2012

Analysis And Mitigation Of Edge Stresses In Multi-Directional Fiber Reinforced Composite Laminates

Srikanth Sundaresh Ghantae
North Carolina Agricultural and Technical State University

ANALYSIS AND MITIGATION OF EDGE STRESSES IN MULTI-DIRECTIONAL FIBER REINFORCED COMPOSITE LAMINATES

by

Srikanth Sundaresh Ghantae

A dissertation submitted to the graduate faculty
in partial fulfillment of the requirements for the degree of
DOCTOR OF PHILOSOPHY

Department: Mechanical Engineering
Major: Mechanical Engineering
Major Professor: Dr. Kunigal Shivakumar

North Carolina A&T State University
Greensboro, North Carolina
2012

ABSTRACT

Ghantae, Srikanth Sundaresh. ANALYSIS AND MITIGATION OF EDGE STRESSES IN MULTI-DIRECTIONAL FIBER REINFORCED COMPOSITE LAMINATES **(Major Professor: Dr. Kunigal Shivakumar)**, North Carolina Agricultural and Technical State University.

Edge delamination in composite laminates with adjacent layers oriented at different fiber angles is a major failure mode because of the existence of high interlaminar stresses and poor interlaminar properties. Mitigation of edge stresses poses a challenge even to date. This research provides a detailed analysis and a potential approach to solve this problem in a carbon/epoxy composite laminate. Two extreme laminates of stacking sequence $(0_n/90_n)_s$ and $(+45_n/-45_n)_s$ subjected to separately applied tensile and thermal loading were considered. These problems have been treated in the literature as a mathematical or bare interface model, wherein the material properties jumped between the adjacent layers of different fiber orientations. A microscopic analysis of laminate cross section showed that the interface was not really bare but there was a thin resin layer of thickness of about 5.0% of the ply thickness. This realization completely changed the modeling and potential modification of the interphase. The region between the plies was represented by a resin layer interphase. A three-dimensional composite finite element (FE) analysis was performed using ANSYS version 12 code. The FE modeling and analysis were verified with the literature for both $(0/90)_s$ and $(+45/-45)_s$ laminates for axial tensile loading as well as temperature change. The resin interphase layer with thicknesses of 2.5%, 5.0% and 7.5% of the ply thickness were

modeled using three different material properties representing: elastic (brittle epoxy), elastic-plastic (toughened epoxy) and non-linear (interleaved polymer nanofiber composite). As the layer thickness became zero, the bare interface results were recovered. Then, for non-linear resin layer the edge stresses reduced indicating that the interleaving of interphase region had a potential to mitigate edge stresses and thus the edge delamination failure.

School of Graduate Studies
North Carolina Agricultural and Technical State University

This is to certify that the Doctoral Dissertation of

Srikanth Sundaresh Ghantae

has met the dissertation requirements of
North Carolina Agricultural and Technical State University

Greensboro, North Carolina
2012

Approved by:

Dr. Kunigal N. Shivakumar Major Professor	Dr. Vinayak N. Kabadi Committee Member
Dr. Mannur J. Sundaresan Committee Member	Dr. Messiah Saad Committee Member
Dr. Ivatury S. Raju (NASA Langley) Committee Member	Dr. Samuel Owusu-Ofori Department Chairperson

Dr. Sanjiv Sarin
Associate Vice Chancellor for Research and
Graduate Dean, School of Graduate Studies

DEDICATION

I dedicate this research work to my dad, Sundaresh Ghantae and my mom, Shantha Sundaresh.

BIOGRAPHICAL SKETCH

Srikanth Sundaresh Ghantae was born on October 20th 1970, in Honnavally, Karnataka State in India. He received a Bachelor of Science in Mechanical Engineering from The University of Mysore, India. He obtained his Master of Science in Mechanical engineering from North Carolina Agricultural and Technical State University, Greensboro, NC in 2000. He has also been employed full time at Volvo Trucks North America, Greensboro, NC, since July, 1998. He is a candidate for Ph.D. degree in Mechanical Engineering.

ACKNOWLEDGMENTS

I am greatly indebted to Dr. Kunigal Shivakumar for being my advisor for my Ph.D. work. I thank the committee members, Drs. Ivatury S Raju, Vinayak Kabadi, Messiha Saad and Mannur Sundaresan for their valuable suggestions and comments. I also thank Volvo Trucks North America for the financial support for my studies. Thanks to my colleague Sarathy Ramachandra for helping me with proof reading and automating the formatting of the document.

I thank the staff and faculty of Center of Composite Material Research, Center of Aviation Safety (CAS) and Department of Mechanical Engineering for their support during my studies and research. My special thanks to Mr. Matthew Sharpe for his help in preparing samples to measure lamina thickness and Dr. Shivalingappa Lingaiah for providing the data for the Nano-fabric.

Finally, my special thanks to my wife Suganthi, son Adithya and daughter Divya, family and friends for their support and encouragement for completing this research.

TABLE OF CONTENTS

LIST OF FIGURES

FIGURE **PAGE**

LIST OF TABLES

CHAPTER 1

INTRODUCTION

1.1 Background

Fiber reinforced composites can be classified into broad categories according to the matrix used: polymer, metal, ceramic and carbon matrix composites. Polymer matrix composites include thermoset (epoxy, polyamide, polyester) or thermoplastic (poly-ether-ether-ketone, polysulfone) resins reinforced with glass, carbon (graphite), aramid (Kevlar), or boron fiber. These composites are used primarily in relatively low temperature applications. Metal matrix composites consist of metals or alloys (aluminum, magnesium, titanium, copper) reinforced with boron, carbon (graphite), or ceramic fibers. The metal matrix composite is limited only by the softening or melting temperature of the metal matrix. Ceramic matrix composites consist of ceramic matrices (silicon carbide, aluminum oxide, glass ceramic, silicon nitride) reinforced with ceramic fibers. The ceramic matrix composites are best suited for very high temperature applications. Carbon/Carbon composites consist of carbon or graphite matrix reinforced with carbon/graphite fibers. They have unique properties of high strength at high temperatures, resistance to extremely high temperature shock coupled with low thermal expansion and density.

Primary building block of composite material is a ply (about 0.005in or .125 mm thick). The required thickness and properties are obtained by stacking several lamina in

different directions and curing them together, the resulting group of plies is referred to as a laminate. The composite laminate used in this research is made of continuous fiber as shown in Figure 1.1. The laminate properties and the constitutive equations can be developed based on the "Classical Laminate Theory (CLT)" by knowing how the plies are laid up to build the laminate that is called the stacking sequence (Jones, 1975), and (Daniel and Isahi, 1994) and the unidirectional lamina constitutive relationships. A general purpose public domain downloadable software mmTexLam is available at http://www.ncat.edu/~ccmradm/ccmr/mmtexlam4.html (Chella and Shivakumar, 2001). The mmTexlam software calculates the lamina and laminate properties of unidirectional, woven as well as braided fibers. The program uses fiber architecture based on different weavings as well as braidings. The computation is based on CLT equations and provides relation between in-plane stresses and strains in the laminate away from the edges. Near the edges, the 3-Dimensional stresses build up to maintain the continuity of the deformation between the plies and the equilibrium condition of the laminate. The interlaminar transverse normal and shear stresses dominate the free edge regions. These stresses can potentially cause delamination and premature failure of structures. Understanding the stress field and finding solutions to mitigate these interlaminar stresses have been subject of interest for the past three decades. The interlaminar stresses exist due to mechanical loading as well as temperature and moisture changes. Types of stresses and their magnitudes at the free edges are explained for two different extreme laminates $(0/90)_s$ and $(+45/-45)_s$ below.

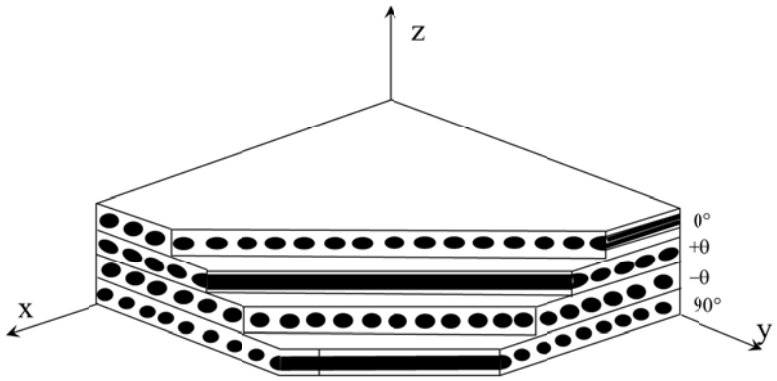

Figure 1.1 Multidirectional laminate and reference coordinate system

1.2 Interlaminar stresses in $(0/90)_s$ and $(+45/-45)_s$ laminates

Figure 1.2a shows a schematic of a $(0/90)_s$ laminate subjected to an uniform tensile axial strain loading of $\varepsilon_{xo.}$ Figure 1.2b shows a cross section of $(0/90)_s$ laminate. Due to the loading, the stress σ_x will be dominant throughout the laminate. σ_y exists in each of the lamina due to the Poisson effect. However, at the interface between the plies with different fiber orientation a different state of stress exists. This has been explained below.

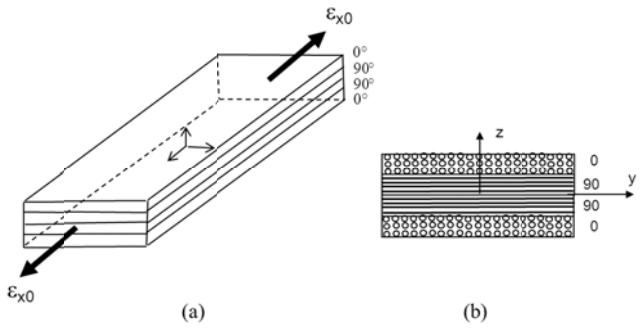

Figure 1.2 Symmetric cross-ply (0/90)s laminate subjected to axial strain (ε_{x0}) (a) full model (b) cross section of laminate

Figure 1.3 shows a free body diagram of a $(0/90)_s$ laminate under uniform extension or axial strain ε_{x0}, if 0° and 90° layers left themselves to undergo contraction, the lateral deformation in 0° is much larger than 90°. When these layers are glued together by lamination, the 0° layer tends to pull 90° layer, while 90° layer pushes (compress) the 0° layer. The pull and push sets up transverse shear stresses (τ_{yz}) on each of the plane layers acting in opposite directions. This must be equilibrated by σ_y acting on each layer. The stresses σ_y and τ_{yz} cause a moment about z direction and in order to satisfy the moment equilibrium condition interlaminar transverse stress σ_z will develop as shown in Figure 1.4. These two stresses above satisfy the equilibrium and continuity conditions of the elasticity at the interface as shown in Figure 1.4. Figure 1.5 shows typical distribution of σ_z and τ_{yz} near the free edge between 0° and 90° layers in the laminate. The stresses that develop at free edge in $(0/90)_s$ is attributed to Poisson's ratio mismatch of layers and are called the edge stresses. The stresses are zero in the interior width of the laminate and peak towards the edges. The interlaminar shear stress τ_{yz} falls to zero at the free edge, since the shear stress cannot exist at the free surface. The normal stress (σ_z) is zero in the middle and increases towards the free edge and is singular at the free edge due to mismatch in material properties. The distance from the edge where the out of plane normal and shear stresses exist is called the edge stress distance (d), and this can exists both in the normal stresses and the shear stresses in the laminate, schematic of the edge distance is shown in Figure 1.5.

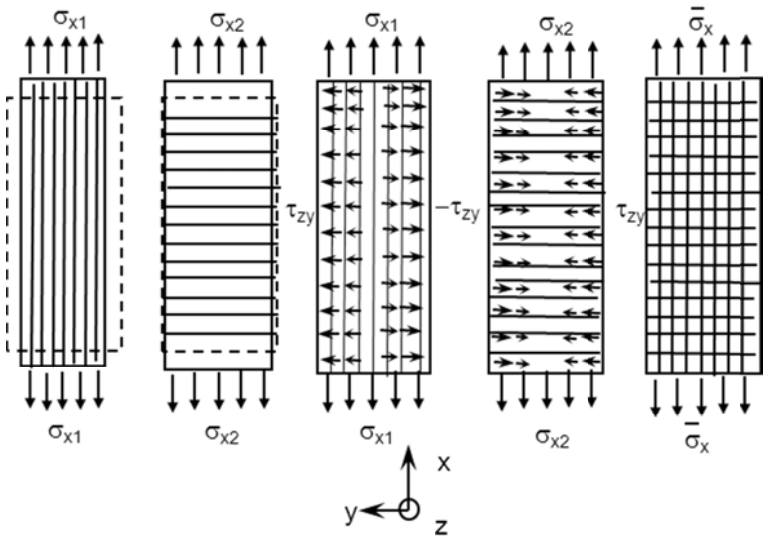

Figure 1.3 Free body diagram of $(0/90)_s$ laminate

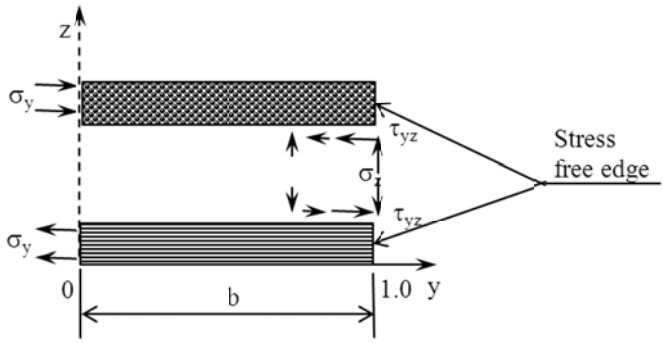

Figure 1.4 Free body diagram of (0/90)s laminate at cross section through the thickness

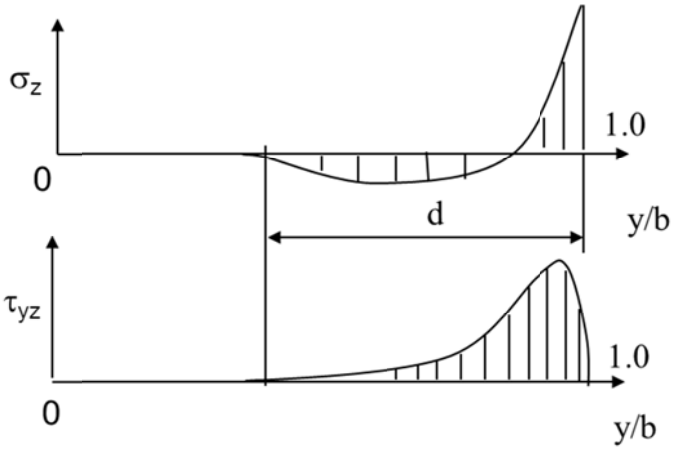

Figure 1.5 Schematic of stress distribution between 0 and 90 interface

Figure 1.6 shows schematic of a $(+45/-45)_s$ laminate subjected to uniform loading ε_{x0}. Similar to the $(0/90)_s$ the axial loading causes σ_x to be dominant in the entire laminate. σ_y also exists in each lamina due to Poisson's ratio. However, at the interface between the +45 and -45 layer a different stress state exists. Figure 1.7 shows a free body diagram of the laminate in the loaded condition under stress σ_x on each layers separately; the layers will undergo shear deformation. When they are bonded together the shear strain must be zero at the free edges. This can happen only with interlaminar transfer of shear stress between the two layers and this gives rise to τ_{xz} and τ_{xy}. In order to satisfy moment equilibrium of τ_{xz} and τ_{xy}, the out of plane normal σ_z stress also exists at the interface. These stresses are zero in the middle part of the specimen and are singular at the free edges. The moment produced by this gives rise to τ_{xy}. Normal σ_z is zero in the middle and peaks at the edges as explained in Daniel and Isahi (Daniel and Isahi, 1994). Figure 1.8 shows typical distribution of edge stresses. Similar to $(0/90)_s$ case the distance from the edge where the stresses exist is called the edge stress distance 'd'.

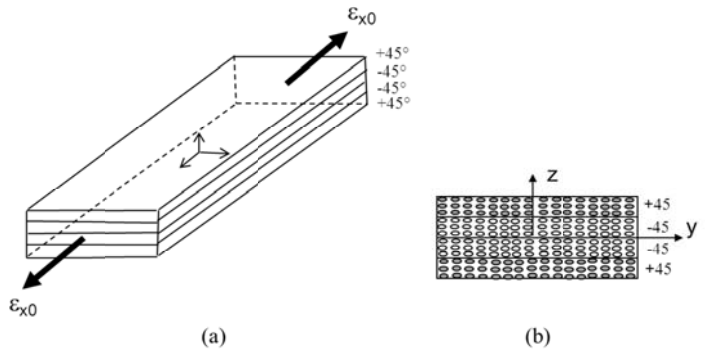

Figure 1.6 Symmetric angle-ply (45/-45)s laminate subjected to axial strain (ε_{x0}) (a) full model (b) cross section

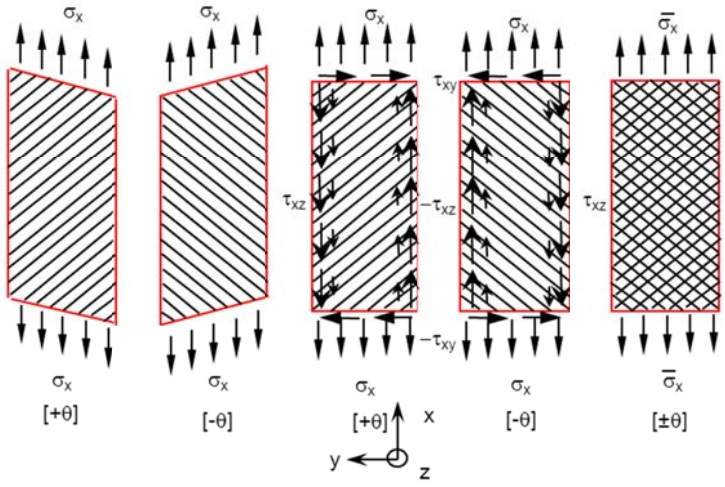

Figure 1.7 Freebody diagram of $(45/-45)_s$ laminate

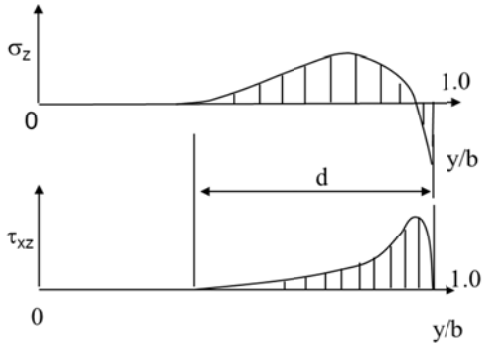

Figure 1.8 Typical stress distribution between 45 and -45 laminate interface

1.3 Literature on interlaminar stresses in composite laminate

In order to understand the effect of interlaminar stresses and predict the stress fields at the free edges a number of research has been performed in the last 30 years, most important publications are reviewed here. Williams (Williams, 1952) was the first to show singularities in anisotropic plates subjected to extension load under mixed boundary conditions at the edges. Pipes and Pagano (Pipes and Pagano, 1970) were the first to demonstrate the existence of interlaminar stresses and singularities at the free edge in

composite laminate. They used a finite difference technique and two dimensional theory of elasticity to study the mechanism and calculate the edge stresses in $(+45/-45)_s$ laminate under tensile loading. In this study, the out of plane shear stress at free edge was forced to zero. They showed that the interlaminar out of plane shear stresses exist only at the region close to the edges and this region is approximately equal to the laminate thickness. Rybichi (Rybichi, 1971) used 3-D Finite Element Analysis (FEA) to obtain approximate stress solution based on complementary energy formulation on symmetric laminate with in plane loading. Edge effects were studied in $(+45/-45)_s$, $(-45/+45)_s$ and $(90/0)_s$ laminates under tensile loading and showed that the out of plane shear stress τ_{yz} is significant at the edges and out of plane shear τ_{xy} can occur at the center section.

Tang and Levy (Tang and Levy, 1975) developed boundary layer theory for laminated composites and analyzed $(+45/-45)_s$ laminate for interlaminar stressed under tensile loading. The results from this theory compared well with the work of Pipes and Pagano (Pipes and Pagano, 1970). Wang and Crossman (Wang and Crossman, 1977) used 2D-FEA to calculate the interlaminar stresses for $(90/0)_s$, $(0/90)_s$, $(+45/-45)_s$ and $(\pm45/0/90)_s$ laminates for uniform tensile loading. They concluded that the physical effect of singularity stresses at the edges were not found and these stresses if found would dissipate in the laminate resulting in stress redistribution. The material property would degrade at locations where the stress redistribution occurred. Wang and Crossman (Wang and Crossman, 1977) extend the analysis for $(90/0)_s$, $(0/90)_s$, $(+45/-45)_s$ and $(\pm45/0/90)_s$ laminates for uniform thermal loading and calculated the interlaminar stresses at the laminate. They concluded that the singularity stresses exist at the boundary region for

laminates under thermal loading. Pagano (Pagano, 1978) proposed theoretical solution using Reissner's variational principle (Reissner, 1950) and layer equilibrium. The stress distribution was calculated for $(+45/-45)_s$ laminate and compared with Wang and Crossman (Wang and Crossman, 1977). Conclusion from this model showed no singularities at the free edges and singularities were mathematical in nature and not realistic.

Raju and Crews (Raju and Crews, 1981) used quasi 3-D FEA to calculate interlaminar stresses for $(0/90)_s$, $(15/-75)_s$, $(30/-60)_s$, $(+45/-45)_s$, $(60/-30)_s$, $(+75/-75)_s$ and $(90/0)_s$ laminates under uniform tensile loading. They showed the existence of singularities for σ_z, τ_{xz} stresses at the free edge of the laminate interface. Wang and Choi (Wang and Choi, 1982) studied boundary layer stress singularities using Lekhnitskii's stress potential and theory of anisotropic elasticity. They compared their results with Pipes and Pagano and Wang and Crossman (Pipes and Pagano, 1970) and (Wang and Crossman, 1977) for $(+45/-45)_s$ laminate. They concluded that the boundary layer stress developed from their theory predicted a boundary layer that was more exact compared to the elasticity and other approximate solutions. Also, concluded that the boundary layer for $(+45/-45)_s$ laminate had the highest boundary layer width of 4.5% for lamina thickness. Wang and Choi (Wang and Choi, 1982) also computed interlaminar stresses at the boundary layer for $(+\theta/-\theta)_s$ laminate. They concluded that the ply orientation and ply thickness had significant effects on the development of in-plane and interlaminar stresses. The boundary layer width due to moisture loading was one-half of laminate thickness, for lamina thickness of 30-70% of the total laminate thickness.

Kassapoglou and Lagace (Kassapoglou and Lagace, 1987) analyzed interlaminar stresses in $(+45/-45)_s$ and $(0/90)_s$ laminates using closed form solution with force balance method and principle of minimum complementary energy. They compared their solutions with Pipes and Pagano and Wang and Crossman (Pipes and Pagano, 1970) and (Wang and Crossman, 1977). Flanagan (Flanagan, 1994) calculated the free edge stresses for $(0/90)_s$ and $(+45/-45)_s$ laminates for tensile loading using the principle of minimum complementary energy. The solution compared well with (Pipes and Pagano, 1970). Lessard et al., (Lessard, Schmidt, and Shokrieh, 1996) used 3-D FEA to calculate stress distribution at the free edge for $(0/90)_s$ laminates, using 'slice method' technique with a 20 noded brick element. Their solution has been shown to agree well with the work of Pipes and Pagano (Pipes and Pagano, 1970) and Kassapoglou and Lagace (Kassapoglou and Lagace, 1987). Icardi et al., (Icardi and Bertetto, 1995) conducted 3D FEA for calculating the interlaminar stresses for $(0/90)_s$ laminate using special elements called "wedge element" to get more accurate singularity stress results at the free edges. Their study concluded that there was no effect on the power of singularity due to the change in lay up, material properties or the geometry of the laminate.

Tahani and Nosier (Tahani and Nosier, 2003) used Reddy's layer wise theory (LWT) (Reddy, 1987) and calculated stress at the free edges for $(0/90)_s$ laminates for mechanical and thermal loading. They compared results with Wang and Crossman (Wang and Crossman, 1977) and found to agree well. Becker et al., (Becker, Peng Jin, and Neuser, 1999) derived closed form solutions to analyze the stresses at free corners in $(0/90)_s$ laminates under thermal loading, they have compared the results with FEA

solution for interlaminar stresses and found they agree well. More recently Nguyen and Caron (Nguyen and Caron, 2009) have derived analytical solution for composite laminates using the M4-5n (Multi-particle model of Multi Layered Materials with five kinematic fields per layer for an n-layer laminate) layer-wise method and the results for the stress fields agree well with Wang and Crossman (Wang and Crossman, 1977).

The study reported above on FEA and derived solutions gave a good representation of stress distributions at the edge of interior of a composite laminate. All the analyses considered that the ply interface properties jumped (as shown in Figure 1.9) from each other depending on the ply orientation (this representation of laminate is called bare interface). The ply thicknesses considered in these studies were too thick compared to the actual composite laminates. The mesh refinement used in these were coarse possibly due to the limitation of the computes at that time.

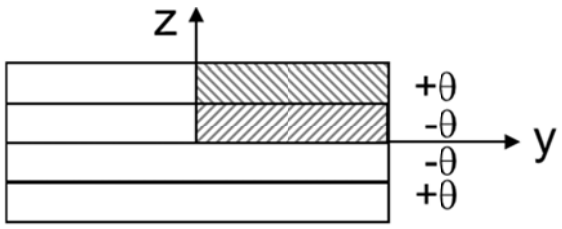

Figure 1.9 Bare interface model

1.4 Interlaminar stress mitigation techniques in multi-directional laminates

Interlaminar edge stresses have been a challenging problem in composite laminates even to this date. Edge delamination failure such as the one shown in Figure

1.10 has been a typical failure mode in laminates. The free edges are very common where there are joints between two parts or at the ends that have been trimmed off. A number of attempts were made to reduce these stresses through various methods during for the past 25 years. Kim (Kim, 1983) conducted experiments to understand effect of addition of glass fabric between two differently oriented lamina. They found that for a laminate with glass fabric interleaved specimen loaded in tensile, no delamination occurred at the interface and they also found that the strength of the laminate increased due to this interleaving. However, the experiments did not give reliable results to show that there was a reduction in stresses compared to the baseline. Mignery et al., (Mignery, Tam, and Sun, 1985) tried stitching the edges as shown in Figure 1.11 of the laminates to suppress the interlaminar out of plane normal stresses in composite laminates. Edge delamination was arrested at and around the stitches in all the stacking sequence studied. The tensile strength of $(+30/-30/90)_s$ increased, tensile strength on $(+30/-30/0)_s$ decreased, and had no effect on $(+45/-45/0_2/90_2)_s$ laminate. However, the stitching did not eliminate the edge delaminations unless they were very close to the edges.

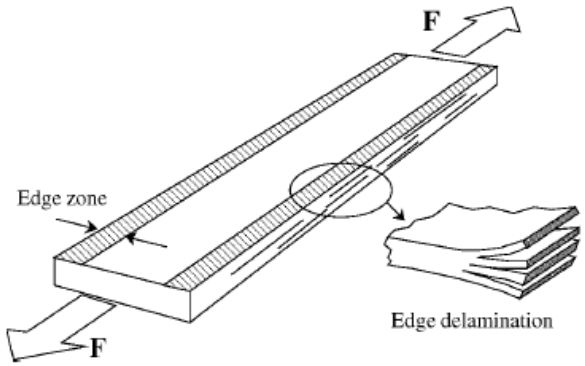

Figure 1.10 Edge delamination mode of failure in a laminate (Tanimoto, 2002)

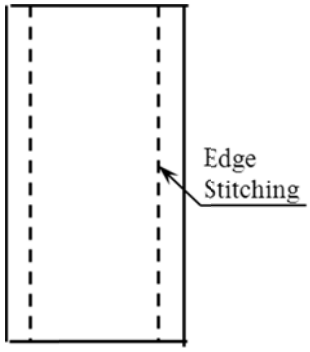

Figure 1.11 Edge Stitching in a laminate

Chan and Jumbo (Chan and Jumbo, 1986) used knitted non-woven fabric or uni-directional tapes as interleaving. They showed no significant improvement in tensile strength due to non-woven fabric or tape interleaving, but found that ultimate strength with non-woven interleaving was lowered. The delamination size of non-woven was small compared to the unidirectional tapes, the reason was not conclusive. Sun and Chu (Sun and Chu, 1991) used notches at the edges to relieve edge stresses. They concluded that the presence of notches could suppress the delamination and also, for an interlaminar shear controlled failure the laminate strength significantly increased. Figure 1.12 shows the technique of edge notching.

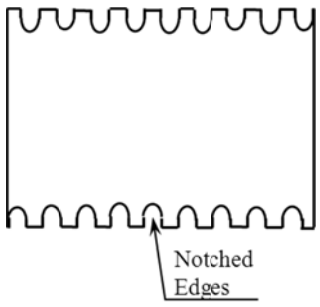

Figure 1.12 Notching of edges in a laminate

Howard et al., (Howard, Gossard, and Jones, 1986) used capping of the edges to mitigate the normal edge stresses and delay the onset of delamination, schematic of edge capping technique is shown in Figure 1.13. This capping reduced the interlaminar stresses for $(+30/-30/0/-30/+30)_s$ and $(+30/-30/90/-30/+30)_s$ laminates but there was no change in the total strain energy release rate. Chan et al (Chan, Rogers, and Aker, 1986) showed that addition of adhesive layer of 0.0105" (2 Ply thickness) thick at the interphase and compared the results between interleaving at the region closer to the edges or the enter width of the specimen as shown in Figure 1.14. They showed that the edge delamination was eliminated until the final failure and also showed that there was an increase in ultimate strength for the interleaved laminate. However, the drawback of this study was that the adhesive film is too thick and was not optimized. This could lead to significant loss of in-plane properties. They also used 3D FEA to show the edge stress regions. However, the study was performed only on the specific laminate stacking sequence and the mesh refinement was not fine enough to obtain good stress distribution. Lagace et al. (Lagace, Mong, and Khulmann, 1993) also studied the effect of adding adhesive layers of 0.008" (0.203mm) on $(+45/-45/0/90)_{4s}$ and $(((+45_2/-45_2)/0)_s/90_5)_{2s}$ composite laminate for tensile properties. The results showed that the addition of adhesive layer suppressed or at least significantly delayed the onset of delamination. The load carrying capacity increased by 50% for the interlayer. However, the thickness of the adhesive layer was higher and led to loss of in-plane strength. Tanimoto (Tanimoto, 2002) and Hojo et al. (Hojo, Matsuda, Tanaka, Ochiai, and Murakami, 2006) proposed interleaving technique such as dispersed particulate interlayers for tensile and impact loading. Figure 1.15 shows

the technique of particle interleaving. They found that interleaving in composite laminates improved axial fatigue strength and modulus. Interleaving also slowed the delamination growth under Mode I loading.

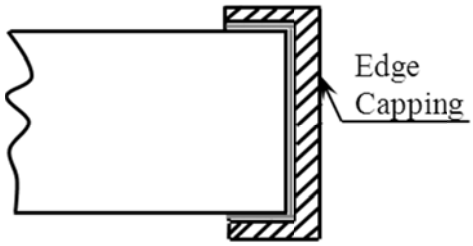

Figure 1.13 Edge cap reinforcement

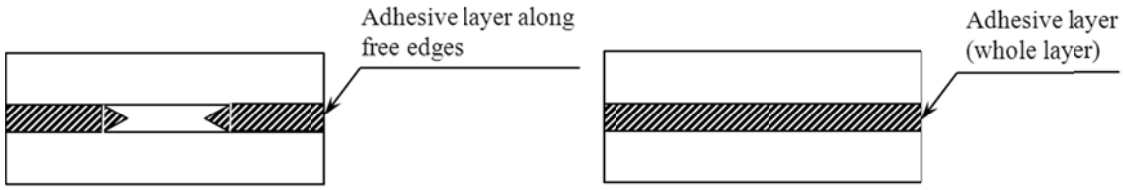

Figure 1.14 Addition of adhesive layer

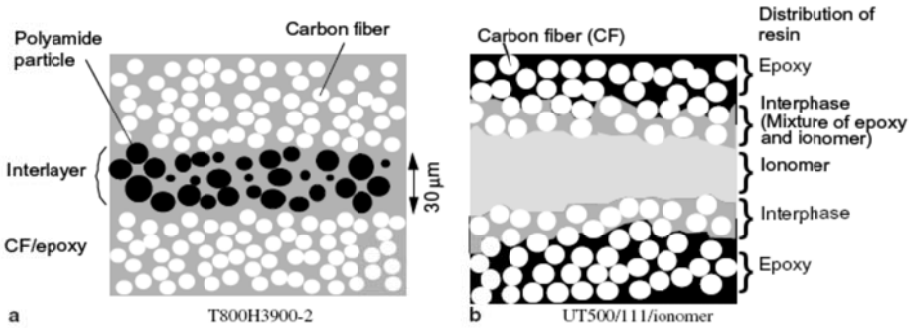

Figure 1.15 Particle/Resin interleaving technique in a laminate (Hojo, Matsuda, Tanaka, Ochiai, and Murakami, 2006)

Shin et al. (Sihn, Kim, Kazumasa, and Tsai, 2007) studied the effect of delamination and tensile strength on the use of thin ply concept and compared against thick plies. Their studies showed that thin plies could suppress the micro-cracking and delamination damages at the edge of the laminate. Thin ply composite laminate also improved the higher allowable strain in the laminate. The ultimate load was higher for thin plies compared to the thick plies. However, the drawback of this technique was the difficulty in manufacturing of the thin ply laminates and the additional processing involved. Also the thinning of plies showed a brittle fracture in a notched laminate.

The techniques discussed above showed some reduction in interlaminar stresses. However, all these techniques had some kind of additional manufacturing processes which are hard to implement in real applications. Furthermore in most cases their modifications add additional cost, weight and in-plane properties for composite components. One outcome of the study of interlaminar edge stresses and edge distance is the thin ply concept. By reducing the thickness of the ply and the edge stress dominance length and eventually the edge stress delamination can potentially be eliminated in the laminates. Another concept still attractive, although it was experimented previously with problems, is the interleaving between the plies. These two research areas continue to be explored.

1.5 Interphase Region in a Multi Directional Laminate

As many researchers studied, including Lagace (P. A. Lagace, 1993), the interface between the plies of dissimilar orientation in a resin layer may behave like linearly

elastic, the elastic-plastic or non-linear elastic depending on the state of stress. The mathematical representation with a bare interface model and a sudden change of the material properties is a modeling simplicity, which could be the root cause of singularity stresses. All the analytical models used to analyze the interfacial stresses so far were based on the mathematical interface. The Figure 1.16 shows a cross section of $(0/90)_s$ laminate with an enlarged view at 0 and 90 interphase region. Notice a finite resin layer, in this case about $2.3x10^{-4}$" (250 μm) or 5% of ply thickness (this representation of laminate is referred in this study as resin interphase model). Crews et al., Raju et al and Smith et al have tried using thin resin layer interphase for cracked specimens, however analysis for models with the resin layer for edge stresses study of realistic geometry under tensile and thermal loading has not been attempted to date (Crews, Shivakumar, and Raju, 1986), (Crews, Shivakumar, and Raju, 1988), (Raju, Crews, and Amanpour, 1988) and (Smith and Shivakumar, 2001). Whether this modeling will significantly impact the interlaminar stresses or not, has not been explored. Extension of the resin layer to behave as an elastic-plastic or non-linear, in case the layer is replaced by an interleaved material such as polymer nano-fiber composite needs to be understood and their impact on interlaminar edge stresses needs to be explored. Because of large variation of geometric parameters and non-linearity of the interphase material the modeling analysis and the interpretation of results are challenging. However, the understanding of stress distribution at and around the region of free edges is very critical to prove the validity of the concepts such as polymer nano-fiber interleaving to relieve or mitigate interlaminar

stresses (Lingaiah, Shivakumar, and Sadler, 2008), (Akangah, Lingaiah, and Shivakumar, 2011) and (Adams and Shivakumar, 2011) .

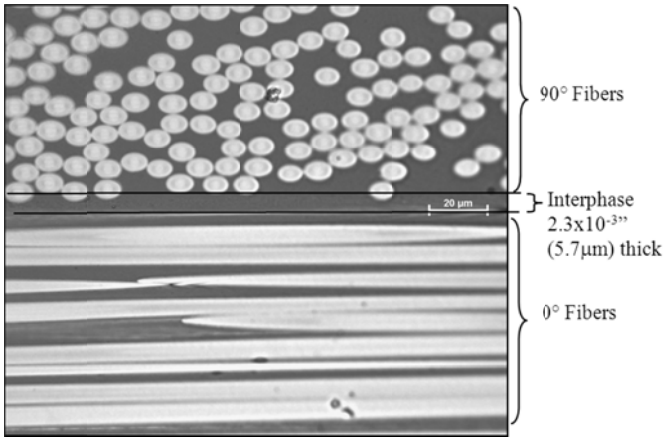

Figure 1.16 Cross-section of realistic laminate

In the present research, two classical laminates namely $(0_n/90_n)_s$ and $(45_n/-45_n)_s$ were selected. Here "n" is the number of plies in a layer. A resin layer interphase with various material properties was interleaved between the composite layers. The thickness was about the same as what was measured in the carbon/epoxy laminate. The models were developed and analyzed using 3D-finite element method. The laminates were loaded by uniform axial stresses and temperature change. The interlaminar edge stresses were computed and examined for all cases.

1.6 Objectives of this research

The goal of the research is to understand the interlaminar stresses between the adjacent plies oriented at different angles with a resin interphase layer subjected to axial

strain and thermal loads. The laminate considered were $(0/90)_s$ cross-ply and $(+45/-45)_s$ angle-ply. The resin interphase layer thickness represents what is observed in real laminate. The resin material were assumed to be isotropic and (a) elastic, (b) elastic-plastic and (c) non-linear elastic. The specific objectives of the research are:

(a) To develop a refined 3-D finite element (FE) model of the bare interface problem and validate the modeling and results with the literature,

(b) To develop a refined FE model of the resin interphase problem and study the difference and trend of the interlaminar stresses for variation of interphase thickness and elastic, elastic-plastic and non-linear properties of the resin layer,

(c) To investigate the effect of ply grouping or the thickness of the ply on interlaminar edge stresses and distance,

(d) To investigate the effect of temperature change on thermal edge stresses for bare and resin interphase model with elastic, elastic-plastic and non-linear properties of resin layer, and

(e) Finally, the conclusion that lead to a necessity of interphase modification of adjacent plies oriented differently to reduce the interlaminar edge stresses.

1.7 Scope of this Dissertation

Chapter 1 describes the background of this research and theory behind interlaminar edge stresses in composite laminates. This chapter also includes literature, challenges and objectives of the research. Chapter 2 describes the bare interface modeling, of $(0/90)_s$ and $(+45/-45)_s$ laminate by 3D-finite element analysis of the model.

This chapter also presents mesh convergence study and comparison with existing literature for a laminate under tensile loading. Chapter 3 presents the results for interlaminar edge stresses within a realistic resin interphase layer between the 0 and 90 and 45 and -45 plies in symmetric laminates. It also presents the effect of ply grouping on the edge stresses and distance. Chapter 4 examines the effect of temperature change on interlaminar stresses in bare and resin layer interphase models. Chapter 5 presents the concluding remarks and future research.

CHAPTER 2

MODELING OF BARE INTERFACE COMPOSITE LAMINATE AND VERIFICATION WITH LITERATURE

In this chapter, 3-D Finite element analysis of two classical laminates, namely $(0/90)_s$ and $(+45/-45)_s$ subjected to an uniform axial strain are presented. The interface region between the layers is treated as a mathematical separation represented as bare interface wherein the material properties jump between the adjacent layers depending on the lamina orientation. A systematic mesh refinement is conducted to get a good description of the stress field. The modeling is verified by comparing with the results from the literature. In addition, some important conclusion regarding the boundary layer region and the grouping of the plies are derived.

2.1 Material system

The material properties considered for this research are a typical high modulus aircraft grade AS4/3501-6 carbon/epoxy material made by of Hexcel® Corporation. This is also chosen because it is commonly used in literature and so that it will be easier to compare the present results with the literature. The unidirectional mechanical and thermal properties are listed in Table 2.1.

Table 2.1 Material Properties of unidirectional AS4/3501-6 carbon/epoxy composite

Elastic Constant	Values msi (GPa)	Elastic Constant	Values
E_1	19.0 (131)	ν_{12}	0.34
E_2	1.89 (13.0)	ν_{13}	0.34
E_3	1.89 (13.0)	ν_{23}	0.35
G_{12}	0.93 (6.41)	α_{12}	$0.5x10^{-6}$ in/in/°F ($0.03x10^{-6}$ mm/mm/°C)
G_{13}	0.93 (6.41)	α_{13}	$15x10^{-6}$ in/in/°F ($0.90x10^{-6}$ mm/mm/°C)
G_{23}	0.70 (4.82)	α_{23}	$15x10^{-6}$ in/in/°F ($0.90x10^{-6}$ mm/mm/°C)

Subscripts 1, 2 and 3 represent material coordinate system, with 1 being the fiber direction

2.2 A $(0_n/90_n)_s$ Laminate subjected to uniform axial strain

2.2.1 Problem definition

Figure 2.1 shows a $(0/90)_s$ laminate subjected to uniform axial strain ε_0. The specimen of length 'L', width '2b' and total laminate thickness 't', with each lamina of thickness 'h'. The geometry of the specimen used throughout this research is L= 4" (101.2mm) and 2b=1" (25.4mm) has been shown in Figure 2.1 The thickness of the specimen used for the verification with the literature is t= 0.5" (12.7 mm) and has been taken from the work of Nguyen and Caron (Nguyen and Caron, 2009) for mesh refinement and verification of the model, for the rest of the research a more realistic

laminate thickness of t=5.1mm (0.2”) for n=10 and t=1mm (0.04”) for n=2 in a $(0_n/90_n)_s$ laminate, where n is the number of layers grouped in the lamina have been used.

The specimen is made of composite laminate with four layers (lamina), each layer is made of continuous fiber layer oriented in 0° or 90°. The stacking sequence of this composite is $(0_n/90_n/90_n/0_n)$ also represented as $(0_n/90_n)_s$ where n is the number of fiber layer in each of the orientation. The 0° lamina is on the top and bottom layer and two of the 90° lamina in between the 0° layers. This stacking sequence represents one extreme cases of the laminate interphase. The schematic of the laminate is shown in Figure 2.1. The cross section of the laminate with the fiber direction is shown in Figure 2.2a. This axial loading of the specimen results in interlaminar edge stresses between the two layers with mismatched fiber orientation. These resulting stresses between the two layers (interphase) have been calculated and analyzed as part of this work.

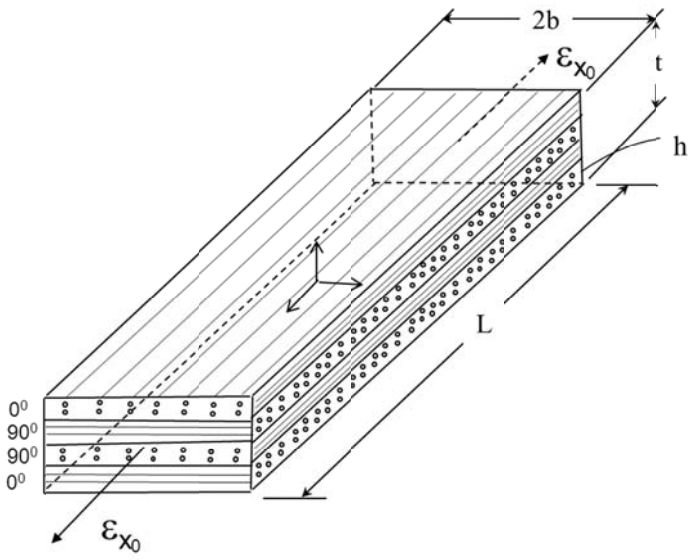

Figure 2.1 Problem and geometry definition

2.2.2 Ply grouping

Cost of manufacturing and grouping number of plies in a layer to minimize interlaminar stresses continues to be a challenge. At least from an academic point of view effect of ply grouping on interlaminar stresses is studied here. The number of plies in a layer is changed from n=1 to n=12 and its influence on interlaminar stress near the edge of $(0_n/90_n)_s$ and $(+45_n/-45_n)_s$.laminate is examined. The sketch showing the concept of ply grouping for n=2 and n=4 is shown in Figure 2.2 a and b respectively.

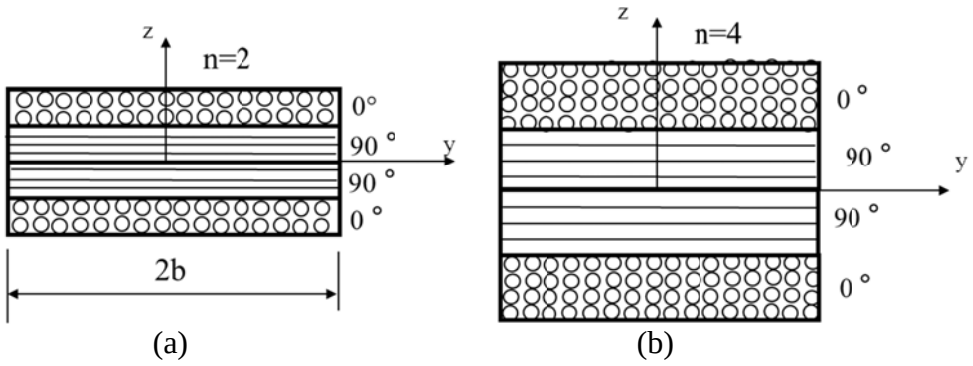

Figure 2.2 Concept of Ply Grouping (a) 2 layers, (b) 4 layers

2.2.3 Mathematical Model

Since the model is symmetric about the x, y and z direction of the specimen, a full physical model shown in Figure 2.3a can be simplified to a $1/8^{th}$ symmetric model. Figure 2.3b illustrates the model used in the analysis. The length of the model is L/2, the width of the model is b, 'h' is the ply thickness and the thickness is h=t/4. The model was constructed such that the inner face of the $1/8^{th}$ model represented a symmetric boundary condition. The area of interest for this research is the interphase region between the two

layers and the stress distribution at the free edges as shown in the Figure 2.3c. As discussed in Chapter 1 for a $(0/90)_s$ laminate the stresses σ_z and τ_{yz} are of interest closer to the free edge. Although this analysis can be easily solved as a generalized 2D plain strain model, it is convenient to use 3-D Modeling technique in commercial FE codes like ANSYS.

2.2.4 Boundary conditions

As described above the mathematical model is simplified to only $1/8^{th}$ of the physical model. The complete model is simulated by applying symmetric boundary condition to the model on three sides at x=0, y=0 and z=0 planes. The axial loading in x direction (ε_{x0}) is applied as an elongation of 1% of length. The boundary conditions and loading has been shown in Figure 2.3b.

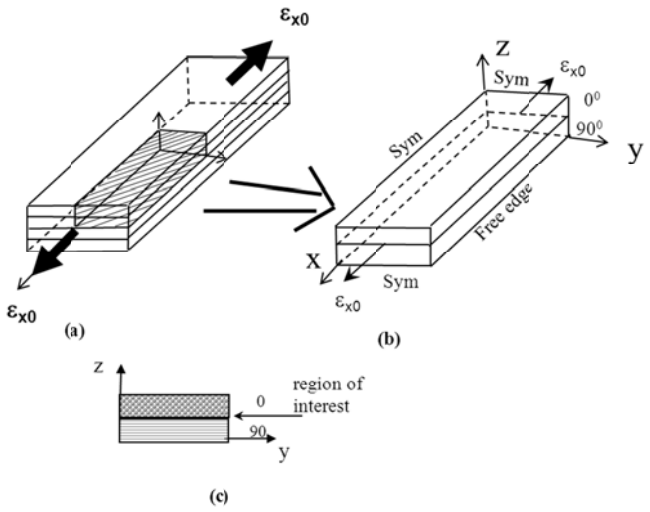

Figure 2.3 Mathematical Model of Bare interface (a) Full model of laminate, (b) Symmetric $1/8^{th}$ model, (c) Cross section of $1/8^{th}$ model

2.3 Finite Element Analysis of $(0_n/90_n)_s$ laminate

2.3.1 ANSYS Finite Element Code and Methodology

A commercial finite element software ANSYS version 11.0 was used in this study. This code has mesh generation as well as linear and non-linear analysis capability. The pre and post processing capabilities of the code were used for modeling the problem and analysis of the results, respectively.

APDL (ANSYS Parametric Design Language), a scripting language that can be used to automate common tasks or even build model in terms of parameters (variables) was used. While all ANSYS commands can be used as part of the scripting language, the APDL commands used in this research are the true scripting commands and encompass a wide range of other features such as repeating a command, macros, if-then-else branching, do-loops, and scalar, vector and matrix operations.

While APDL is the foundation for sophisticated features such as design optimization and adaptive meshing, it also offers many conveniences that can be used in routine analyses (ANSYS® Theory Reference, 2009). A typical APDL code used in the analysis has been listed in Appendix A.

2.3.2 Three Dimensional Hexahedron Element

Three-dimensional eight noded, iso-parametric elements were used to model the specimen. The element had three degrees of freedom at each node and can model from isotropic to general anisotropic materials. The element used in the software is represented as “SOLID 46”. Solid46 (3-D Layered Structural Solid) is a layered version of the 8-node

structural solids (SOLID45) and has 3 degrees of freedom at each node, this element is designed to model layered thick shells or solids. The element allows up to 100 different material layers. If more than 100 layers are required, a user-input constitutive matrix option is available. The element may also be stacked as an alternative approach. The element has three degrees of freedom at each node translations in the nodal x, y, and z directions. Number of layers, thickness of the layers, fiber orientation and material properties have to been defined in order to use the element. Figure 2.4 shows a sketch of SOLID46 element with identification labels for the nodes (I-P) and faces (1-6).

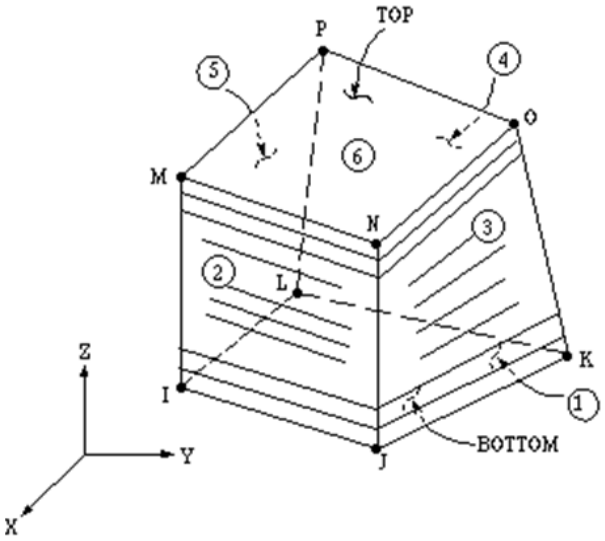

Figure 2.4 Sketch of SOLID-46 element (ANSYS® Theory Reference, 2009)

2.3.3 Finite Element Mesh and Mesh Refinement

In order to obtain a good stress field response from the finite element model developed a number of different models were analyzed based on the model meshing, A

typical idealization for the baseline model is shown in Figure 2.5. Several other idealizations were used to establish the rate of convergence of the solution, accuracy of the modeling and to resolve oscillatory singularity issues. Figure 2.6 presents various mesh refinements used to study the convergence across the width of the specimen.

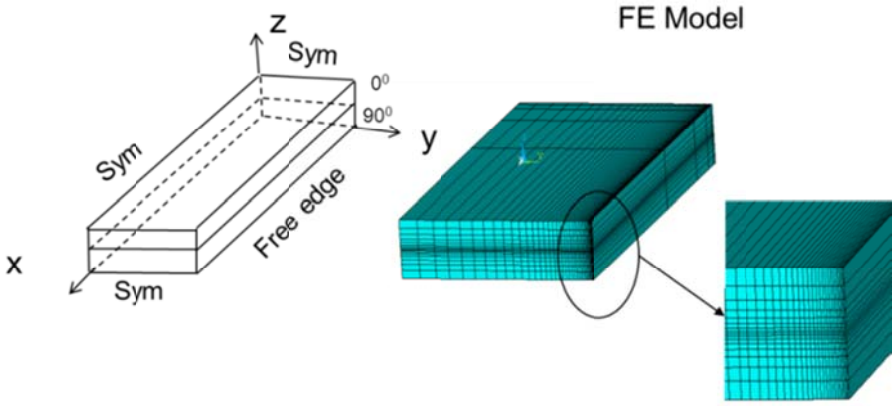

Figure 2.5 Typical FEA Model Idealization

The model has been constructed by defining key points at the corners of each of the model. The key points are used to build the volume that represents the lamina. Each layer is represented by different volumes but have common edges. This is done to attach different material properties for each volume in the laminate. The edges of volume are broken into segments that will then be used to mesh the volume. Boundary conditions are then applied to the volume for solving the model. The output is generated by choosing the location of the nodes and its corresponding six stresses at each of the nodes. The location and stress data are then saved into an output file for data analysis.

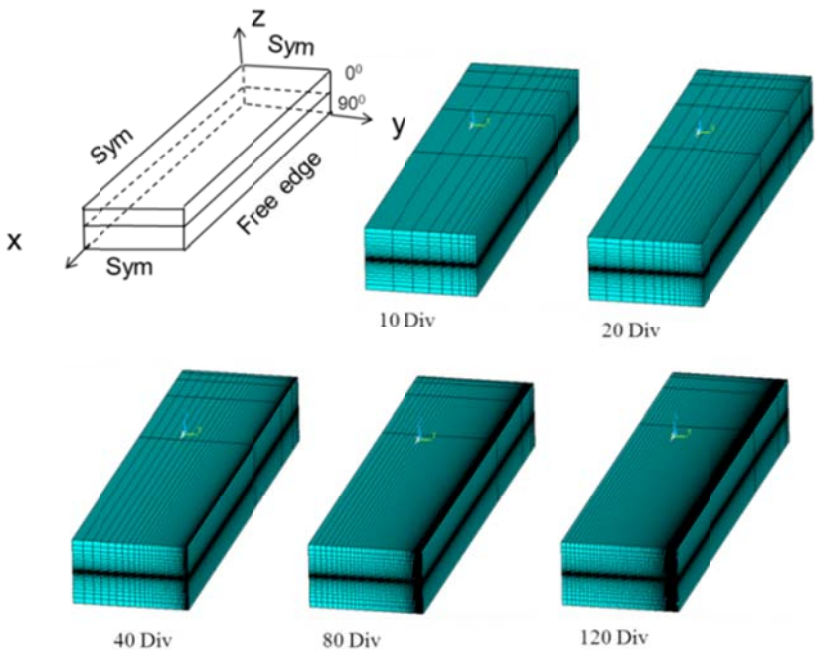

Figure 2.6 Mesh Refinement along Y-Direction

The model representing a tensile specimen has been studies and FE Analysis were performed. Different mesh refinement study was performed to achieve the best results and singularity results at the free edge of the specimen. The mesh was finer towards y=b (closer to the free edge) and z=h (at the interphase of lamina) which is the area of interest.

Five widthwise refinements were considered. The models had 10, 20 40, 80 and 120-graded divisions in the width direction. All the models were graded to have smaller elements near the outer free edges and larger divisions in the middle width of the specimen. All five idealizations are presented in Figure 2.6 these models were analyzed. then the σ_x and τ_{yz} distribution along the width closer to x=0 were plotted. Number of nodes and elements in the model is shown in Table 2.2

Table 2.2 Mesh Refinement along y-Direction

Model	x-Div	y-Div	z-Div	Grading	No. of Elements	No. of nodes
1	5	40	4	4	800	6,400
2	5	40	8	8	1,600	12,800
3	5	40	16	16	3,200	25,600
4	5	40	32	32	6,400	51,200
5	5	40	64	64	12,800	102,400

The thickness refinement was studied for 4, 8, 16, 32 and 64 divisions for each of the lamina thickness, whereas, x and y remaining constant at 5 and 40 divisions. The number of divisions in the length direction is constant because the stresses are constant across the length of the specimen. Figure 2.7 shows different thickness idealizations. σ_z and τ_{yz} were plotted at 1-node behind the free edge. Table 2.3 shows the number of element that was used in each of the models for this refinement study.

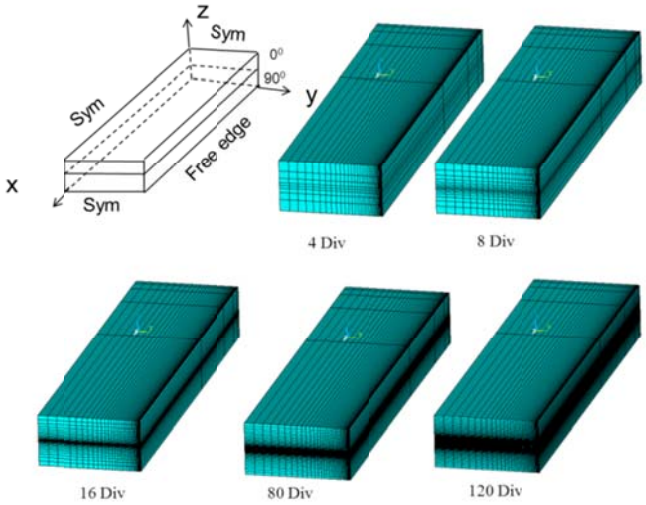

Figure 2.7 Mesh Refinement along Z-Direction

Table 2.3 Mesh Refinement along z-Direction

Model	x-Div	y-Div	z-Div	Grading	No. of Elements	No. of nodes
1	5	10	16	10	800	6,400
2	5	20	16	20	1,600	12,800
3	5	40	16	40	3,200	25,600
4	5	80	16	80	6,400	51,200
5	5	120	16	120	9,600	76,800

2.3.4 Analysis Procedure

Using the method described above the mathematical model and the material attributes. The model was idealized using the 3-D SOLID46 as explained in the mesh refinement section. The material properties and the fiber orientation was defined. The boundary conditions were imposed as explained in section 2.3.4. The linear elastic analysis of the model was conducted using the ANSYS Sparse solver. The results were obtained from the solved model at the critical regions using the post processing module to output all stress and strains. The ANSYS total nodal stress at each of the nodes in x, y, z , xy, yz, xz direction in the critical regions were used in this analysis. Average axial normal stress σ_{x0} was computed by extracting the reaction at x=0 plane on the specimen and dividing by the area of cross section. The reaction load for the models used for mesh refinement analysis were found to be 55,511 lbs, the average σ_x was found to be 55,390 ksi. To verify this value the average stress was also calculated using the Young's modulus equation $\sigma=E_x\varepsilon_0$. The laminate E_x was found to be 5.539 $x10^6$ psi from the

mmTexlam code available in [3]. The calculated average stress for 1% axial strain (ε_0) is 55,390 psi which is exactly the same as the FE result. Analysis was repeated for different mesh and the interlaminar stresses were examined at critical regions.

2.4 Results of $(0_n/90_n)_s$ Laminate

2.4.1 Refinement Study for $(0/90)_s$ Laminate

As explained previously mesh refinement study was conducted in y and z directions of the model, the results are presented. Figure 2.8a shows the distribution of interlaminar normal $\sigma_z(y,h)$ normalized by σ_{x0} for different refinement in y-direction. The graded discretization ranged from 10-120 divisions. The abscissa is normalized by half-width (b) of the specimen and the ordinate is normalized value of σ_z. Figure 2.8b shows an enlarged view of the 10% of the width from the free edge. The general shape of the curves agree very well with the results shown in (Daniel and Isahi, 1994). The normal stress is zero on the inside of the laminate and is singular at the free edge. As it can be seen except for 10 divisions mesh refinement, the rest of the refinements show a very close agreement with others. Also, the curves are very smooth for mesh higher than 10 divisions. Furthermore, the result of mesh refinement of 40 divisions and higher refinements shows identical results.

Figure 2.9 shows the interlaminar out of plane shear stress distribution for τ_{yz} across the half-width of the laminate along the interphase. Here the overall shape of the curve shows that it is in agreement with reference (Daniel and Isahi, 1994). The result

from mesh refinement of 20 and higher shows the curve to be smooth and goes to zero at the free edges as it should be. Figure 2.9b shows the enlarged view of 10% of the free edge. Here the results for the mesh with 40 divisions and above shows a better value and is in close agreement with others. Based on the results from the width wise refinement studies 40 graded divisions have been chosen for y-axis in this research.

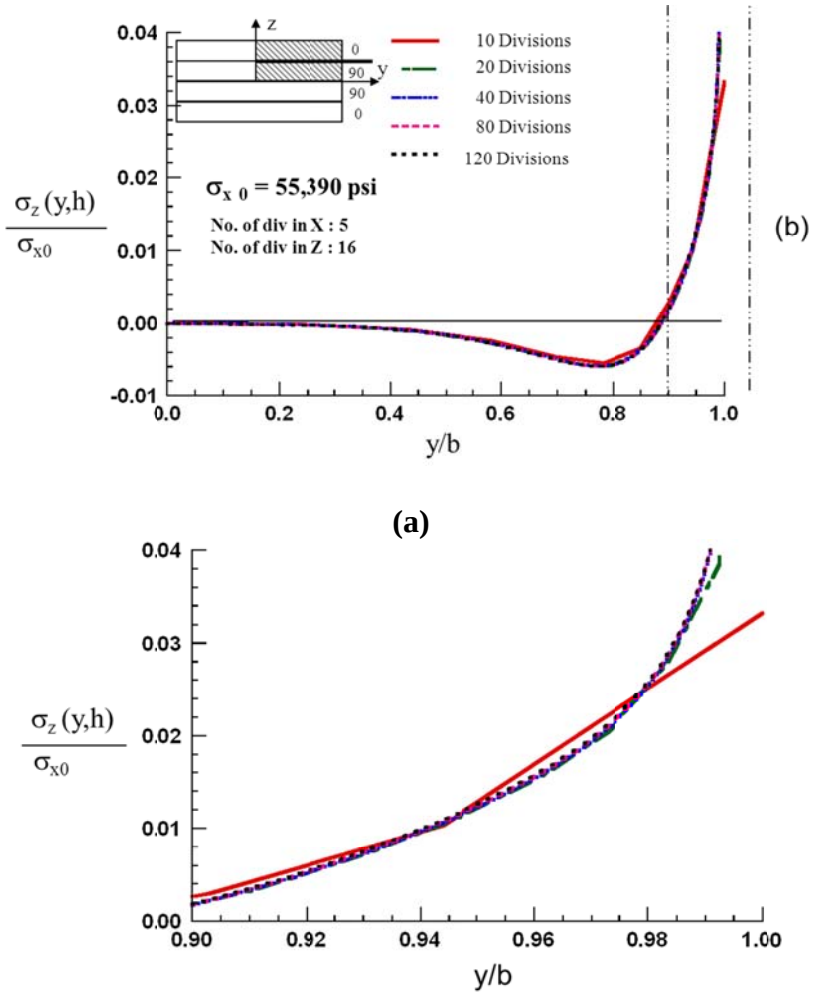

Figure 2.8 Distribution of normalized interlaminar normal stress σ_z across the width of the laminate $(0/90)_s$ (a) half-width of laminate (b) 10% of width from free edge for different width wise refinement

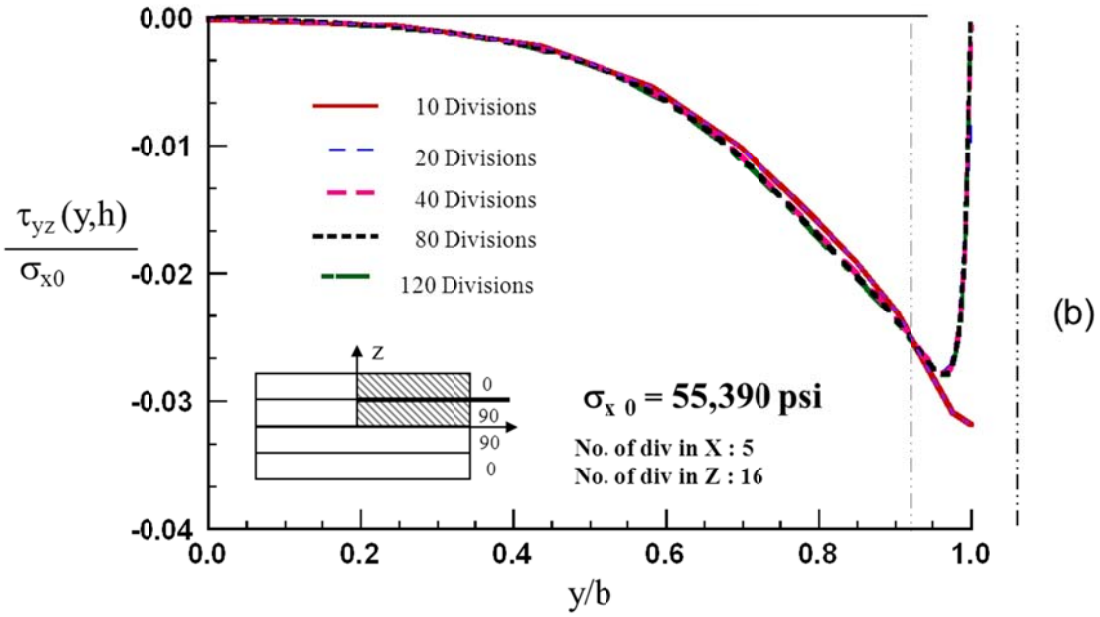

(a)

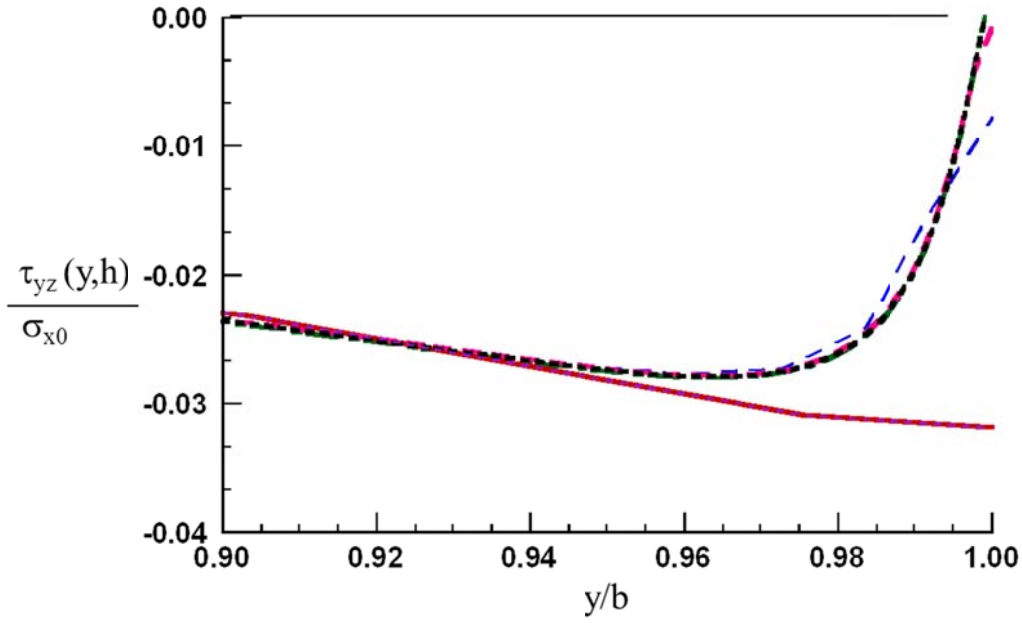

(b)

Figure 2.9 Distribution of normalized interlaminar normal stress τ_{yz} across the width of the laminate $(0/90)_s$ (a) half-width of laminate (b) 10% of width from free edge for different width wise refinement.

The mesh for the model in y-direction has been determined, in this part the results from the z-direction refinement has been discussed. Figures 2.10 to 2.13 show the stress distribution for the thickness refinement study.

Figure 2.10a shows the distribution of interlaminar shear stress normalized by σ_{x0} for different values of z-direction refinements from 4 graded divisions to 64 graded divisions for half-width of the specimen. The stresses are close to 0 in the middle and increases towards the free edges. At the free edge the stress is singular due to the difference in the material properties between the lamina. The overall stresses distribution matches the figures from Daniel and Isahi (Daniel and Isahi, 1994). But as the number of divisions increases the σ_z increase at free edge, which is an indication of singularity of σ_z at free edge. Figure 2.10b shows and enlarged view of the normalized interlaminar stress σ_z closed to the free edge of the specimen. Here it can be seen that models with 4 divisions are more shows very good and same stress distribution. However, the model with 16 graded divisions show a better and smooth distribution in agreement with the figures in Daniel and Isahi (Daniel and Isahi, 1994) of the stress compared to the other models.

Figure 2.11 shows the normalized stress distribution for τ_{yz} with respect to y/b for different divisions in z. From Figure 2.10 and Figure 2.11, it can be seen that the models with 16 divisions will clearly describe stresses at the free edge. This mesh refinement is used throughout the study.

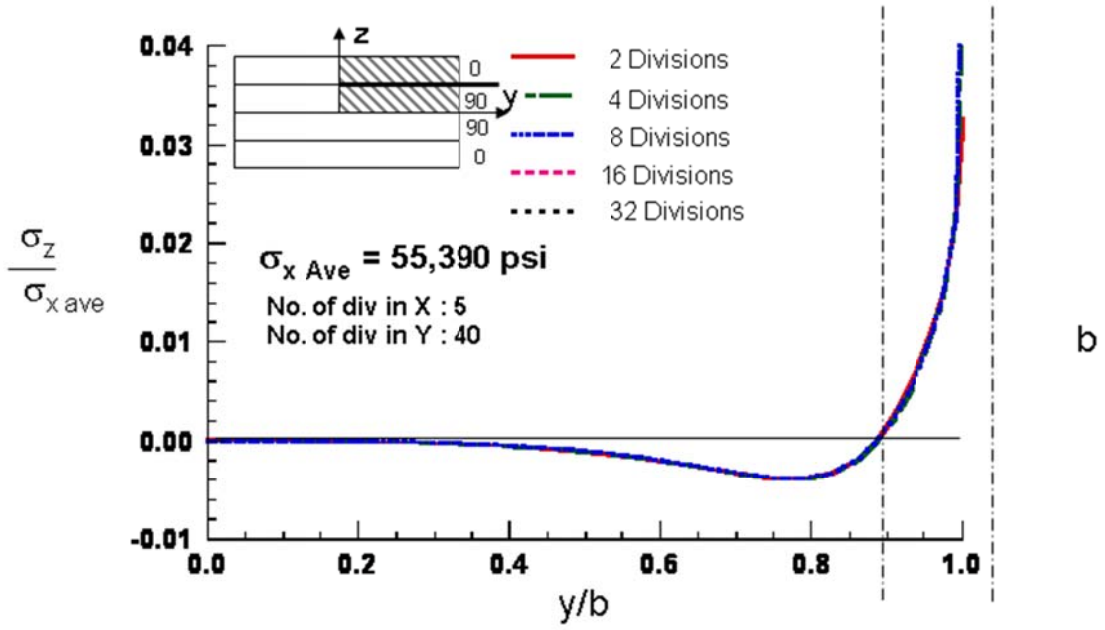

(a)

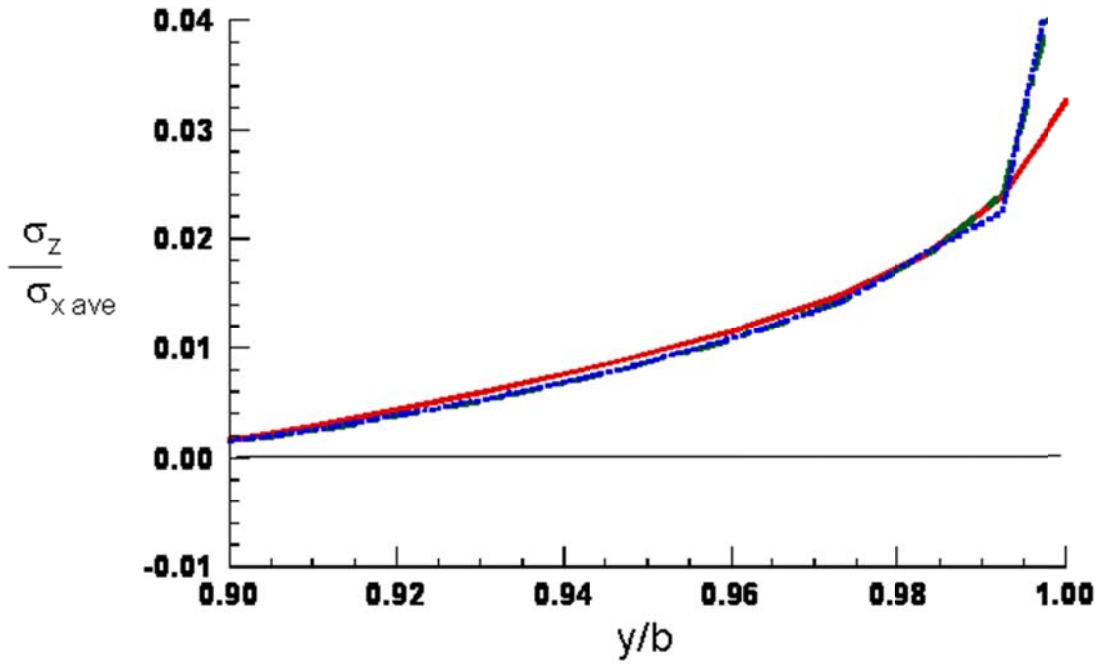

(b)

Figure 2.10 Distribution of normalized interlaminar normal stress σ_z across the width of the laminate $(0/90)_s$ (a) half-width of laminate (b) 10% of width from free edge for different thickness refinement

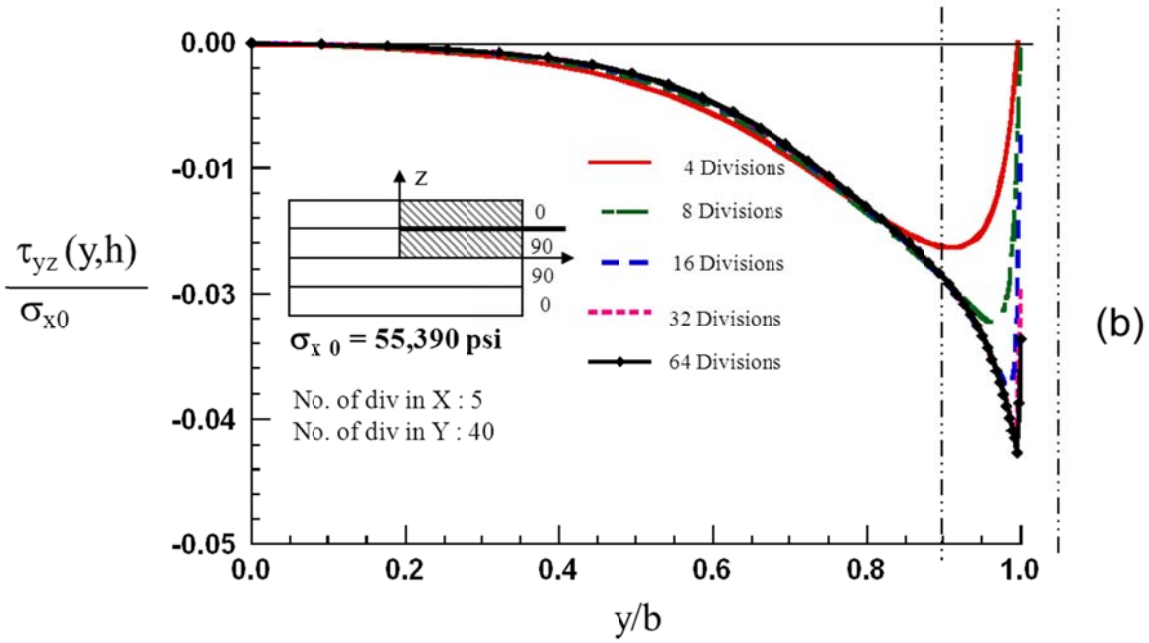

(a)

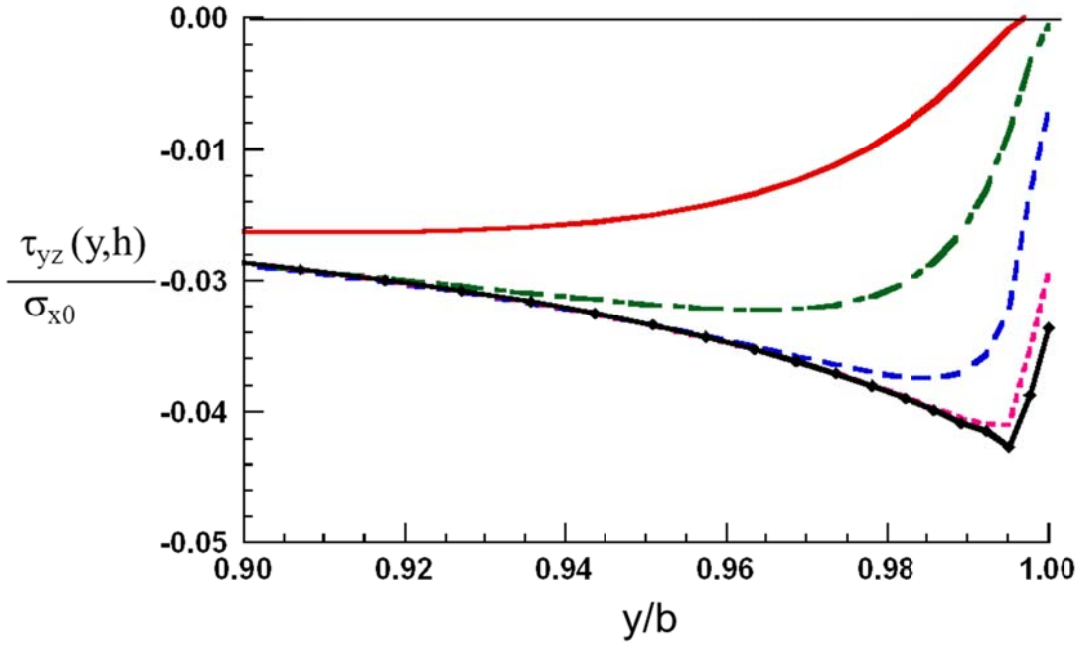

(b)

Figure 2.11 Distribution of normalized interlaminar normal stress τ_{yz} across the width of the laminate $(0/90)_s$ (a) half-width of laminate (b) 10% of width from free edge for different thickness refinement

Figure 2.12 and Figure 2.13 shows distribution of normalized stresses σ_z and τ_{yz} through the thickness of the specimen at the free edge. Based on the figures it can be seen that the distribution of stresses is continuous and similar to the results from the work of Pipes and Pagano (Pipes and Pagano, 1970). The distribution of stresses is better for any models more than 8 divisions in thickness direction. As the number of divisions increases the stress distribution becomes smoother at the interface the stresses increases as the number of divisions increases indicating singularity at that location.

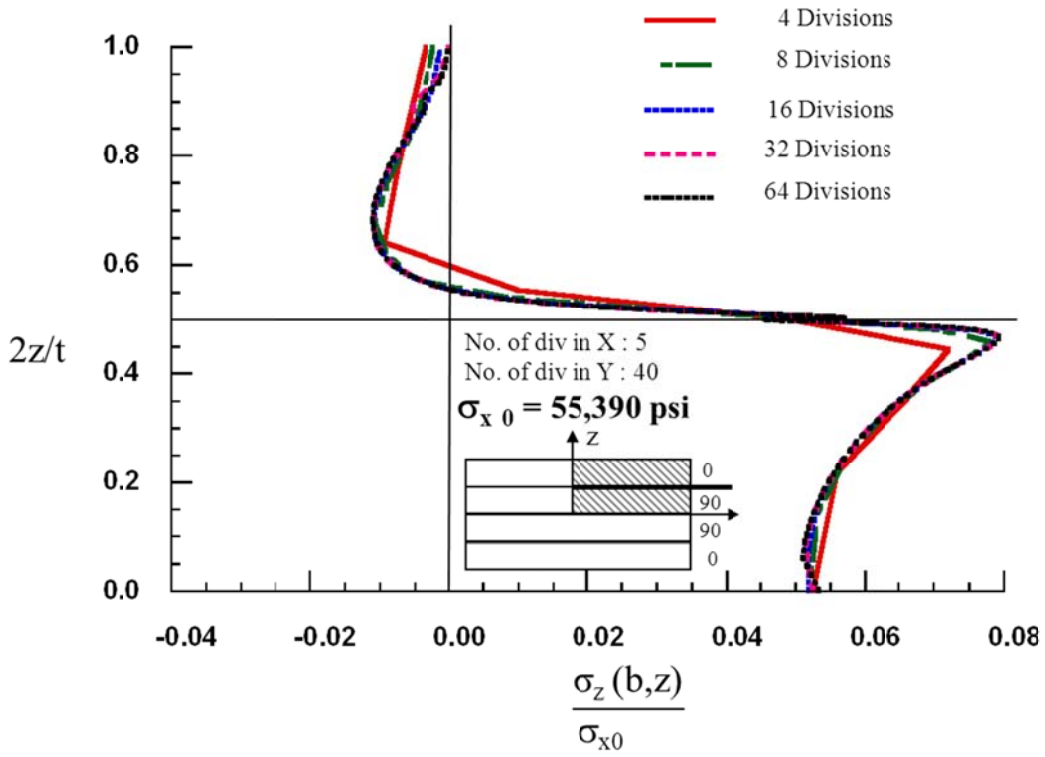

Figure 2.12 Distribution of normalized interlaminar normal σ_z through the thickness at free edge for (0/90)s laminate, for mesh refinement in z-direction

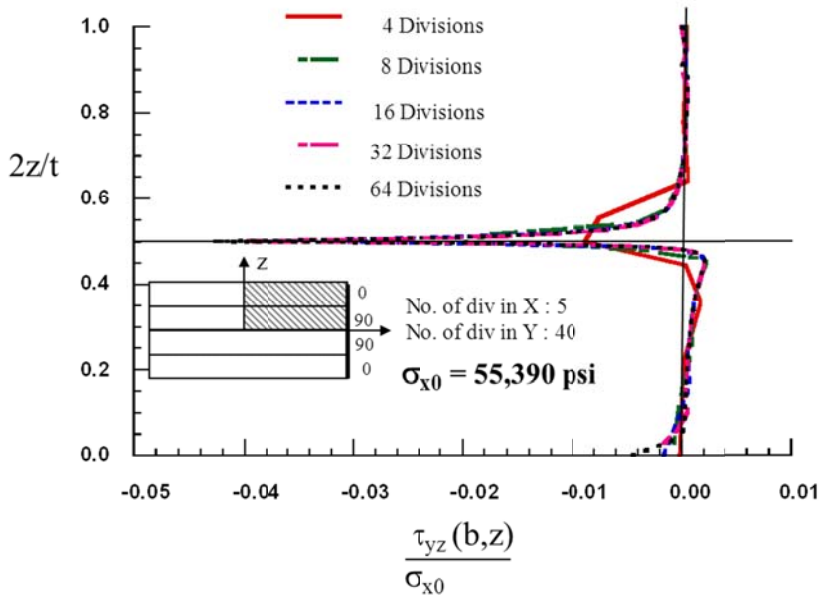

Figure 2.13 Distribution of normalized interlaminar normal τ_{yz} through the thickness at free edge for (0/90)s laminate, for mesh refinement in z-direction

Based on the above results a graded division of 40 has been selected for the width of the specimen and a graded division of 16 has been selected in the thickness direction for this research. Since the loading considered is a uniform extension (ε_{x0}) in x-direction the stresses are constant in x-plane. A coarse 5 graded division model has been selected for x-axis meshing.

2.4.2 Verification of Modeling

Based on mesh refinement study FEA model has been established and is now ready for further study to verify the accuracy of the model with existing literature. For $(0/90)_s$ model work of Nguyen and Caron (Nguyen and Caron, 2009), Wang and Crossman (Wang and Crossman, 1977) and Pagano (Pagano, 1978) have been chosen.

Wang and Crossman conducted numerical analysis using finite element method to study the stress fields of cross-ply laminates. The stress distribution close to the free edges were studied for the singular behavior of the stresses. Pagano proposed an approximate and simple solutions theory for predicting the stress distribution across the interphase of the laminate using the layer equilibrium principle. Nguyen and Caron derived a new layer wise model using the M4-5n was proposed. All the results shown seem to agree with each other very well as shown in the work of Nguyen and Caron for a cross ply laminate.

Figure 2.14 shows the distribution of normalized stress normalized σ_z across the half-width of the specimen. The model used in the present work is plotted to compare with existing literature. The results have been plotted at the 0 and 90 interphase. As it can be seen that the results obtained in the present research matches well with the results in literature Wang and Crossman (Wang and Crossman, 1977) and Nguyen and Caron (Nguyen and Caron, 2009). The present results show a smoother curve probably due to a more refined meshing.

Similarly, Figure 2.15 shows the normalized distribution of τ_{yz} across the width of the specimen. The results from present research have been compared with the results in the literature and has been found to agree very well. Figure 2.16 shows the normalized value of σ_z through the thickness of the specimen. Comparing to the previous work, the stress values at the free edge seems to be defined well in the present work however the overall results agree well in this case also. This is because of the higher mesh refinement compared to the existing literature.

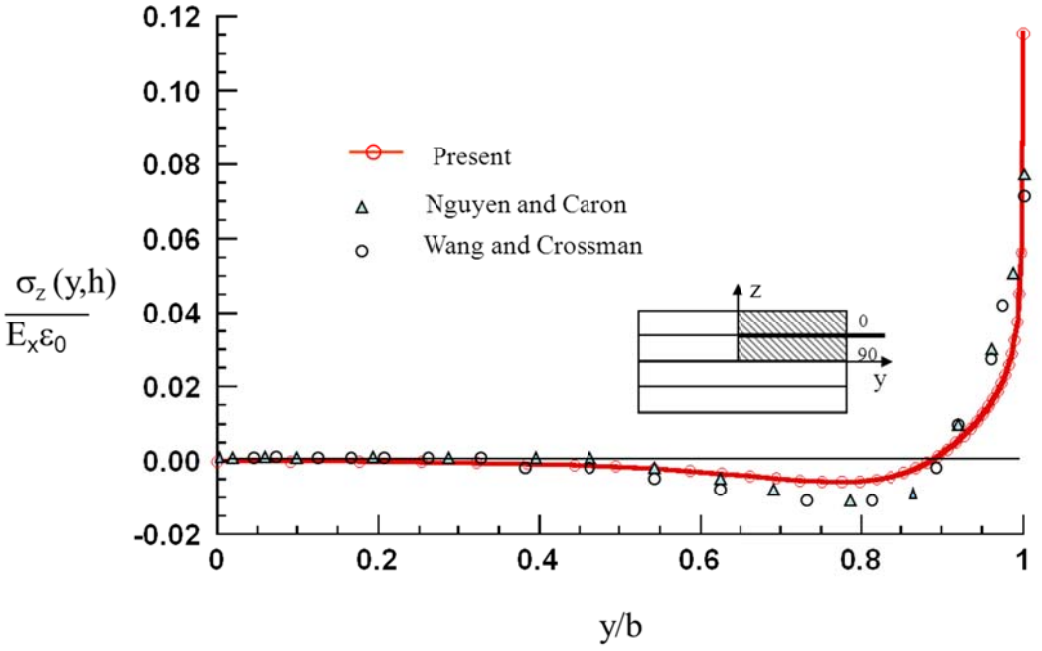

Figure 2.14 Distribution of normalized interlaminar normal σ_z across the width of laminate $(0/90)_s$ for comparison with literature

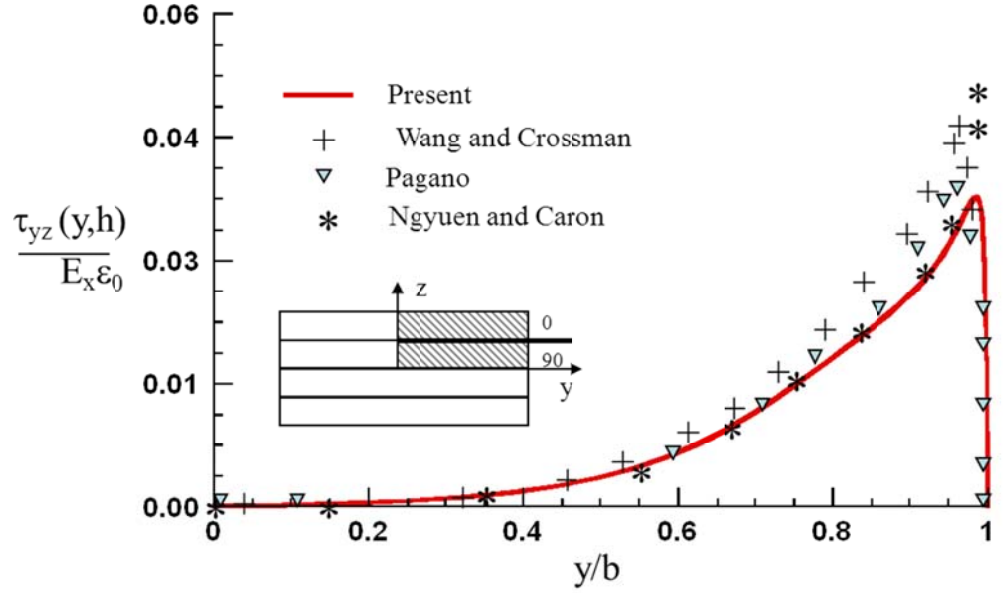

Figure 2.15 Normalized τ_{yz} across the width for comparison with literature for (0/90)s laminate, bare interface

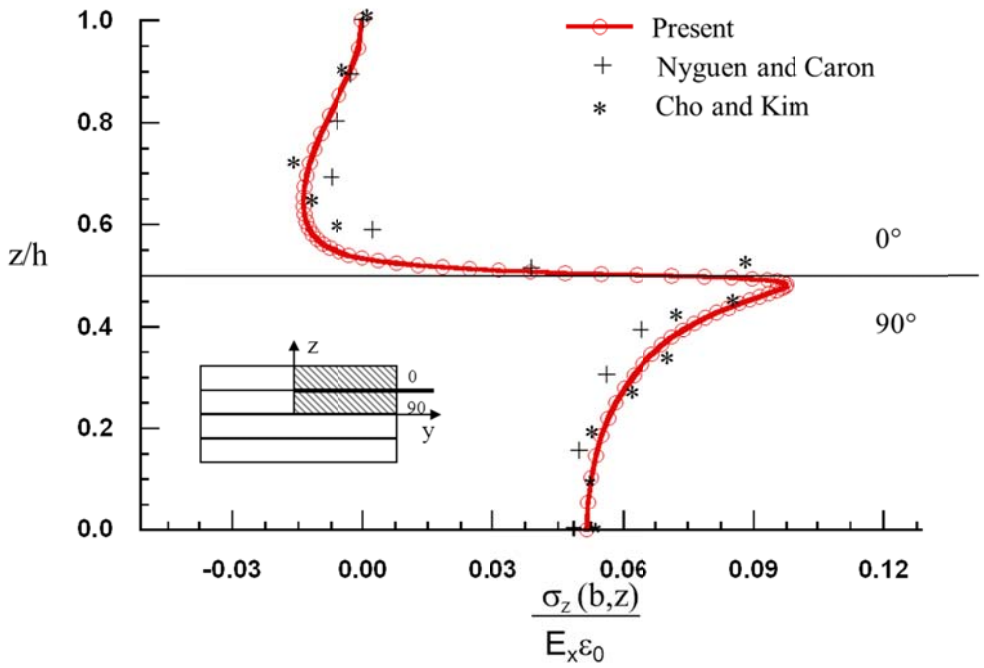

Figure 2.16 Normalized σ_z across the width for comparison with literature for $(0/90)_s$ laminate, bare interface at the free edge

Based on the mesh refinement study and comparison of the interlaminar stress results of the present work with the previous literature, it can be concluded that the FEA models developed for $(0/90)_s$ is accurate for all other analysis and further work.

2.4.3 Effect of Ply Grouping

A number of plies in the same direction are lumped together for ease of manufacturing and handling for a multi directional laminate, making the laminate thick. It is more desirable that the stacking be in single layers for design, but there must be a trade-off between manufacturability and optimization. This method of using multiple plies in the same direction is called ply-grouping. A schematic of ply grouping of two and

four layers have been shown in Figure 2.2 a and b. The distance from the free edge to the point where the interlaminar edge stresses exists at the interphase is called the edge stress distance, since the edge stresses are zero in the center and it is very difficult to find the exact location on the width where the stress is zero, the value has been determined based on the 0.05% stress level from zero line, the edge distance and the 0.05% criteria have been shown in Figure 2.17.

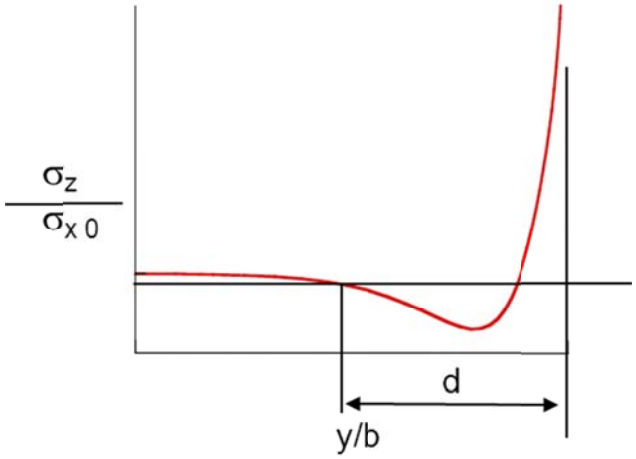

Figure 2.17 Edge stress distance

This section details the study of effect of ply grouping on the edge distance in a laminate. Figure 2.18 and Figure 2.19, shows the graph for normalized σ_z and τ_{yz} across the width of laminate for n varying from 1 to 10, respectively. A distance over which σ_z or τ_{yz} is greater than 0.05% of axial stress is considered to be the edge distance. As the number of plies decreases in the lamina the edge distance also decreases. Figure 2.20 shows the plot of normalized edge distance for different ply grouping. . For $(0/90)_s$ the

edge distance is about 1.25 times the thickness of the laminate. The data relevant to the edge distance for $(0_n/90_n)_s$ has been presented in Table 2.4.

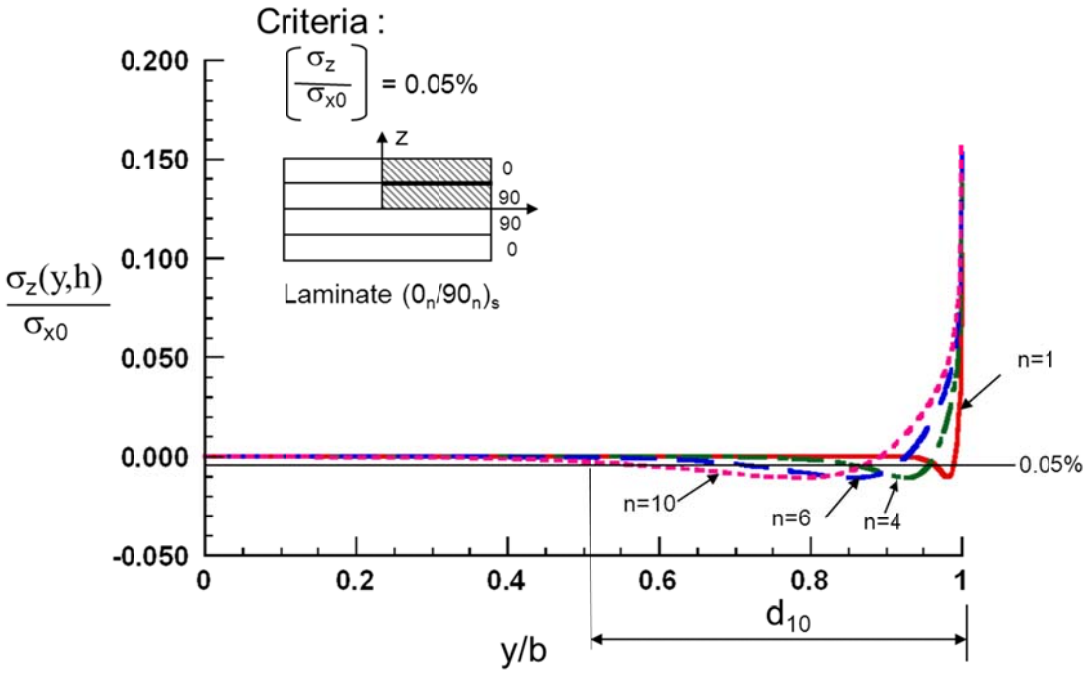

Figure 2.18 Effect of Grouping of Plies on σ_z in a laminate for a laminate $(0_n/90_n)_s$

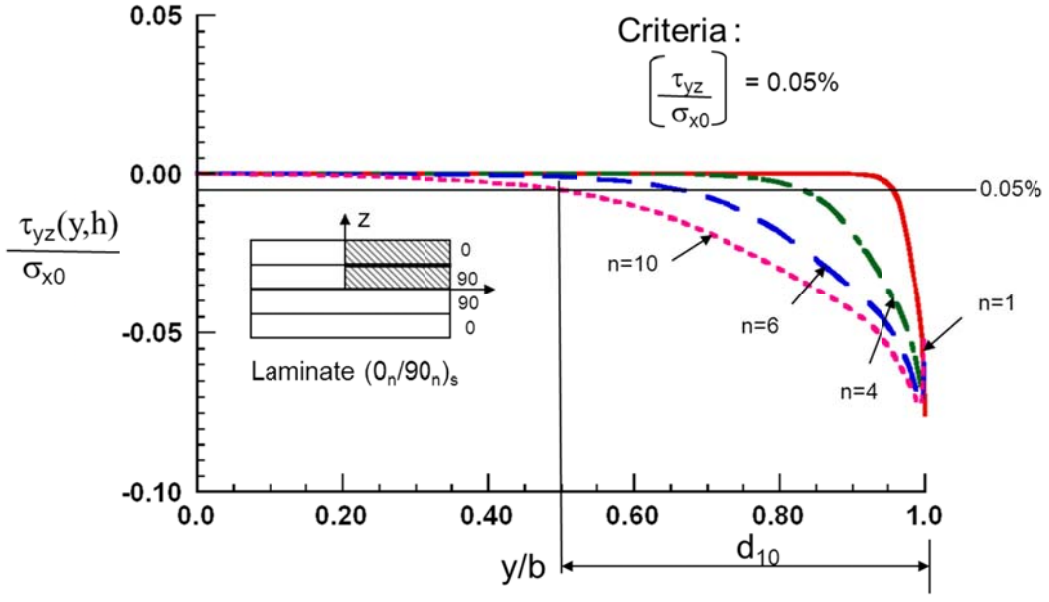

Figure 2.19 Effect of Grouping of Plies on τ_{yz} in a laminate for a laminate $(0_n/90_n)_s$

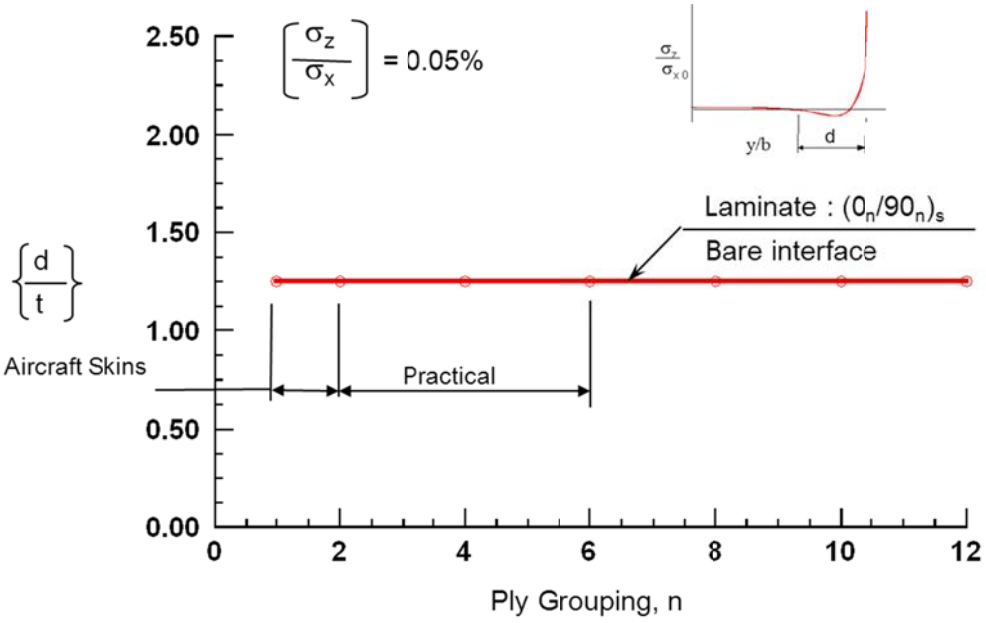

Figure 2.20 Variation of Edge Distance with Ply Grouping

Table 2.4 Variation of edge distance with ply grouping for $(0_n/90_n)_s$ laminate for bare interface

2b (width)	No. of plies	Lamina thickness	Edge distance, in	[d/t] %
0.5	1	0.02	0.045	1.25
0.5	2	0.04	0.090	1.25
0.5	4	0.08	0.180	1.25
0.5	6	0.12	0.270	1.25
0.5	8	0.16	0.360	1.25
0.5	10	0.20	0.450	1.25
0.5	12	0.24	0.540	1.25

Effect of width of the panel on edge distance was studied and found that the width did not have any effect on the edge distance except for n=1 for the panel width of 0.5", 1" and 1.5". Variation of normalized σ_z with the width of the specimen for the last 10% towards the edge of the specimen, for different thickness of the ply between .0005-0.005", has also been studied. Based on the plot it can be concluded that as the thickness of the ply reduces the edge distance and the interlaminar stresses decreases These results have been shown in Appendix B. Thus proving the concepts of previous research studied by various authors in Shin et al. (Sihn, Kim, Kazumasa, and Tsai, 2007).

2.5 Results of $(+45_n/-45_n)_s$ Laminate

2.5.1 Problem definition

This section outlines the results for developing a model for cross ply $(+45_n/-45_n)_s$ laminate. The geometry of the specimen is the same as that of $(0_n/90_n)_s$ case as shown in Figure 2.21 which has been used by Pipes and Pagano (Pipes and Pagano, 1970) and Raju and Crews (Raju and Crews, 1981). The Ply orientation and the stacking sequence have been illustrated in Figure 2.21a and b. As in the case of $(0_n/90_n)_s$ the ply grouping considered for this study of interlaminar stresses are also n=2 and n=10, an example of ply grouping for $(+\theta_n/-\theta_n)_s$ has been illustrated in Figure 2.22a and b.

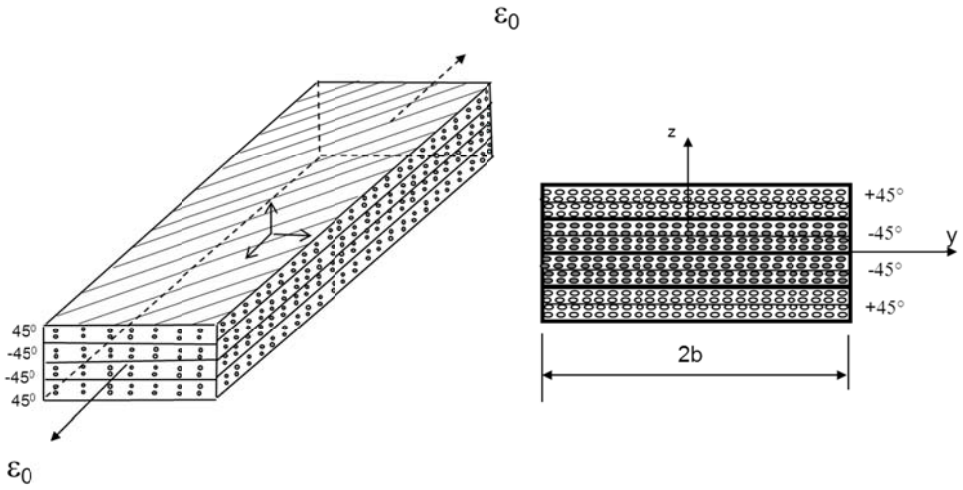

(a) **(b)**

Figure 2.21 Schematic of $(+45_n/-45_n)_s$ laminate (a) Full laminate (b) cross section of laminate

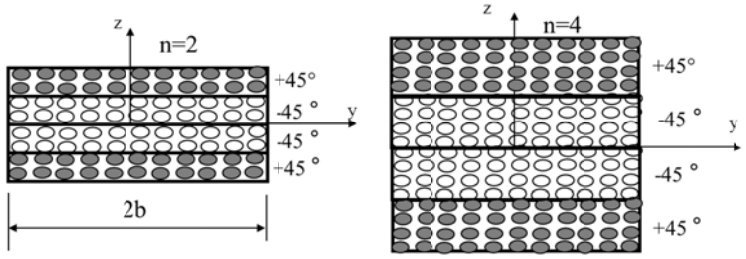

Figure 2.22 Concept of Ply Grouping for $(+45_n/-45_n)_s$ laminate

2.5.2 Modeling

For the $(+45_n/-45_n)_s$ modeling technique used and the finite element mesh generation is the same as that of $(0_n/90_n)_s$ laminate. Figure 2.23 shows the mathematical model that is considered for the $(+45_n/-45_n)_s$ case. Figure 2.23a shows the full physical model and the $1/8^{th}$ model part that is considered as the mathematical model. Although

the model appears to be symmetric in x, y and z direction. Due to the fiber orientation the mode is not symmetrical in y-direction. But the stress response has been shown to be anti-symmetric about the y=0 plane Wang and Crossman (Wang and Crossman, 1977) and Raju and Crews (Raju and Crews, 1981).

Hence, for simplicity 1/8th of a Figure 2.23b shows the boundary condition and the stacking of the +45° and -45° layers in the model. Figure 2.23c shows the interphase between +45 and -45, region of interest where the stresses are studied as part of this research. The mesh refined model of 40 divisions in y-direction, 16 divisions in z-direction for each ply and 5 divisions in x-direction same as the one considered for $(0_n/90_n)_s$ has also been used for the $(+45_n/-45_n)_s$ analysis.

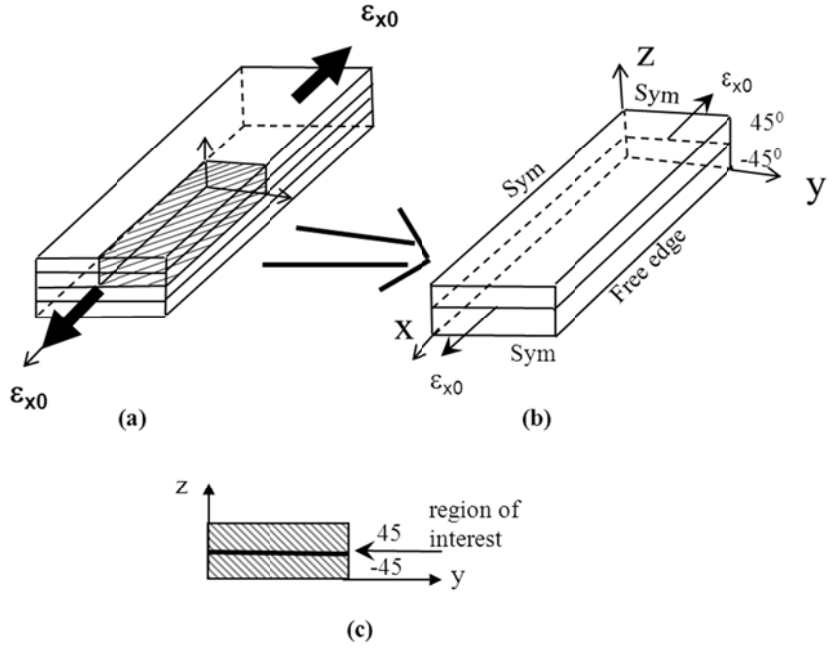

Figure 2.23 Mathematical Model of Bare interface for $(+45_n/-45_n)_s$ laminate (a) Full Model of laminate, (b) Symmetric 1/8th Model, (c) Cross section of 1/8th model

2.5.3 Verification of Modeling

Similar to the $(0_n/90_n)_s$ case the current model $(+45_n/-45_n)_s$ was also verified against the current literature for its accuracy. Raju and Crews (Raju and Crews, 1981) studied the stress distribution at the free edges of the cross ply laminate using finite element method, the results from this work has been used to compare the results of the present model developed in this research. Figure 2.24 shows the comparison between the results for existing literature and the current results for distribution of normal stress σ_z normalized across the half-width. As it can be observed, the current results agree very well with the literature. Figure 2.25 shows the comparison between the results for existing literature and the current results for distribution of shear stress τ_{xz} across the half-width of the laminate. The results agree very well with the results from the present model.

Figure 2.26 shows the distribution of normal stress through the thickness of the specimen at the free edge. The figure shows that the current results agree very well with the existing literature. Based on the comparison of the it can be concluded that the current model $(+45_n/-45_n)_s$ agrees well with the literature and is accurate enough for further analysis work.

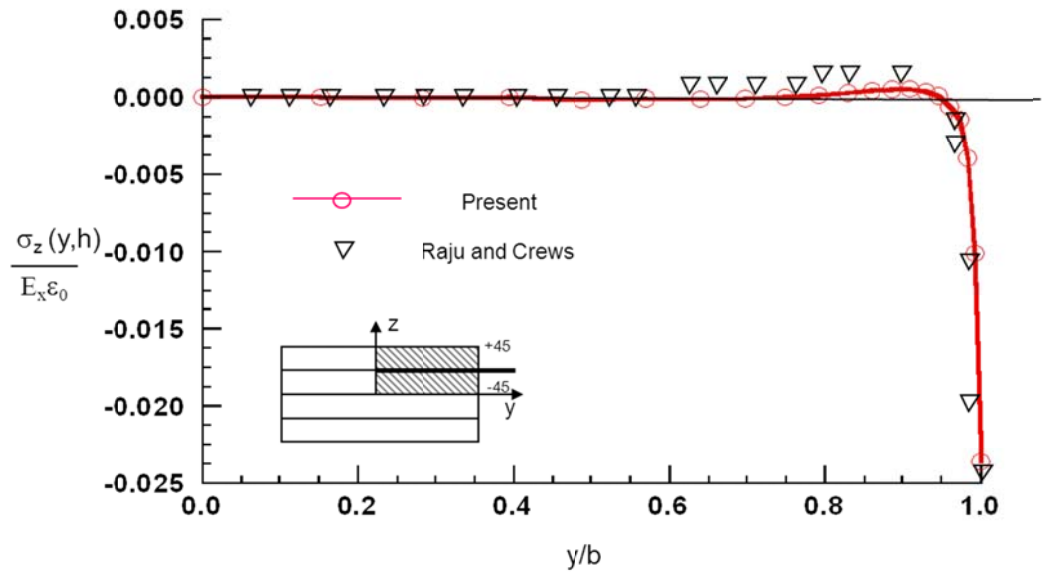

Figure 2.24 Normalized σ_z across the width for comparison with literature for (+45/-45)s laminate, Bare interface

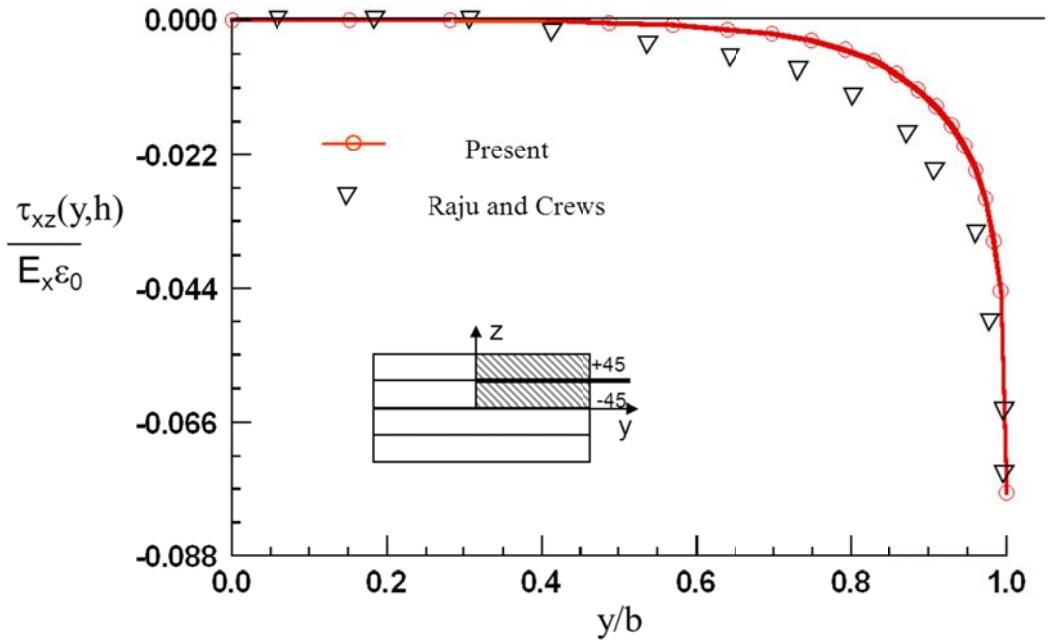

Figure 2.25 Normalized τ_{xz} across the width for comparison with literature for $(+45/-45)_s$ laminate, Bare interface

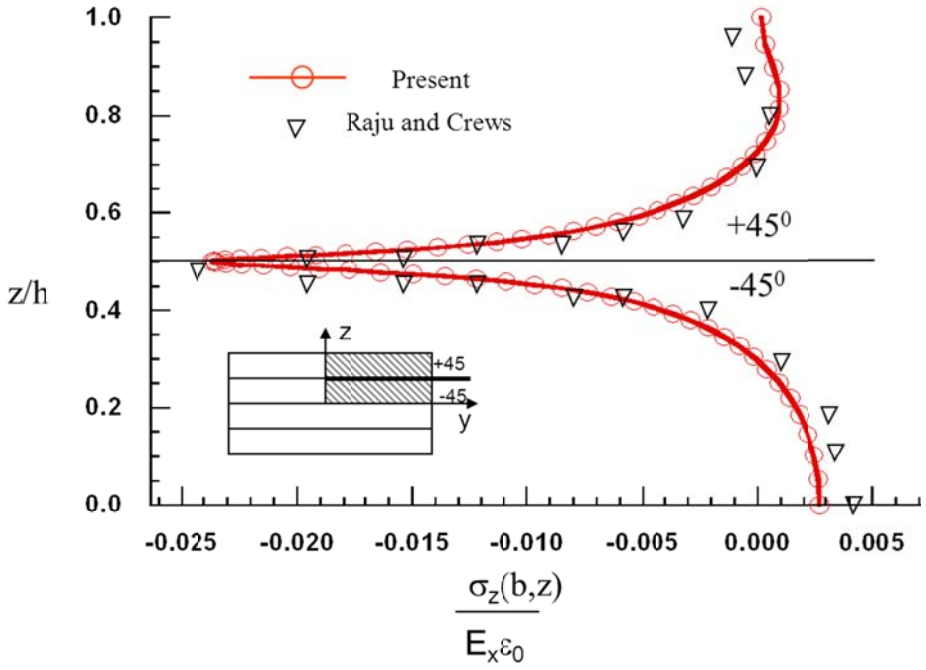

Figure 2.26 Normalized σ_z through the thickness for comparison with literature for $(+45/-45)_s$ laminate, Bare interface

2.5.4 Effect of Ply Grouping

A study was performed to understand the effect of ply grouping on the interlaminar edge stresses. An example of ply grouping of two and four for $(+\theta_n/-\theta_n)_s$ has been shown in Figure 2.22. Figure 2.27 and Figure 2.28 shows the normalized σ_z and τ_{xz} for different values for ply grouping respectively. For the $(+45_n/-45_n)_s$ case the normalized edge distance is higher for single ply laminate at 1.75 times laminate thickness and decreases as the number of plies increases and remains constant around 0.83 times the thickness of the laminate. The results has also been compared to the work of Pipes and Pagano who concluded that the edge distance is equal to the thickness of the

laminate this has been shown in Figure 2.29. (Pipes and Pagano, 1970). The data for edge distances for $(+45_n/-45_n)_s$ have been presented in Table 2.5

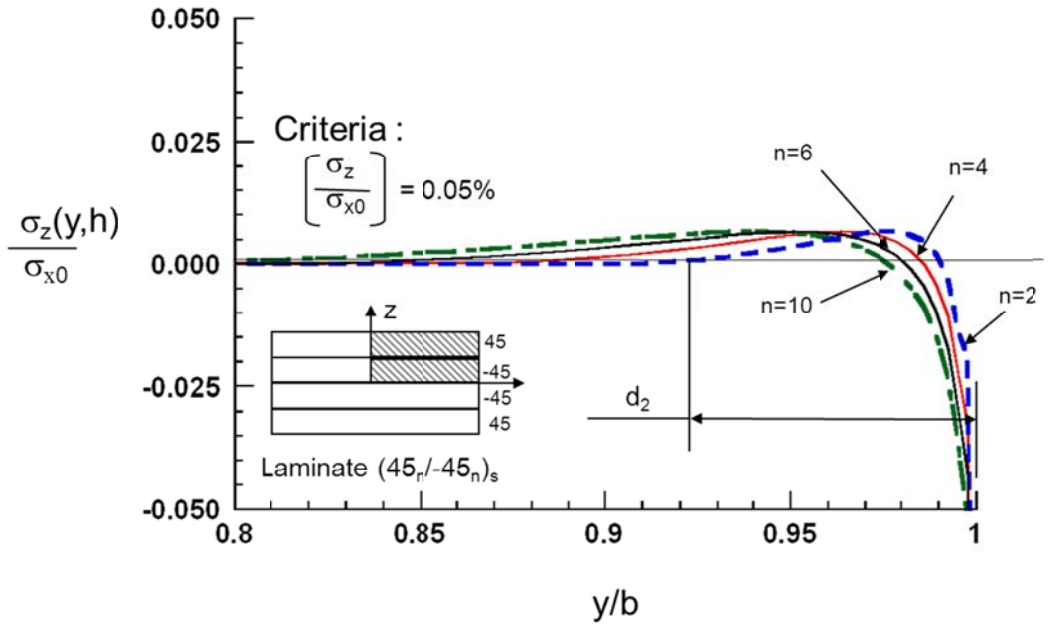

Figure 2.27 Effect of Grouping of Plies on σ_x in a laminate for a laminate $(+45_n/-45_n)_s$

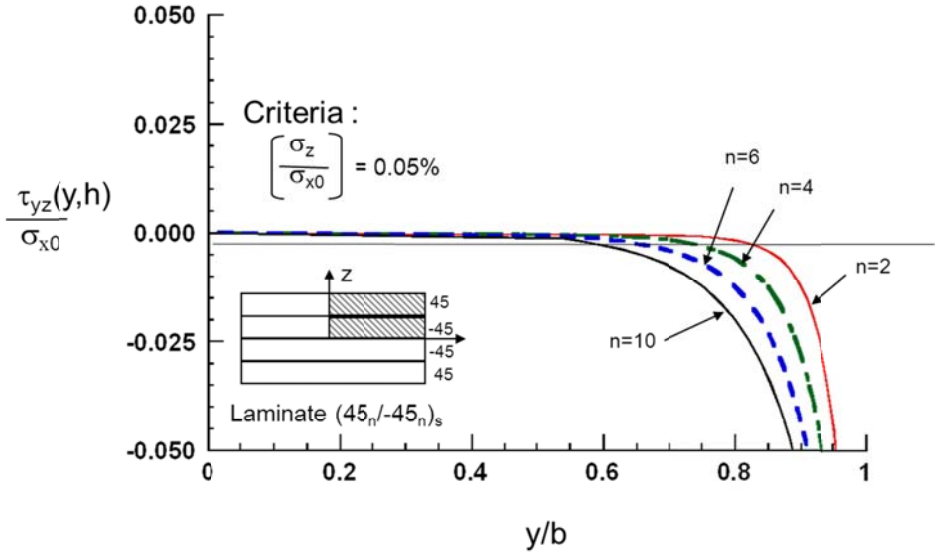

Figure 2.28 Effect of Grouping of Plies on τ_{xz} in a laminate for a laminate $(+45_n/-45_n)_s$

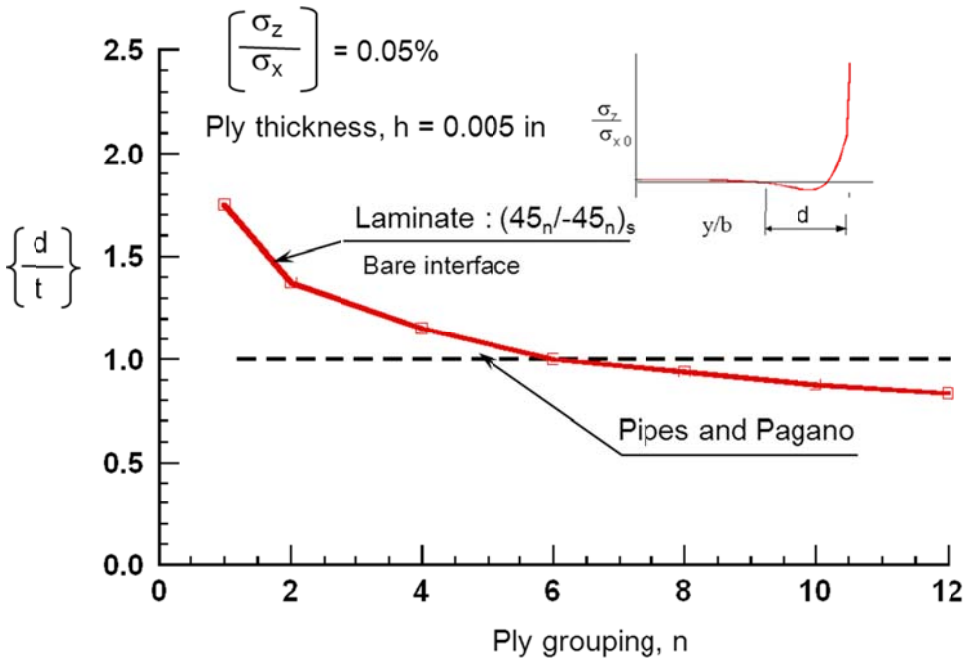

Figure 2.29 Effect of Grouping of Plies in a laminate for a $(+45_n/-45_n)_s$ (Pipes and Pagano, 1970)

Table 2.5 Variation of edge distance with ply grouping for $(45_n/-45_n)_s$ laminate for bare interface

2b (width)	No. of plies	Lamina thickness	Edge distance, in	[d/t] %
0.5	1	0.02	0.07	1.75
0.5	2	0.04	0.11	1.38
0.5	4	0.08	0.20	1.25
0.5	6	0.12	0.24	1.00
0.5	8	0.16	0.30	0.94
0.5	10	0.20	0.35	0.88
0.5	12	0.24	0.40	0.83

Effect of edge distance with ply grouping for the different panel width was studied. The results indicate that the width of the panel does not have any effect on the change in ply grouping. Variation of normalized τ_{xz} with the width of the specimen for the last 5% towards the edge of the specimen, for different thickness of the ply between .0005-0.005" this has been shown in Appendix B. Based on the plot it can be concluded that as the thickness of the ply reduces the edge distance and the interlaminar stresses decreases. Thus proving the concepts of previous research studied by various authors in (Sihn, Kim, Kazumasa, and Tsai, 2007)

2.6 Summary

A finite width $(0_n/90_n)_s$ and $(+45_n/-45_n)_s$ laminates subjected tensile stress was modeled using 3-D finite element model. A mesh refinement study was conducted to demonstrate the accuracy of the interlaminar stresses near the free edges. A 40 graded division in the width direction and 16 graded divisions through the thickness in each lamina were found to give a good description of the interlaminar stresses and was used in this research. The finer division was chosen closer to the free edge across the width and towards the lamina interphase in the thickness direction. The results from the present model agreed very well with the literature A study of the effect of edge distance over which the interlaminar stresses was performed. The edge distance (based on the 0.05% axial stress criteria) is about 1.25 times the laminate thickness for $(0_n/90_n)_s$ laminate and varies from 1.75 to 0.8 times the laminate thickness for ply grouping of one to twelve for

$(+45_n/-45_n)_s$ laminate. The refined FE model developed here and is used in the analysis of problems in Chapter 3 and 4.

CHAPTER 3

MODELING AND ANALYSIS OF RESIN INTERPHASE LAYER COMPOSITE LAMINATES

As previously stated that the interphase regions between dissimilarly oriented plies consisting of thin layer of resin which provides the transition between the plies. This chapter will focus on measuring the interphase thickness, analysis of the $(0_n/90_n)_s$ and $(+45_n/-45_n)_s$ laminates including the resin layer and assessing the interlaminar stresses at the edges. Variation of the edge stresses were also assessed for different approximation of resin layer properties namely, elastic, elastic-plastic and non-linear material. The non-linear material is representation of nano fabric composite layer that is envisioned by polymer nano fabric interleaving. Because the modeling involves a layer of resin between adjacent plies this model will be termed here as "realistic model"

3.1 Measurement of Interphase Resin Layer Thickness

In order to measure the actual thickness of the interphase layer a good microscopic picture is necessary. To obtain this picture, the laminate specimen cross section surface has to be prepared and polished using a polishing machine, such as Buehler polishing machine shown in Figure 3.1. The laminate specimen was first prepared using an epoxy potting material to make it easier to polish as shown in Figure 3.2 and was prepared and polished using 600, 900 and 1200 grit papers for coarse,

intermediate and fine polishing respectively. The thickness of the interphase is determined using the cross section. The resin interphase layer thickness has been measured using the Nikon Optical microscope, a sample of the image obtained and is shown in Figure 3.3.

Figure 3.1 Specimen polishing machine

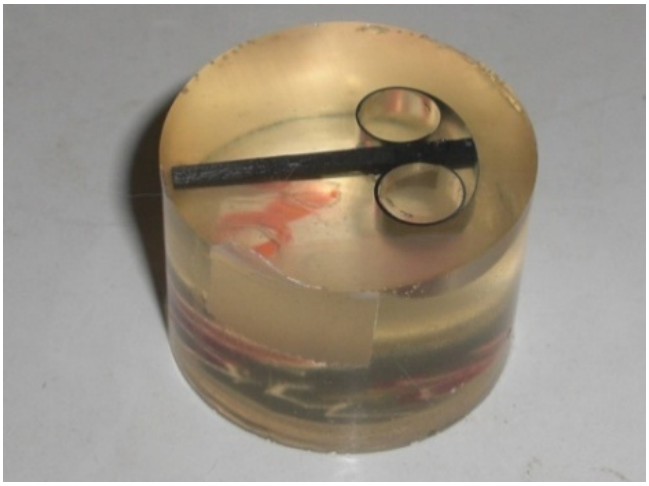

Figure 3.2 Casted laminate in a resin

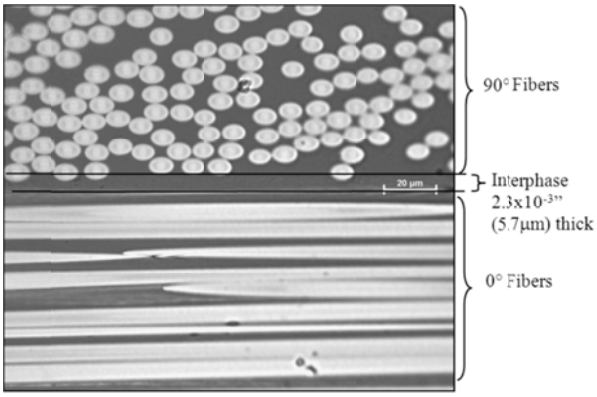

Figure 3.3 Optical microscopy of 0/90 interphase

Figure 3.4 shows the schematic section of an interphase layer to indicate the criteria that has been used for measuring the interphase thickness. Figure 3.5a shows the cross section of the laminate to measure the thickness of the lamina and the interphase for $(0/90)_s$ laminate. From the Figure it can be seen that the ply thickness is about 0.01" (250 μm) for each ply and 2.3 $x10^{-4"}$ (5.7μm) of the interphase thickness. The percentage of the interphase with reference to ply thickness is about 4.5%.

The interphase thickness was also measured for laminate with a nano-fabric interleave. Figure 3.5b shows a cross section of the laminate with lay-up $(0/i/90/i/45)_s$. The nano fabric is too small for it to be visible in the optical microscope. A close up view has been shown to measure the thickness of the interleave. Based on the figure the thickness of the interphase is about 1.3 $x10^{-4"}$ (3.3 μm) and the thickness of the lamina is about 0.006" (150 μm). The percentage of nano interphase thickness with the lamina thickness is about 4.5%. Based on the thickness calculations the percentage thickness that is used in this research is 2.5%, 5% and 7.5% of the ply thickness to cover the extremities of the interphase thickness. Based on this selection the thickness selected for both

$(0_n/90_n)_s$ and $(+45_n/-45_n)_s$ laminate for 2.5%, 5% and 7.5% are $1.25x10^{-4"}$ (3.175 μm), $2.5x10^{-4"}$ (6.350 μm) and $3.75x10^{-4"}$ (9.525μm) respectively.

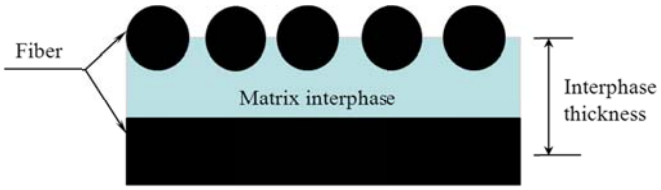

Figure 3.4 Approximating interphase resin layer

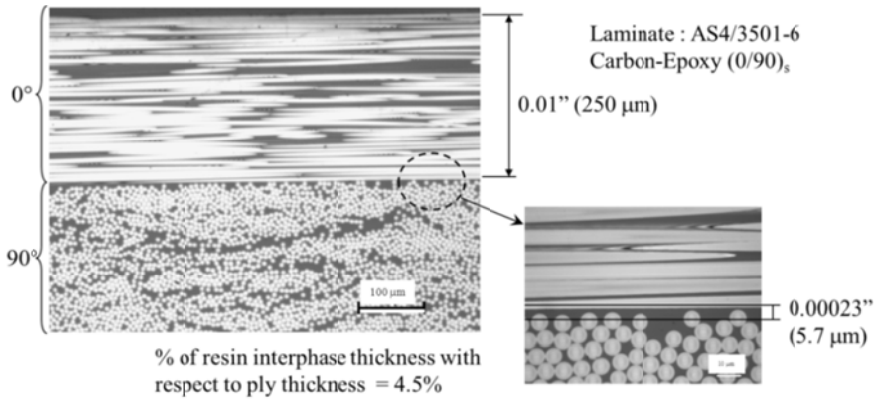

(a)

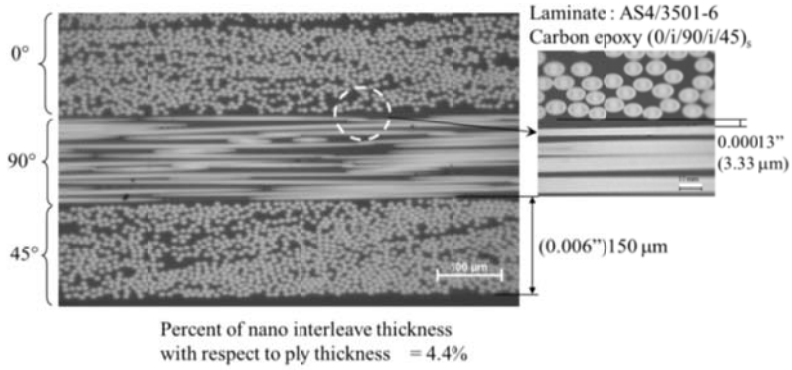

(b)

Figure 3.5 Cross section of laminate (a) for $(0/90)_s$ laminate(b) for nano interleave $(0/i/90/i/45)_s$ laminate

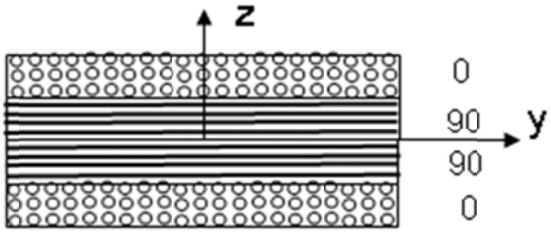

Figure 3.6 Bare interface model

3.2 Material Properties of Interphase Region

The unidirectional material properties of AS4/3501-6 carbon/epoxy used for the laminate are listed in the Table 2.1. The matrix used in the interphase region is assumed to be Epoxy (3501-6) that has 3 different properties; Elastic (E=0.5msi(3.5GPa), n =0.3), elastic-plastic (E = 0.5msi (3.5GPa) for $0<\varepsilon<3\%$ and σ =10ksi (69MPa) for $\varepsilon > 3\%$) and lastly nonlinear as shown in Figure 3.7. The non-linear matrix interphase stress-strain curve was assumed to be an approximate representation of electrospun Nylon 66 nano-fabric/Epoxy material. The stress strain curve was determined using constituent material properties as described below.

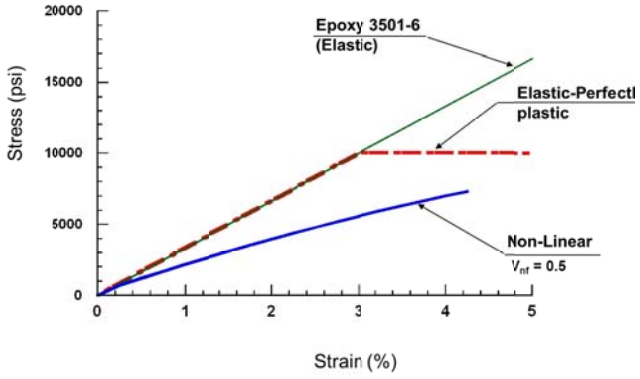

Figure 3.7 Different Material Properties used for Matrix Interphase

The individual material properties and the stress-Strain curve of electro-Spun nano Nylon-66 fabric (Lingaiah, Shivakumar, and Sadler, 2008) and the Epoxy 3501-6 (Daniel and Isahi, 1994) was used and are shown Figure 3.8. Using the rule of Mixtures (Daniel and Isahi, 1994) and based on the volume fraction of the nano-fabric the stress strain curve was determined. The mechanical properties of the composite has also been shown in Figure 3.7 to compare with the linear-elastic and the elastic-plastic interphase material properties.

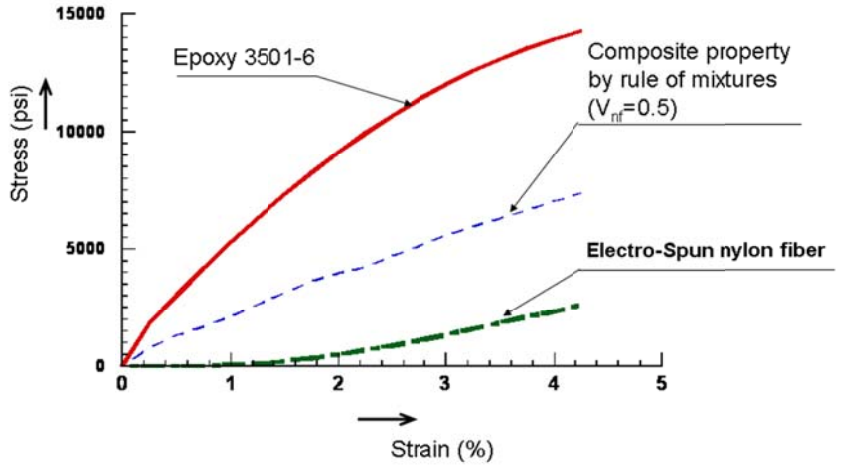

Figure 3.8 Component material properties of Nano and Epoxy

3.3 Modeling of Composite laminate with Resin interphase layer

As stated previously analysis reported to date were on mathematical interphase models. The resin layer, which actually exists between the two layers was considered, here the resin layer is approximated to 2.5% , 5% and 7.5% of the ply thickness and the same two classical problems were analyzed using 3-D FEA. To understand the state of

stress within and outside the interphase layer three types of resin material properties were considered, they are Linear elastic, Elastic-plastic and Non-linear models.

To study the effect of ply grouping each layer was assumed to be consisting of different number of plies (n=2 to n=10). The ply thickness was assumed to be 0.005”(0.127 mm), The region of interlaminar stress dominance also called as boundary layer thicknesses was assessed for different ply groups.

The overall problem geometry and loading is same as the problem analyzed in Chapter 2. The length of the specimen is L=4”(101.2mm), the width of the specimen is 2b=1”(25.4mm), total laminate thickness of h=4t, where t is the thickness of the lamina. The lamina thickness (h) is sum of the fiber layer and the interphase thickness. But this problem has interphase region between 0° and 90° plies and +45° and -45° plies. The interphase thickness are $1.25x10^{-4}$” (3.2 μm), $2.5x10^{-4}$” (6.4 μm) and $3.75x10^{-4}$” (9.5μm) for 2.5%, 5% and 7.5% of the ply thickness respectively.

Figure 3.10 a and b shows the mathematical model of the problem and symmetric $1/8^{th}$ of the geometry. The loading is uniform axial strain in x-direction. Figure 3.10c shows a cross section of the laminate with (+θ/-θ)s laminate and the interphase between the +θ and –θ layers.

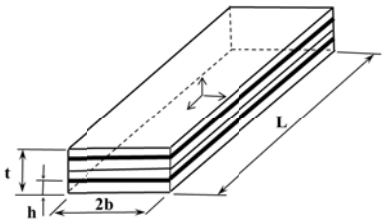

Figure 3.9 Schematic of laminate with the interphase region

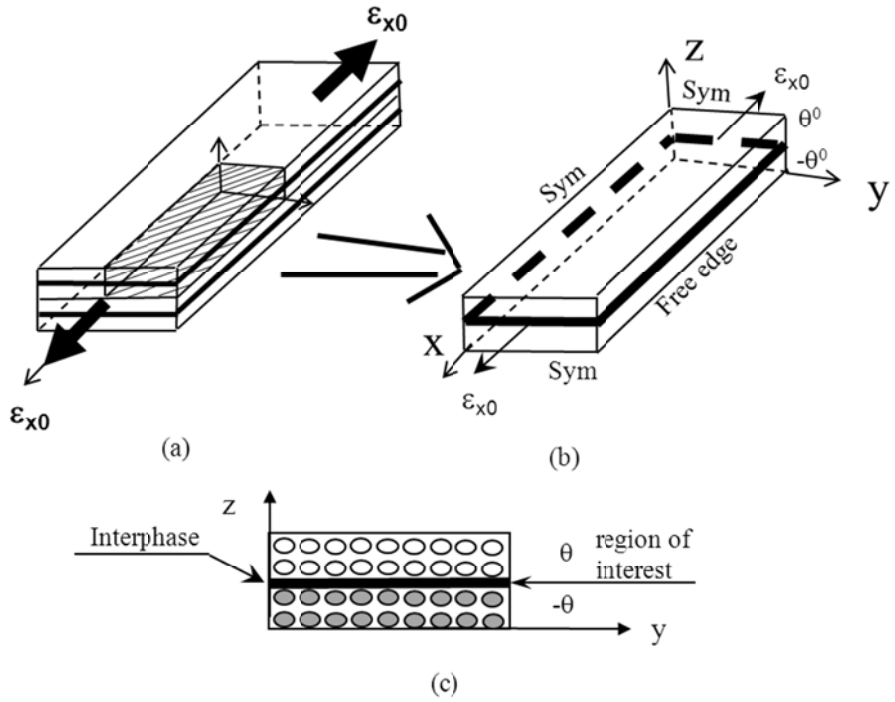

Figure 3.10 Mathematical model of $(+\theta/-\theta)_s$ laminate (a) Full Model of laminate, (b) Symmetric 1/8th Model, (c) Cross Section of 1/8th Model

3.4 Finite Element Analysis

Figure 3.11 shows the FE idealization through the thickness of the layer between the lamina. The 3D FE considered for the interphase region of the model has 40 graded divisions in y-direction, 5 equal divisions in x-direction and 4 graded divisions in z-direction. The meshing of the lamina region is the same as the bare interface model shown in Chapter 2. The grading was selected such that the element sizes reduced towards the free edge and to the center of interphase region. Within the interphase region the refinement was away from the center. Then the 3-D solid model was developed and analyzed in the same manner as explained in Chapter 2. Because the model is refined

enough based on the convergence study made in Chapter 2 , the same model was used throughout the study. Also, the same model was used for the $(+45_n/-45_n)_s$ laminate analysis.

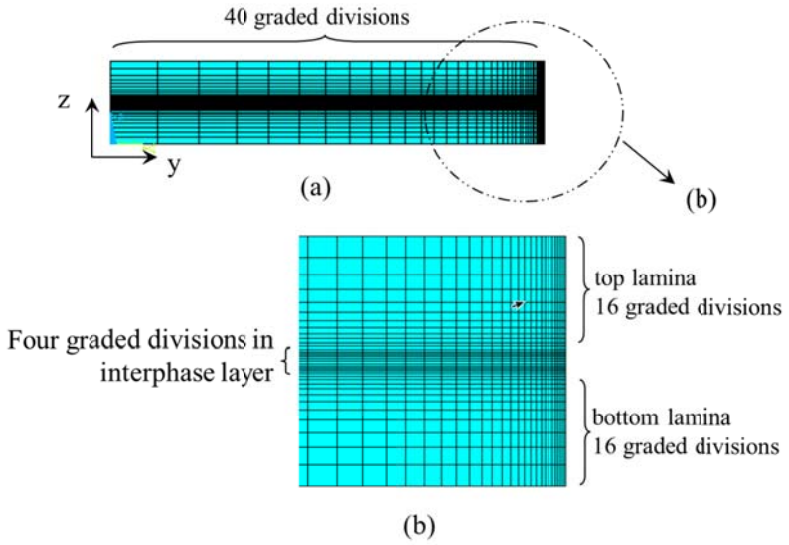

Figure 3.11 Finite element idealization through the thickness with the interphase layer (a) Full width, (b) Closer to the free edge

The various critical regions where the interlaminar stress output was obtained is presented in Figure 3.12. The ANSYS total nodal stress σ_x, σ_y, σ_z, τ_{xy}, τ_{yz}, τ_{xz} at in the critical regions were examined. Average axial normal stress σ_{x0} was computed by extracting the reaction at x=0 plane on the specimen and dividing by the area of cross section. Various values of σ_{x0} for analysis that has been performed in this chapter are performed in Table 3.1. In this chapter analysis have been conducted for two different laminates $(0_n/90_n)_s$ and $(+45_n/-45_n)_s$, different thickness of the interphase and for different material of the interphase namely elastic, elastic-plastic and non-linear.

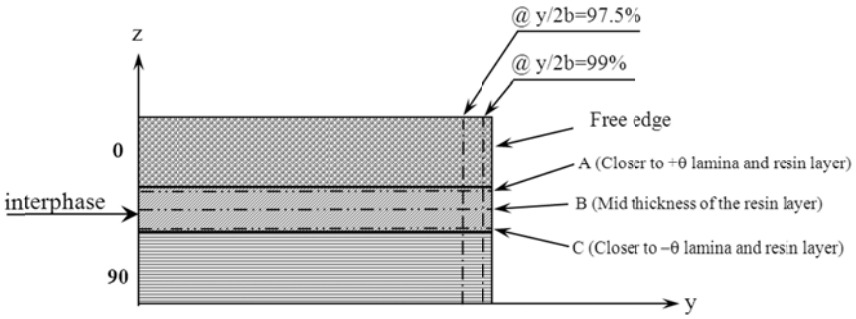

Figure 3.12 Region of interest for study of edge stresses.

Table 3.1 Average normal stress (σ_{x0}) ksi (MPa) for different laminate models

Laminate interphase (% of ply thickness)	$(0_n/90_n)_s$	$(+45_n/-45_n)_s$
Bare interface	**118 (813)**	**30.5 (210.3)**
Ply Thickness 2.5%	**109 (751)**	**31.0 (214.0)**
Ply Thickness 5.0%	**108 (744)**	**30.5 (210.3)**
Ply Thickness 7.5%	**106 (731)**	**30.0 (207.0)**

3.5 Results

Results are grouped into three parts as follows:

1. Elastic interphase materials of $(0_2/90_2)_s$ and $(+45_2/-45_2)_s$ laminates to differentiate response between bare interface and resin interphase
2. Ply grouping to understand how the ply grouping impacts interlaminar edge stresses
3. Elastic plastic and nonlinear resin material to assess the impact of material non-linearity on interlaminar edge stresses

These results expected to answer the questions if the modeling of resin interphase region is necessary and if the non-linearity of the interphase material will help to mitigate the edge stresses in cross-ply and angle-ply laminates.

3.5.1 Elastic Interphase Material

In this section the results for the analysis of resin interphase model compared with different thickness of resin interphase has been presented.

3.5.1.1 $(0_2/90_2)_s$ laminate with a resin interphase

Figure 3.13 to Figure 3.15 show the variation of interlaminar normal stress along the laminate width. The figures indicate results for three different resin layer and thicknesses namely 2.5%, 5% and 7.5% of the laminate ply thickness (h). Because there could be three possible plots in the interphase region these three plots are shown. Figure 3.13a is for the region (A) at the 0° ply and the resin interphase, Figure 3.14a is at the mid thickness of the resin layer (B) and Figure 3.15a is at the resin interphase and the 90° ply. In all these cases σ_z appears to show a singularity response. The σ_z stress distribution very close to the free edge is shown in Figure 3.13b, Figure 3.14b and Figure 3.15b for regions A, B and C respectively. Because the case A and C represent the mathematical interphase, the σ_z response shows singularity. However, for the case B (thin ply layer only), σ_z is less severe compared to the bare interface. As the resin layer thickness increases (2.5%, 5% and 7.5%) the magnitude of σ_z at the free edge reduces see Figure 3.14b), indicating that the stresses in the resin layer is non-singular. The stress distribution of σ_z shows it is trending towards 0, this could be due to the mechanical

properties of interface and the 90° layer being nearly similar in the axial direction. The singularity as stated by previously in many investigations (Wang and Crossman, 1977) is an artifact of mathematical modeling.

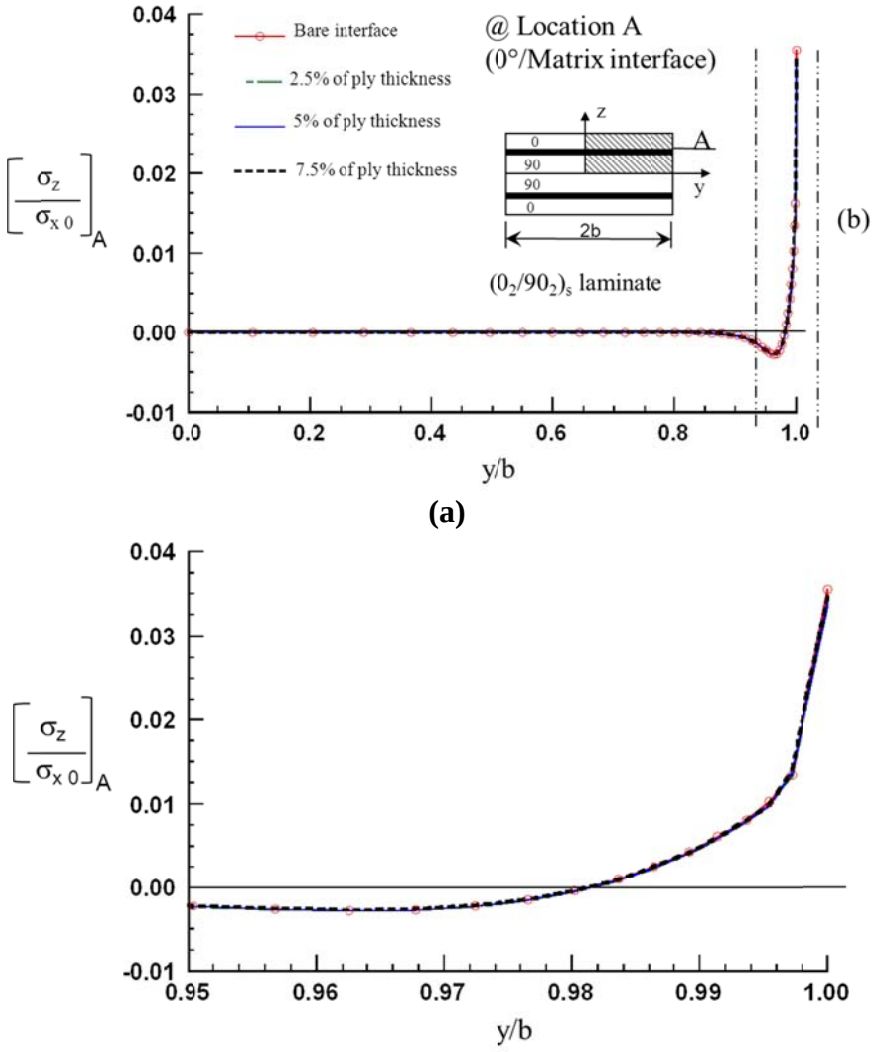

(a)

(b)

Figure 3.13 Distribution of interlaminar normal stress σ_z across the width for $(0_2/90_2)_s$ laminate at 0 and matrix interphase(a) one-half width (b) near the edge

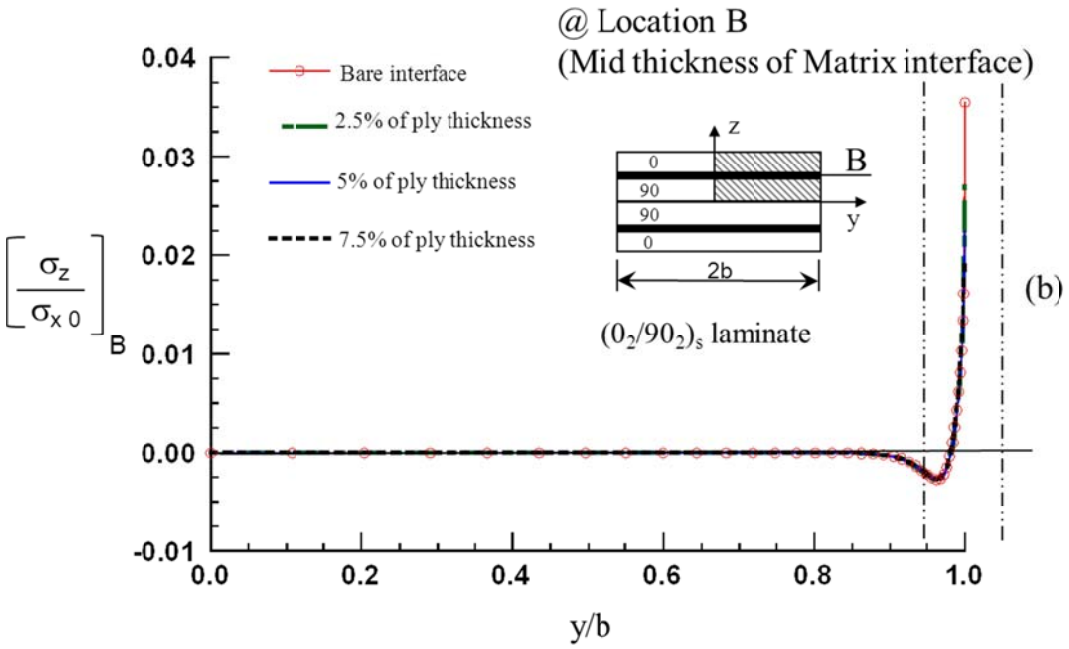

(a)

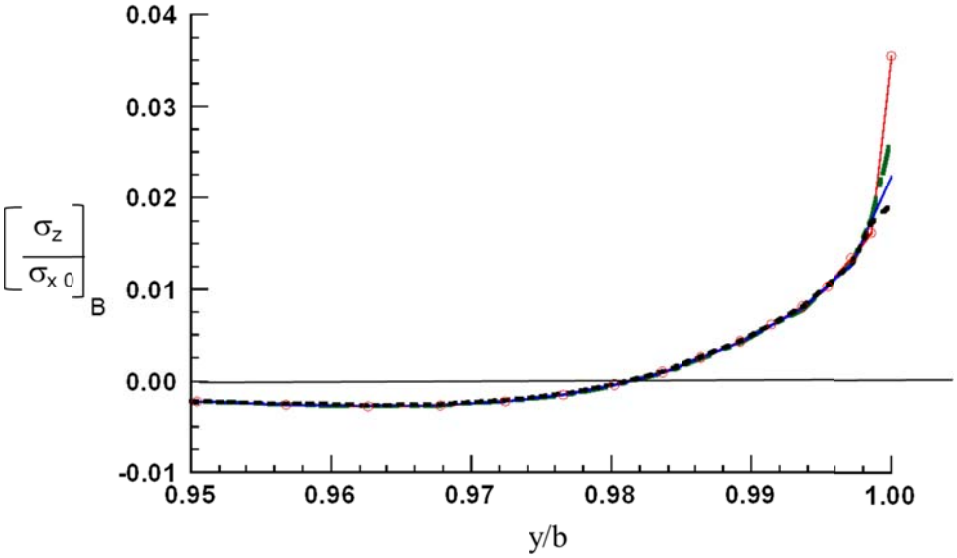

(b)

Figure 3.14 Distribution of interlaminar normal stress σ_z across the width for $(0_2/90_2)_s$ laminate at mid thickness of matrix interphase (a) one-half width (b) near the edge

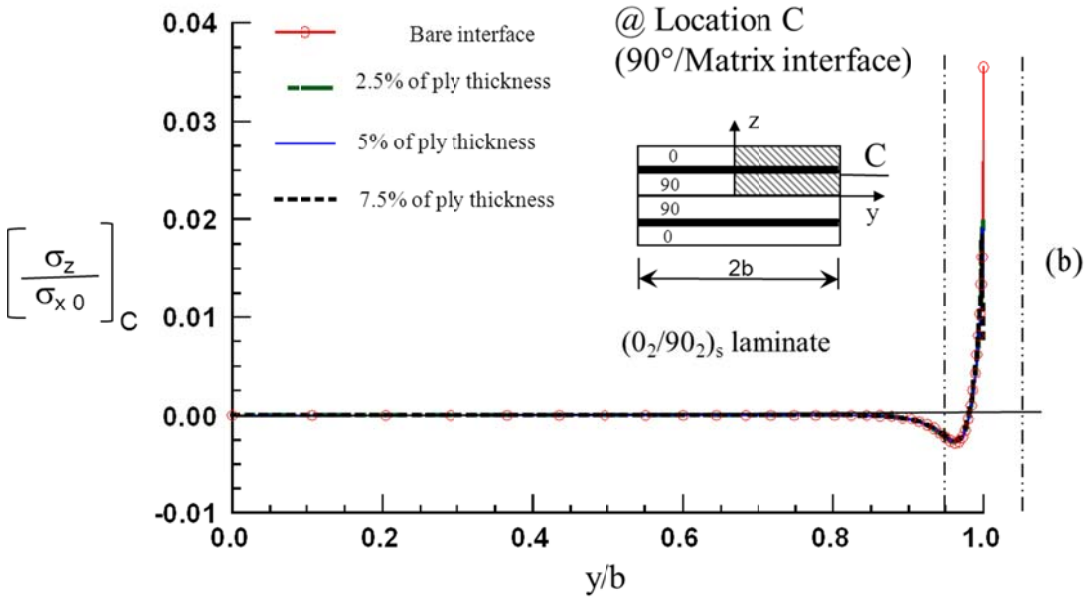

(a)

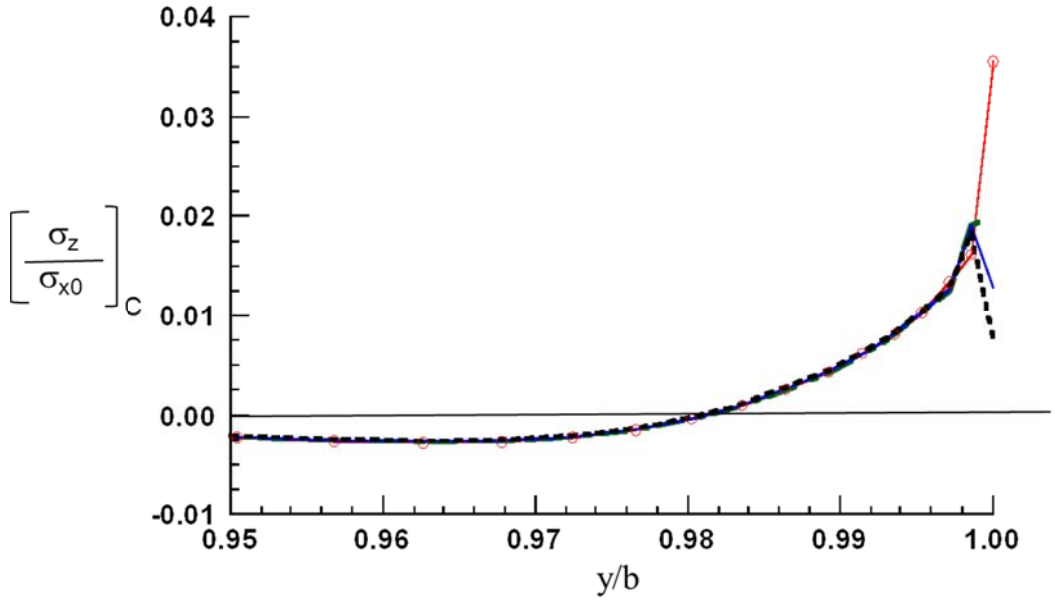

(b)

Figure 3.15 Distribution of interlaminar normal stress σ_z across the width for $(0_2/90_2)_s$ laminate at matrix interphase and 90° lamina (a) one-half width (b) near the edge

Figure 3.16 to Figure 3.18 shows the variation of interlaminar shear stress (τ_{yz}) along the width of the laminate at location A, B and C respectively for resin layer thickness 2.5%, 5.0% and 7.5% of the ply thickness. The response of the curves at interfaces (A and C) is similar to those in the literature. The response, at location B, at mid-thickness of the resin layer the stress response is smoother, lower and turning sooner to 0 for resin interphase models compared to the bare interface. Similar to the case of σ_z the stress τ_{yz} in location C is trending towards 0, this can also be attributed to material properties being similar in x-axis.

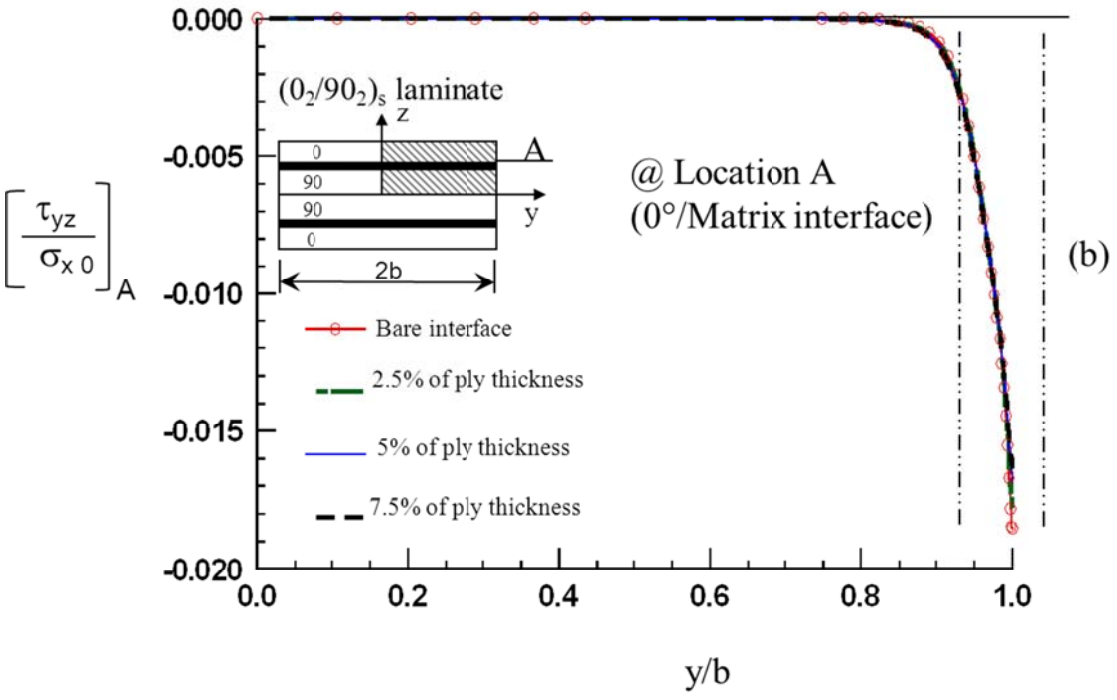

(a)

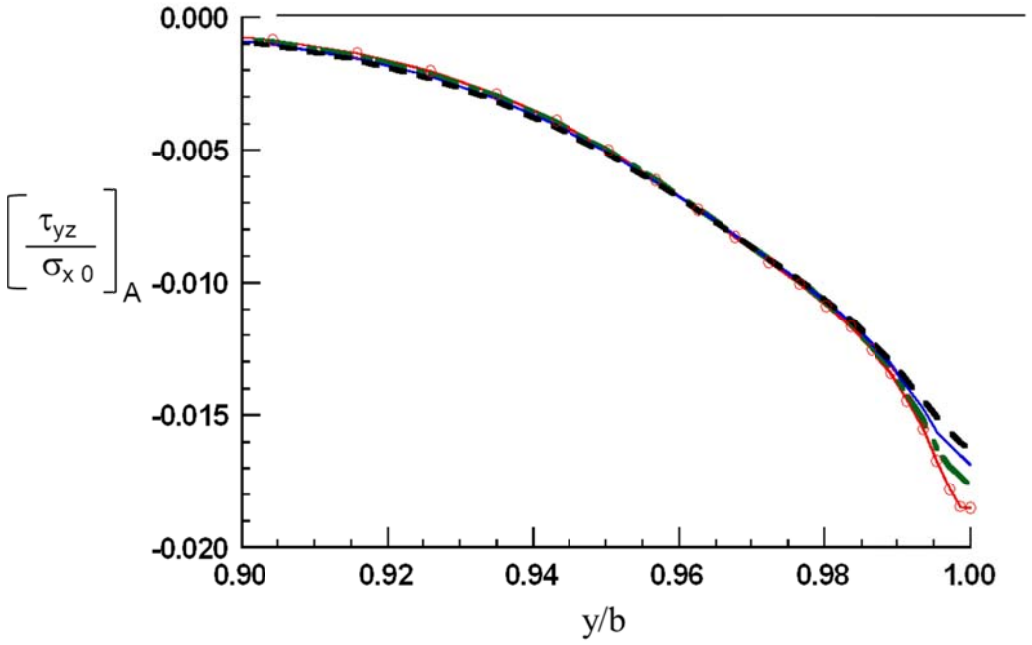

(b)

Figure 3.16 Distribution of interlaminar shear stress τ_{yz} across the width for $(0_2/90_2)_s$ laminate at 0° and matrix interphase (a) one-half width (b) near the edge

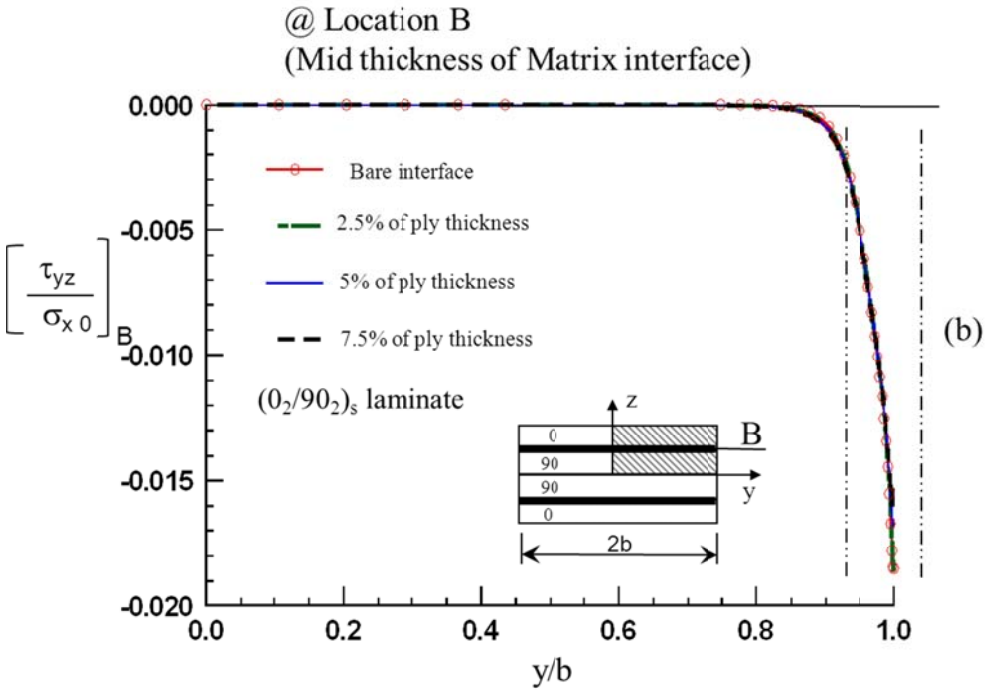

(a)

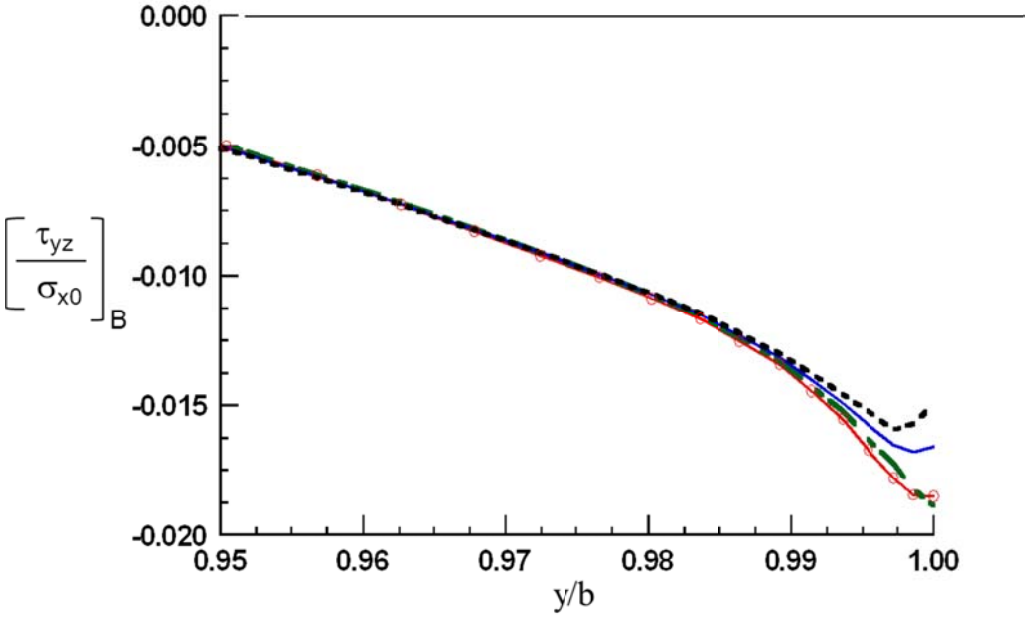

(b)

Figure 3.17 Distribution of interlaminar shear stress τ_{yz} across the width for $(0_2/90_2)_s$ laminate at mid thickness of matrix interphase (a) one-half width (b) near the edge

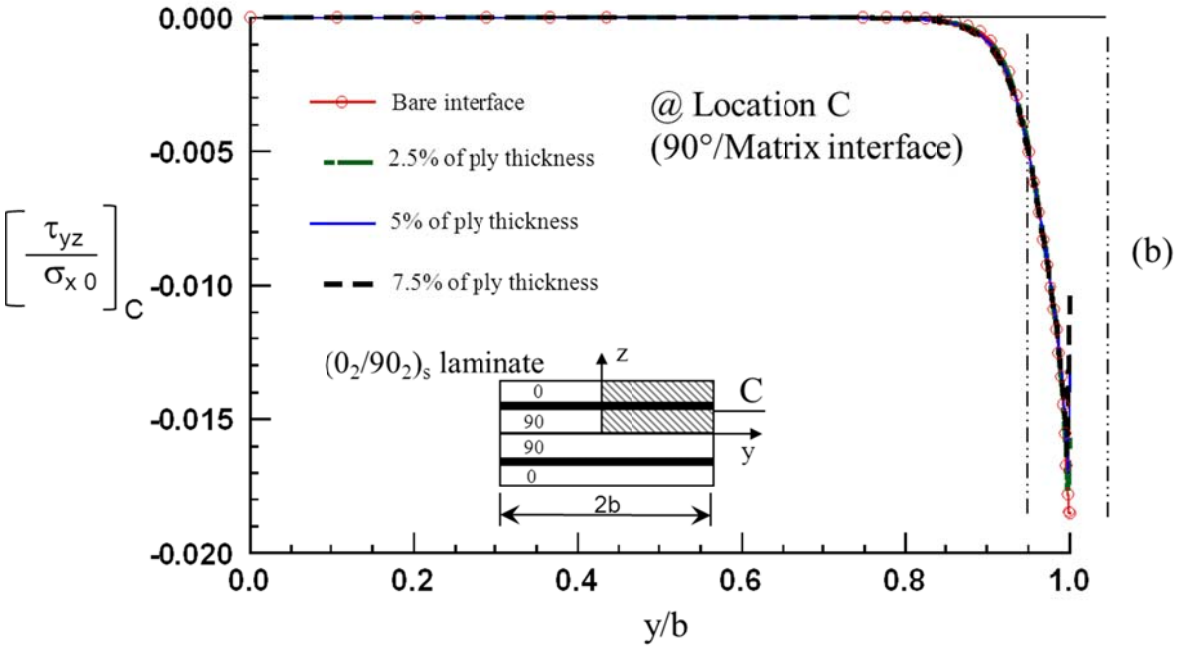

(a)

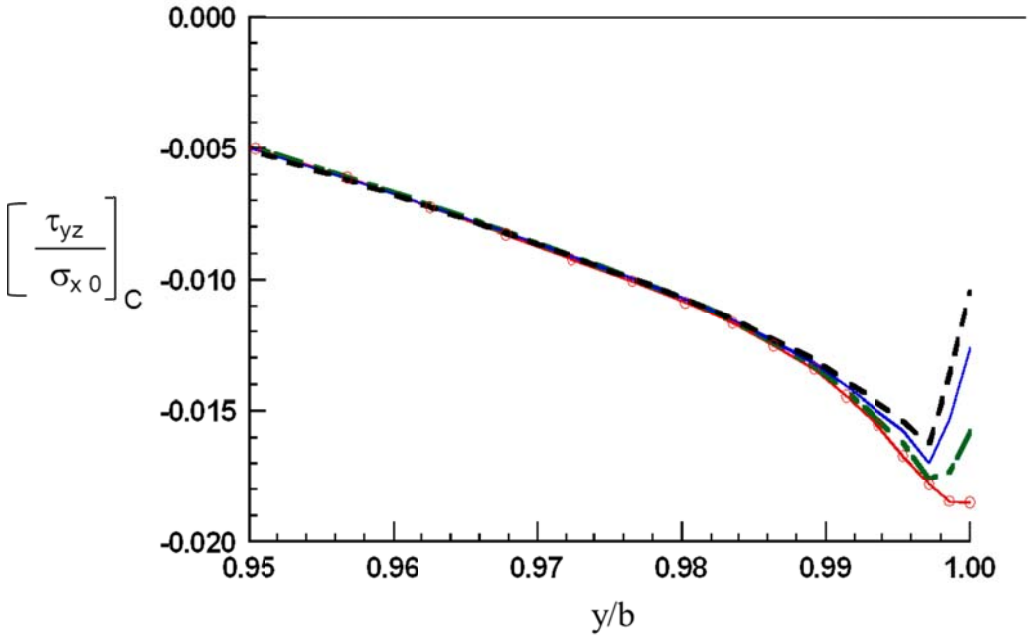

(b)

Figure 3.18 Distribution of interlaminar shear stress τ_{yz} across the width for $(0_2/90_2)_s$ laminate at matrix and 90° interphase (a) one-half width (b) near the edge

Figure 3.19 to Figure 3.21 shows the variation of interlaminar normal stress (σ_x) through the thickness of the laminate at 2.5% of half-width, 1.0% of half width and at free edge respectively. The Figure 3.19 and Figure 3.20 shows that the stresses are continuous and are very close to the bare interface model. However, Figure 3.21 shows that the stresses are lower than the bare interface, but these are singularity stresses that was seen in the width-wise plot. The plot indicates that the overall interlaminar normal and shear stresses are higher throughout the thickness of the laminate compared to the bare interface. But it still has the same trend as that of the bare interface model.

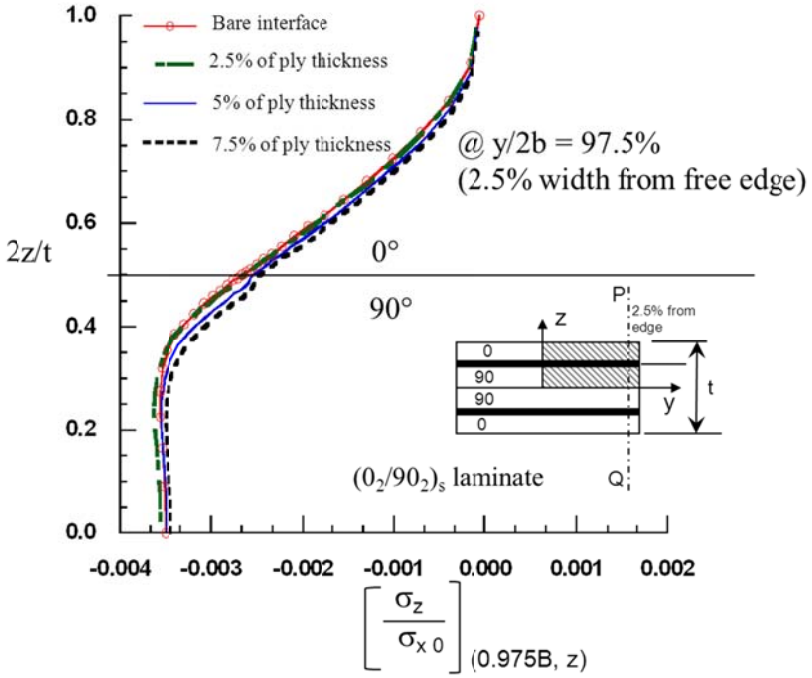

Figure 3.19 Distribution of normal stress σ_z through the thickness for $(0_2/90_2)_s$ laminate at 2.5% width from edge (P-Q), for realistic matrix material

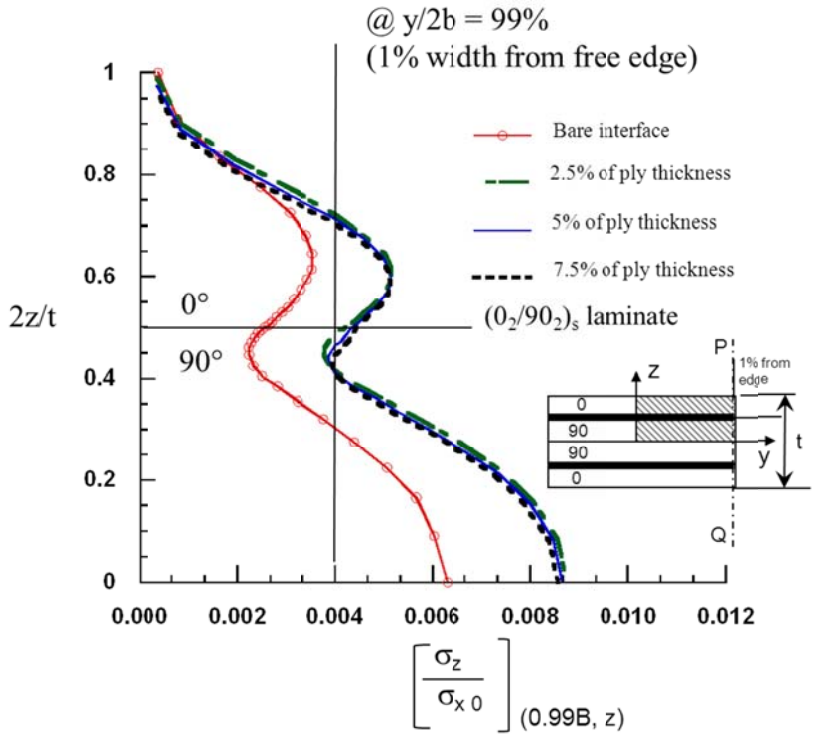

Figure 3.20 Distribution of normal stress σ_z through the thickness for $(0_2/90_2)_s$ laminate at 1% width from edge (P-Q), for realistic matrix material

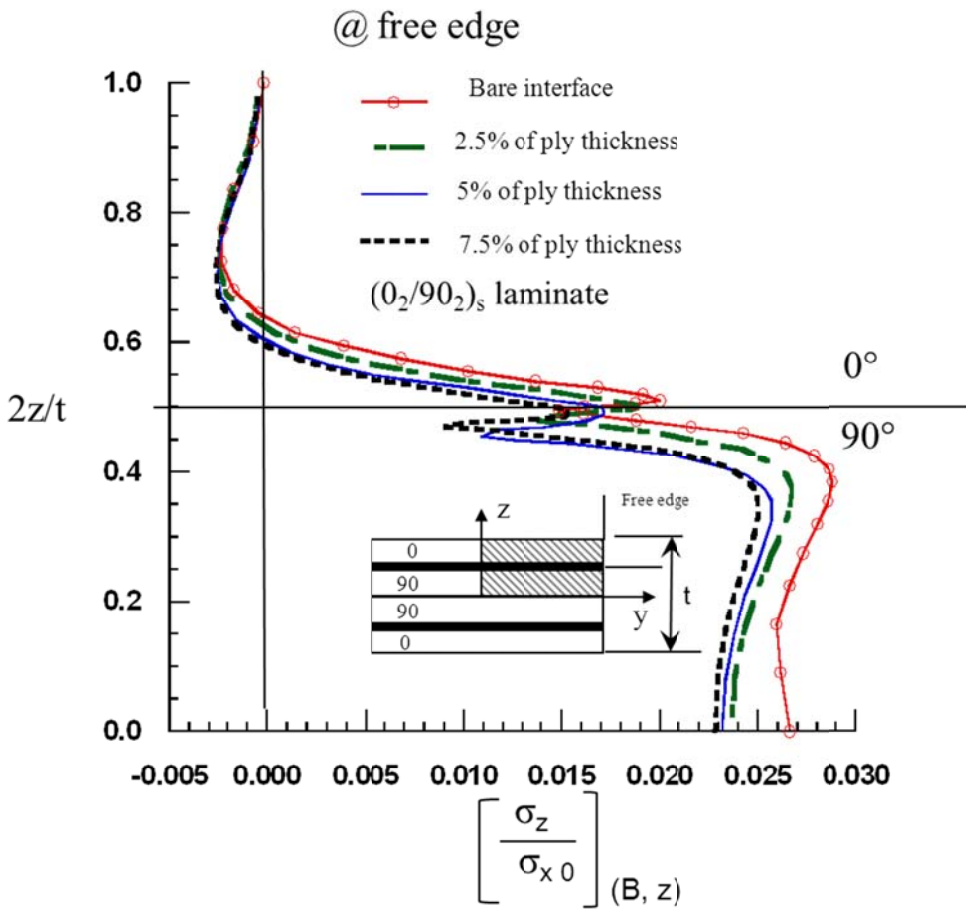

Figure 3.21 Distribution of normal stress σ through the thickness for $(0_2/90_2)_s$ laminate at free edge, for realistic matrix material

Figure 3.22 to Figure 3.24 shows the variation of interlaminar shear stress through the thickness of the laminate at 2.5% of half-width, 1.0% of half width and at free edge respectively. The Figure 3.22 and Figure 3.23 show that the stresses are continuous and are very close to the bare interface model. However, Figure 3.24 shows that the stresses are lower than the bare interface, but these are singularity stresses was seen in the width-wise plot.

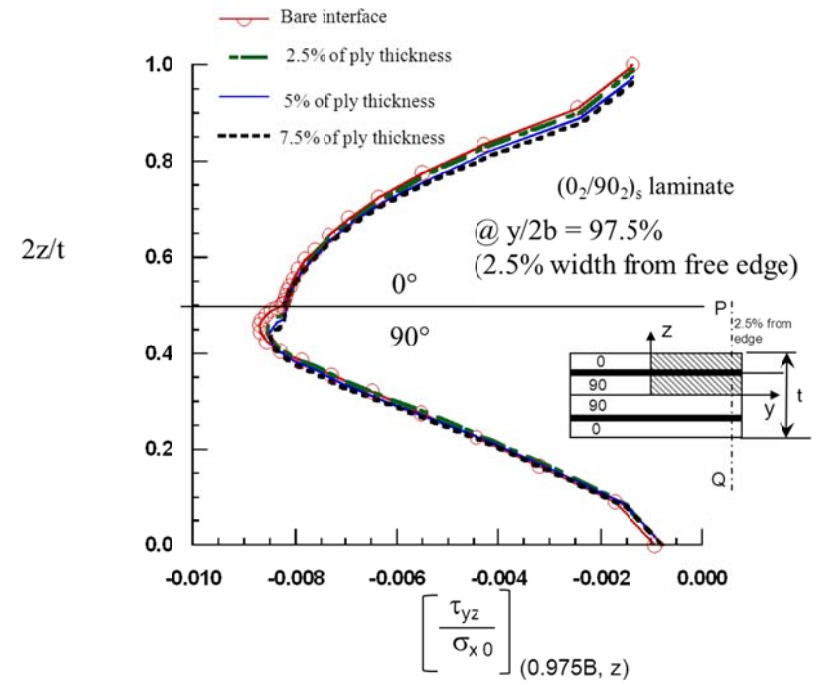

Figure 3.22 Distribution of shear stress τ_{yz} through the thickness for $(0_2/90_2)_s$ 2.5% of width from the edge (P-Q), for realistic matrix material

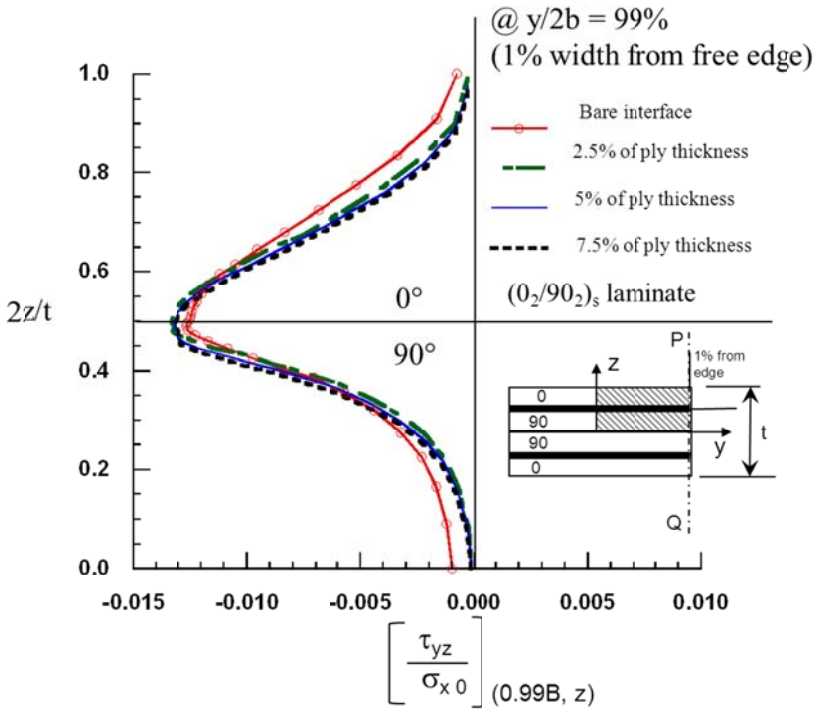

Figure 3.23 Distribution of shear stress τ_{yz} through the thickness for $(0_2/90_2)_s$ 1% of width from the edge (P-Q), for realistic matrix material

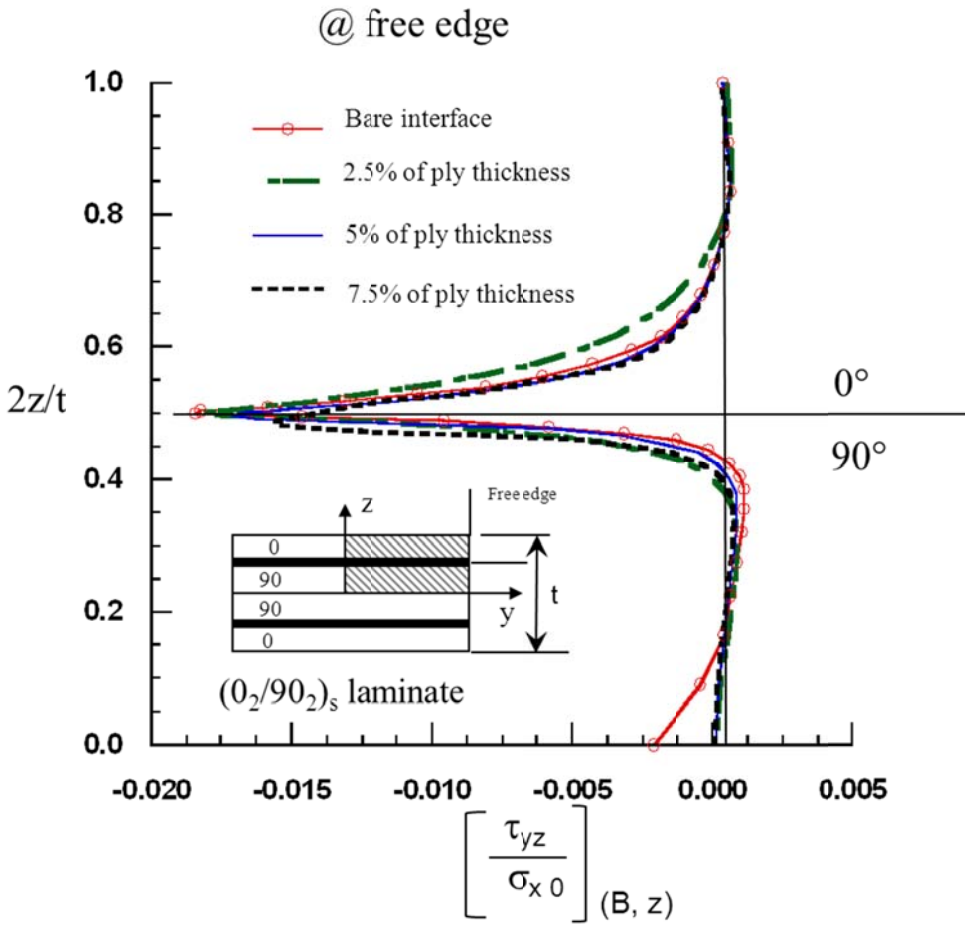

Figure 3.24 Distribution of shear stress τ_{yz} through the thickness for $(0_2/90_2)_s$ at free edge, for realistic matrix material

Interlaminar edge stresses have been studied for $(0_{10}/90_{10})_s$ laminates and found that the response is similar to 2 ply. These plots have been shown in Appendix C.

Based on the analysis of the interlaminar stresses compared with the base interphase and a resin interphase layer of 2.5%, 5.0% and 7.5% of the ply thickness for a cross ply laminate. It can be concluded that there is no significant effect of adding a layer of resin interphase that is linear elastic in properties, on the normal and stresses for FEA

analysis. However, normal stresses and the shear stresses turn to 0 sooner for the resin interphase compared to bare interface.

3.5.1.2 Angle-ply $(+45_2/-45_2)_s$ laminate with a resin interphase

Once again the interlaminar stress σ_z and τ_{xz} along interphase region between +45 and -45 plies are examined for bare and resin interphase models. Figure 3.25-Figure 3.27 shows the variation of interlaminar normal stress (σ_z) along the width of the laminate for $(+45_2/-45_2)_s$ laminate. The figures include the results of different resin layer thickness namely 2.5%, 5.0% and 7.5% of the ply thickness. The response of the curves is similar to those from the literature. Figure 3.25b - Figure 3.27b shows the σ_z at A, B and C respectively close to the free edges. The location A and C represent the bare interface and the response is similar to the bare interface results in this region. The results at location B at the middle of the resin interphase, the stress response is smoother and the stress value decreases in the resin layer thickness.

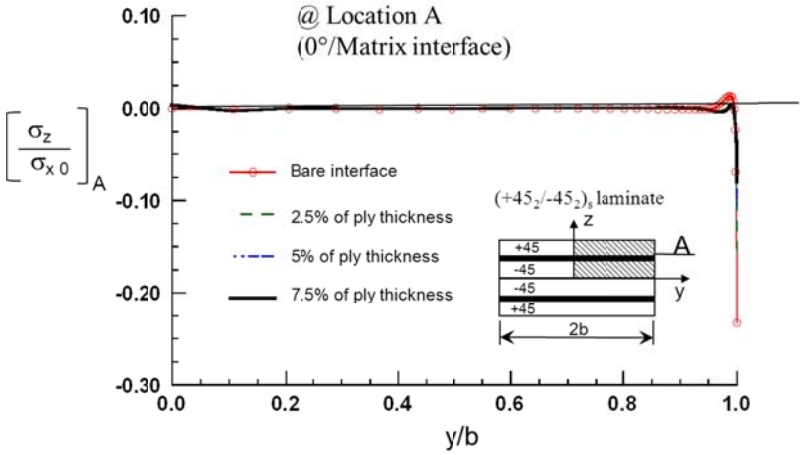

(a)

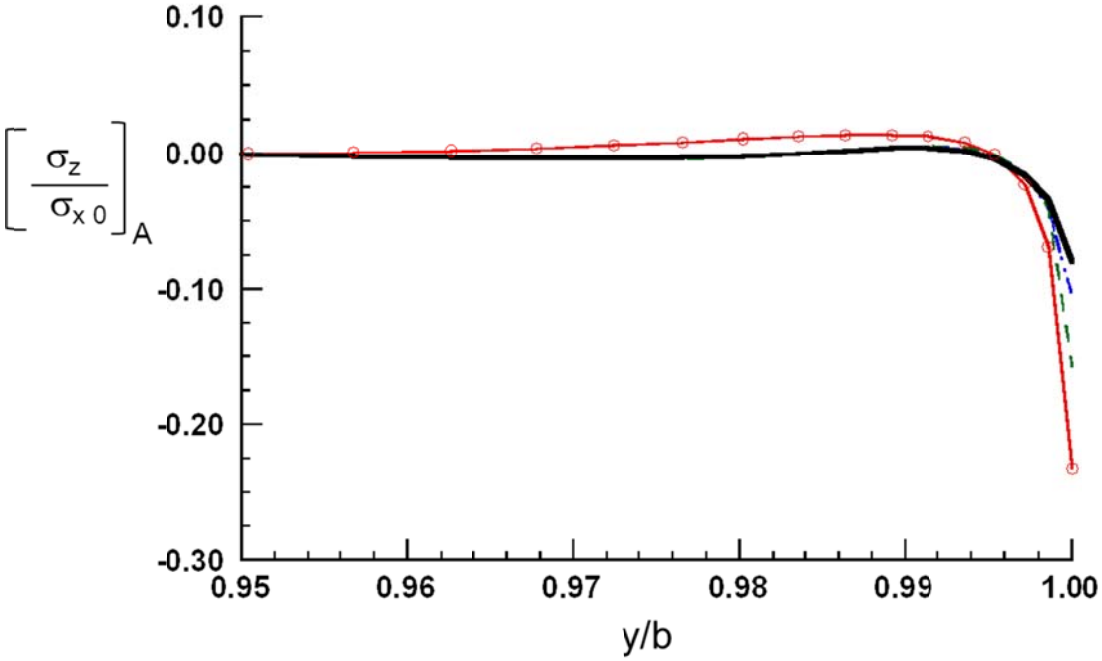

(b)

Figure 3.25 Distribution of normal stress σ_z for $(+45_2/-45_2)_s$ laminate at 0 ° and Matrix interphase (a) One-half width (b) Near the edge across the width

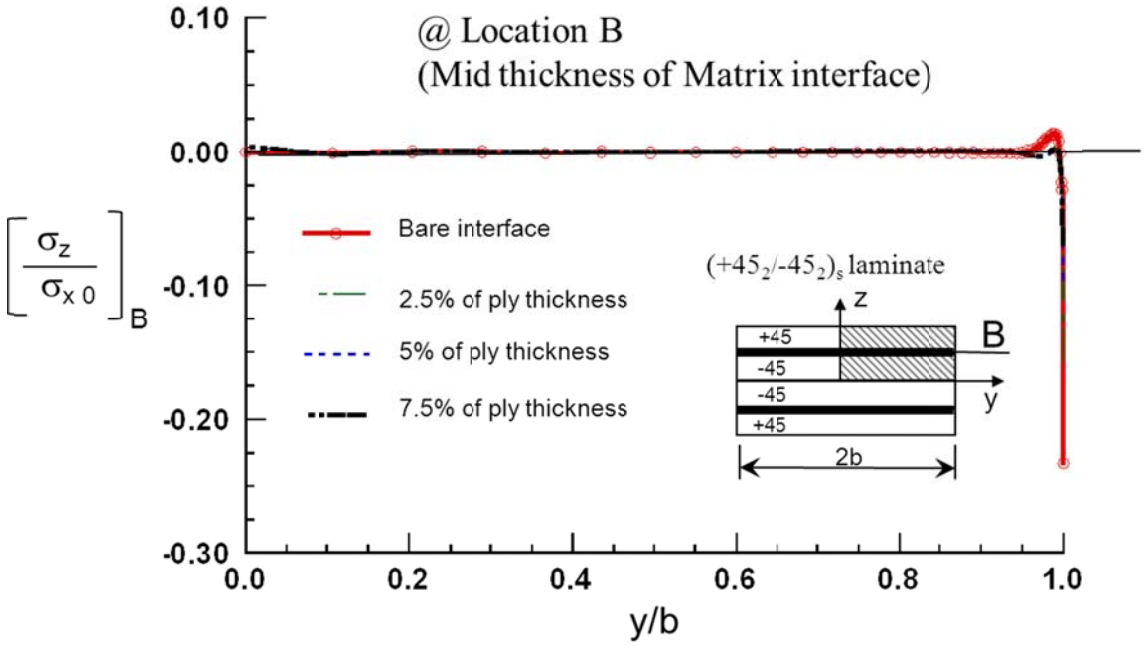

(a)

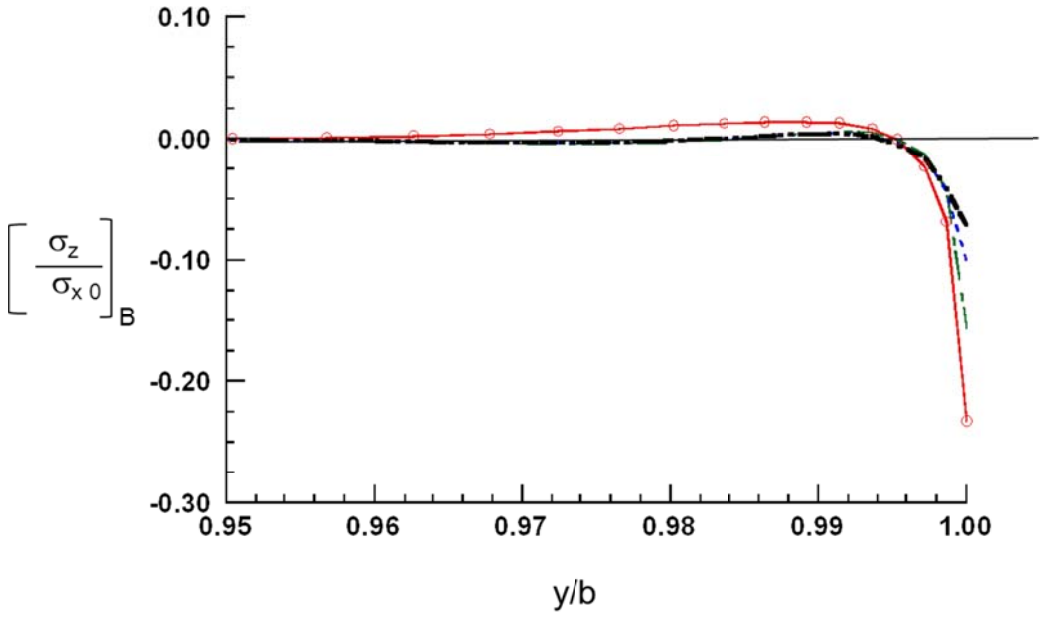

(b)

Figure 3.26 Distribution of normal stress σ_z for $(+45_2/-45_2)_s$ laminate at the mid-thickness of the interphase (a) One-half width (b) Near the edge across the width

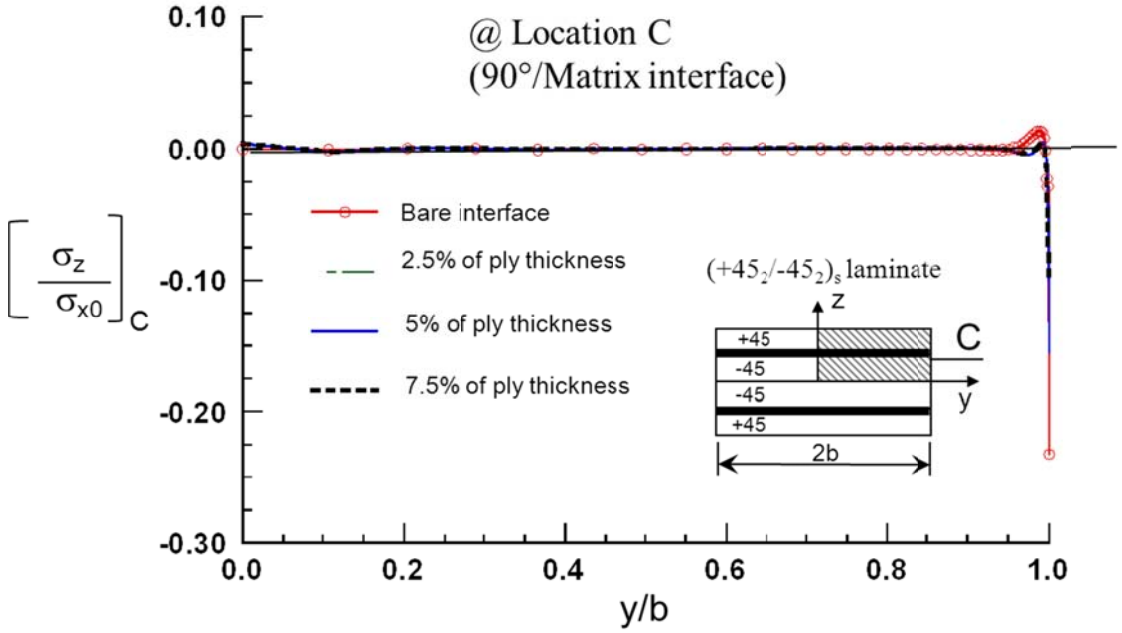

(a)

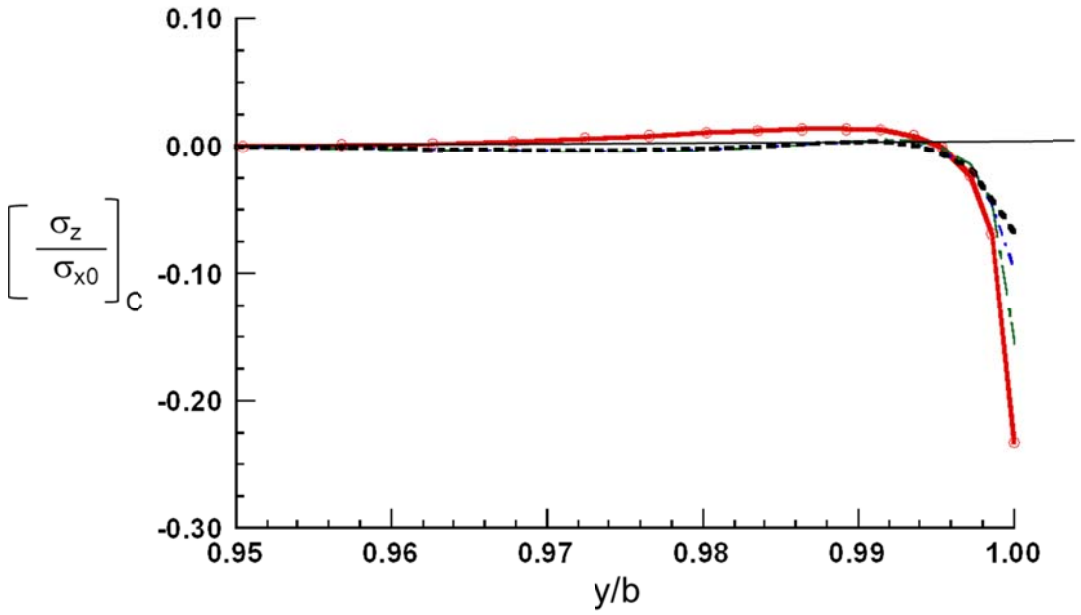

(b)

Figure 3.27 Distribution of normal stress σ_z for $(+45_2/-45_2)_s$ laminate at 90 ° and matrix interphase (a) One-half width (b) Near the edge across the width for $(+45_2/-45_2)_s$

Figure 3.28 to Figure 3.30 shows the variation of interlaminar shear stress (τ_{xz}) along the width of the laminate for $(+45_2/-45_2)_s$. laminate. The figures include the results of different resin layer thickness namely 2.5%, 5.0% and 7.5% of the ply thickness. The response of the curves is similar to those from the literature. Figure 3.28 to Figure 3.30b shows the distribution of shear stresses at A, B and C respectively close to the free edges. The location at A and C represent the bare interface while the location B represents the mid-location of the resin layer still shows that the interphase model helps lower the stresses at regions 1% from the free edge. The shear stress at location B for this laminate is also lower at the free edge, as the thickness of the resin interphase layer increases the stress values at the free edge is lower as seen in Figure 3.29.

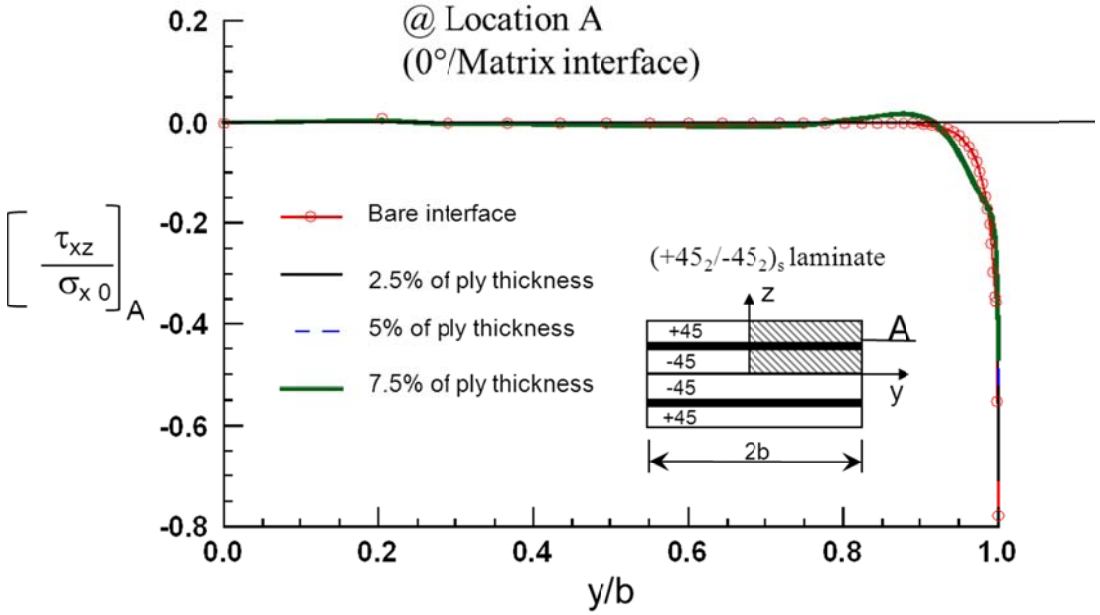

(a)

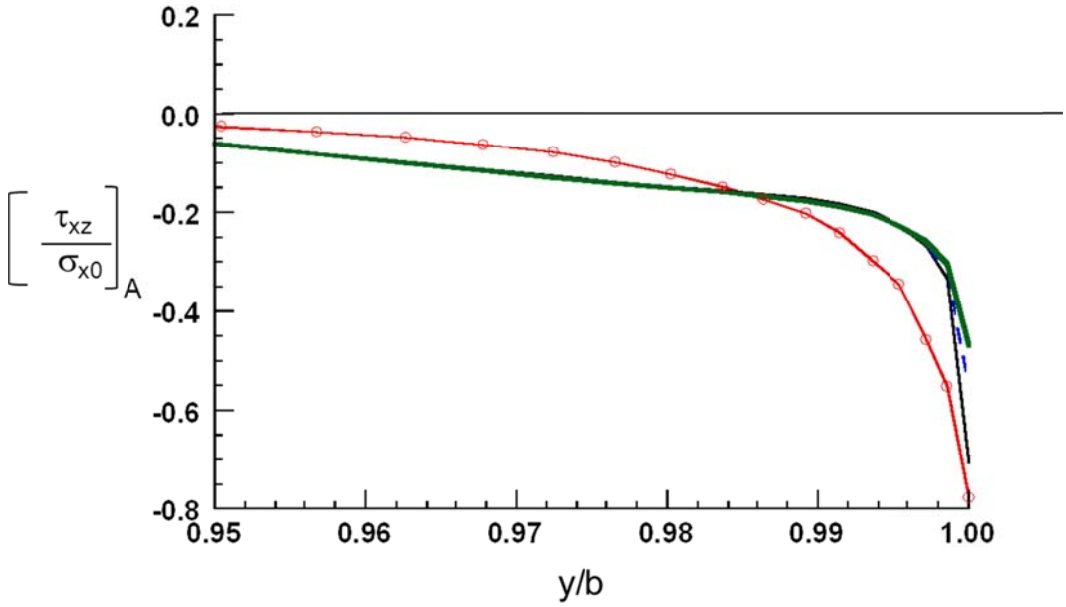

(b)

Figure 3.28 Distribution of shear stress τ_{xz} for $(+45_2/-45_2)_s$ laminate at 0 ° and matrix interphase (a) One-half width (b) Near the edge across the width

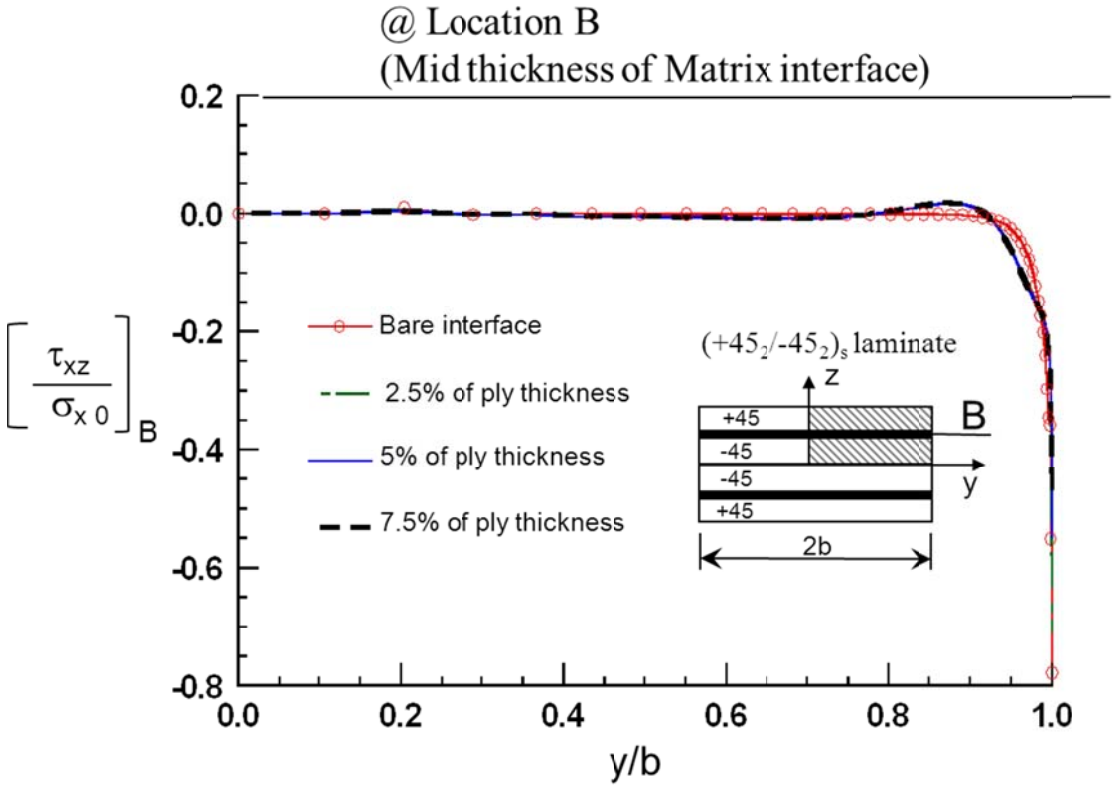

(a)

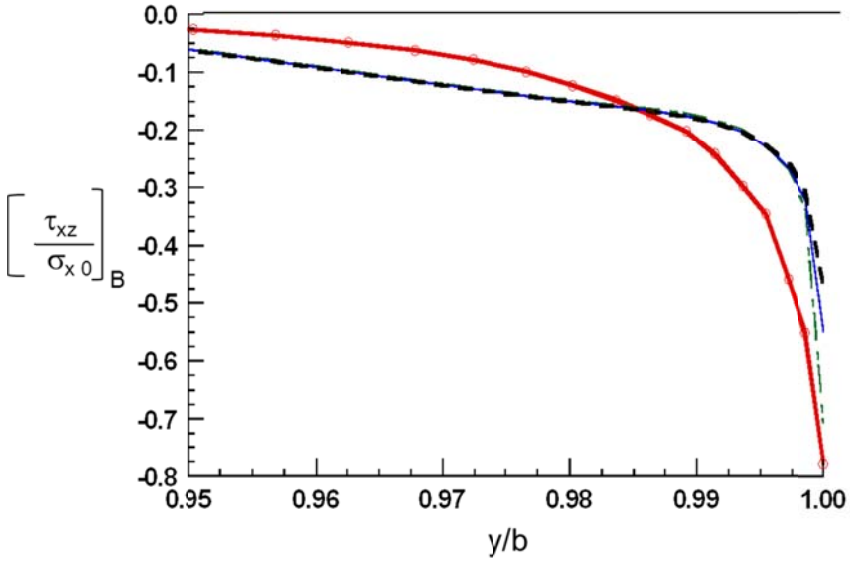

(b)

Figure 3.29 Distribution of shear stress τ_{xz} for $(+45_2/-45_2)_s$ laminate at the mid-thickness of the interphase (a) One-half width (b) Near the edge across the width

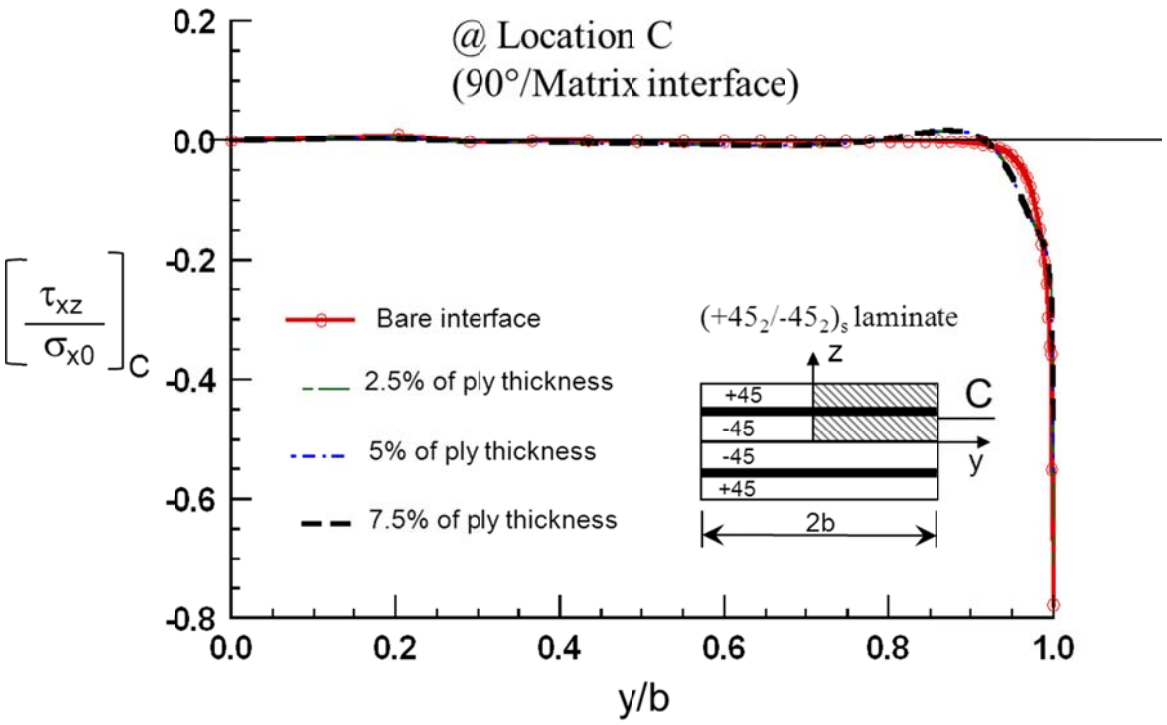

(a)

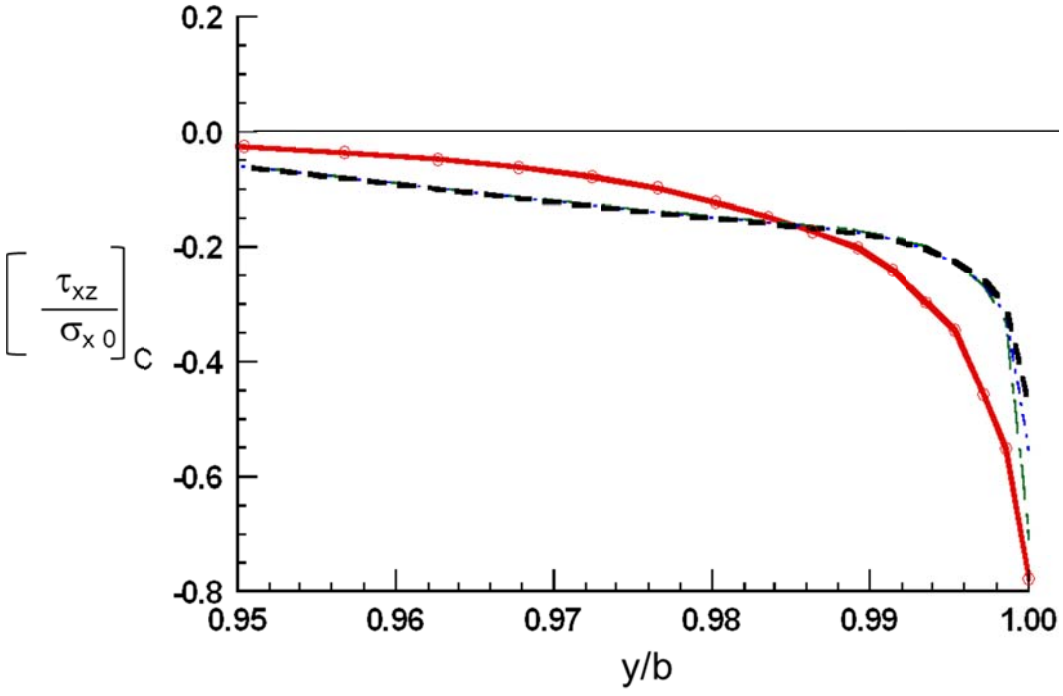

(b)

Figure 3.30 Distribution of shear stress τ_{xz} for $(+45_2/-45_2)_s$ laminate at 90 ° and matrix interphase (a) One-half width (b) Near the edge across the width

Figure 3.31 to Figure 3.33 show the normal stress distribution through the thickness for 2.5%, 1% from the free edge and at the free edge. The distribution is similar to that of bare interface, except at 2.5% from the edge. But, the stresses are continuous across the thickness of the laminate.

Figure 3.31 shows the plot for through the thickness for normal stress at distance of 2.5% width from free edge. Here it can be seen that the stresses for the interphase model is much lower than the bare interface models between the lamina. A similar trend can be seen at 1% and 0.5% distance from the free edge. This has been shown in Figure 3.32 and Figure 3.33.

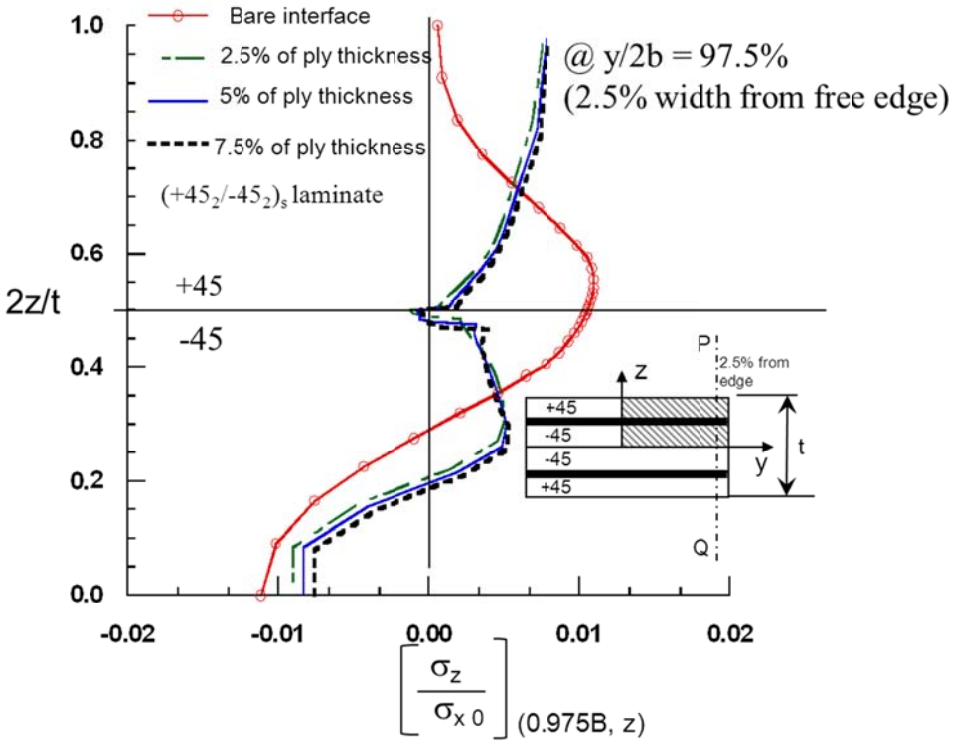

Figure 3.31 Distribution of normal stress σ_z through the thickness, for $(+45_2/-45_2)_s$ laminate at 2.5% width from the edge (P-Q), for realistic matrix material

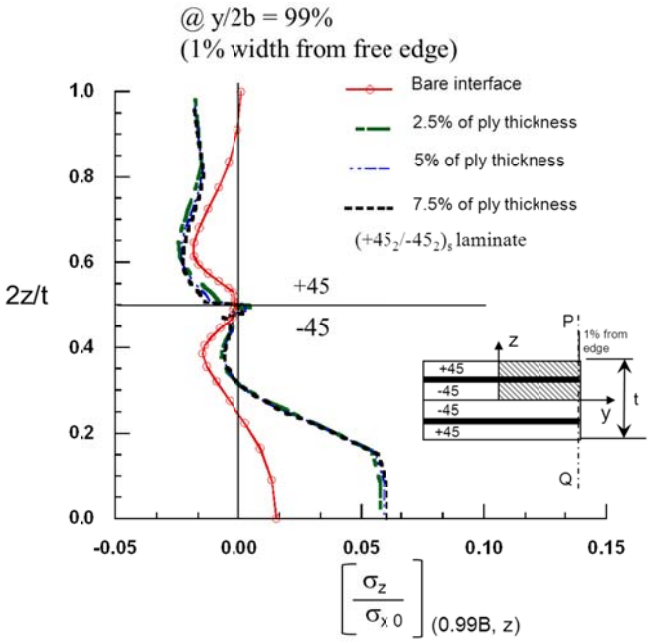

Figure 3.32 Distribution of normal stress σ_z through the thickness, for $(+45_2/-45_2)_s$ laminate at 1% width from the edge (P-Q), for realistic matrix material

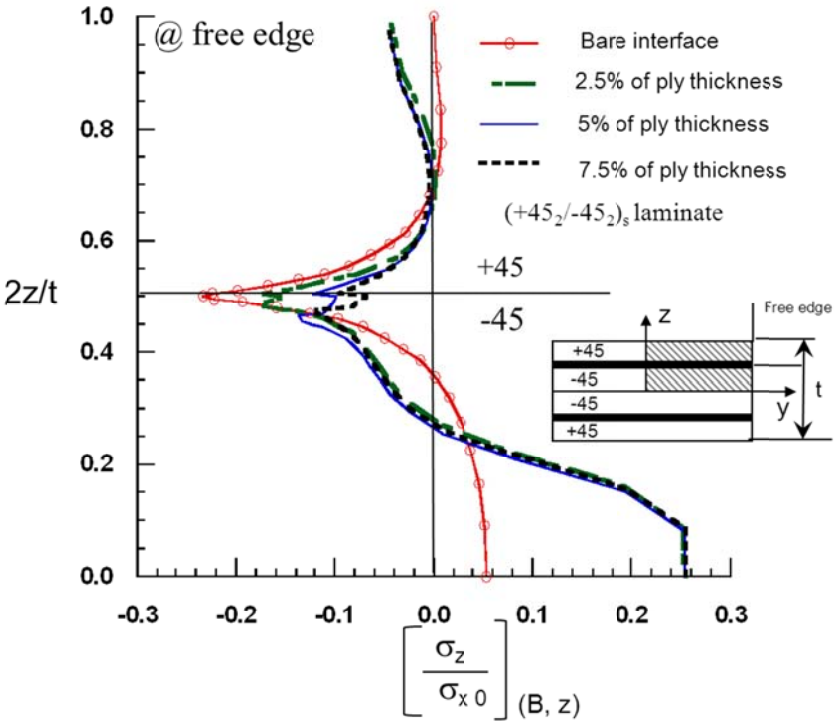

Figure 3.33 Distribution of normal stress σ_z through the thickness, for $(+45_2/-45_2)_s$ laminate at free edge, for realistic matrix material

Figure 3.34 to Figure 3.36 show the shear stress distribution through the thickness for 2.5%, 1% from the free edge and at the free edge. The distribution is similar to that of bare interface and is continuous. Similarly to the normal stress the shear stresses are also lower in for the interphase models compared to the bare interface based on the Figure 3.34-Figure 3.36.

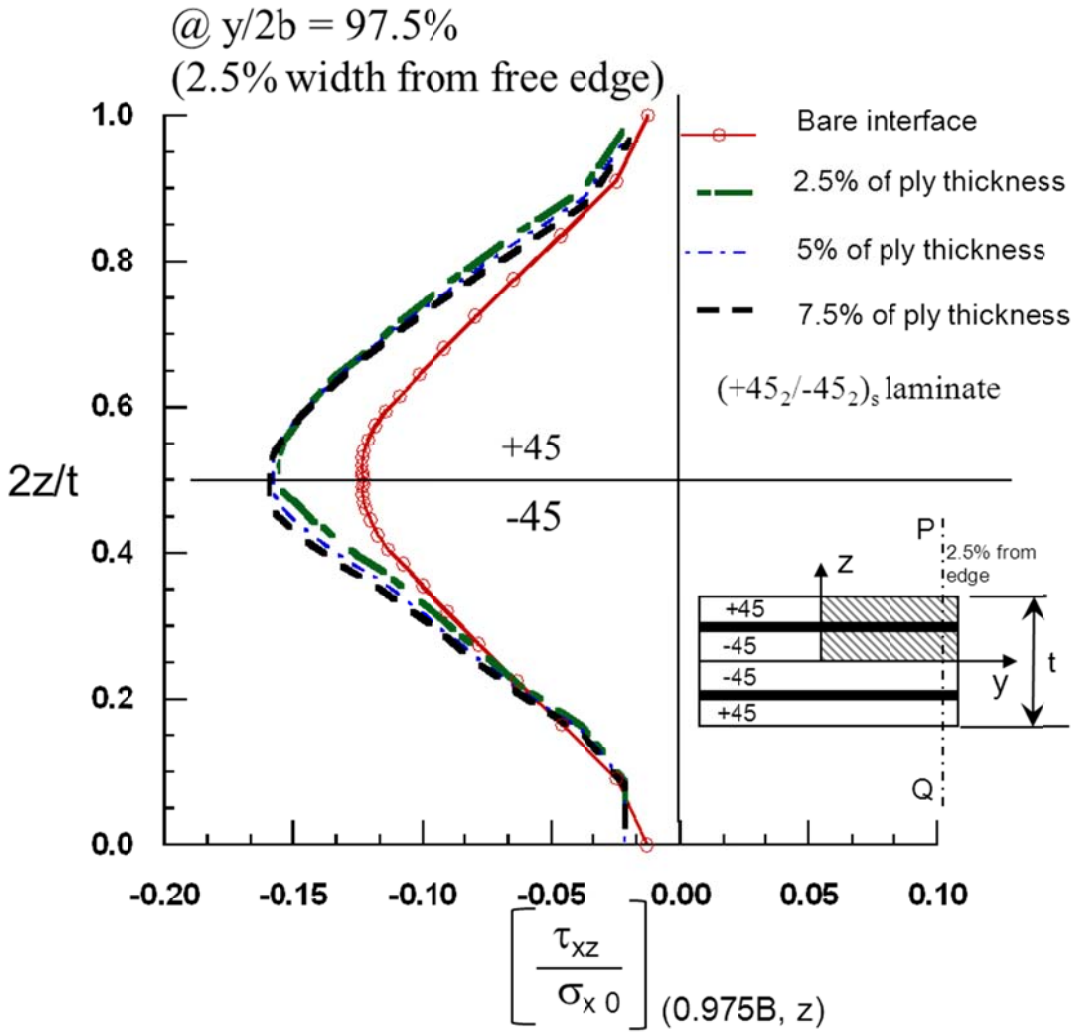

Figure 3.34 Distribution shear stress τ_{xz} through the thickness, for $(+45_2/-45_2)_s$ laminate at 2.5% width from the edge (P-Q), for realistic matrix material

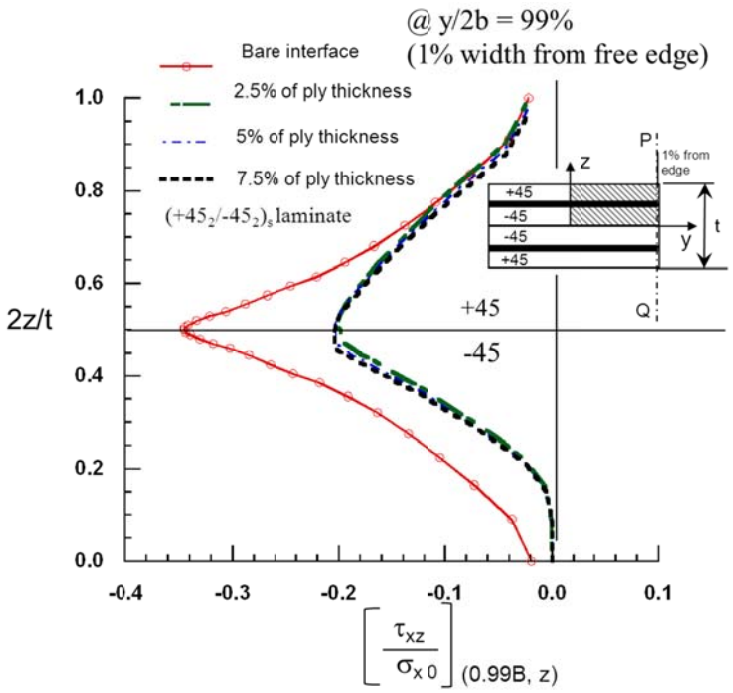

Figure 3.35 Distribution shear stress τ_{xz} through the thickness, for $(+45_2/-45_2)_s$ laminate at 1% width from the edge (P-Q), for realistic matrix material

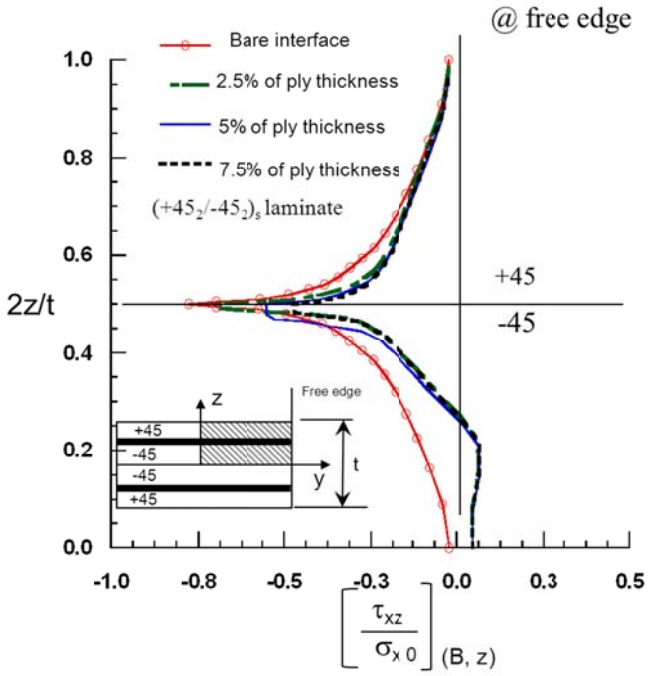

Figure 3.36 Distribution shear stress τ_{xz} through the thickness, for $(+45_2/-45_2)_s$ laminate at free edge, for realistic matrix material

Interlaminar edge stress studies have been performed for $(+45_{10}/-45_{10})_s$ and the results are found to be similar to the 2-ply laminate and these results are shown in Appendix C.

Based on the analysis, the interlaminar normal stresses have a little effect on the thickness of the interphase layer and prediction of stresses for angle ply laminate $(+45_2/-45_2)_s$. The interlaminar shear stresses are lower at the last 1% from the free edge compared to bare interface. The singularity effect vanishes as the resin interphase thickness increases.

The above analysis concludes that the resin interphase layer smoothens the interlaminar edge stresses. Furthermore, the interlaminar stress reduces as the resin layer thickness increases.

3.5.2 Effect of Ply Grouping and Lamina thickness on the interlaminar stresses

3.5.2.1 $(0_2/90_2)_s$ Laminate

To study the effect of the ply grouping analysis was performed on different ply grouping on the $(0_n/90_n)_s$ laminates. Figure 3.37 shows a schematic of 2 and 4 layers of $(0/90)_s$ laminate. Each layer makes up of 1 thickness of the fiber diameter. For a 2 layer laminate there are totally eight times the diameter of the fiber. For the 4 layer there are totally 16 times of the diameter for the selected laminate.

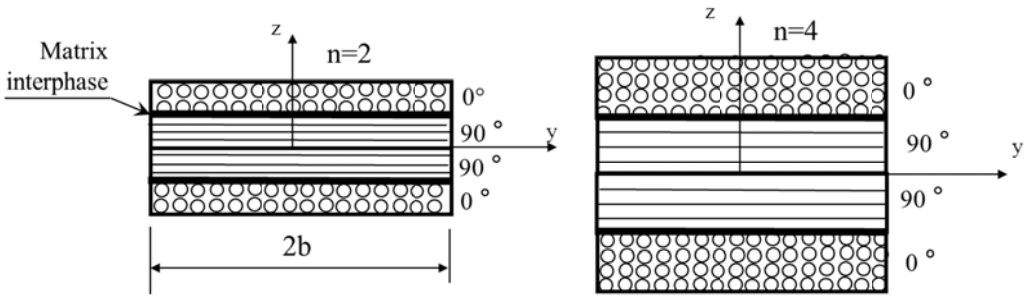

Figure 3.37 Schematic of $(0_2/90_2)_s$ laminate with matrix interphase

Figure 3.38 and Figure 3.39 shows the distribution of normalized normal stress σ_z and shear stress across the width of the specimen respectively, for different ply thickness from 1-10. From the figure it can be seen that the edge distance d reduces as the number of ply reduces. The rate of reduction in stress has been found to be same as bare interface model at 1.25 times the laminate thickness, this is shown in Figure 3.40.

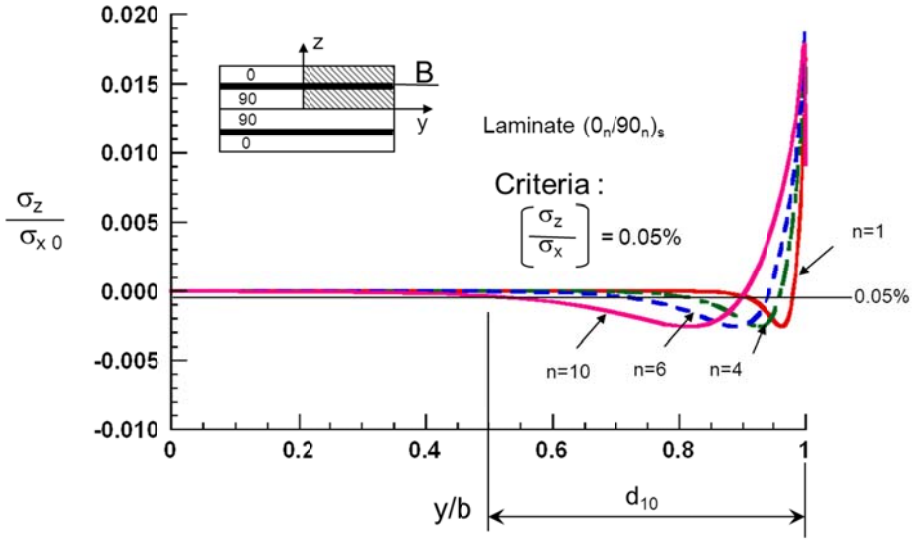

Figure 3.38 Distribution of normal stress σ_z across the width, for different ply grouping at the mid-thickness of the interphase , for realistic matrix material

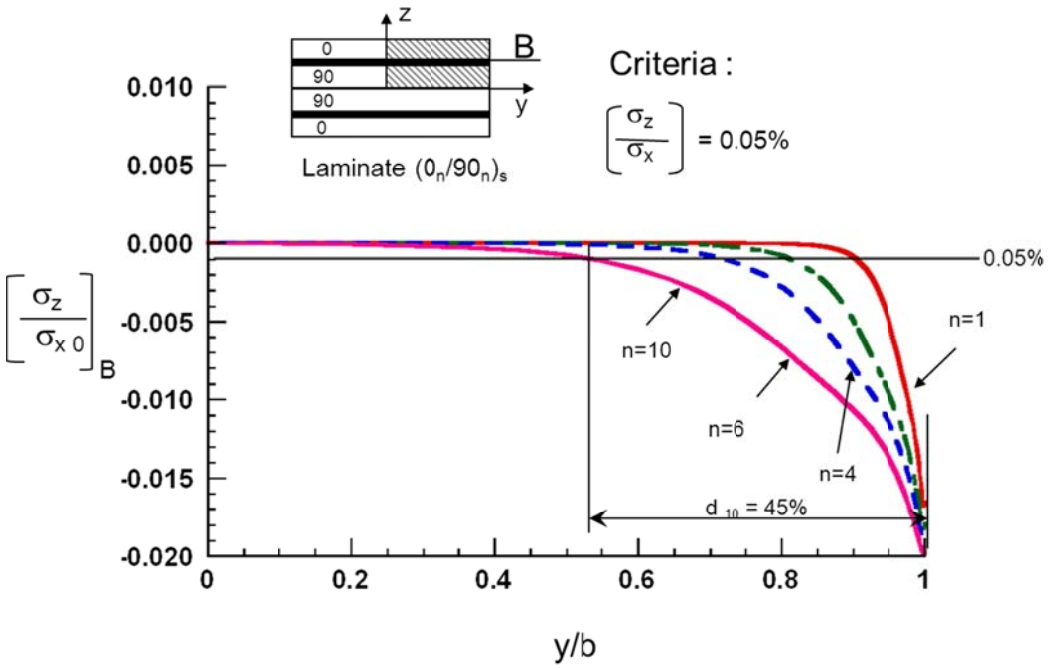

Figure 3.39 Distribution of shear stress τ_{yz} across the width, for different ply grouping at the mid-thickness of the interphase , for realistic matrix material

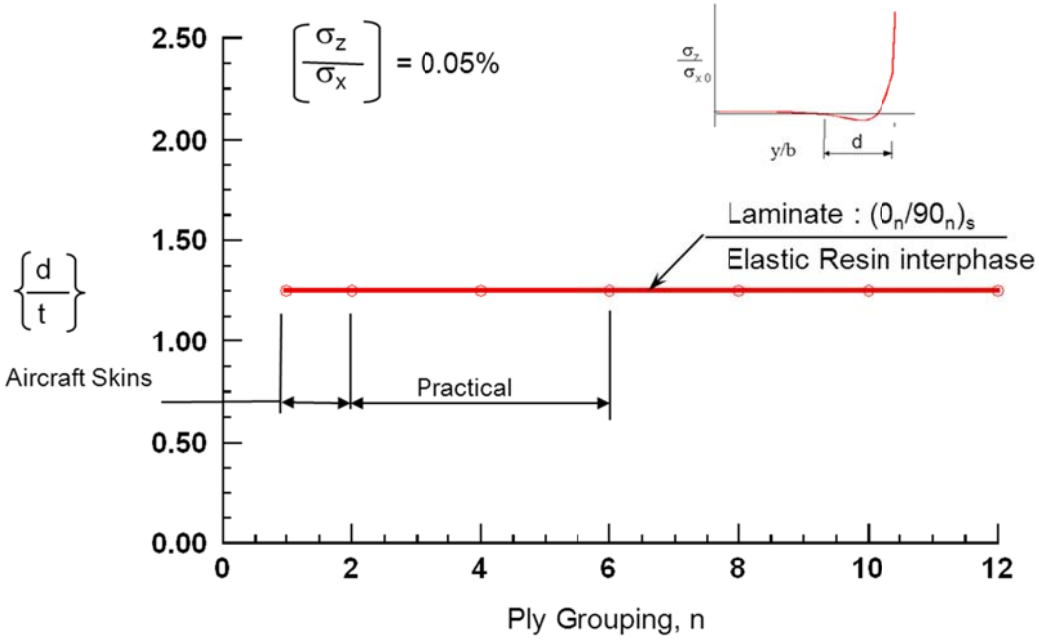

Figure 3.40 Distribution of edge distance (d) for different ply grouping, for $(0_n/90_n)_s$ for resin interphase

In order to study the effect of the lamina thickness analysis was performed for different lamina thickness from 0.0005-0.005". The normalized distribution of stresses for different lamina thickness were plotted and they are presented in Appendix C. As the ply thickness decreases the edge distance decreases, this observation supports some of the experiments and theory conducted in the literature. Based on the analysis, both the laminates with interphase and the bare interface for cross-ply laminate yield nearly same edge stress distances.

3.5.2.2 $(+45_2/-45_2)_s$ Laminate

In order to study the effects of the ply-grouping and the ply thickness analysis was performed on different ply grouping and lamina thicknesses. Figure 3.41 shows example of ply thickness 2 and 4 for $(+\theta_n/-\theta_n)_s$ laminate.

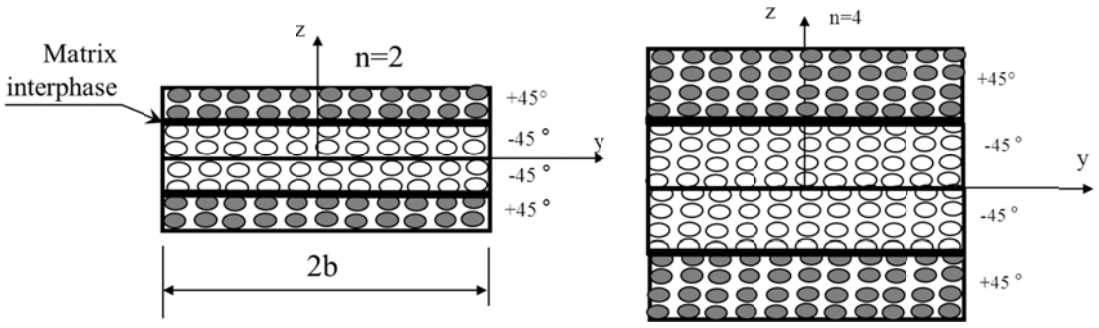

Figure 3.41 Schematic of Ply thickness for n=2 and n=4 with matrix interphase

Figure 3.42 and Figure 3.43 shows normalized normal stress (σ_z) and shear stress (τ_{xz}) for different ply grouping from 1-10. Based on the plot it can be seen that as the edge distance decreases with the number of layers in the lamina. Using the data from the plot the edge distance has been calculated for each of the layer thicknesses and then normalized with respect to the thickness of the laminate. The normalized edge distance is around 1.75 times the laminate thickness for single ply but reduces to around 0.6 times the thickness for the $(+45_n/-45_n)_s$ laminates subjected to the tensile loading of the laminate shown by Figure 3.44.

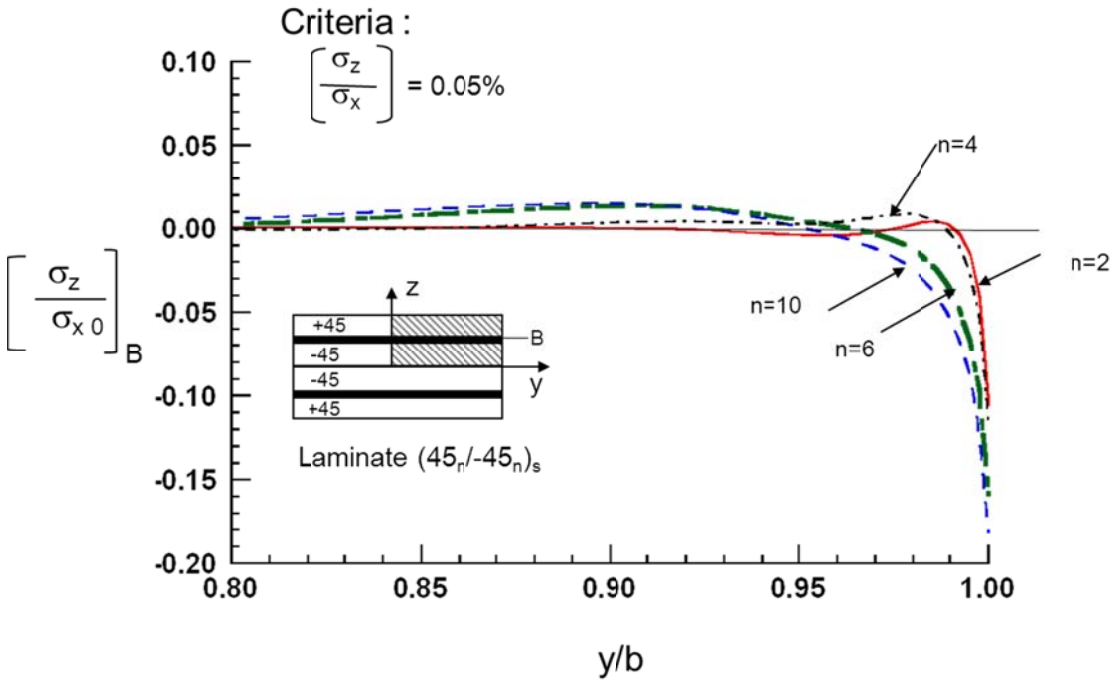

Figure 3.42 Distribution of normal stress σ_z across the width, for $(+45_n/-45_n)_s$ laminate at the mid-thickness of the interphase for different ply grouping, for realistic matrix material

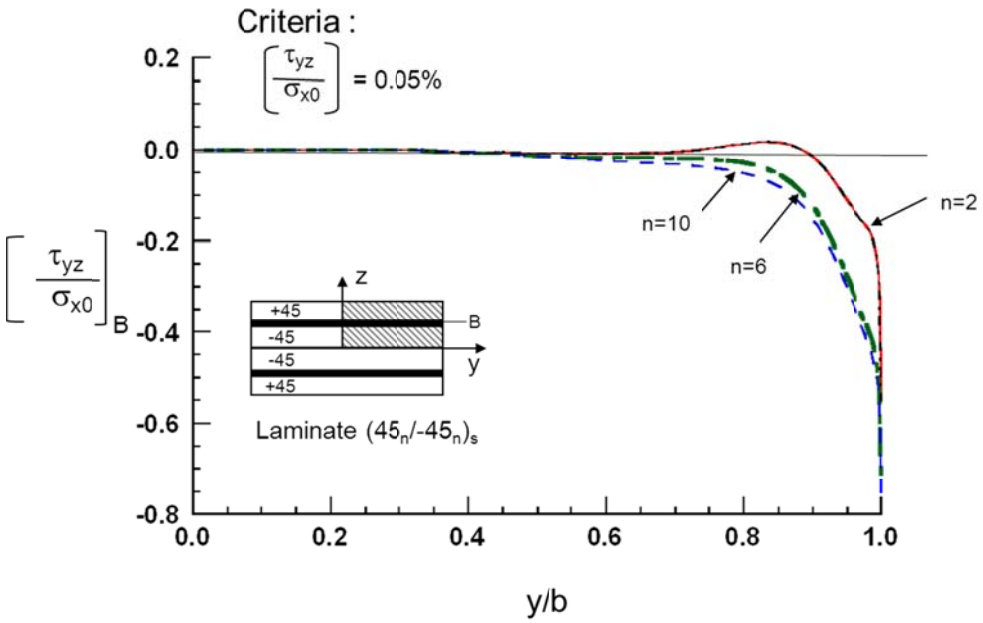

Figure 3.43 Distribution of shear stress τ_{xz} across the width, for $(+45_n/-45_n)_s$ laminate at the mid-thickness of the interphase for different ply grouping, for realistic matrix material

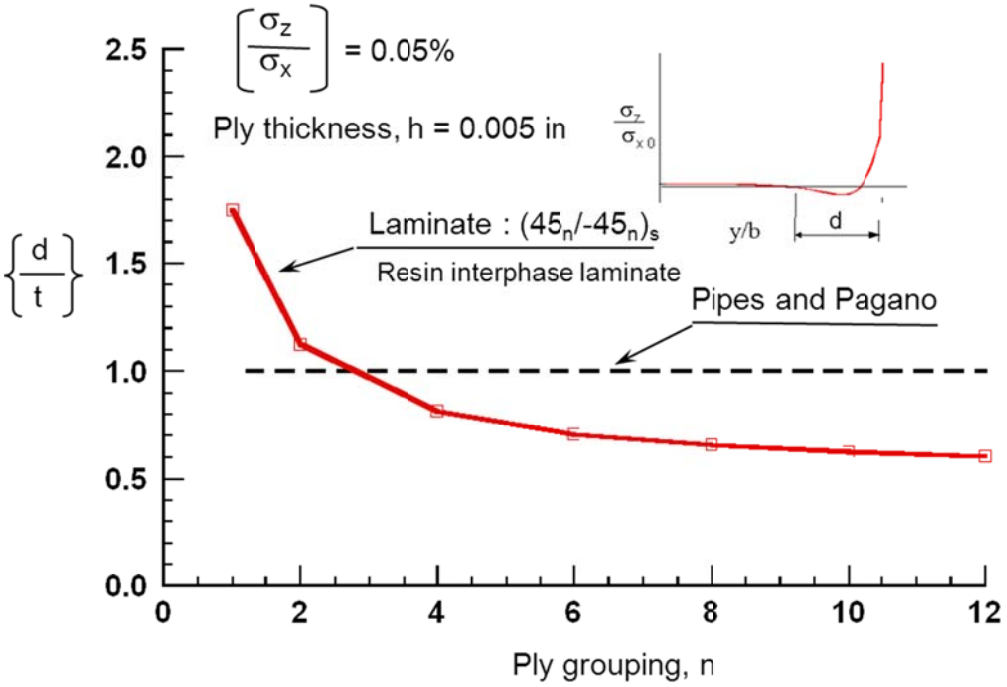

Figure 3.44 Distribution of edge distance with ply grouping for $(+45_n/-45_n)_s$ (Pipes and Pagano, 1970)

Table 3.2 Variation of edge distance with ply grouping for $(45_n/-45_n)_s$ laminate for resin layer interphase

2b	n	t	d in	[t/b]	[d/t] %
0.5	1	0.02	0.07	4	1.75
0.5	2	0.04	0.09	8	1.13
0.5	4	0.08	0.13	16	0.81
0.5	6	0.12	0.17	24	0.71
0.5	8	0.16	0.21	32	0.66
0.5	10	0.20	0.25	40	0.63
0.5	12	0.24	0.29	48	0.60

In order to study the effect of the lamina thickness analysis was performed for different lamina thickness from 0.0005”-0.005” for a (+45/-45)s laminate. As the ply thickness decreases the edge distance decreases, this observation supports some of the experiments and theory conducted in the literature. These figures have been shown in Appendix C

Based on the analysis for variation in ply grouping for cross-ply and angle ply laminate. The following can be concluded, the ply grouping has no effect on the modeling of resin interphase for $(0_n/90_n)_s$ laminate and remains at 1.25 times the laminate thickness like the bare interface. The ply grouping has small effect on the modeling of the resin interphase for $(+45_n/-45_n)_s$ laminate and is about 1.75 times of the laminate thickness for single ply and reduces to 0.6 times for 12 ply.

3.5.3 Interlaminar Stresses with Elastic Plastic and Non-Linear interphase

In this section the study of the interlaminar edge stress effect of change in interphase material from a linear elastic to elastic-plastic and non-linear has been presented.

3.5.3.1 Cross-ply $(0_2/90_2)_s$ laminate with an Elastic Plastic interphase

Figure 3.45 shows distribution of normal stress σ_z at location B closer to the free edge of the interphase, the stresses go to mathematical singularity for the bare interface However, the elastic-plastic interphase model shows that the stresses are lower compared to the bare interface. The singularity effect is reduced compared to the bare interface.

Figure 3.46 shows distribution of shear stress τ_{yz} at location B closer to the free edge of the interphase, The shear stress go turns towards 0 sooner compared to the bare interface, thus reducing the effect of the edges.

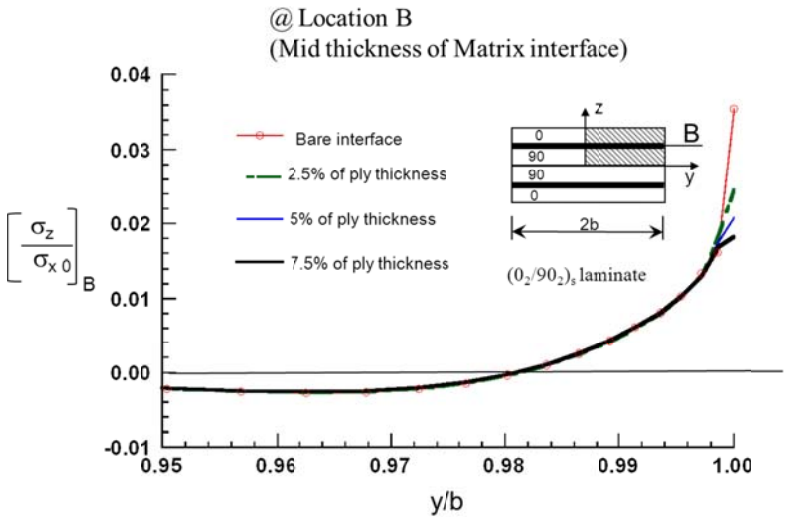

Figure 3.45 Distribution of normal σ_z across the width for $(0_2/90_2)_s$ laminate at the mid-thickness of the interphase (B), for elastic-plastic matrix material

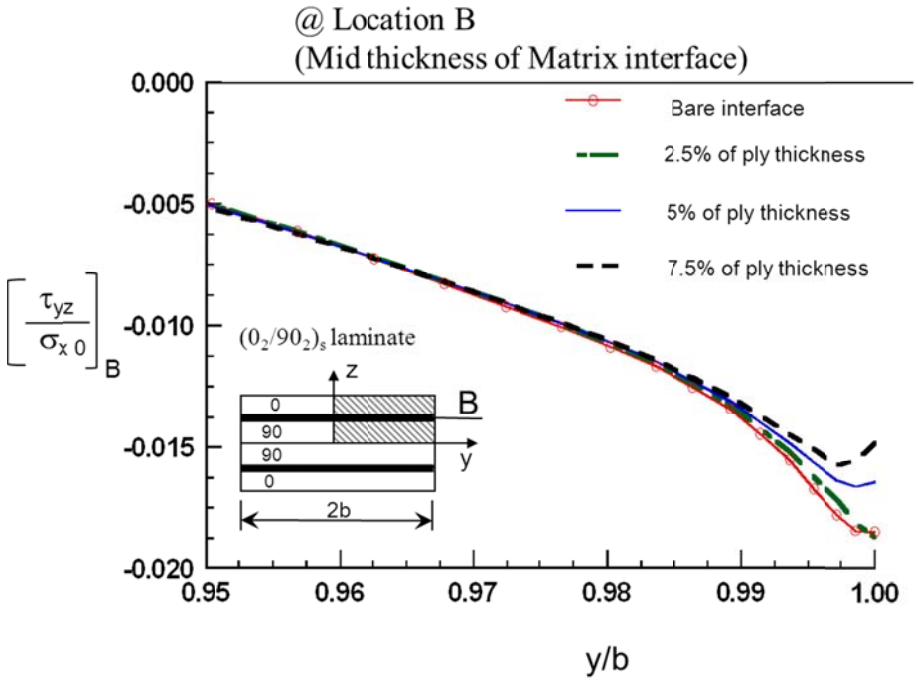

Figure 3.46 Distribution of shear stress τ_{yz} across the width for $(0_2/90_2)_s$ laminate at the mid-thickness of the interphase, for elastic-plastic matrix material

Additional plots for 10 ply thickness laminate and through the thickness plots at 1% close to the edges showed not much change in the stresses and are presented in Appendix B.

Based on the analysis the edge stresses of a laminate with Elastic-Plastic interphase has minimal significance at a region 1% from free edge. However, the region 0.2% closer to the edge shows that the singularity stress effect is vanished.

Figure 3.47 shows a contour plot of Von-Mises stresses for the interphase area and compared to the yield strength of the matrix. For 1% of the strain the value it can be seen that the matrix has not yielded yet in the laminate. The highest stress is at the interphase between the 0° and 90° interphase.

Figure 3.48 and Figure 3.49 shows comparison of Elastic and Elastic plastic interphase for strains from 0.9-1.1%. The interphase is not yielded till 1% of the strain but fully yielded at 1.1% of the strain.

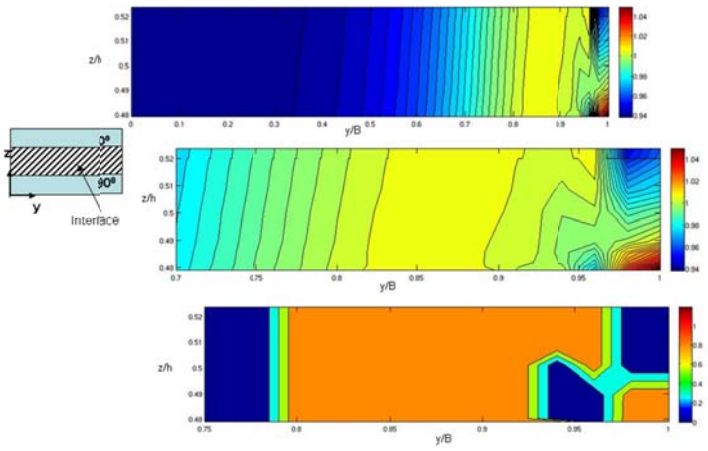

Figure 3.47 Contour plot of $(0_n/90_n)_s$ laminate under Tensile loading, comparison of Von-Mises stress with yield strength for linear interphase laminate at 1% strain in the interphase only

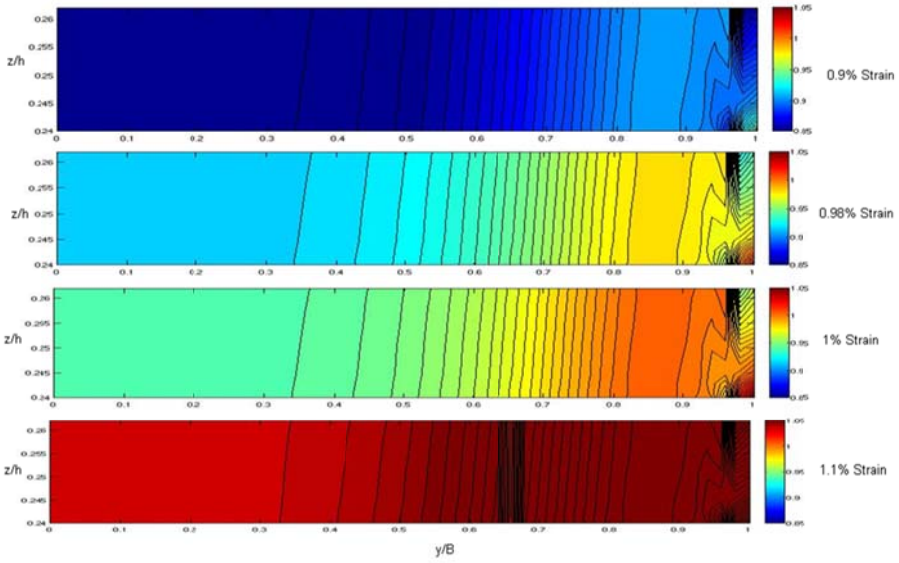

Figure 3.48 Contour plot of $(0_n/90_n)_s$ laminate under Tensile loading, comparison of Von-Mises stress with yield strength for elastic matrix interphase laminate at for 0.98-1.1% strain in the interphase only

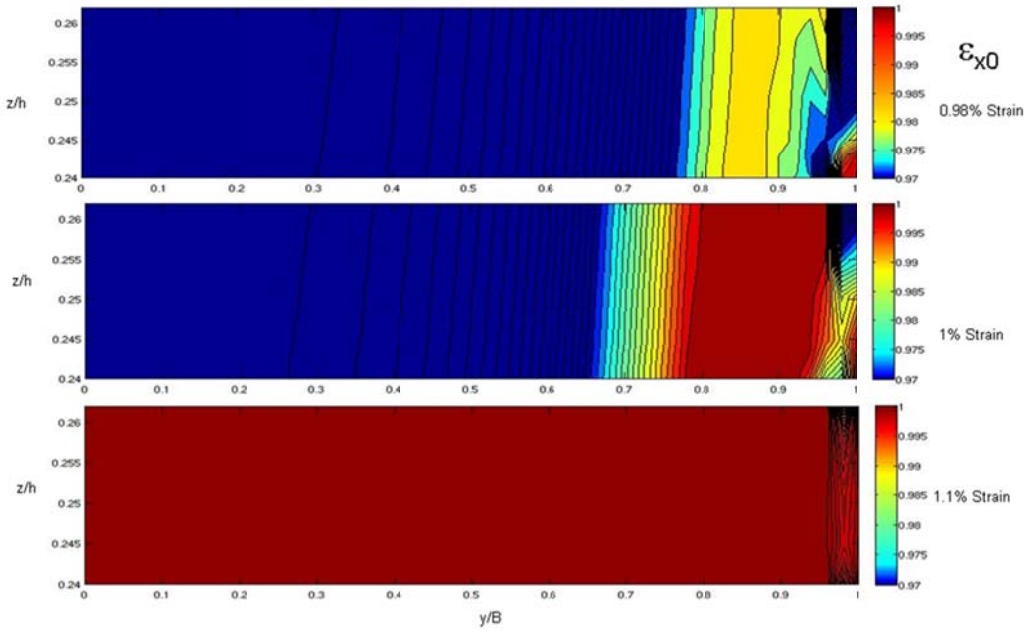

Figure 3.49 Contour plot of $(0_n/90_n)_s$ laminate under Tensile loading, comparison of Von-Mises stress with yield strength for elastic-plastic interphase laminate at for 0.98-1.1% strain in the interphase only

3.5.3.2 Angle-ply $(+45_2/-45_2)_s$ laminate with an Elastic Plastic interphase

Figure 3.50 shows the variation of normal stress distribution across the width of the specimen for $(+45_2/-45_2)_s$ laminate, for different thickness of the interphase at location B (Mid of the interphase) lamina for an elastic-plastic interphase. The stresses are closer to zero for the non-linear interphase. The normal stress are compressive and is mathematically singular at the edges for the bare interface, for the elastic-plastic the singularity stresses do not exist for this laminate.

Figure 3.51 shows the distribution of interlaminar shear stresses across the width of the laminate at location B. The stress is much higher at the free edges but the elastic-

plastic interphase reaches a maximum value and a milder singularity or the singularity does not exist.

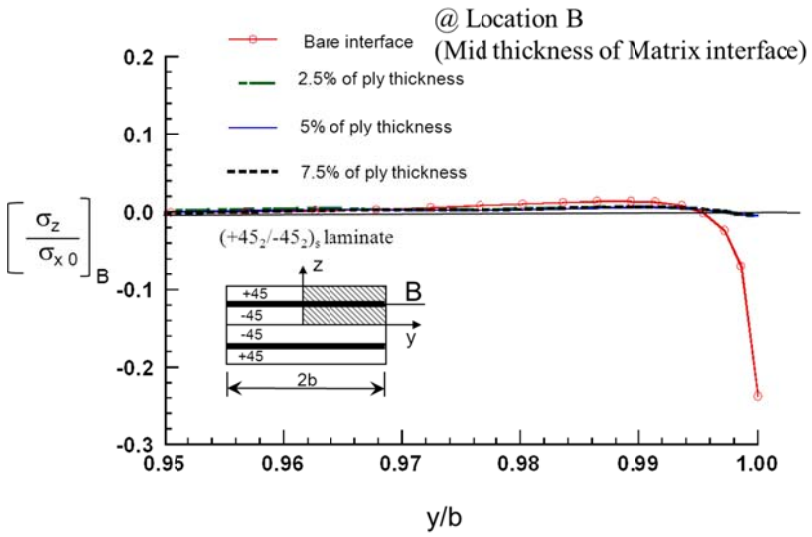

Figure 3.50 Distribution of normal stress σ_z across the width for $(+45_2/-45_2)_s$ laminate at the mid-thickness of the interphase (B), for Elastic-Plastic matrix material

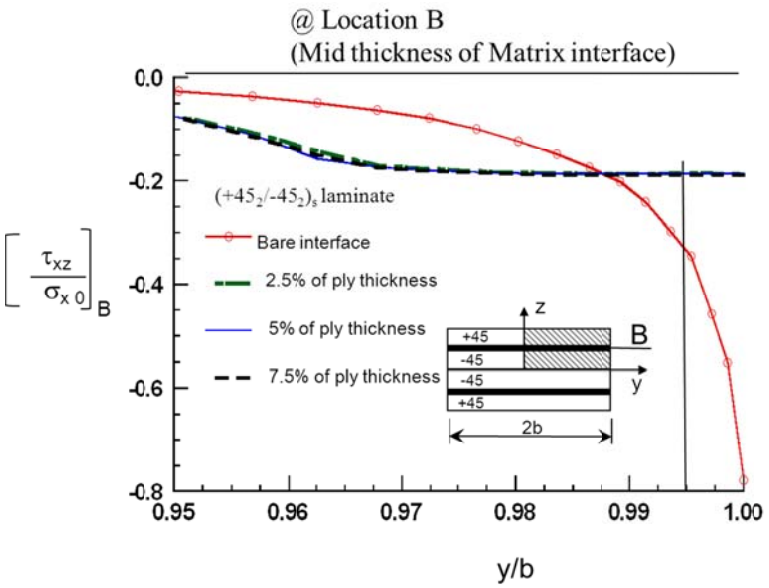

Figure 3.51 Distribution of interlaminar shear τ_{xz} across the width for $(+45_2/-45_2)_s$ laminate at the mid-thickness of the interphase (B), for Elastic-Plastic matrix material

Interlaminar edge stress analysis for $(+45_{10}/-45_{10})_s$ has been performed and the results are similar to the 2-ply case. These plots along with additional through the thickness plots for $(+45_2/-45_2)_s$ have been shown in Appendix B.

Based on the analysis, both laminates with interphase and without the resin interphase layer for angle ply $(+45_{10}/-45_{10})_s$ nearly the same results. There is a considerable change in stress field by introducing an elastic-plastic resin layer.

3.5.3.3 Cross-ply $(0_2/90_2)_s$ laminate with a Non-Linear interphase

Figure 3.52 shows distribution of interlaminar normal stress σ_z at location B, the stress becomes singularity at the bare interface while the stress is finite and much lower for non-linear resin layer. The σ_z decreases as the non-linear thickness increases.

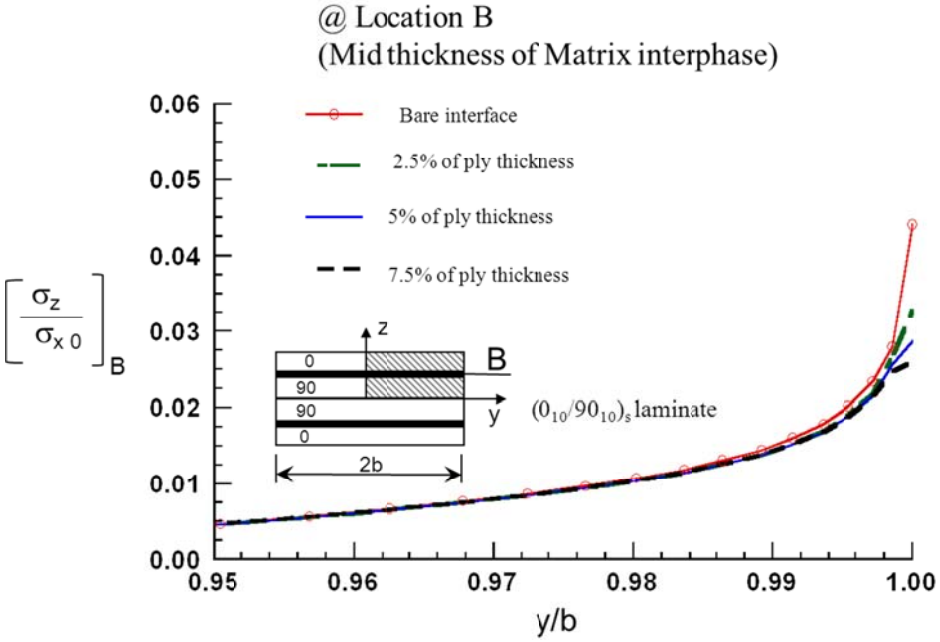

Figure 3.52 Distribution of interlaminar normal stress σ_z across the width for $(0_2/90_2)_s$ laminate at the mid-thickness of the interphase (B), for non-linear matrix material

Figure 3.53 shows the distribution of shear stress (τ_{yz}) for bare interface and different interphase thickness for elastic-plastic material for $(0_2/90_2)_s$ laminate at location B, the stresses are lower for the resin interphase than the bare interface and turn towards zero. The stresses reduce as the interphase layer becomes thicker.

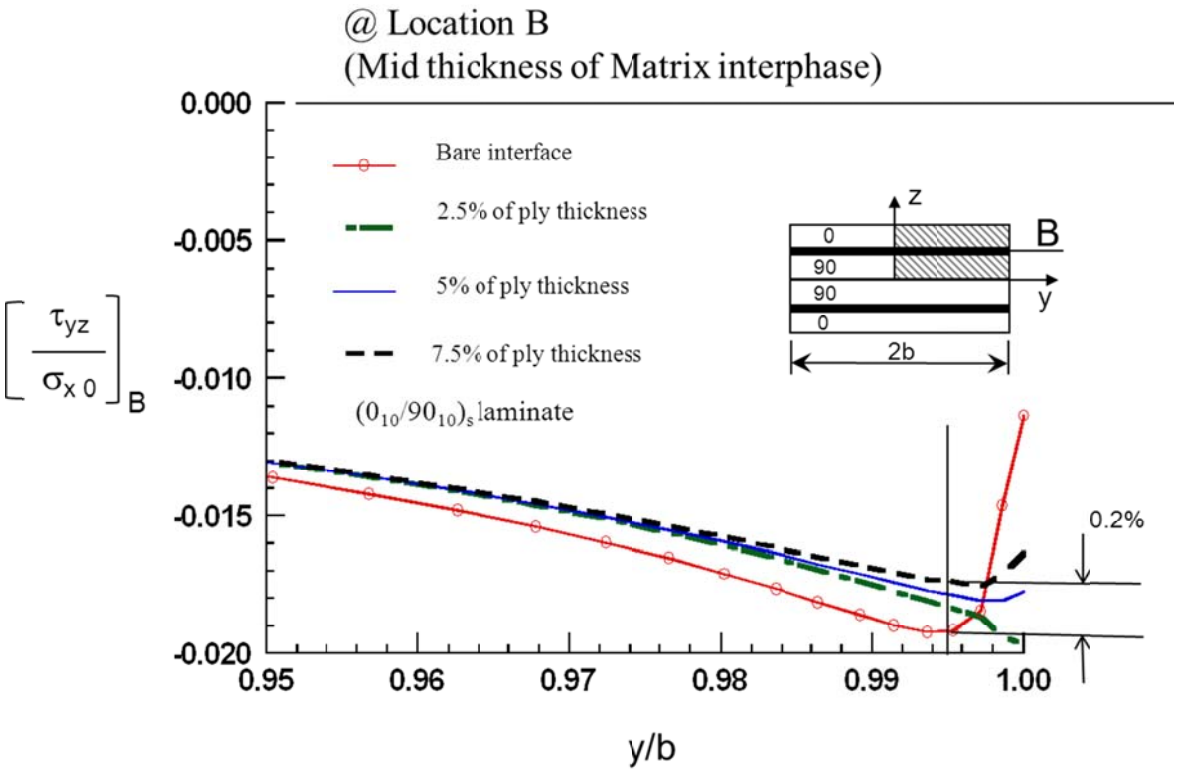

Figure 3.53 Distribution of interlaminar shear τ_{xz} across the width for $(0_2/90_2)_s$ laminate at the mid-thickness of the interphase (B), for non-linear matrix material

Interlaminar edge stress effect studies have also been performed for $(0_{10}/90_{10})_s$ laminate with elastic-plastic interphase and is similar to 2-ply case, these figures along with additional through the thickness figures are presented in Appendix C.

Based on the analysis there is no significant reduction in the normal stress σ_z for the change in thickness or the change in the material type at 1% closer to the edge. However, there is a significant reduction in τ_{yz} at the free edge of the interphase compared to the bare interface.

3.5.3.4 Angle-ply $(+45_2/-45_2)_s$ laminate with a Non-Linear interphase

Figure 3.54 shows the variation of normal stress distribution across the width of the specimen for $(+45_2/-45_2)_s$ laminate, for different thickness of the interphase closer to the edge near the 0° lamina for a non-linear interphase. The normal stresses are compressive and is mathematically singular at the edges for the bare interface, However, for the non-linear interphase for different thickness shows the stress are very close to zero and do not show the presence of singularity as expected.

Additional plots for 10 ply thickness laminate and through the thickness plots showed similar results as the 2-ply case and are presented in Appendix C. They all show results that are similar to the 2 ply thick. Hence the ply grouping did not generally change the trend of the stress values.

In summary a non-linear resin layer interphase between +45 and -45 plies reduces both σ_z and τ_{yz} to finite value and very much smaller than σ_x.

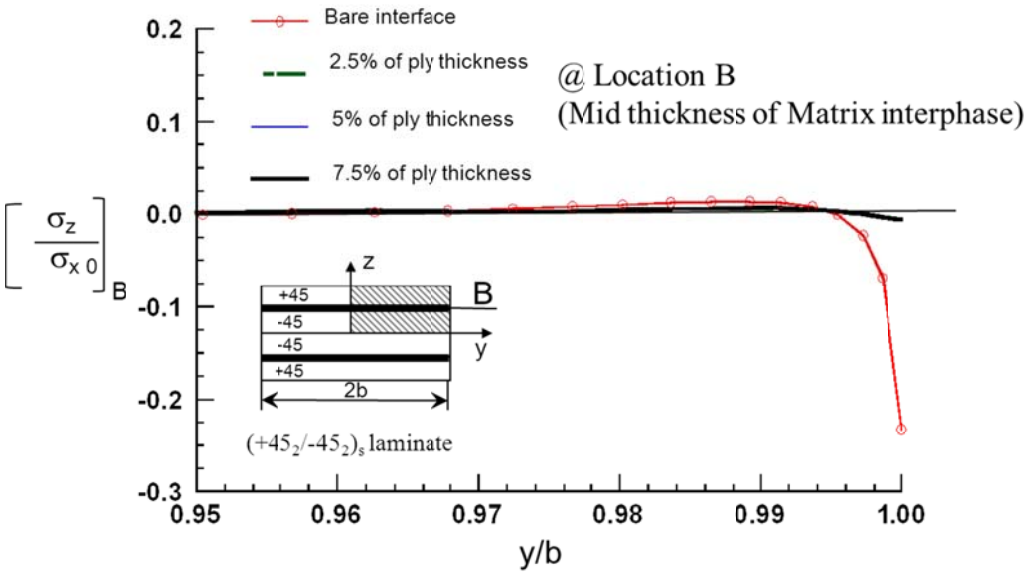

Figure 3.54 Distribution of interlaminar normal stress σ_z across the width for $(45_2/-45_2)_s$ laminate at the mid-thickness of the interphase (B), for non-linear matrix material

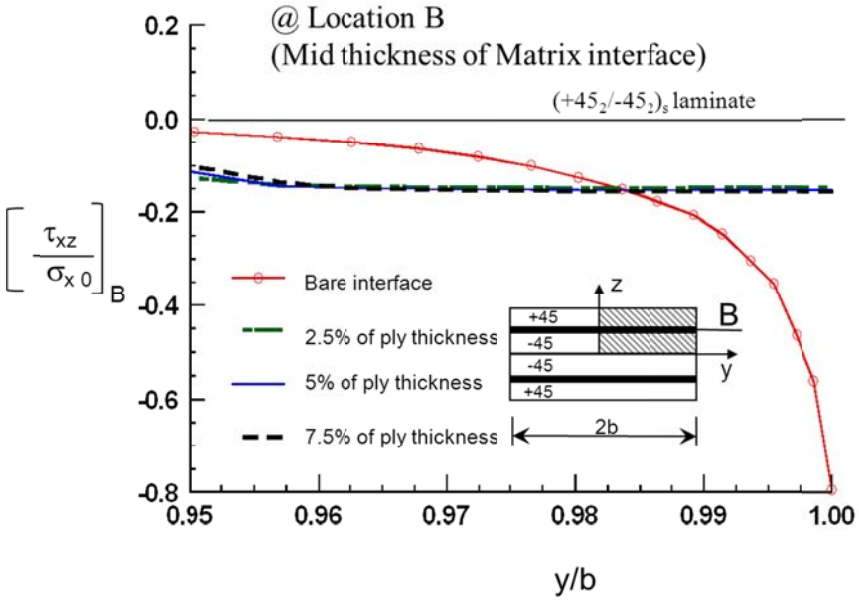

Figure 3.55 Distribution of interlaminar shear τ_{xz} across the width for $(+45_2/-45_2)_s$ laminate at the mid-thickness of the interphase (B), for non-linear matrix material

Based on the analysis of the laminates with elastic-plastic and non-linear interphase the following conclusions can be made, addition of interphase layer with an elastic-plastic or non-linear interphase may eliminate the mathematical singularity effect for the interlaminar edge stresses for both $(0_n/90_n)_s$ and $(+45_n/-45_n)_s$ laminates. The interlaminar normal stresses have near zero values at the edges for $(+45_n/-45_n)_s$ laminates for the model with interphase compared to the bare interface model. The interlaminar shear stresses are lower for the interphase model compared to the bare interface and plateaus in the regions closer to the free edges,

3.6 Summary

FEA analysis was conducted for a composite laminate $(0_2/90_2)_s$ and $(+45_2/-45_2)_s$ with a resin layer between the differently oriented plies. The thickness of the resin layer considered was 2.5%, 5.0% and 7.5% of the ply thickness. Elastic, elastic-plastic and non-linear properties were used for modeling the resin layer.

The analysis showed that the resin interphase layer reduced interlaminar stress near the edge; for a thin resin layer the bare interface results were recovered. The non-linear resin layer significantly reduced the interlaminar stresses at the edges and their values were finite and small. Therefore, using a non-linear resin matrix could be a viable approach to mitigate edge stresses in composite laminate.

In addition, the effect of the ply grouping was examined for n ranging from one to twelve. The edge distance (based on the 0.05% axial stress criteria) is about 1.25 times

the laminate thickness for $(0_n/90_n)s$ laminate and varies from 1.75 to 0.6 times the laminate thickness for ply grouping of one to twelve for $(+45_n/-45_n)_s$ laminate.

CHAPTER 4

INTERLAMINAR STRESSES DUE TO TEMPERATURE CHANGE IN COMPOSITE LAMINATES

As stated previously in Chapter 1, the interlaminar stresses exists interlaminar edge stresses also exist at the interphase for loading due to environmental effects such as temperature and moisture. In this chapter, the effect of an uniform thermal loading with and without the interphase region has been analyzed and the interlaminar stresses are assessed at different regions of the laminate. Also, the effect of edge stresses have been studied for different material interphases.

4.1 Interlaminar stresses in laminates due to thermal loading

Figure 4.1a shows the geometry of the laminate and loading of incremental temperature change ΔT= 100°F (37.7°C). This temperature change has been applied for the entire laminate. Figure 4.1b and c shows the first laminate stacking sequence considered which is the $(0_n/90_n)_s$ and $(+45_n/-45_n)_s$ respectively.

To study the physical effect of the thermal loading, Figure 4.2 and Figure 4.3 show the free body diagram of $(0_n/90_n)_s$ laminate under uniform thermal loading. The 0° lamina experiences a very small amount of linear thermal expansion in the longitudinal direction because the co-efficient of thermal expansion is low in this direction, but in the

lateral direction the width undergoes a expansion of Δw. For the 90°, the lamina experiences a higher expansion in the longitudinal direction of ΔL.

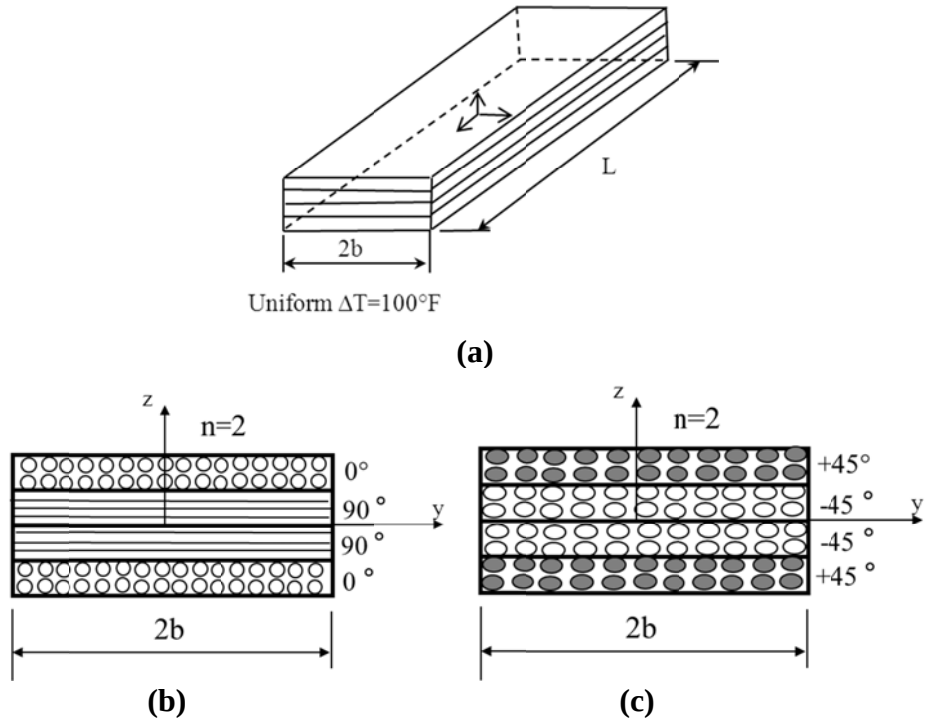

Figure 4.1 Geometric Model of laminate (a) Geometry and loading (b) $(0/90)_s$ laminate (c) $(+45/-45)_s$ laminate

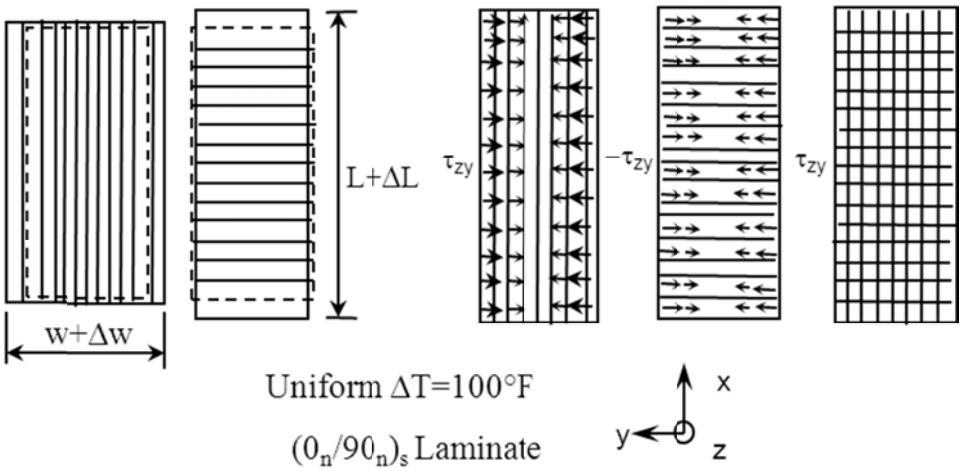

Figure 4.2 Free body diagram for $(0_n/90_n)_s$ laminate under uniform thermal loading

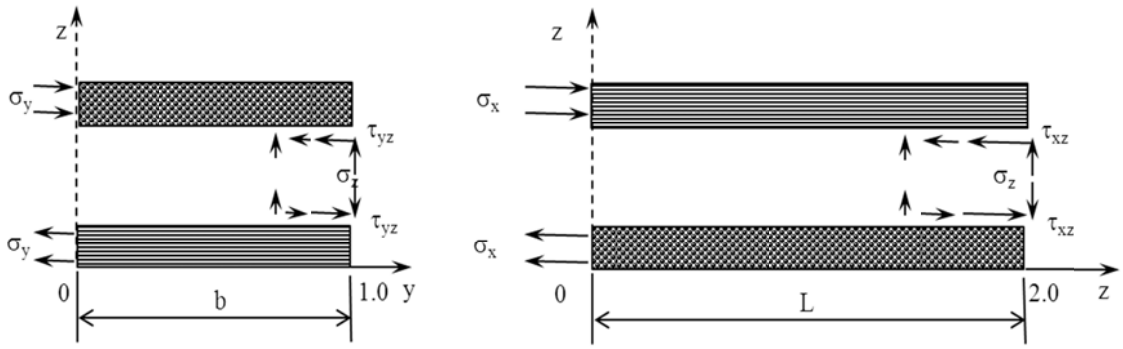

Figure 4.3 Free body diagram for a laminate under thermal loading for cross section of the laminate (a) Longitudinal cross section, (b) Lateral cross section

The expansion is very low in the lateral direction. When the two layers are bonded together the layers get pulled in the opposite direction against the thermal expansion, due the effect of push and pull between the layers shear stress in τ_{yz} exists at the interphase and in order to satisfy moment equilibrium condition of the laminate, the normal stress σ_z exists at the region closer to the free edges. However, in the longitudinal direction the stresses should exist at the free edges since the 0° layer expands much lower than the 90° layer. From the free body diagram in Figure 4.3b, similar to the longitudinal section the free edge of the laminate in x-direction also experiences interlaminar edge stresses. Because of the push and pull and to satisfy the moment equilibrium condition the shear stress τ_{xz} and σ_z exists at the region closer to the free edges. The stresses in the free edge in the longitudinal direction have not been studied in this research.

For the $(+45_n/-45_n)_s$ laminate the free body diagram has been shown in Figure 4.4. In this case the +45 layer the thermal expansion will deform the layer in the diagonal direction lateral to the fibers, for the -45 layer the thermal expansion happens on the

opposite side. When the two layers are bonded together they are pulled back to the rectangular shape. Due to the effect of layer deformation the shear stress τ_{yz} exists at the free edge. To satisfy the moment equilibrium τ_{xy} exists. Also, the transverse normal σ_z stress exists. Hence the normal stress σ_z and shear stress τ_{xz} exists in the laminate under thermal loading for $(+45_n/-45_n)_s$ laminate.

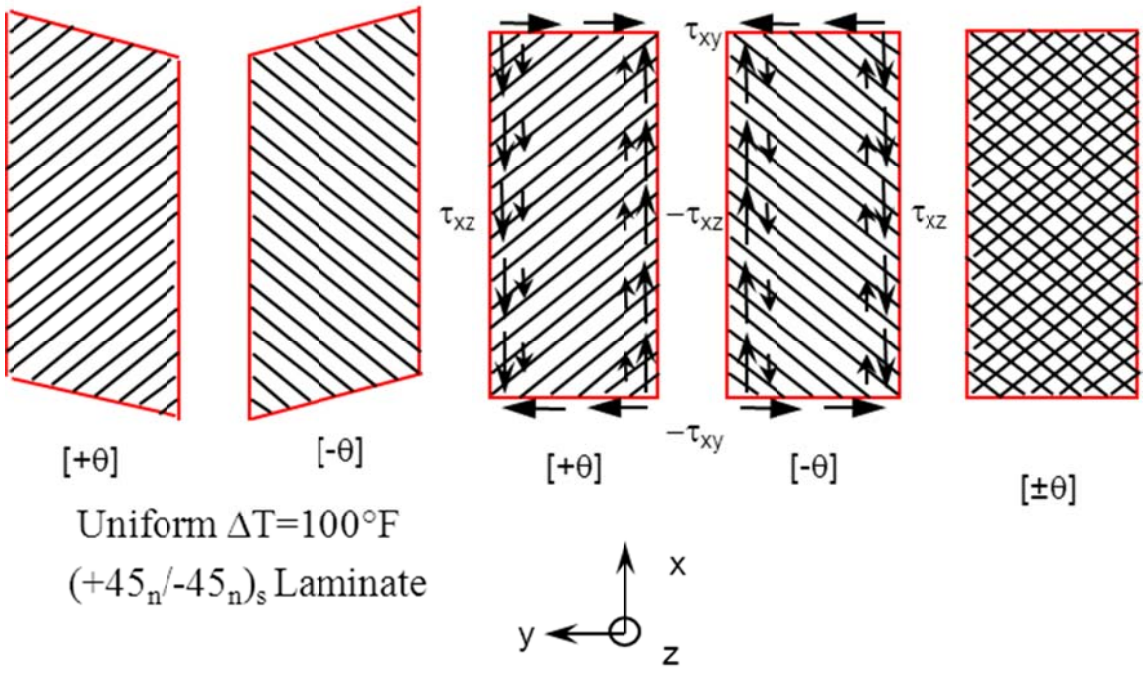

Figure 4.4 Freebody diagram of $(+45_n/-45_n)_s$ laminate under thermal loading

4.2 Material, mathematical modeling and FEA

The unidirectional material property of AS4/3501-6 carbon/epoxy used for the laminate has been shown in

Table 2.1. The interphase material to represent the realistic material model considered for the thermal loading analysis is the same as in section 3.4.

The geometry of the model is the same as the ones used in the previous section. Here also the FE model used is of a $1/8^{th}$ symmetric model with a uniform thermal loading of 100° F. Figure 4.5 shows the schematic of the full model and the symmetric model considered for this analysis. The FEA model used in this analysis is also the same as the one described on section 3.6.

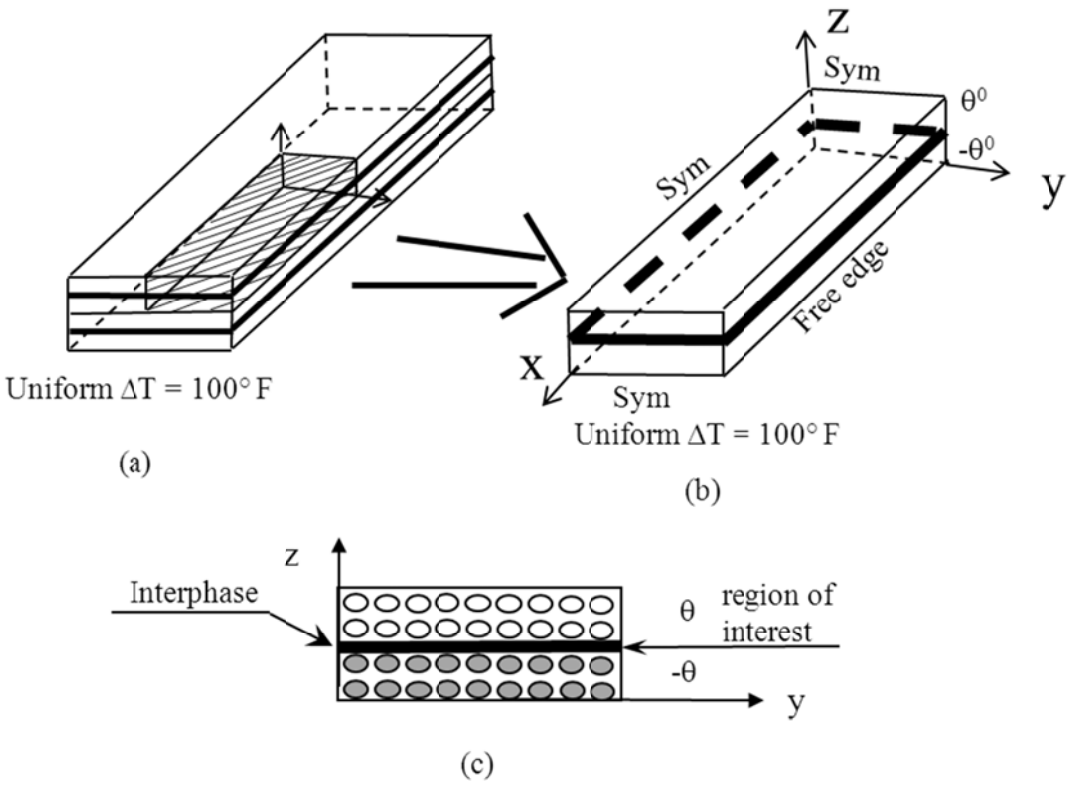

Figure 4.5 Mathematical Model (a) Full model of laminate, (b) Symmetric $1/8^{th}$ Model, (c) Cross Section of $1/8^{th}$ model

4.3 Verification of Modeling

Interlaminar stresses due to uniform thermal loading were also studied. (Wang and Crossman, 1977) and (Nguyen and Caron, 2009) have studied this on the bare interface between $(0/90)_s$ and $(+45/-45)_s$ laminates. In order to validate the current model so that the model can be used for further analysis, the present results have been compared to the results from previous literature. A new layer-wise finite element was used in order to under thermal load (Nguyen and Caron, 2009). Finite element analysis was used to study the effect of thermal loading on the laminates. The stress results across the width and thickness have been presented in psi/°F. Based on the previous studies, Figure 4.6 shows the stress distribution of σ_z psi/ °F across the width of the specimen comparing the current results with that of results in the literature, as shown in the free body diagram the interlaminar normal stress exists and it has a similar response as the tensile specimen. Figure 4.7 shows the interlaminar edge shear stress τ_{yz} psi/°F across the width of the specimen for $(0/90)_s$ laminate, the response is the same effect as compared to the tensile specimen. To ensure continuity of the stress response thought the thickness Figure 4.8 shows the comparison of the stress response for the present model with that of research in (Nguyen and Caron, 2009).

Based on the results for validation of the models, it shows that the model is good for further work to analyze the interlaminar stresses with interphase at the free edge.

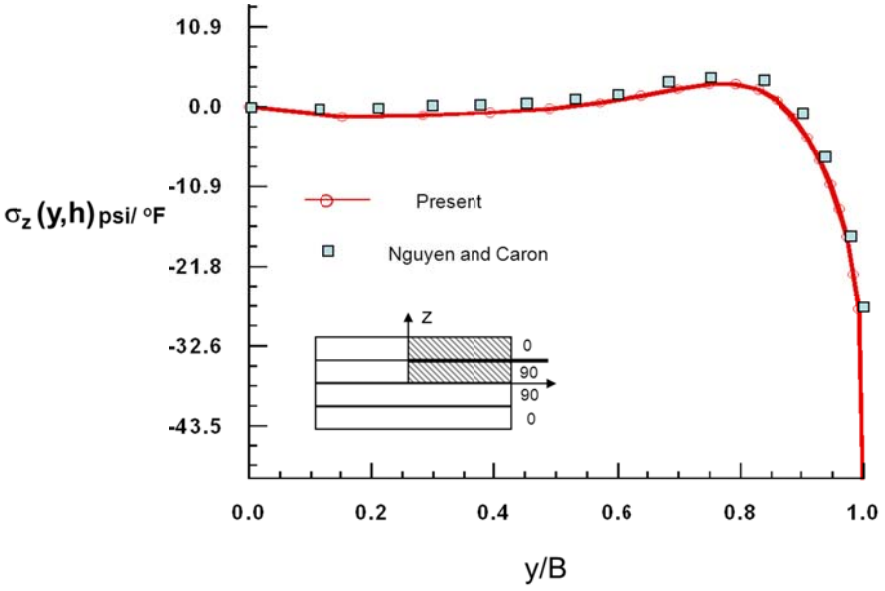

Figure 4.6 Distribution of interlaminar normal stress σ_z across the width for comparison with literature for $(0/90)_s$ laminate, bare interface for unit thermal loading

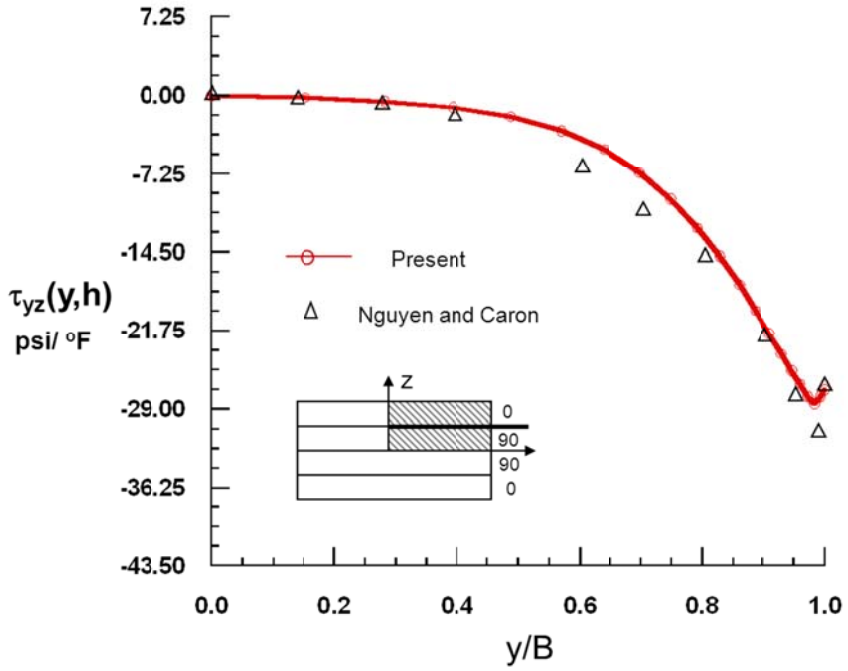

Figure 4.7 Distribution of interlaminar shear stress τ_{yz} across the width for comparison with literature for $(0/90)_s$ laminate, bare interface for unit thermal loading

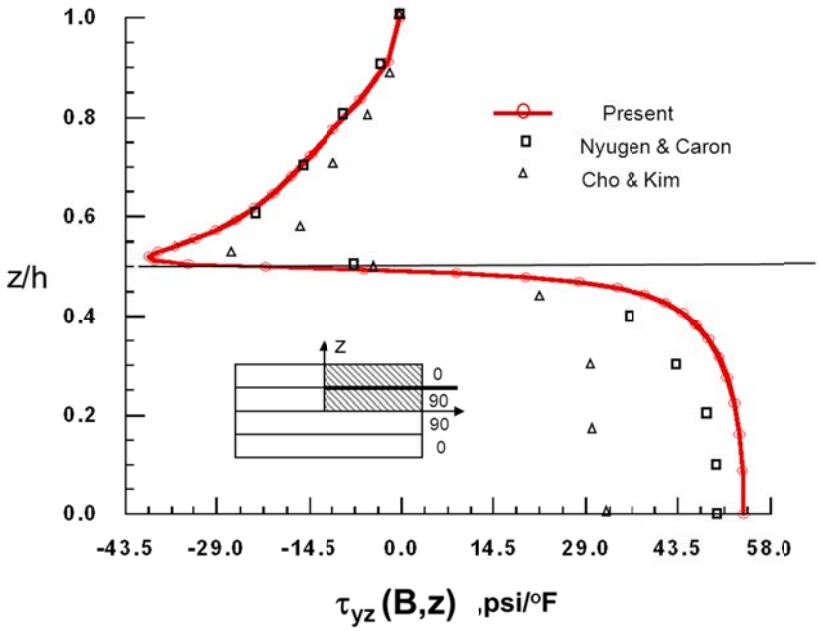

Figure 4.8 Normalized τ_{xz} Stress distribution through the thickness for $(0/90)_s$ laminate at free edge

Similarly, analysis was performed on $(+45/-45)_s$ laminate for effect on change in temperature and has been shown in Figure 4.9 for normal stress agree very well with those from the literature. However, in this case the length of the laminate had to be increased 10 times in order to avoid anti-clastic bending similar to the model used in the literature. Figure 4.10 shows the shear interlaminar edge stress across the width of the specimen here the stress distribution in the current results shows that it is sharper compared to the results in literature, this is attributed to the finer mesh used in the present analysis compared to the literature.

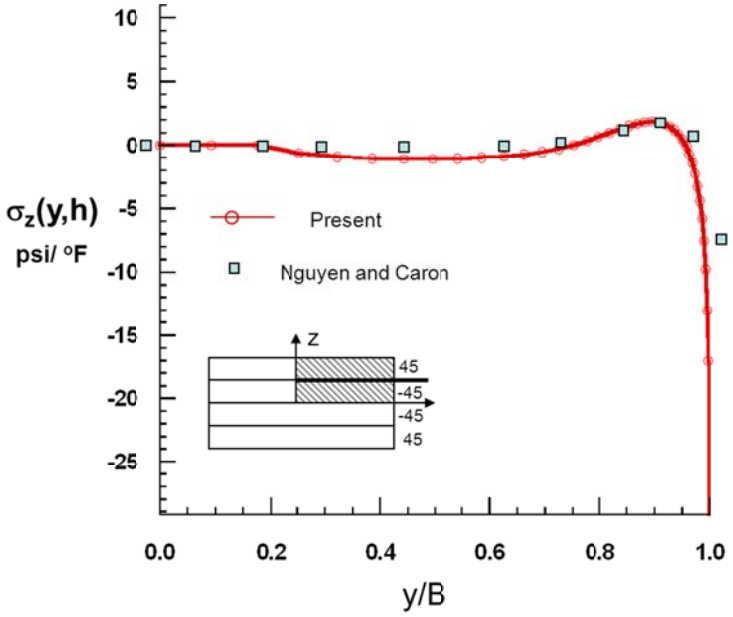

Figure 4.9 Distribution of interlaminar normal stress σ_z across the width for comparison with literature for $(+45/-45)_s$ laminate, bare interface for unit thermal loading

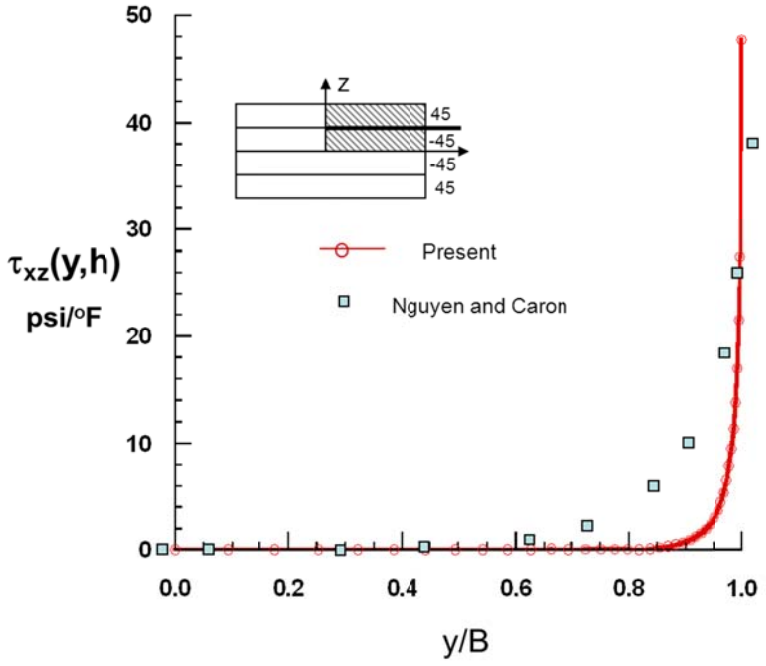

Figure 4.10 Distribution of interlaminar shear stress τ_{yz} across the width of the specimen for comparison with literature for (+45/-45)s laminate, bare interface for unit thermal loading

4.4 Results

The results of the thermal analysis for $(0_n/90_n)_s$ and $(+45_n/-45_n)_s$ laminates has been presented in this section. First, the results from comparison of different resin interphase thickness using a linear elastic material with bare interface are derived. Then the results from comparison of different interphase material such as elastic-plastic and nonlinear material for 5.0% thickness of the interphases are presented.

4.4.1 Interlaminar analysis of realistic laminate

The existence of matrix interphase layer between the two differently oriented lamina had been ignored in the analysis that has been performed in previous literature. In this section the results comparing the interlaminar stress results for bare interface and effect of changing the interphase thickness of 2.5%, 5.0% and 7.5% are presented. The results from this will show the effect of adding the interphase layer between two differently oriented lamina on the interlaminar edge stresses for the $(0_n/90_n)_s$ and $(+45_n/-45_n)_s$ laminate for thermal loading.

Figure 4.11 shows the distribution of interlaminar normal stresses (σ_z) for $(0_2/90_2)_s$ across the width of the specimen closer at location 5.0% closer to the free edge. The stress distribution is very similar to the $(0_2/90_2)_s$ tensile specimen where in the normal stresses are 0 in the middle section of the laminate and the increases towards the free edges, here the stresses range from 1 psi/ °F to -16 psi/ °F. Based on the figure it can be concluded that the interphase thickness of 2.5%-7.5% has minimum effect on the normal stress compared to the bare interface, except the free edge where the singularity

effect vanishes for the model at the free edges for model with interphase. The stress values at the free edges are also lower compared to the bare interface.

Figure 4.12 shows the distribution of interlaminar shear stresses (τ_{yz}) for $(0_2/90_2)_s$ across the width of the specimen closer at location 5.0% closer to the free edge. The stress distribution ranges from 0 psi/ °F to 4 psi/ °F. Based on the figure it can be concluded that using the resin interphase in the model the shear stress trends to zero faster for the resin interphase layer than the bare interface model. The stress values at the free edges are also lower compared to the bare interface.

Figure 4.13 shows the normal stress distribution across the width for $(45_2/-45_2)_s$ for uniform thermal loading comparing bare interface with different interphase thicknesses 2.5, 5.0 and 7.5% of the ply thickness The stresses have near zero values in the region far away from the free edge of the laminate and increases to 5 psi/ °F. From the figure it can be seen that the addition of interphase layer has no significant effect on the stress prediction except for the free edges where the effect of the singularity vanishes for the model with interphase. The stress values at the free edges are also lower compared to the bare interface.

Figure 4.14 shows the plot of interlaminar shear stresses (τ_{yz}) for $(45_2/-45_2)_s$ across the width of the specimen closer at location 5.0% closer to the free edge. The stress distribution of the model with interphase is same as that of the bare interface, but the magnitude of stresses is lower. The stress values at the free edges are also lower compared to the bare interface.

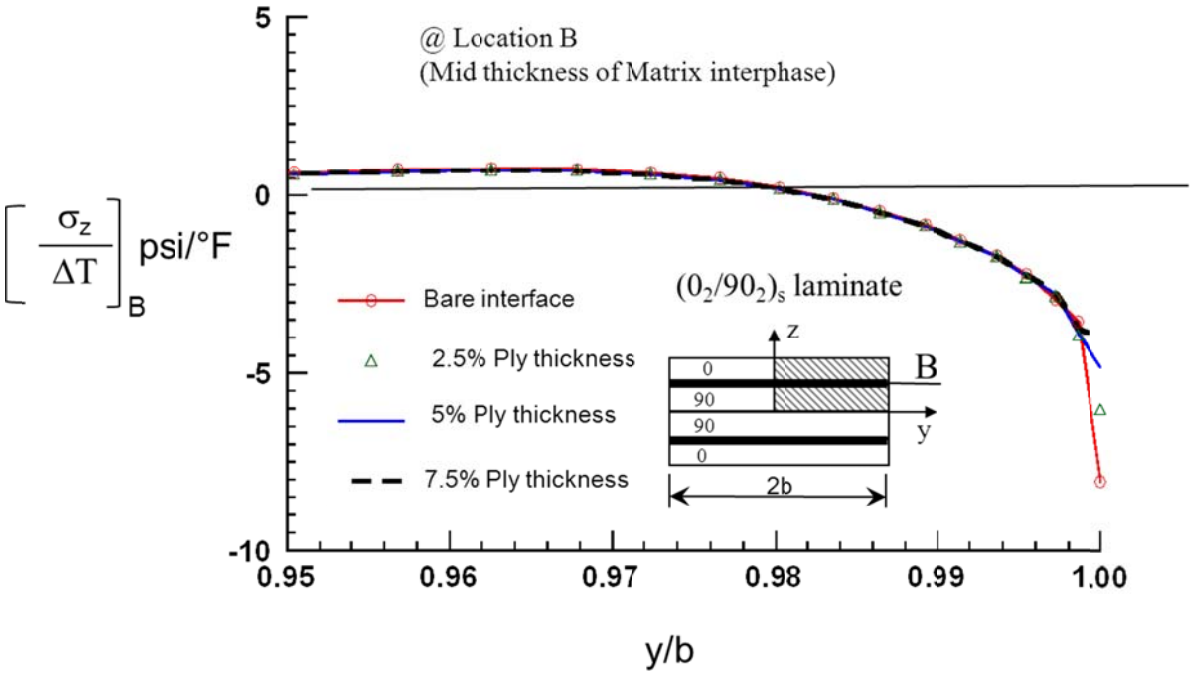

Figure 4.11 Distribution of interlaminar normal stress σ_z across the width for $(0_2/90_2)_s$ laminate at the mid-thickness of the interphase (B), for comparing different matrix material thickness

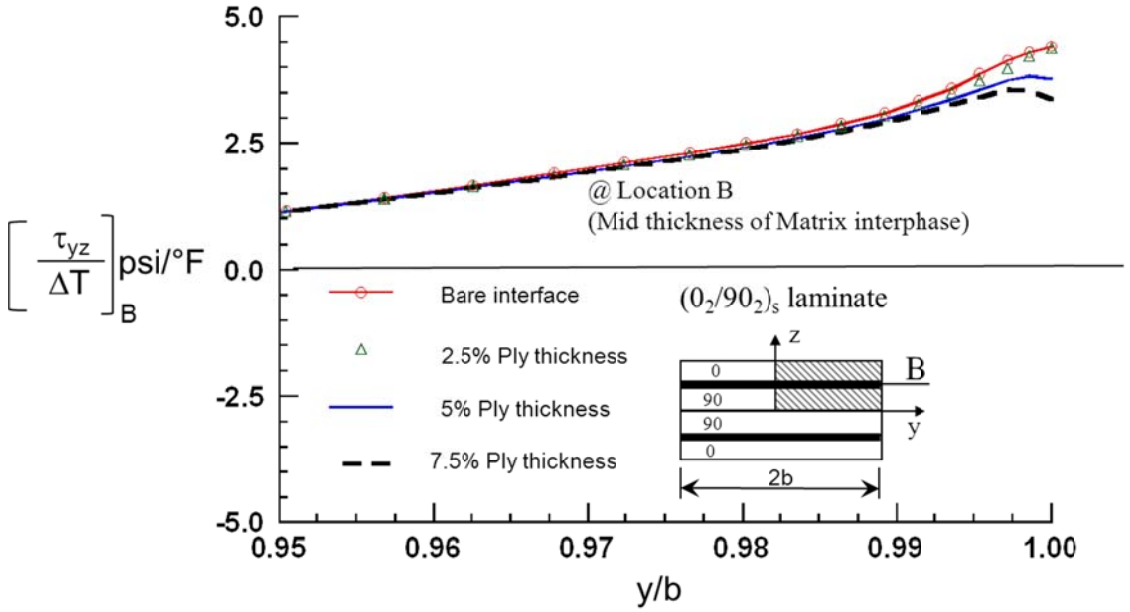

Figure 4.12 Distribution of interlaminar shear stress τ_{yz} across the width for $(0_2/90_2)_s$ laminate at the mid-thickness of the interphase (B), for comparing different matrix material thickness

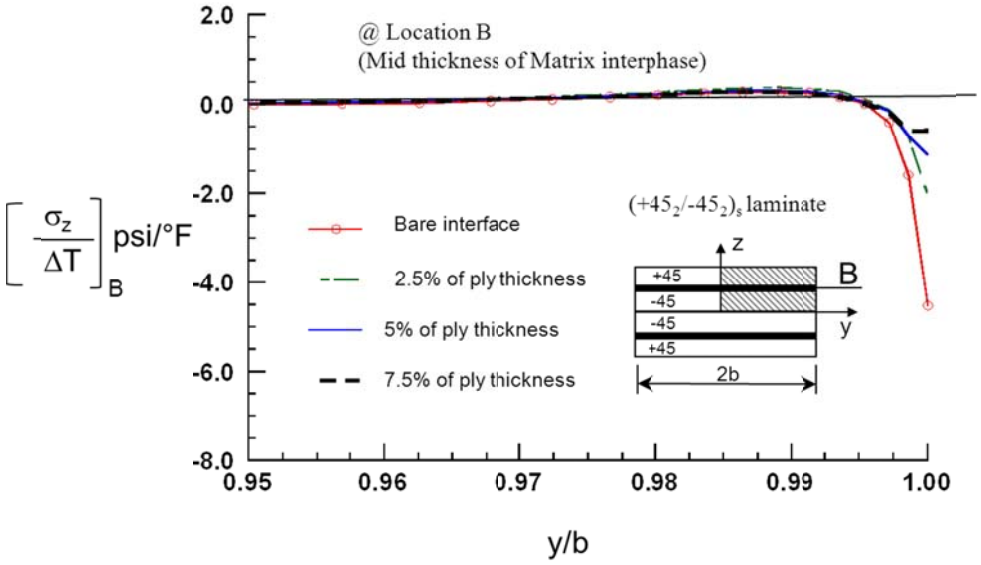

Figure 4.13 Distribution of interlaminar normal stress σ_z across the width for $(+45_2/-45_2)_s$ laminate at the mid-thickness of the interphase (B), for comparing different matrix material thickness

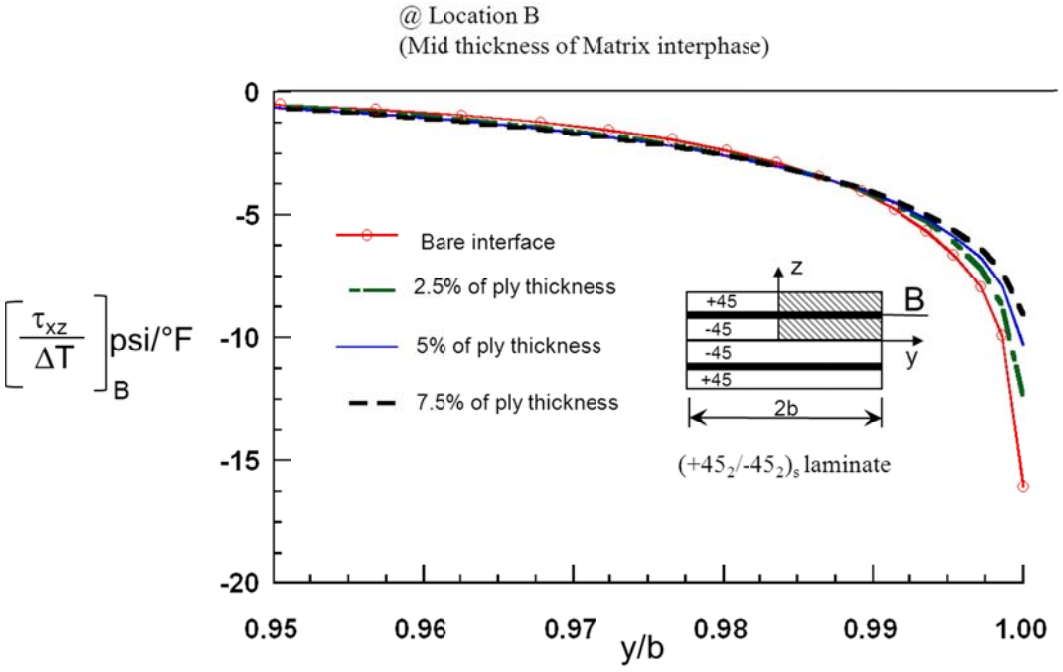

Figure 4.14 Distribution of interlaminar shear stress τ_{xz} across the width for $(+45_2/-45_2)_s$ laminate at the mid-thickness of the interphase (B), for comparing different matrix material thickness

Additional analysis for laminate with 10-plies have been conducted and the results have been shown in Appendix D. Based on the analysis the interlaminar edge stress distribution has no effect on addition of the interphase layer in the laminate model. As the thickness increases the singularity effect reduces. As the thickness of the interphase layer reduces the solution goes closer to the bare interface model.

4.4.2 Interlaminar analysis of different material interphases

Previous section showed the effect of interlaminar edge stresses for addition of a linear elastic matrix material at the interphase. In this section FE studies have been conducted to see the effect on the interlaminar edge stresses if the interphase is changed from elastic to elastic-plastic and non-linear to bring out the effect of plasticity at the interphase has been presented. This result will show if the use of a tougher interlayer such as the addition Electro-spun nano nylon 66 fibers will help in reducing the interlaminar edge stresses for the $(0_n/90_n)_s$ and $(+45_n/-45_n)_s$ laminate for thermal loading.

Figure 4.15 shows the distribution of interlaminar normal stresses (σ_z) for $(0_2/90_2)_s$ across the width of the specimen closer to the free edge for different material properties of the matrix interphase. The stress varies from zero in the region away from the laminate and increases closer to the free edge from 0-7psi/ °F. From the figure it can be seen that the stress response of the model with different material interphase show the same stress distribution on the interior of the free edge. However, at the free edge the effect of singularity vanishes.

Figure 4.16 shows the distribution of interlaminar shear stresses (τ_{yz}) for $(0_2/90_2)_s$ across the width of the specimen closer at location 5.0% closer to the free edge for

different material properties of the interphase. The stress distribution ranges from 0 psi/ °F to 4 psi/ °F. Based on the figure it can be seen that adding an interphase of an elastic-plastic or non-linear material has no influence on the stress response on the interior of the free edge. However, the stresses trend towards zero faster than that of the bare interface model. The stress values at the free edges are also lower compared to the bare interface model.

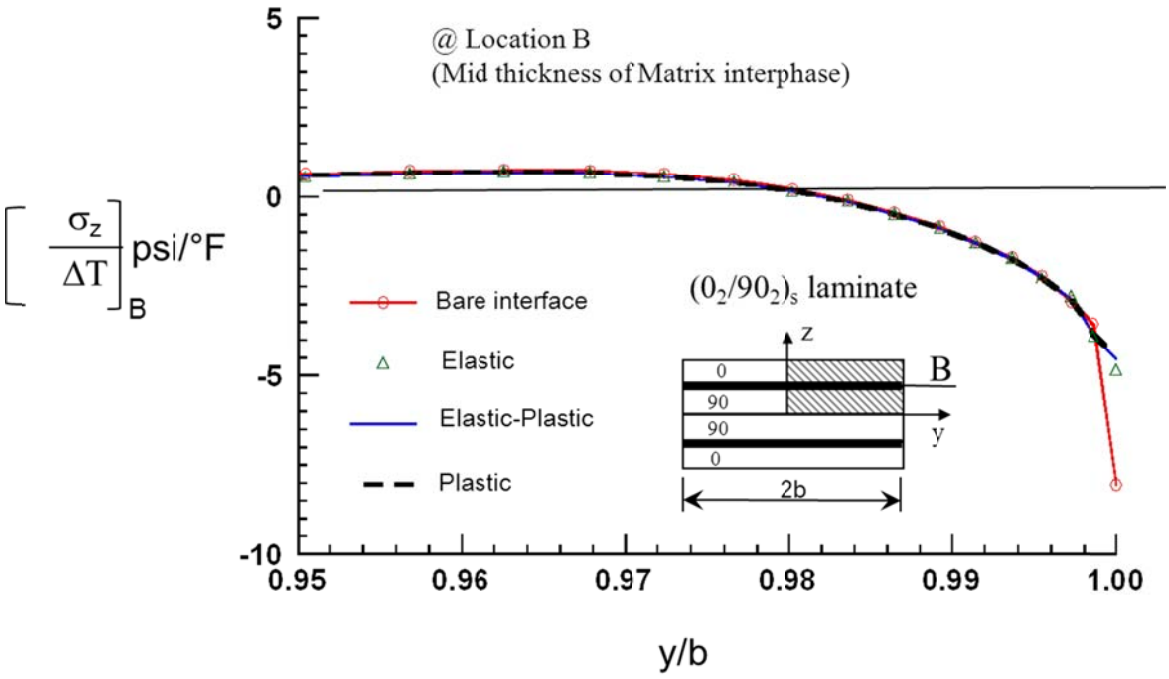

Figure 4.15 Distribution of interlaminar normal σ_z across the width for $(0_2/90_2)_s$ laminate at the mid-thickness of the interphase (B), for comparing different matrix material near the edge

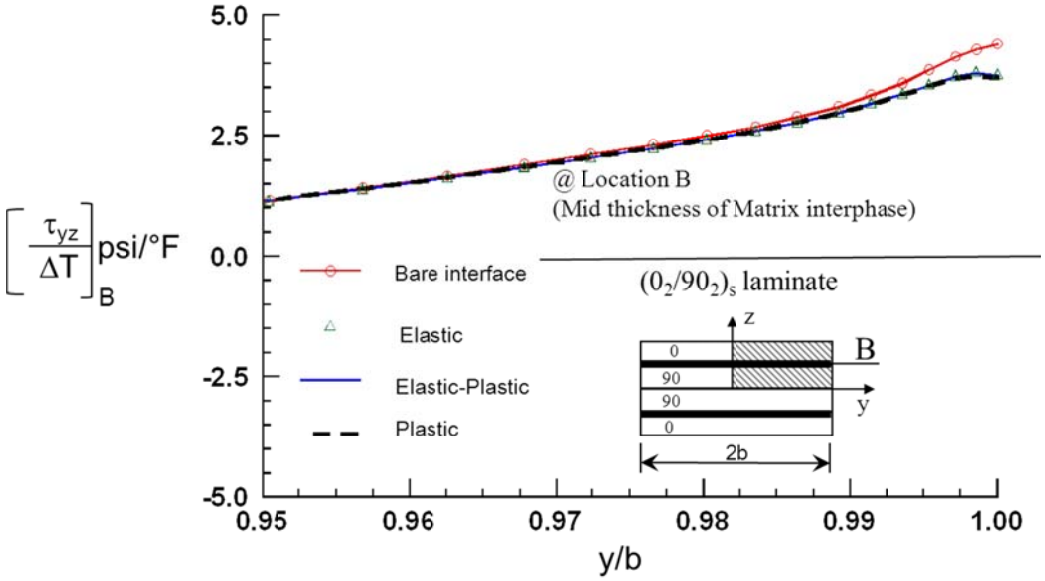

Figure 4.16 Distribution of interlaminar shear τ_{yz} across the width for $(0_2/90_2)_s$ laminate at the mid-thickness of the interphase (B), for comparing different matrix material near the edge

Figure 4.17 shows the distribution of interlaminar normal stresses (σ_z) for $(+45_2/-45_2)_s$ across the width of the specimen closer to the free edge for different properties of the interphase. The stress varies from 0 in the middle of the laminate and increases closer to the free edge from 0 to -5 psi/ °F. From the figure it can be seen that the interlaminar normal stresses are same for the entire width of the laminate except for the free edge where the effect of singularity stress are much lower for different interphase material compared to the bare interface .

Figure 4.18 shows the plot of interlaminar shear stresses (τ_{yz}) for $(+45_2/-45_2)_s$ across the width of the specimen closer at location 5.0% closer to the free edge for different material properties of the interphase. The stress distribution ranges from 0 psi/ °F to -16 psi/ °F. Based on the figure it can be concluded that using an elastic-plastic or a

non-linear interphase material in place resin interphase in the model does not have much effect on the stresses on the interior of the laminate. However, the stresses close to the free edge are lower and the effect of singularity vanishes.

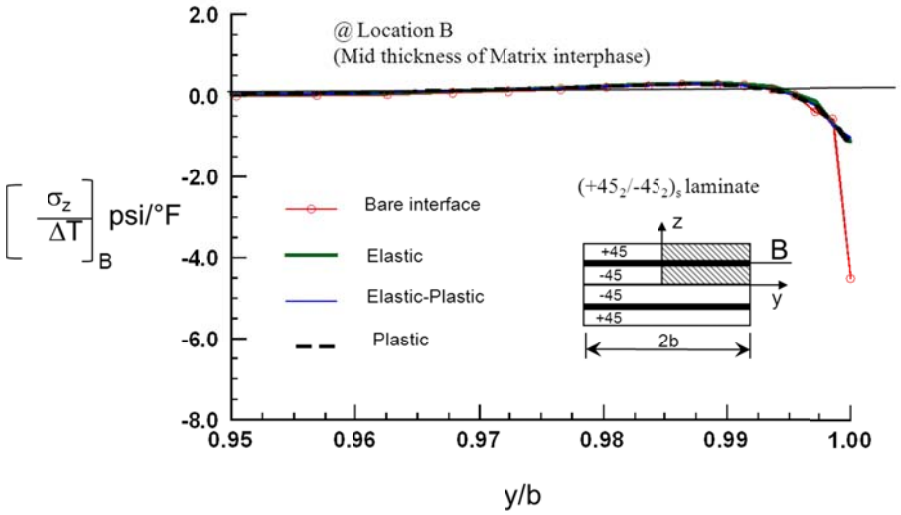

Figure 4.17 Distribution of interlaminar normal stress σ_z across the width for $(+45_2/-45_2)_s$ laminate at the mid-thickness of the interphase (B), for comparing different matrix material near the edge

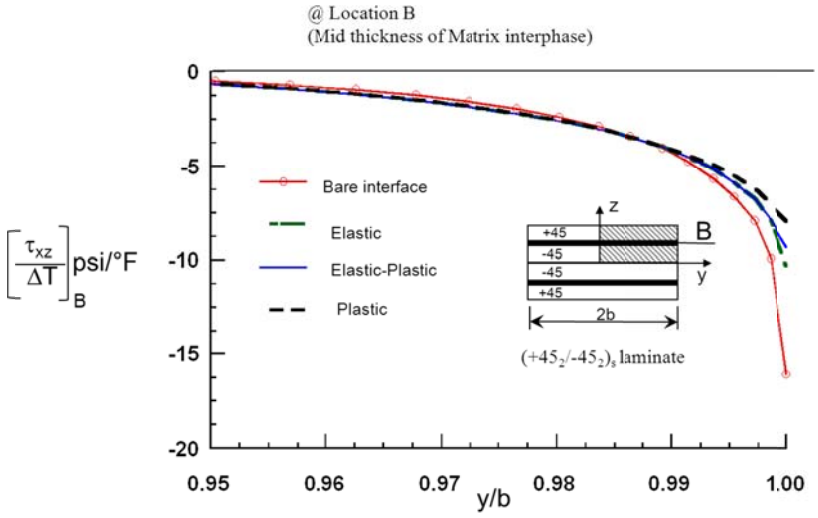

Figure 4.18 Distribution of interlaminar shear stress τ_{xz} across the width for $(+45_2/-45_2)_s$ laminate at the mid-thickness of the interphase (B), for comparing different matrix material. near the edge

Analyses for the effect of interlaminar edge stresses on a laminate with 10-plies have been conducted and the results show a similar response in comparison to bare interface model. These figures have been shown in Appendix D. Based on this analysis it can be concluded that the change in material properties from linear elastic material to elastic-plastic or non-linear material at the interphase did not have any effect on the stress response on the interior of the laminate. However, the effect on the singularities at the edges have been reduced considerably.

4.5 Summary

Effect of temperature change on interlaminar edge stresses for $(0_n/90_n)_s$ and $(+45_n/-45_n)_s$, laminate models was studied using the models that was used for tensile loaded laminate in Chapter 3. The elastic bare interface model analysis reproduced the results in the literature. In the elastic resin layer model the edge stresses were similar to that of the bare interface model. Whereas, the nonlinear resin layer model reduced both σ_z and τ_{xz} stresses at the edge to be finite values and are much lower than that of elastic resin layer model. Therefore, using a non-linear resin matrix could be a viable approach to mitigate edge stresses in composite laminates due to temperature change.

CHAPTER 5

CONCLUDING REMARKS AND FUTURE WORK

5.1 Concluding remarks

Edge delamination in composite laminates with adjacent layers oriented at different fiber angles is a major failure mode because of the existence of high interlaminar stresses and poor interlaminar properties. Mitigation of edge stresses poses a challenge even to date. This research provides a detailed analysis and a potential approach to solve this problem in a carbon/epoxy composite laminate. Two extreme laminates of stacking sequence $(0_n/90_n)_s$ and $(+45_n/-45_n)_s$ subjected to separately applied tensile and thermal loading were considered. These problems have been treated in the literature as a mathematical or bare interface model, wherein the material properties jumped between the adjacent layers of different fiber orientations. A microscopic analysis of laminate cross section showed that the interface was not really bare but there was a thin resin layer of thickness of about 5.0% of the ply thickness. This realization completely changed the modeling and potential modification of the interphase.

The region between the plies was represented by a resin layer interphase. A three-dimensional composite finite element (FE) analysis was performed using ANSYS version 12 code. The FE modeling and analysis were verified with the literature for both $(0/90)_s$ and $(+45/-45)_s$ laminates for axial tensile loading as well as temperature change. The resin interphase layer with thicknesses of 2.5%, 5.0% and 7.5% of the ply thickness were

modeled using three different material properties representing: elastic (brittle epoxy), elastic-plastic (toughened epoxy) and non-linear (interleaved polymer nanofiber composite). As the layer thickness became zero, the bare interface results were recovered. Then, for non-linear resin layer the edge stresses reduced indicating that the interleaving of interphase region had a potential to mitigate edge stresses and thus the edge delamination failure.

The FE modeling and analysis were verified with the literature for both $(0/90)_s$ and $(+45/-45)_s$ laminates for axial tensile loading as well as temperature change. The laminate of length 'L', width '2b' and thickness 't' subjected to uniform tensile strain of 1% was modeled by 3D SOLID46 elements. Because of the symmetry $1/8^{th}$ of the laminate was modeled for $(0_n/90_n)_s$ laminate and the same model was used for $(+45_n/-45_n)_s$ laminate. A mesh refined concept of finer elements near high stress gradient region was followed. A converged refined model had 3,200 elements and 25,600 nodes was used for detailed investigation.

5.1.1 Validation of bare interface models

The bare interface models for $(0_n/90_n)_s$ and $(+45_n/-45_n)_s$ laminates subjected to tensile loading were analyzed. Calculated the interfacial interlaminar normal and shear stresses and were compared with the work of Nguyen and Caron (Nguyen and Caron, 2009) and Wang and Crossman (Wang and Crossman, 1977) and have been found to agree very well. The analysis was repeated for thermal loading and the results were also found to agree well with work of Nguyen and Caron (Nguyen and Caron, 2009).

The bare interface analysis was extended to study the ply grouping (n), for n=1, 2, 4, 6 and 10. The result concluded that edge stress distance is 1.25 times the thickness of the laminate for $(0_n/90_n)_s$ and varied between 1.75 to 0.80 as the ply thickness increases from 1 to 12

5.1.2 Resin layer interphase model with tensile loading

Three thicknesses of resin layer models were analyzed 2.5%, 5.0% and 7.5% of ply thickness, which represent 50%, 100% and 150% of the estimated thickness of resin layer in AS4/3501-6 carbon/epoxy composite. Three types of resin properties were used: (1) elastic (brittle), (2) elastic-plastic (toughened) and (3) non-linear, a polymer nano fabric reinforced resin. Interlaminar stresses (σ_z, τ_{yz} and τ_{xz}) were examined near the free edge and were compared with bare interface results.

The conclusions from these analyses are:

Elastic resin

- The interlaminar edge stresses were same as the bare interface model results for thin resin
- As the thickness of the resin interphase layer increased, the edge stresses reduced.
- Thick resin interphase layer reduces the interlaminar stresses at the edges but also could potentially reduce the in plane properties of the laminate.
- The effect of ply grouping on the laminate due to the addition of resin interphase layer remained the same as the bare interface model.

Elastic-plastic and non-linear resin

- The magnitude of the edge stresses (σ_z and τ_{yx}) were reduced and did not show the

singularity effect as in case of bare interface model.

- The use of resin interphase modeling reduced the interlaminar edge stress compared to bare interface modeling.
- The non-linearity effect can be achieved by using an interphase layer consisting of an Electro-spun polymer nano fiber with resin.

5.1.3 Effect of thermal loading

Temperature or the moisture change in composite laminate also causes edge stresses in a loaded laminate because of differential expansion coefficient in different directions. Temperature and moisture have similar effect. In this research only the temperature change was investigated. Both the bare interface and resin layer interphase models with three different interlayer thicknesses and three material properties were analyzed for a temperature increment of 100°F. Interlaminar stresses at mid-length of the specimen were examined. These results showed the following conclusion:

- The elastic bare interphase model can reproduce the results in the literature
- The results from elastic resin interphase model has similar trend as the bare interface model
- Nonlinear resin interphase reduced both σ_x and τ_{xz} stresses to be finite and much lower than the elastic resin interphase.

Finally, use of a non-linear resin layer made of combining ductile polymer nano-fibers and resin matrix can be a viable approach to mitigate the edge stress in composite laminate under thermal loading as well as mechanical loading.

5.2 Future work

The present research was focused on analysis of edge stresses and their mitigation by polymer nanofiber resin composite layer. Based on this study, it is important to conduct the following research:

- Results of the present analyses needs to be validated with experiments.
- In the present analysis a hypothetical resin layer properties were used at the interphases, however, the analysis needs to be repeated with actual electrospun Nylon 66 nano-fabric/Epoxy properties.
- Combined concept of "thin ply" and polymer nanofiber interleaved composite needs to be examined to determine the combined effect.

REFERENCES

ANSYS® Theory Reference. (2009). Ansys, Inc.

Adams, E., and Shivakumar, K. (2011). Mitigation of Edge Delamination in Polymeric Composites by Polymer Nanofabric Interleaving – Static Tensile Test. *ICCM.*

Akangah, P., Lingaiah, S., and Shivakumar, K. (2011). Effect of Nylon-66 nano-fiber interleaving on impact damage resitance of epoxy/cabon fiber composite laminate. *Composite Structures, 92*, 1432-1439.

Becker, W., Peng Jin, P., and Neuser, P. (1999). Interlaminar stresses at the free corners of a laminate. *Composite Structures, 45*, 155-162.

Chan, W. S., and Jumbo, D. E. (1986). A Comparision of the Structural Behavior of Laminates made of Knitted Nonwoven Fabric and Lamiantes made of Conventional Unidirectional tapes. *SAMPE J, 22*, 21-26.

Chan, W. S., Rogers, C., and Aker, S. (1986). Improvement of Edge Delamination Strength of Composite Laminates Using Adhesive Later. *ASTM STP 893, 266*, 266-285.

Chella, P. R., and Shivakumar, K. (2001). mmTEXlam – A Graphical user Interfaced Design Code for Laminated Textile Fabric Composites. *AIAA*, 1571. Retrieved from http://www.ncat.edu/~ccmradm/ccmr/mmtexlam4.html

Crews, J. H., Shivakumar, K. N., and Raju, I. S. (1986, November). Factors Influencing Elastic Stresses in Double Cantilever Beam Specimens. *Adhesively Bonded Joints: Testing, Analysis, and Design, ASTM STP 981, W. S. Johnson, Ed) American Society for Testing and Materials*, 49.

Crews, J. H., Shivakumar, K. N., and Raju, I. S. (1988, Januvary). Fiber-Resin Micromechanics Analysis of Delamination Front. *NASA TM 100540.*

Daniel, I. M., and Isahi, O. (1994). *Engineering Mechanics of Composite Materials.* New York: Oxford University Press Inc.

Flanagan, G. (1994). An efficient stress function approximation for the freeedge stresses in laminates. *Int J Solids Struct, 31*, 941-952.

Hojo, M., Matsuda, S., Tanaka, M., Ochiai, S., and Murakami, A. (2006). Mode I Delamination fatigue properties of interlayer-Toughened CF/epoxy laminates. *Compostie Science and Technology*, 665-675.

Howard, W. E., Gossard, T. J., and Jones, R. M. (1986). Reinforcement of composite laminate free-edges with U-shaped caps. *AIAA,Paper No 86-0972*.

Howard, W. E., Gossard, T., and Jones, R. (1986). Reinforcement of composite laminate free edges with U-shaped caps. *27th Structures, Structural Dynamics and Materials Conference*, 472-485.

Icardi, U., and Bertetto, A. (1995). An evaluation of the influence of geometry and of material properties at free edges and at corners of composite laminates. *Comput Struct, 57*, 555–571.

Jones, R. M. (1975). *Mechanics of Composite Materials.* New York: Hemisphere Publishing Corporation.

Kassapoglou, C., and Lagace, P. A. (1987). Closed form solutions for the interlaminar stress field in angle-ply and cross-ply laminates. *J Comput Mater, 21*, 292–308.

Kim, R. Y. (1983). Prevention of Free-edge Delamination. *Proc. 28th National SAMPE Symp*, (pp. 200-209).

Lagace, P. A., Mong, R. L., and Khulmann, C. W. (1993). Suppression of delaminateion in a gradient stress field in graphite/epoxy laminates. *Proc. ICCM-9*, (pp. 705-713).

Lekhnitskii, S. (1963). Theory of Elasticity of an Anisotropic Body. *Holden Day, San Fransisco*.

Lessard, L. B., Schmidt, A. S., and Shokrieh, M. M. (1996). Three-dimensional stress analysis of free-edge effects in a simple composite cross-ply laminate. *Int J Solids Struct, 33*(15), 2243–2259.

Lingaiah, S., Shivakumar, K., and Sadler, R. (2008). Electrospinning of Nylon-66 Polymer nano-fabrics. *AIAA*, (p. 1787).

Lorriot, T., Marion, G., Harry, R., and Wargnier, H. (2003). Onset of free-edge delamination in composite laminates under tensile loading. *Composites: Part B, 34*, pp. 459-471.

Mignery, L., Tam, T., and Sun, C. (1985). The use of stitiching to suppress Delamination in laminated composite. *ASTM STP 876 W.S.Johnson, Ed, American Socienty of Testing and Materials*, pp. 371-385.

Mittelstedt, C., and Wilfried, B. (2003). Free-corner Effects in Cross-ply Lamiantes : An approximate Higher oder Theroy Solution. *Journal of Composite Materials, 37*, 2043-2068.

Nguyen, V., and Caron, J. (2009). Finite element analysis of free-edge stresses in composite laminates under mechanical an thermal loading. *Composites Science and Technology, 69*, 40-49.

Pagano, N. J. (2004). Stress fields in composite laminates. *Int J Solids Struct, 14*, 385-400.

Pipes, B. R., and Pagano, N. J. (1970). Interlaminar stresses in composite laminates under uniform axial extension. *J Comput Mater, 4:*, 538–548.

Raju, I. S., and Crews, J. H. (1981). Interlaminar stress singularities at a straight free edge in composite laminates. *Comput Struct, 14*, 21–28.

Raju, I. S., Crews, J. H., and Amanpour, M. A. (1988). Convergence of strain energy release rate components for edge delaminated composite laminates. *Engineering Fracture Mechanics, 30*(3), 383-396.

Reddy, J. N. (1987). A generalization of two-dimensional theories of laminated composite plates. *Commun Appl Numer Meth, 3*, 173-180.

Reissner, E. (1950). On Variational Theorem in Elasticity. *Journal of Mathematical Physics, 29*, 90.

Rybichi, E. F. (1971). Approximate three-dimensional solutions for symmetric laminates under in plane loading. *J Comput Mater, 5*, 354–360.

Sihn, S., Kim, R. Y., Kazumasa, K., and Tsai, S. W. (2007). Expertimental studies of thin=ply lamianted composite. *Composite Science and Technology, 67*, 996-1008.

Smith, S., and Shivakumar, K. (2001). Modified Mode-I Cracked Sandwich Beam (CSB) Fracture Test. *AIAA paper*, 2001-1221.

Sun, C., and Chu, G. (1991). Reducing Free Edge Effect on Laminate Strength by Edge Modification. *Compos. Mater, 25*(142), 142-161.

Tahani, M., and Nosier, A. (2003). Free edge stress analysis of general cross-ply composite laminates under extension and thermal loading. *Composite Structures, 60*, 91-103.

Tahani, M., and Nosier, A. (2003). Three-dimensional interlaminar stress analysis at free edges of general cross-ply composite laminates. *Material Design, 24*, 121-130.

Tang, S., and Levy, A. (1975). A boundary layer theory – part II: extension of laminated finite strip. *J Compos Mater, 9*, 42–52.

Tanimoto, T. (2002). Interleaving methodology for property tailoring of CFRP laminates. *Composite Interfaces, 9*(1), . 25–39.

Wang, A., and Crossman, F. W. (1977). Edge Effects on Thermally Induced Stresses in Composte laminates. *Journal of Composte Materials, 11*, 300-312.

Wang, A., and Crossman, F. W. (1977). Some new results on the edge effect in symmetric composite laminates. *J Compos Mater, 11*, 92–106.

Wang, S. S., and Choi, I. (1982). Boundary-layer effects in composite laminates: part1 – free-edge stress singularities. *J Appl Mech*, 541-548.

Wang, S. S., and Choi, I. (1982). Boundary-layer effects in composite laminates: Part2 – free-edge stress singularities. *J Appl Mech, 49*, 549-560.

Wang, S. S., and Choi, I. (1982). Infulence of Fiber Orientation and Ply Thickness on Hygroscopic Boundary-Layer Stresses in Angle-Ply Composite Laminate. *Journal of Composite Materials, 16*, 244-258.

Williams, M. W. (1952). Stress singularities resulting from various boundary conditions in angular corners of plates in extension. *Journal of applied mechanics*, 20-28.

APPENDIX A

APDL CODE USED IN THIS RESEARCH

This section shows a typical APDL script used for the analysis of the interlaminar stresses.

```
!-----------------------------------
!  Comments
!-----------------------------------
/COM,3-D Full Model: 5x1x0.12 model Plain stress condition
/TITLE,Solid46, 00/90 laminate., width 40 unequal Division , 1/8th model W/gCGEN = 4 Ele
!Non-Linear analysis for an interleaved Elastic Plastic specimen in Tensile model
! of Crack length vs width of specimen
/BEGIN
/CONFIG,NCONT,7000
/NERR,200000,200000
/PREP7
!---------------------------------
! Define all the Required Variables
!---------------------------------
*DIM,NODY11,,div1   ! List of Nodes belonging to the Line in Y Axis
*DIM,NODY12,,div1   ! List of Nodes belonging to the Line in Y Axis
*DIM,NODY13,,div1   ! List of Nodes belonging to the Line in Y Axis
*DIM,NODY14,,div1   ! List of Nodes belonging to the Line in Y Axis
*DIM,NODY15,,div1   ! List of Nodes belonging to the Line in Y Axis
*DIM,NODY16,,div1   ! List of Nodes belonging to the Line in Y Axis
*DIM,NODY17,,div1   ! List of Nodes belonging to the Line in Y Axis

*DIM,NODZ1,,div2   ! List of Nodes belonging to the Line in Z Axis
*DIM,NODZ2,,div2   ! List of Nodes belonging to the Line in Z Axis
*DIM,NODZ3,,div2   ! List of Nodes belonging to the Line in Z Axis
*DIM,NODZ4,,div2   ! List of Nodes belonging to the Line in Z Axis
*DIM,NODZ5,,div2   ! List of Nodes belonging to the Line in Z Axis

*DIM,YLOCB,,div1    ! Location in Y Direction
*DIM,YLOCT,,div1    ! Location in Y Direction
*DIM,ZLOC,,div2    ! Location in Y Direction
```

```
*DIM,STXXYB,,div1
*DIM,STYYYB,,div1
*DIM,STXYYB,,div1
*DIM,STZZYB,,div1
*DIM,STYZYB,,div1
*DIM,STXZYB,,div1

*DIM,STXXYT,,div1
*DIM,STYYYT,,div1
*DIM,STXYYT,,div1
*DIM,STZZYT,,div1
*DIM,STYZYT,,div1
*DIM,STXZYT,,div1

*DIM,STXXZ,,div2
*DIM,STYYZ,,div2
*DIM,STXYZ,,div2
*DIM,STZZZ,,div2
*DIM,STYZZ,,div2
*DIM,STXZZ,,div2
!-----------------------------------
!  List of input parameters
!-----------------------------------
divx=5
div=40          ! Total No. of Divisions
grad=40         ! Gradient
div1=div+1
divz=16
gradz=16
div2=2*divz+5
theta = 0
!---------------------------------
!Scaler Parameters in Standard SYSTEM
!---------------------------------
L=2          !specimen length
W=0.5       !specimen width
t1=0.0475  !Specimen thickness 1
t2=0.0025!Specimen thickness for interleave
div1=div +1
grad2=1/grad
!-----------------------------------
!Element types
!-----------------------------------
```

```
ET,1,SOLID46        !Plane Stress 3-D 8-Noded Structural Solid ELEMENT
KEYOPT,1,2,0        !with KEYOPT(2)=0 i.e. Constant thickness layer input
!-----------------------------------
!Element types for interleave
!-----------------------------------
ET,2,SOLID45        !Plane Stress 3-D 8-Noded Structural Solid ELEMENT
!-----------------------------------
!Real Constants
!-----------------------------------
!-----for angle=+ theta deg.----------------------
r, 1, 1,0, 1,1, ,       ! Real 1 for Mat 1,NL, LSYM, LP1, LP2, ,,
rmore, 0, , , , ,   !  Kref=0 i.e. midplane ref.
rmore, 1,theta,0.005  ! Mat, theta, Thick.

!-----for angle=- theta deg.----------------------
r, 2, 1,0, 1,1, ,       ! Real 1 for Mat 1,NL, LSYM, LP1, LP2, ,,
rmore, 0, , , , ,   !  Kref=0 i.e. midplane ref.
rmore, 1,90, 0.005  ! Mat, theta, Thick.
!-----------------------------------
!Material properties1 -Standard System.
!-----------------------------------
MP,EX,1,20e6         !Orthotropic composite material
MP,EY,1,2.1e6        !convert Msi into Psi units
MP,EZ,1,2.1e6
MP,NUXY,1,0.022
MP,NUXZ,1,0.022
MP,NUYZ,1,0.21
MP,GXY,1,0.849e6
MP,GXZ,1,0.849e6
MP,GYZ,1,0.849e6
!-----------------------------------
!Material properties2 -Standard System.
!-----------------------------------
mptemp,1,0
mpdata,ex,2,,.3384e6,
mpdata,prxy,2,,0.3,
tb,MELAS,2,17
tbtemp,0
tbpt,defi,0,0,,,,,
tbpt,defi,0.0025,750,,,,,
tbpt,defi,0.005,1500,,,,,
tbpt,defi,0.0075,2300,,,,,
tbpt,defi,0.01,3100,,,,,
tbpt,defi,0.0125,3945.762,,,,,
```

```
tbpt,defi,0.015,4585.84,,,,,
tbpt,defi,0.0175,5294.56,,,,,
tbpt,defi,0.02,5717.78,,,,,
tbpt,defi,0.0225,6031.44,,,,,
tbpt,defi,0.025,6650.9,,,,,
tbpt,defi,0.0275,7159.06,,,,,
tbpt,defi,0.03,7734.76,,,,,
tbpt,defi,0.0325,8138,,,,,
tbpt,defi,0.035,8542.4,,,,,
tbpt,defi,0.0375,8946.8,,,,,
tbpt,defi,0.04,9399.6,,,,,
tbpt,defi,0.0425,9749.8,,,,,
!-----------------------------------
!Key points-Global
!-----------------------------------
k,1,0,0,0
k,2,0,w,0
k,3,L,w,0
k,4,L,0,0
k,5,0,0,t1
k,6,0,w,t1
k,7,L,w,t1
k,8,L,0,t1
k,9,0,0,(t1+t2)
k,10,0,w,(t1+t2)
k,11,L,w,(t1+t2)
k,12,L,0,(t1+t2)

k,13,0,0,(2*t1+t2)
k,14,0,w,(2*t1+t2)
k,15,L,w,(2*t1+t2)
k,16,L,0,(2*t1+t2)
!---------------------------------
!Volume of undelaminated part of specimen
!---------------------------------
v,1,2,3,4,5,6,7,8!Lam 1
v,5,6,7,8,9,10,11,12                !Interlayer
v,9,10,11,12,13,14,15,16 ! Lam 2
!-----------------------------------
! Turn model check off because of
! Shape warnings
!-----------------------------------
SHPP,OFF,ASPECT
!-----------------------------------
```

```
!Lesize for Length-10 lines
!---------------------------------
lesize,4,,,divx,grad2
lesize,12,,,divx,grad2
lesize,20,,,divx,grad2
lesize,28,,,divx,grad2


lesize,2,,,divx,grad
lesize,8,,,divx,grad
lesize,16,,,divx,grad
lesize,24,,,divx,grad
!---------------------------------
!Lesize for thickness- 24 lines
!---------------------------------
lesize,5,,,divz,1/gradz
lesize,13,,,4,1
lesize,21,,,divz,gradz


lesize,9,,,divz,gradz
lesize,17,,,4,1
lesize,25,,,divz,1/gradz
lesize,11,,,divz,gradz
lesize,19,,,4,1
lesize,27,,,divz,1/gradz
lesize,7,,,divz,gradz
lesize,15,,,4,1
lesize,23,,,divz,1/gradz
!---------------------------------
!Lesize for Width-10 lines
!---------------------------------
lesize,3,,,div,grad
lesize,10,,,div,grad
lesize,18,,,div,grad
lesize,26,,,div,grad
lesize,1,,,div,grad2
lesize,6,,,div,grad
lesize,14,,,div,grad
lesize,22,,,div,grad
!---------------------------------
!Meshing of laminates
!---------------------------------
type,1
```

```
mat,1
real, 2        !for 90 deg. angle
vmesh,1,1,1
allsel
type,2
mat,2          !for interleave
vmesh,2,2,1
allsel

type,1
mat,1
real,1         ! for 0 Deg angle
vmesh,3,3,1
allsel
!-----------------------------------
! Displacement boundary conditions
!-----------------------------------
NSEL,S,LOC,X,L,L
D,ALL,UX,0.02
ALLSEL
NSEL,S,LOC,X,0,0
D,ALL,UX,0
ALLSEL
!----------------------------------------
! Boundary condition for Symmetry
!----------------------------------------
NSEL,S,LOC,Y,0,0
D,ALL,UY,0
ALLSEL
NSEL,S,LOC,Z,0,0
D,ALL,UZ,0
ALLSEL
!-------------------------------------
! Solving the system
!-------------------------------------
NLGEOM,OFF
ANTYPE,0
OUTRES,ALL,ALL
ALLSEL
/SOL
/STATUS,SOLU
SOLVE
FINISH
!-------------------------------------
```

! Collecting the results
!----------
/POST26 ! Post Processing for Interlaminar Stresses
NUMVAR, 75 ! Set Max number of variables

! Node Numbers data in Y Axis
*set,NODY11(1),1640,1856,1871,1886,1901,1916,1931,1946,1961,1976,
*set,NODY11(11),1991,2006,2021,2036,2051,2066,2081,2096,2111,2126,
*set,NODY11(21),2141,2156,2171,2186,2201,2216,2231,2246,2261,2276,
*set,NODY11(31),2291,2306,2321,2336,2351,2366,2381,2396,2411,2426,
*set,NODY11(41),936

*set,NODY12(1),1641,1857,1872,1887,1902,1917,1932,1947,1962,1977
*set,NODY12(11),1992,2007,2022,2037,2052,2067,2082,2097,2112,2127
*set,NODY12(21),2142,2157,2172,2187,2202,2217,2232,2247,2262,2277
*set,NODY12(31),2292,2307,2322,2337,2352,2367,2382,2397,2412,2427
*set,NODY12(41),937

*set,NODY13(1),1626,1687,1691,1695,1699,1703,1707,1711,1715,1719
*set,NODY13(11),1723,1727,1731,1735,1739,1743,1747,1751,1755,1759
*set,NODY13(21),1763,1767,1771,1775,1779,1783,1787,1791,1795,1799
*set,NODY13(31),1803,1807,1811,1815,1819,1823,1827,1831,1835,1839
*set,NODY13(41),919

*set,NODY14(1),4532,4700,4703,4706,4709,4712,4715,4718,4721,4724
*set,NODY14(11),4727,4730,4733,4736,4739,4742,4745,4748,4751,4754
*set,NODY14(21),4757,4760,4763,4766,4769,4772,4775,4778,4781,4784
*set,NODY14(31),4787,4790,4793,4796,4799,4802,4805,4808,4811,4814
*set,NODY14(41),4356

*set,NODY15(1),4530,4543,4547,4551,4555,4559,4563,4567,4571,4575
*set,NODY15(11),4579,4583,4587,4591,4595,4599,4603,4607,4611,4615
*set,NODY15(21),4619,4623,4627,4631,4635,4639,4643,4647,4651,4655
*set,NODY15(31),4659,4663,4667,4671,4675,4679,4683,4687,4691,4695
*set,NODY15(41),4351

*set,NODY16(1),6547,6763,6778,6793,6808,6823,6838,6853,6868,6883
*set,NODY16(11),6898,6913,6928,6943,6958,6973,6988,7003,7018,7033
*set,NODY16(21),7048,7063,7078,7093,7108,7123,7138,7153,7168,7183
*set,NODY16(31),7198,7213,7228,7243,7258,7273,7288,7303,7318,7333
*set,NODY16(41),5843

*set,NODY17(1),6548,6764,6779,6794,6809,6824,6839,6854,6869,6884

```
*set,NODY17(11),6899,6914,6929,6944,6959,6974,6989,7004,7019,7034
*set,NODY17(21),7049,7064,7079,7094,7109,7124,7139,7154,7169,7184
*set,NODY17(31),7199,7214,7229,7244,7259,7274,7289,7304,7319,7334
*set,NODY17(41),5844

! Node Numbers data in Z Axis

*set,NODZ1(1),151,2068,2069,2070,2071,2072,2073,2074,2075,2076,
*set,NODZ1(11),2077,2078,2079,2080,2081,2082,1747,4744,4745,4746,
*set,NODZ1(21),4603,6988,6989,6990,6991,6992,6993,6994,6995,6996,
*set,NODZ1(31),6997,6998,6999,7000,7001,7002,6667
*set,NODZ2(1),175,2158,2159,2160,2161,2162,2163,2164,2165,2166,
*set,NODZ2(11),2167,2168,2169,2170,2171,2172,1771,4762,4763,4764,
*set,NODZ2(21),4627,7078,7079,7080,7081,7082,7083,7084,7085,7086,
*set,NODZ2(31),7087,7088,7089,7090,7091,7092,6691
,
*set,NODZ3(1),199,2248,2249,2250,2251,2252,2253,2254,2255,2256,
*set,NODZ3(11),2257,2258,2259,2260,2261,2262,1795,4780,4781,4782,
*set,NODZ3(21),4651,7168,7169,7170,7171,7172,7173,7174,7175,7176,
*set,NODZ3(31),7177,7178,7179,7180,7181,7182,6715

*set,NODZ4(1),223,2338,2339,2340,2341,2342,2343,2344,2345,2346,
*set,NODZ4(11),2347,2348,2349,2350,2351,2352,1819,4798,4799,4800,
*set,NODZ4(21),4675,7258,7259,7260,7261,7262,7263,7264,7265,7266,
*set,NODZ4(31),7267,7268,7269,7270,7271,7272,6739

*set,NODZ5(1),243,2413,2414,2415,2416,2417,2418,2419,2420,2421,
*set,NODZ5(11),2422,2423,2424,2425,2426,2427,1839,4813,4814,4815,
*set,NODZ5(21),4695,7333,7334,7335,7336,7337,7338,7339,7340,7341,
*set,NODZ5(31),7342,7343,7344,7345,7346,7347,6759

*cfopen,OUTY11-2-50Pc-thk-def-0090.txt
! Do Loop Begins Here
*DO,i,1,div1,1

! Location of the Nodes in Y
*GET,YLOCB(i),NODE,NODY11(i),LOC,Y

! Stress XX in Y axis
*GET, STXXYB(i), NODE, NODY11(i), S, X

! Stress YY in Y axis
*GET, STYYYB(i), NODE, NODY11(i), S, Y
```

```
! Stress ZZ in Y axis
*GET, STZZYB(i), NODE, NODY11(i), S, Z

! Stress xy in Y axis
*GET, STXYYB(i), NODE, NODY11(i), S, XY

! Stress yz in Y axis
*GET, STYZYB(i), NODE, NODY11(i), S, YZ
*ENDDO
! Stress xz in Y axis
*GET, STXZYB(i), NODE, NODY11(i), S, XZ
*vwrite,YLOCB(1),STXXYB(1),STYYYB(1),STZZYB(1),STXYYB(1),STYZYB(1),S
TXZYB(1)
('  'F7.4,'  '4F12.3,'  '4F12.3,'  '4F12.3,'  '4F12.3,'  '4F12.3,'  '4F12.3)

*cfclos


*cfopen,OUTY12-50Pc-thk-def-0090.txt
! Do Loop Begins Here
*DO,i,1,div1,1

! Location of the Nodes in Y
*GET,YLOCB(i),NODE,NODY12(i),LOC,Y

! Stress XX in Y axis
*GET, STXXYB(i), NODE, NODY12(i), S, X

! Stress YY in Y axis
*GET, STYYYB(i), NODE, NODY12(i), S, Y

! Stress ZZ in Y axis
*GET, STZZYB(i), NODE, NODY12(i), S, Z

! Stress xy in Y axis
*GET, STXYYB(i), NODE, NODY12(i), S, XY

! Stress yz in Y axis
*GET, STYZYB(i), NODE, NODY12(i), S, YZ
*ENDDO
! Stress xz in Y axis
*GET, STXZYB(i), NODE, NODY12(i), S, XZ
*vwrite,YLOCB(1),STXXYB(1),STYYYB(1),STZZYB(1),STXYYB(1),STYZYB(1),S
TXZYB(1)
```

```
(' 'F7.4,' '4F12.3,' '4F12.3,' '4F12.3,' '4F12.3,' '4F12.3,' '4F12.3)

*cfclos

*cfopen,OUTY13-50Pc-thk-def-0090.txt
! Do Loop Begins Here
*DO,i,1,div1,1

! Location of the Nodes in Y
*GET,YLOCB(i),NODE,NODY13(i),LOC,Y

! Stress XX in Y axis
*GET, STXXYB(i), NODE, NODY13(i), S, X

! Stress YY in Y axis
*GET, STYYYB(i), NODE, NODY13(i), S, Y

! Stress ZZ in Y axis
*GET, STZZYB(i), NODE, NODY13(i), S, Z

! Stress xy in Y axis
*GET, STXYYB(i), NODE, NODY13(i), S, XY

! Stress yz in Y axis
*GET, STYZYB(i), NODE, NODY13(i), S, YZ
*ENDDO
! Stress xz in Y axis
*GET, STXZYB(i), NODE, NODY13(i), S, XZ
*vwrite,YLOCB(1),STXXYB(1),STYYYB(1),STZZYB(1),STXYYB(1),STYZYB(1),S
TXZYB(1)
(' 'F7.4,' '4F12.3,' '4F12.3,' '4F12.3,' '4F12.3,' '4F12.3,' '4F12.3)
*cfclos
! Printing Results
*vwrite,YLOCB(1),STXXYB(1),STYYYB(1),STZZYB(1),STXYYB(1),STYZYB(1),S
TXZYB(1)
(' 'F7.4,' '4F12.3,' '4F12.3,' '4F12.3,' '4F12.3,' '4F12.3,' '4F12.3)
*cfclos
*cfopen,OUTY14-50Pc-thk-def-0090.txt
! Do Loop Begins Here
*DO,i,1,div1,1
! Location of the Nodes in Y
*GET,YLOCB(i),NODE,NODY14(i),LOC,Y
! Stress XX in Y axis
*GET, STXXYB(i), NODE, NODY14(i), S, X
```

```
! Stress YY in Y axis
*GET, STYYYB(i), NODE, NODY14(i), S, Y
! Stress ZZ in Y axis
*GET, STZZYB(i), NODE, NODY14(i), S, Z
! Stress xy in Y axis
*GET, STXYYB(i), NODE, NODY14(i), S, XY
! Stress yz in Y axis
*GET, STYZYB(i), NODE, NODY14(i), S, YZ
*ENDDO
! Stress xz in Y axis
*GET, STXZYB(i), NODE, NODY14(i), S, XZ
*vwrite,YLOCB(1),STXXYB(1),STYYYB(1),STZZYB(1),STXYYB(1),STYZYB(1),S
TXZYB(1)
(' 'F7.4,' '4F12.3,' '4F12.3,' '4F12.3,' '4F12.3,' '4F12.3,' '4F12.3)
*cfclos
*cfopen,OUTY15-50Pc-thk-def-0090.txt
! Do Loop Begins Here
*DO,i,1,div1,1
! Location of the Nodes in Y
*GET,YLOCB(i),NODE,NODY15(i),LOC,Y
! Stress XX in Y axis
*GET, STXXYB(i), NODE, NODY15(i), S, X
! Stress YY in Y axis
*GET, STYYYB(i), NODE, NODY15(i), S, Y
! Stress ZZ in Y axis
*GET, STZZYB(i), NODE, NODY15(i), S, Z
! Stress xy in Y axis
*GET, STXYYB(i), NODE, NODY15(i), S, XY
! Stress yz in Y axis
*GET, STYZYB(i), NODE, NODY15(i), S, YZ
*ENDDO
! Stress xz in Y axis
*GET, STXZYB(i), NODE, NODY15(i), S, XZ
*vwrite,YLOCB(1),STXXYB(1),STYYYB(1),STZZYB(1),STXYYB(1),STYZYB(1),S
TXZYB(1)
(' 'F7.4,' '4F12.3,' '4F12.3,' '4F12.3,' '4F12.3,' '4F12.3,' '4F12.3)
*cfclos
*cfopen,OUTY16-50Pc-thk-def-0090.txt
! Do Loop Begins Here
*DO,i,1,div1,1
! Location of the Nodes in Y
*GET,YLOCB(i),NODE,NODY16(i),LOC,Y
! Stress XX in Y axis
*GET, STXXYB(i), NODE, NODY16(i), S, X
```

```
! Stress YY in Y axis
*GET, STYYYB(i), NODE, NODY16(i), S, Y
! Stress ZZ in Y axis
*GET, STZZYB(i), NODE, NODY16(i), S, Z
! Stress xy in Y axis
*GET, STXYYB(i), NODE, NODY16(i), S, XY
! Stress yz in Y axis
*GET, STYZYB(i), NODE, NODY16(i), S, YZ
*ENDDO
! Stress xz in Y axis
*GET, STXZYB(i), NODE, NODY16(i), S, XZ
*vwrite,YLOCB(1),STXXYB(1),STYYYB(1),STZZYB(1),STXYYB(1),STYZYB(1),S
TXZYB(1)
(' 'F7.4,' '4F12.3,' '4F12.3,' '4F12.3,' '4F12.3,' '4F12.3,' '4F12.3)
*cfclos
*cfopen,OUTY17-50Pc-thk-def-0090.txt
! Do Loop Begins Here
*DO,i,1,div1,1
! Location of the Nodes in Y
*GET,YLOCB(i),NODE,NODY17(i),LOC,Y
! Stress XX in Y axis
*GET, STXXYB(i), NODE, NODY17(i), S, X
! Stress YY in Y axis
*GET, STYYYB(i), NODE, NODY17(i), S, Y
! Stress ZZ in Y axis
*GET, STZZYB(i), NODE, NODY17(i), S, Z
! Stress xy in Y axis
*GET, STXYYB(i), NODE, NODY17(i), S, XY
! Stress yz in Y axis
*GET, STYZYB(i), NODE, NODY17(i), S, YZ
*ENDDO
! Stress xz in Y axis
*GET, STXZYB(i), NODE, NODY17(i), S, XZ
*vwrite,YLOCB(1),STXXYB(1),STYYYB(1),STZZYB(1),STXYYB(1),STYZYB(1),S
TXZYB(1)
(' 'F7.4,' '4F12.3,' '4F12.3,' '4F12.3,' '4F12.3,' '4F12.3,' '4F12.3)
*cfclos
!-----------------------------------------------------------------------------------------
*cfopen,OUTZ1-50Pc-thk-def-0090.txt
! Do Loop Begins Here
*DO,i,1,div2,1
! Location of the Nodes in Z
*GET,ZLOC(i),NODE,NODZ1(i),LOC,Z
! Stress x in Z axis
```

```
*GET, STXXZ(i), NODE, NODZ1(i), S, X
! Stress y in Z axis
*GET, STYYZ(i), NODE, NODZ1(i), S, Y
! Stress z in Z axis
*GET, STZZZ(i), NODE, NODZ1(i), S, Z
! Stress xy in Z axis
*GET, STXYZ(i), NODE, NODZ1(i), S, XY
! Stress yz in Z axis
*GET, STYZZ(i), NODE, NODZ1(i), S, YZ
! Stress xz in Z axis
*GET, STXZZ(i), NODE, NODZ1(i), S, XZ
*ENDDO
! Printing Results
*vwrite,ZLOC(1),STXXZ(1),STYYZ(1),STZZZ(1),STXYZ(1),STYZZ(1),STXZZ(1)
(' 'F7.4,' '4F12.3,' '4F12.3,' '4F12.3,' '4F12.3,' '4F12.3,' '4F12.3)
*cfclos
*cfopen,OUTZ2-50Pc-thk-def-0090.txt
! Do Loop Begins Here
*DO,i,1,div2,1
! Location of the Nodes in Z
*GET,ZLOC(i),NODE,NODZ2(i),LOC,Z
! Stress x in Z axis
*GET, STXXZ(i), NODE, NODZ2(i), S, X
! Stress y in Z axis
*GET, STYYZ(i), NODE, NODZ2(i), S, Y
! Stress z in Z axis
*GET, STZZZ(i), NODE, NODZ2(i), S, Z
! Stress xy in Z axis
*GET, STXYZ(i), NODE, NODZ2(i), S, XY
! Stress yz in Z axis
*GET, STYZZ(i), NODE, NODZ2(i), S, YZ
! Stress xz in Z axis
*GET, STXZZ(i), NODE, NODZ2(i), S, XZ
*ENDDO

! Printing Results
*vwrite,ZLOC(1),STXXZ(1),STYYZ(1),STZZZ(1),STXYZ(1),STYZZ(1),STXZZ(1)
(' 'F7.4,' '4F12.3,' '4F12.3,' '4F12.3,' '4F12.3,' '4F12.3,' '4F12.3)
*cfclos
*cfopen,OUTZ3-50Pc-thk-def-0090.txt
! Do Loop Begins Here
*DO,i,1,div2,1
! Location of the Nodes in Z
*GET,ZLOC(i),NODE,NODZ3(i),LOC,Z
```

```
! Stress x in Z axis
*GET, STXXZ(i), NODE, NODZ3(i), S, X
! Stress y in Z axis
*GET, STYYZ(i), NODE, NODZ3(i), S, Y
! Stress z in Z axis
*GET, STZZZ(i), NODE, NODZ3(i), S, Z
! Stress xy in Z axis
*GET, STXYZ(i), NODE, NODZ3(i), S, XY
! Stress yz in Z axis
*GET, STYZZ(i), NODE, NODZ3(i), S, YZ
! Stress xz in Z axis
*GET, STXZZ(i), NODE, NODZ3(i), S, XZ
*ENDDO
! Printing Results
*vwrite,ZLOC(1),STXXZ(1),STYYZ(1),STZZZ(1),STXYZ(1),STYZZ(1),STXZZ(1)
(' 'F7.4,' '4F12.3,' '4F12.3,' '4F12.3,' '4F12.3,' '4F12.3,' '4F12.3)
*cfclos
*cfopen,OUTZ4-50Pc-thk-def-0090.txt
! Do Loop Begins Here
*DO,i,1,div2,1
! Location of the Nodes in Z
*GET,ZLOC(i),NODE,NODZ4(i),LOC,Z
! Stress x in Z axis
*GET, STXXZ(i), NODE, NODZ4(i), S, X
! Stress y in Z axis
*GET, STYYZ(i), NODE, NODZ4(i), S, Y
! Stress z in Z axis
*GET, STZZZ(i), NODE, NODZ4(i), S, Z
! Stress xy in Z axis
*GET, STXYZ(i), NODE, NODZ4(i), S, XY
! Stress yz in Z axis
*GET, STYZZ(i), NODE, NODZ4(i), S, YZ
! Stress xz in Z axis
*GET, STXZZ(i), NODE, NODZ4(i), S, XZ
*ENDDO

! Printing Results
*vwrite,ZLOC(1),STXXZ(1),STYYZ(1),STZZZ(1),STXYZ(1),STYZZ(1),STXZZ(1)
(' 'F7.4,' '4F12.3,' '4F12.3,' '4F12.3,' '4F12.3,' '4F12.3,' '4F12.3)
*cfclos
*cfopen,OUTZ5-50Pc-thk-def-0090.txt
! Do Loop Begins Here
*DO,i,1,div2,1
! Location of the Nodes in Z
```

```
*GET,ZLOC(i),NODE,NODZ5(i),LOC,Z
! Stress x in Z axis
*GET, STXXZ(i), NODE, NODZ5(i), S, X
! Stress y in Z axis
*GET, STYYZ(i), NODE, NODZ5(i), S, Y
! Stress z in Z axis
*GET, STZZZ(i), NODE, NODZ5(i), S, Z
! Stress xy in Z axis
*GET, STXYZ(i), NODE, NODZ5(i), S, XY
! Stress yz in Z axis
*GET, STYZZ(i), NODE, NODZ5(i), S, YZ
! Stress xz in Z axis
*GET, STXZZ(i), NODE, NODZ5(i), S, XZ
*ENDDO
! Printing Results
*vwrite,ZLOC(1),STXXZ(1),STYYZ(1),STZZZ(1),STXYZ(1),STYZZ(1),STXZZ(1)
(' 'F7.4,' '4F12.3,' '4F12.3,' '4F12.3,' '4F12.3,' '4F12.3,' '4F12.3)
*cfclos
! /EXIT,NOSAV
```

APPENDIX B

ADDITIONAL FIGURES FROM CHAPTER 2

In this section some of the figures that have been referred in chapter 2 and not critical for the overall conclusions has been shown here. Studies to show the effect of the width of the laminate and the ply thickness, also, the through the thickness plot comparing the existing literature for the tensile loading specimen has been shown here.

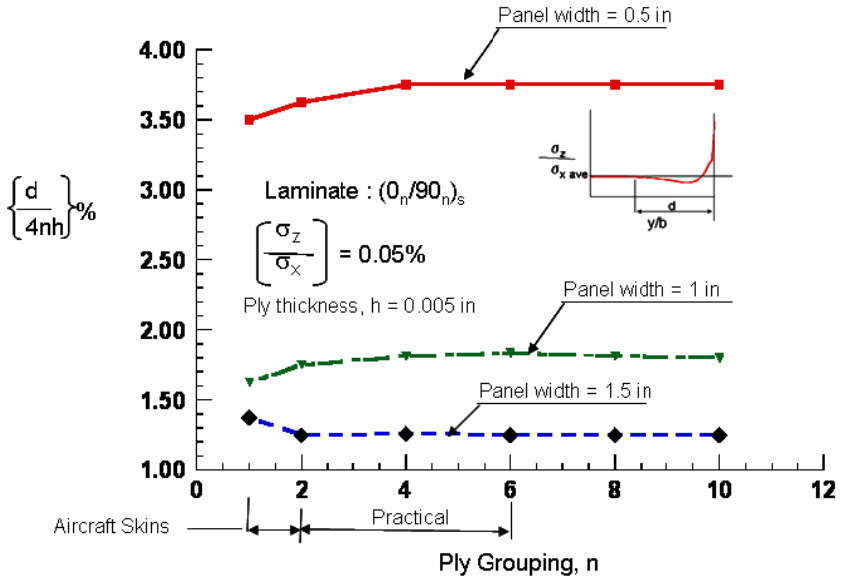

Figure B.1 Effect of edge distance on ply grouping for (0n/90n)s

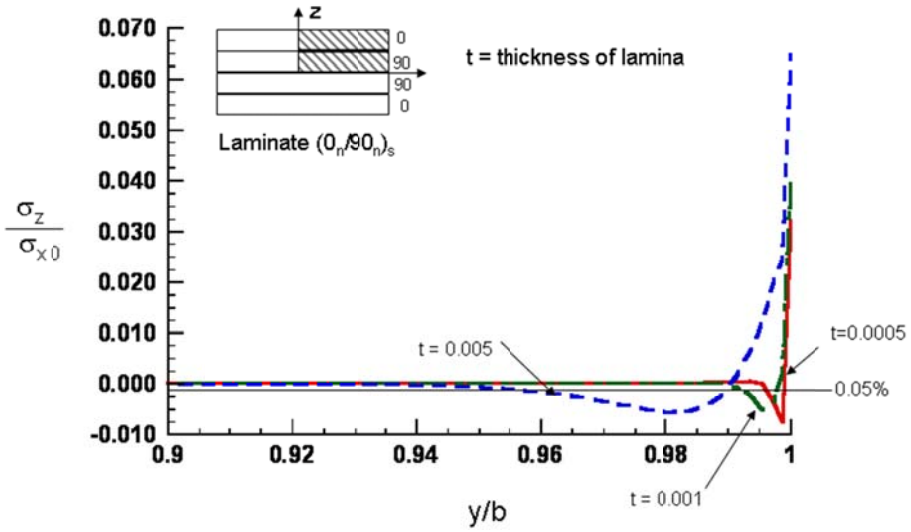

Figure B.2 Normalized σ_x Interlaminar stresses across the width for 10% width from free edge for different ply thickness for $(0_n/90_n)_s$

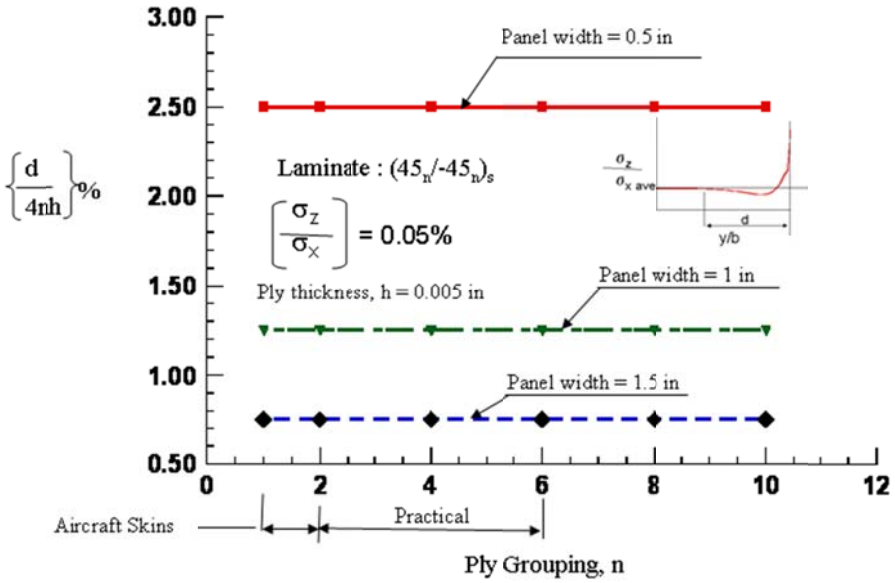

Figure B.3 Effect of edge distance on ply grouping for $(+45_n/-45_n)_s$

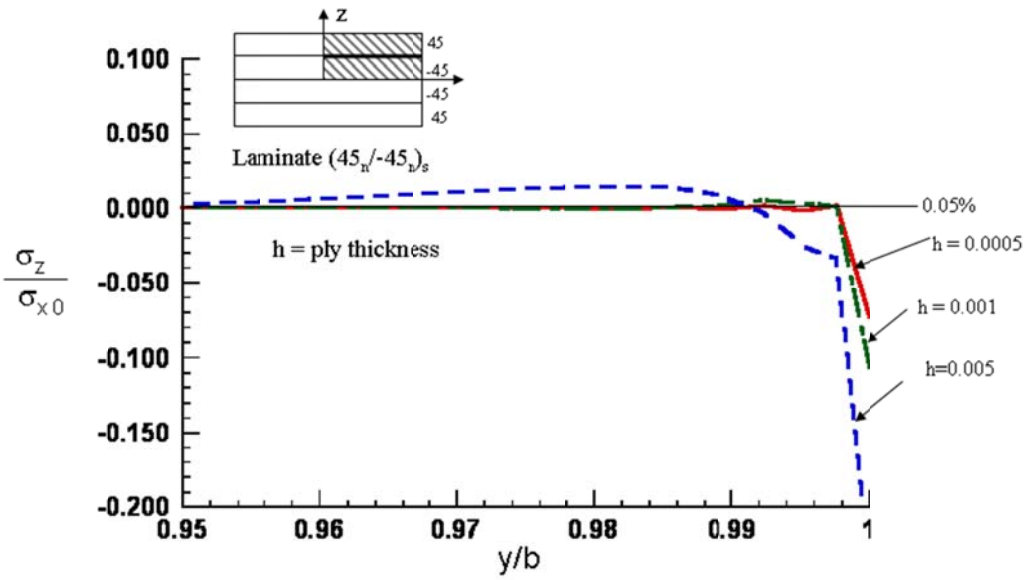

Figure B.4 Normalized σ_x Interlaminar stresses across the width for 10% width from free edge for different ply thickness $(+45_n/-45_n)_s$

APPENDIX C

ADDITIONAL FIGURES FROM CHAPTER 3

In this section some of the figures that have been referred in chapter 3 and not critical for the overall conclusions have been shown here. Studies to show the effect of the width of the laminate and the ply thickness, also, the through the thickness plot for different interphase studies have been shown here. Figure C.1 – Normal Stress for different ply thickness, Figure C.2-Figure C.3 $(0_2/90_2)_s$ laminate Stress distribution of Resin interphase. Figure C.4-Figure C.9 $(0_{10}/90_{10})_s$ laminate Stress distribution of Realistic Laminate. Figure C10 to C 11 $(0_{10}/90_{10})_s$ laminate Stress distribution of Elastic-Plastic material, Figure C12 to C13 $(0_2/90_2)_s$ laminate Stress distribution of Non-Linear material, Figure C14 to C15 $(0_{10}/90_{10})_s$ laminate Stress distribution of Non linear material, Figure C16 to C19 $(45_{10}/45_{10})_s$ laminate Stress distribution of Elastic Material, Figure C20 to C21 $(45_{10}/45_{10})_s$ laminate Stress distribution of Elastic-Plastic Material, Figure C23 to C24 $(45_2/45_2)_s$ laminate Stress distribution of Elastic plastic material, Figure C25 to C28$(45_2/45_2)_s$ laminate Stress distribution of Non-linear material, Figure C29 to C32 $(45_2/45_2)_s$ laminate Stress distribution of Non-Linear material

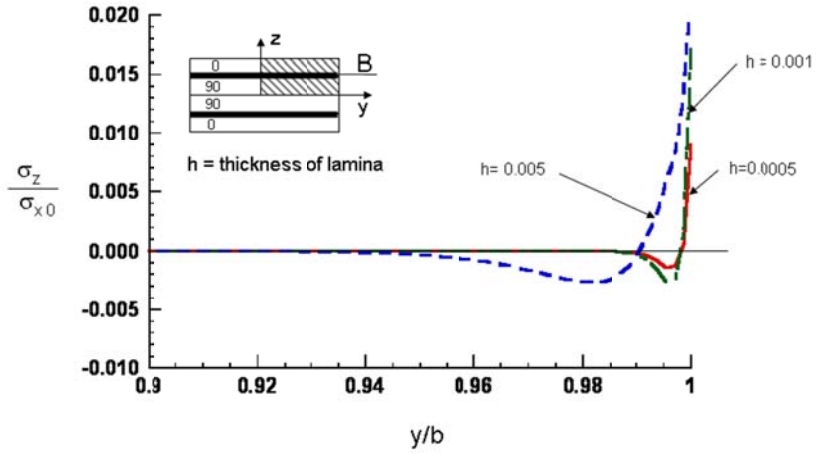

Figure C.1 Normalized σ_z Stress distribution across the width, for different ply

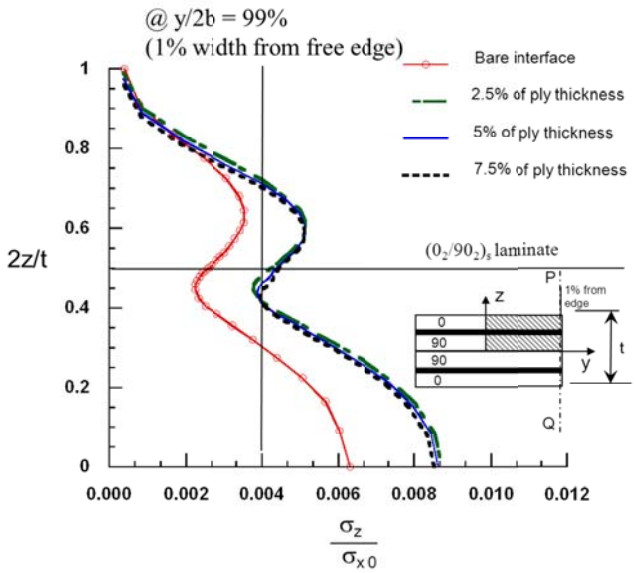

Figure C.2 Normalized σ_z Stress distribution through the thickness, for $(0_2/90_2)_s$ laminate at 1% from the free edge, for elastic-plastic matrix material

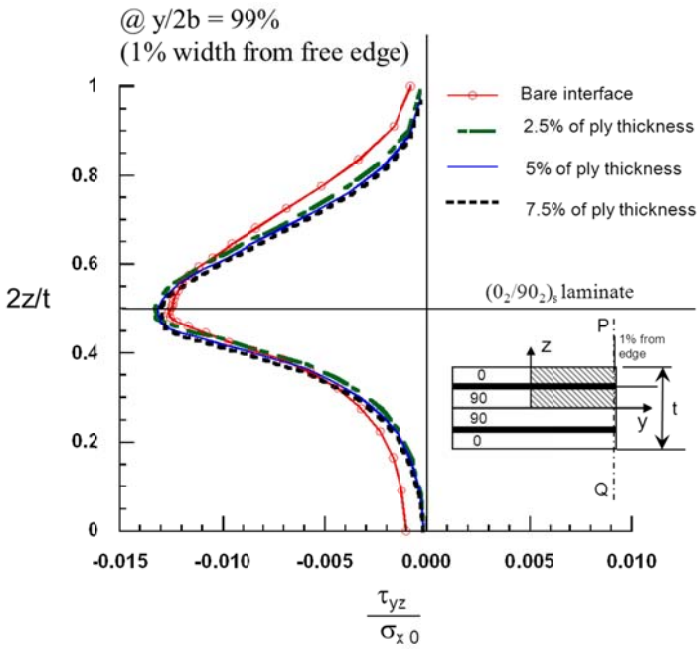

Figure C.3 Normalized τ_{yz} Stress distribution through the thickness, for $(0_2/90_2)_s$ laminate at 1% width from the edge (P-Q), for elastic-plastic matrix material

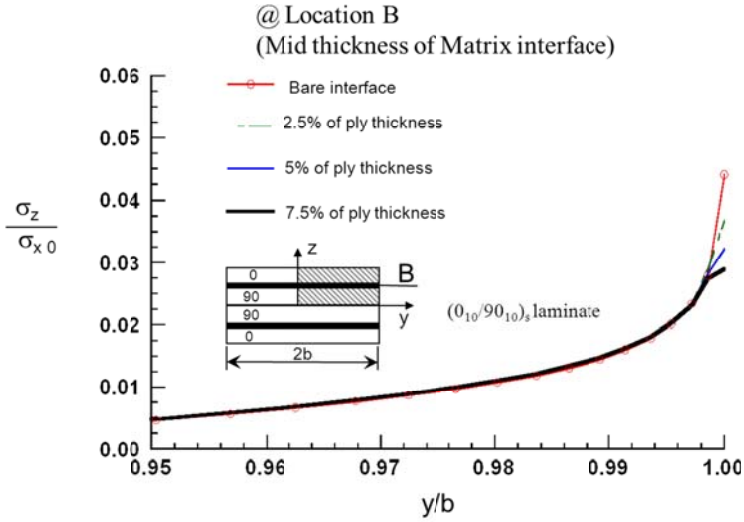

Figure C.4 Normalized σ_z Stress distribution across the width for $(0_{10}/90_{10})_s$ laminate at the mid-thickness of the interphase (B), for elastic-plastic matrix material

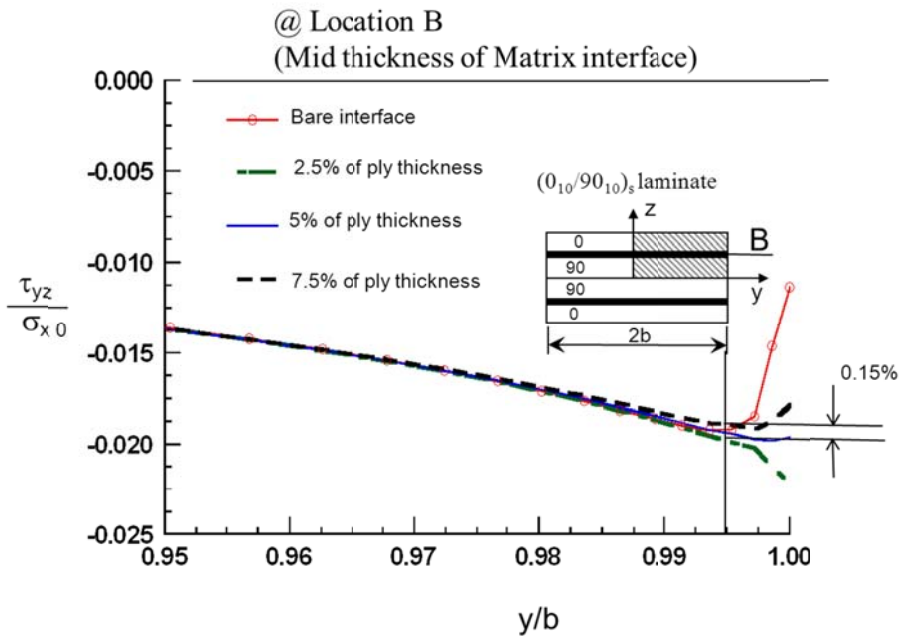

Figure C.5 Normalized τ_{yz} Stress distribution across the width for $(0_{10}/90_{10})_s$ laminate at the mid-thickness of the interphase (B), for elastic-plastic matrix material

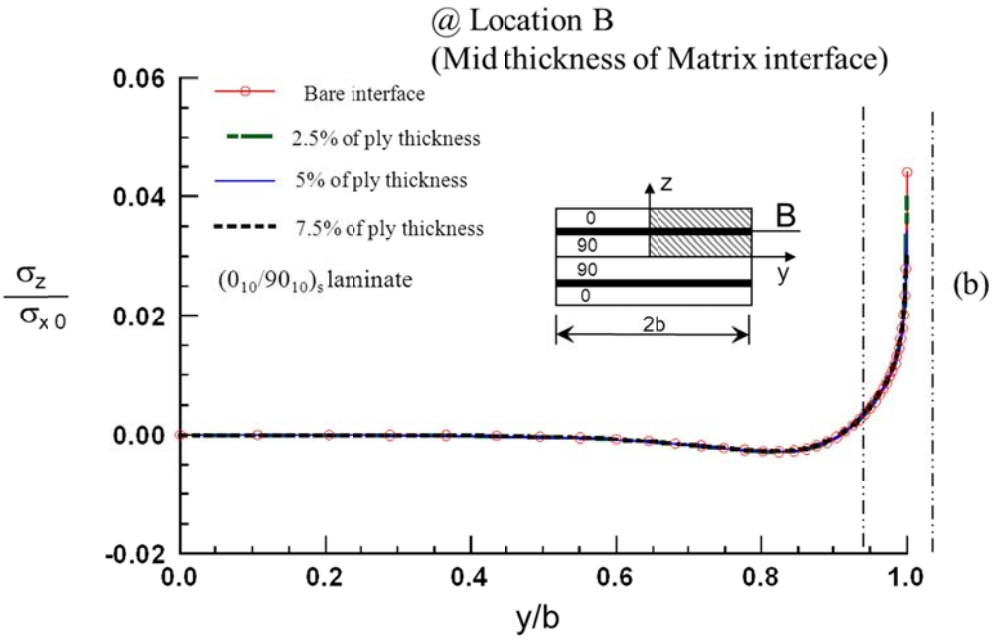

(b)

(a)

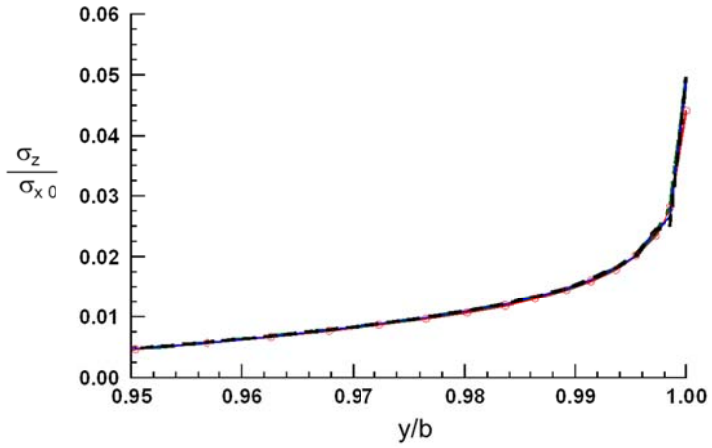

(b)

Figure C.6 Normalized σ_z Stress distribution (a) One-half width (b) Near the edge across the width for $(0_{10}/90_{10})_s$ laminate at the mid-thickness of the interphase (B), for realistic matrix material

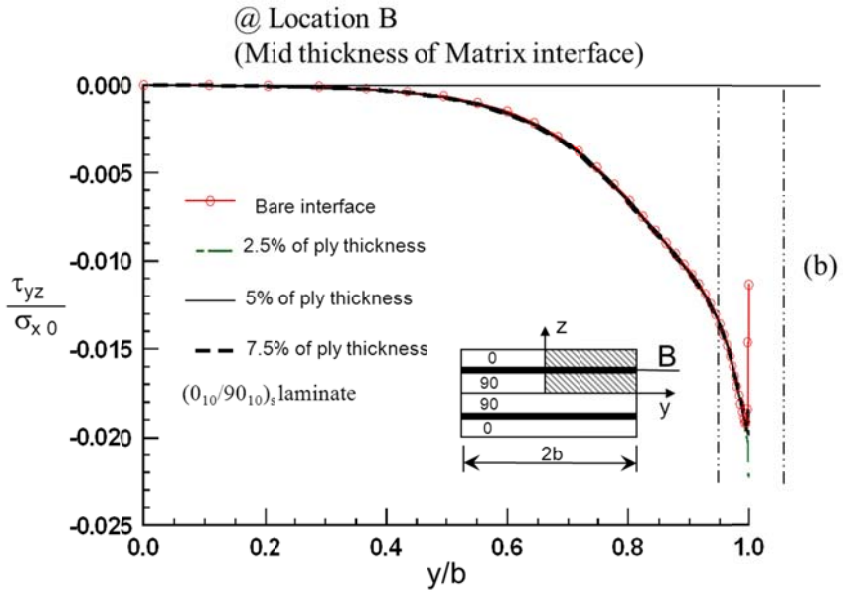

(a)

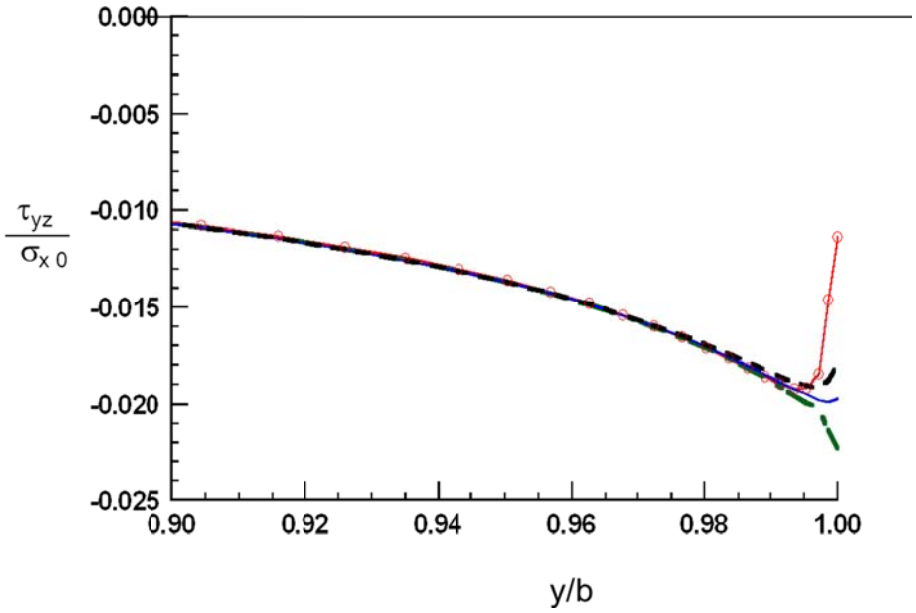

(b)

Figure C.7 Normalized τ_{yz} Stress distribution (a) One-half width (b) Near the edge across the width for $(0_{10}/90_{10})_s$ laminate at the mid-thickness of the interphase (B), for realistic matrix material.

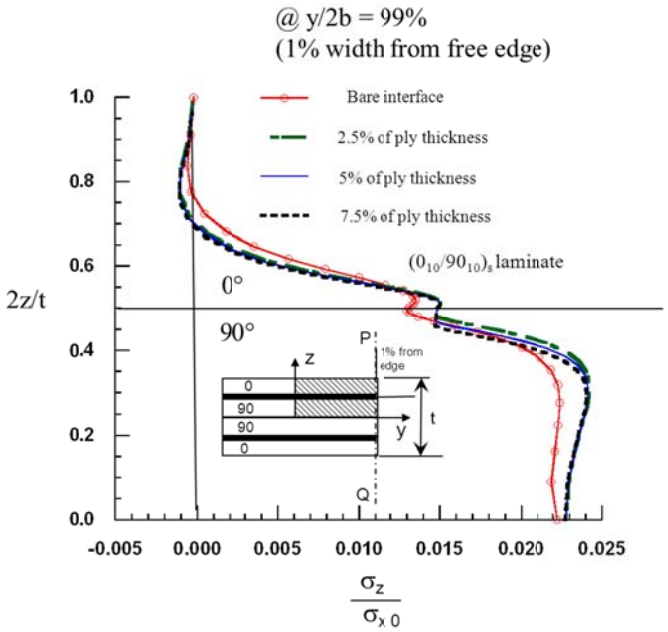

Figure C.8 Normalized σ_z Stress distribution through the thickness, for $(0_{10}/90_{10})_s$ laminate at 1% width from the edge (P-Q), for realistic matrix material

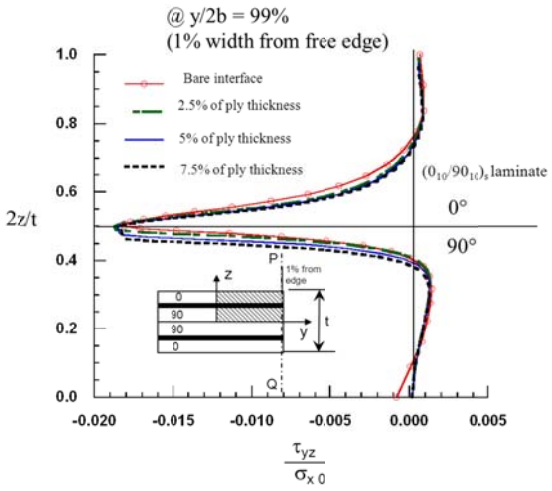

Figure C.9 Normalized τ_{yz} Stress distribution through the thickness, for $(0_{10}/90_{10})_s$ laminate at 1% from the edge (P-Q), for realistic matrix material

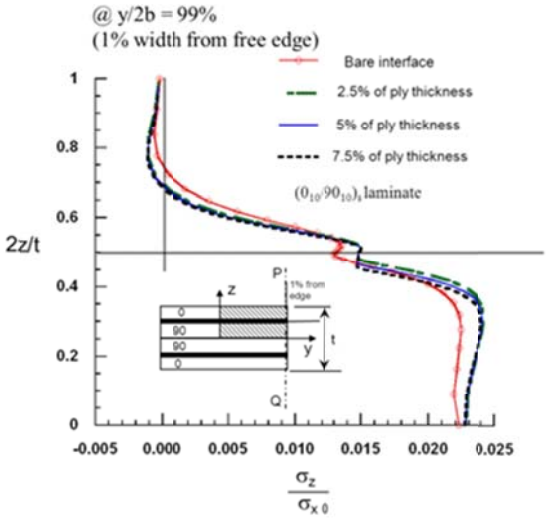

Figure C.10 Normalized σ_z Stress distribution through the thickness for $(0_{10}/90_{10})_s$ laminate at 1% width from the free edge, for elastic-plastic matrix material

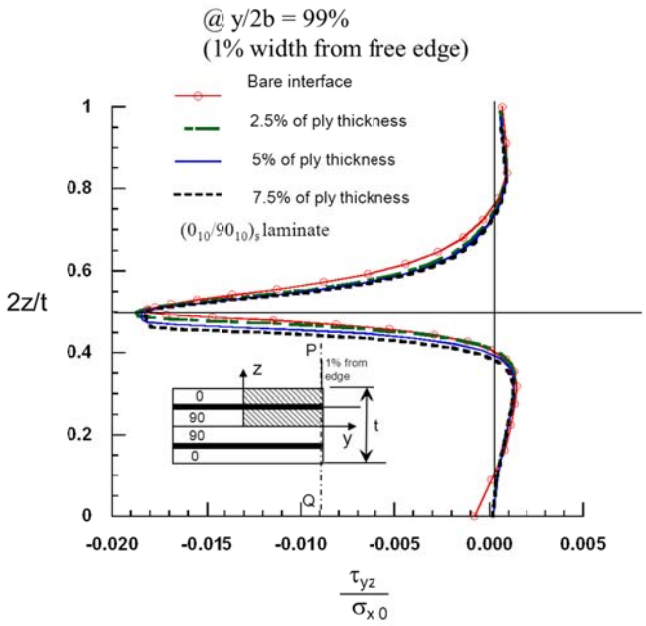

Figure C.11 Normalized τ_{yz} Stress distribution through the thickness for $(0_{10}/90_{10})_s$ laminate at 1% from the edge (P-Q), for elastic-plastic matrix material

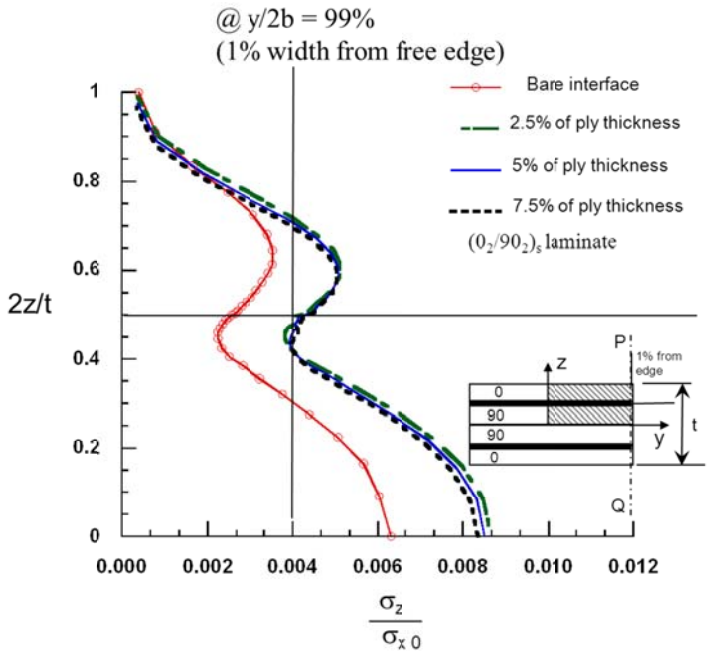

Figure C.12 Normalized σ_z Stress distribution through the thickness, for $(0_2/90_2)_s$ laminate at 1% from the edge (P-Q), for non-linear matrix material

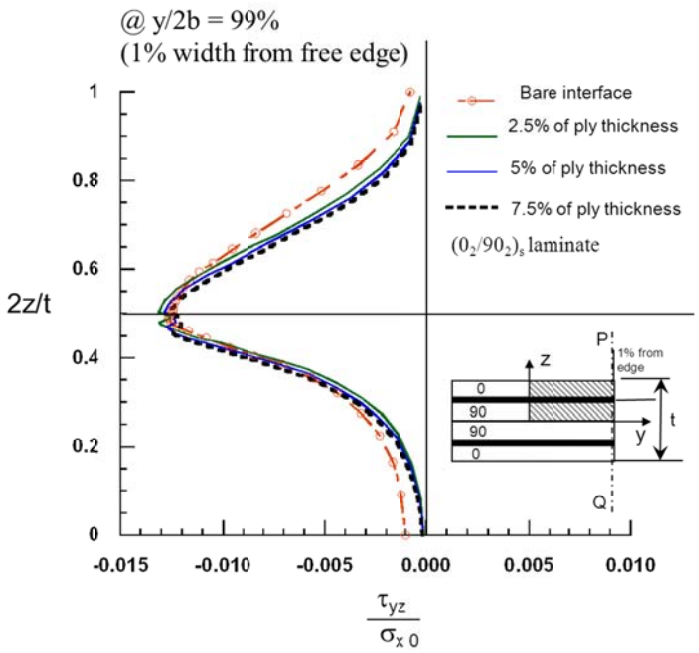

Figure C.13 Normalized τ_{yz} Stress distribution through the thickness, for $(0_2/90_2)_s$ laminate at 1% from the edge (P-Q), for non-linear matrix material

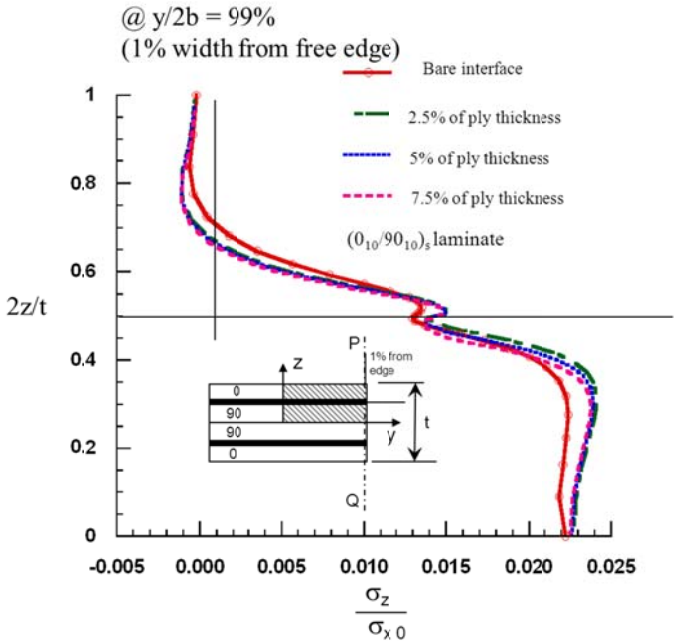

Figure C.14 Normalized σ_z Stress distribution through the thickness, for $(0_{10}/90_{10})_s$ laminate at 1% from the edge (P-Q), for non-linear matrix material

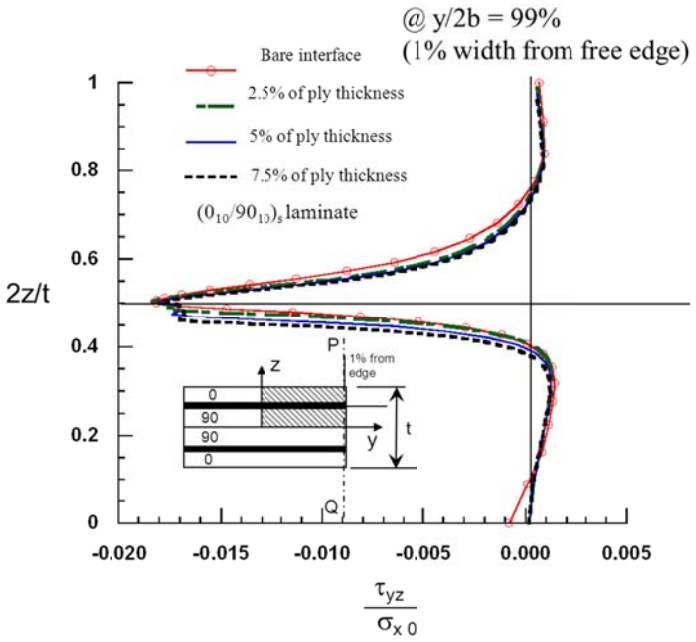

Figure C.15 Normalized τ_{yz} Stress distribution through the thickness, for $(0_{10}/90_{10})_s$ laminate at 1% from the edge (P-Q), for non-linear matrix material

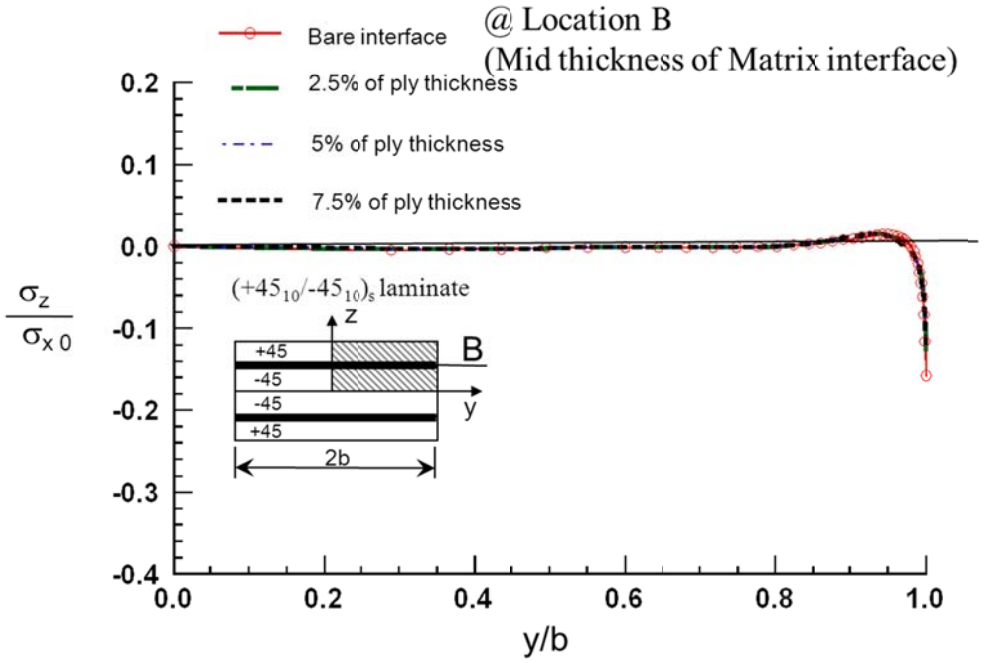

(a)

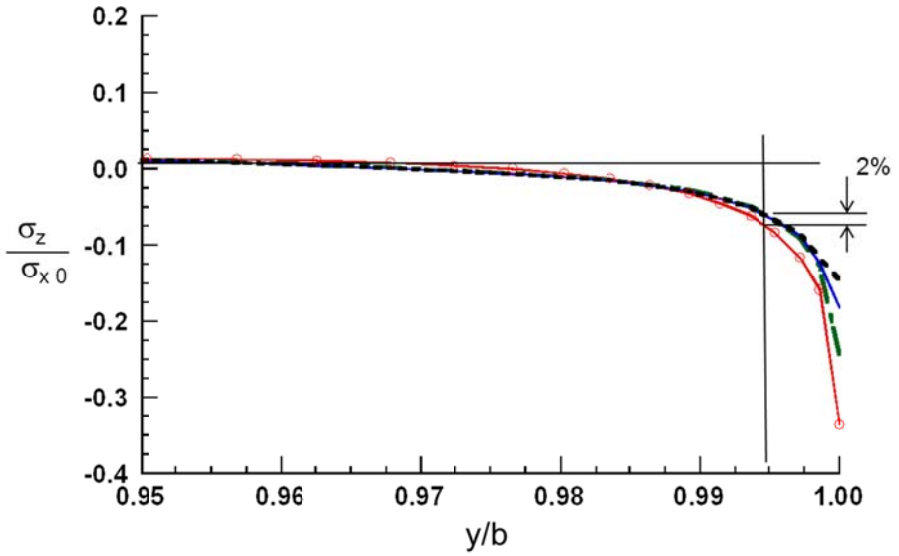

(b)

Figure C.16 Normalized σ_z Stress distribution (a) One-half width (b) Near the edge across the width for $(+45_{10}/-45_{10})_s$ laminate at the mid-thickness of the interphase (B), for realistic matrix material

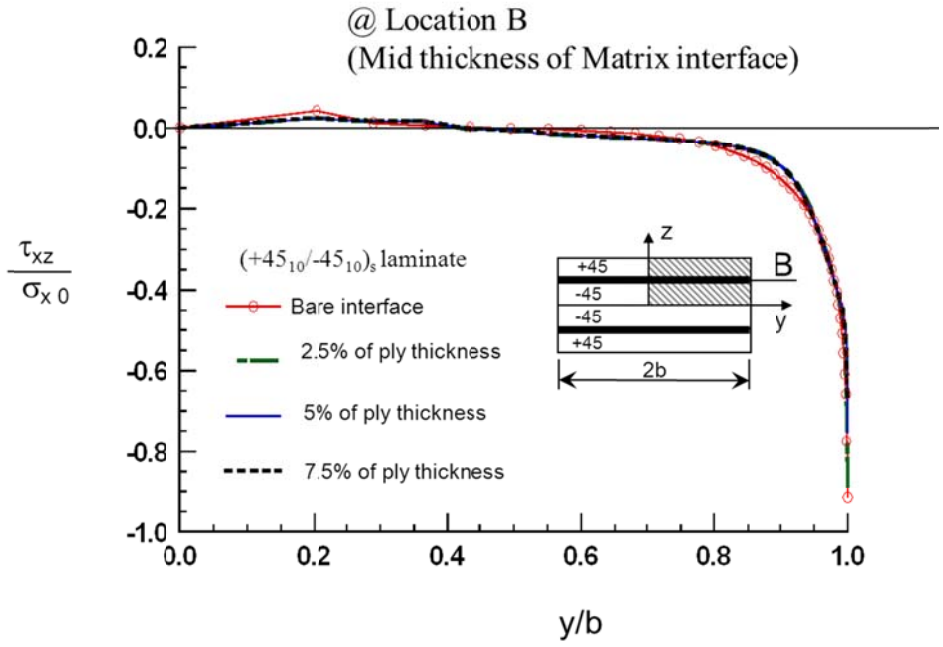

(a)

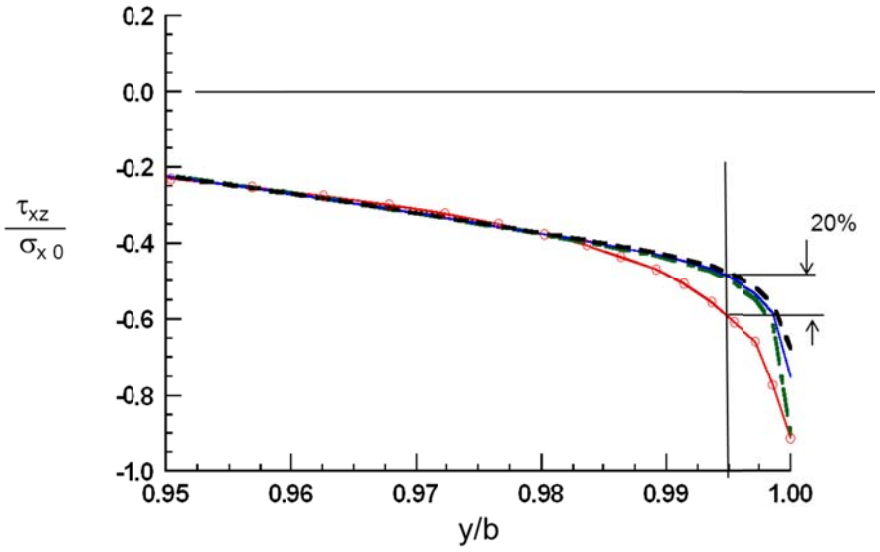

(b)

Figure C.17 Normalized τ_{xz} Stress distribution across the width for $(+45_{10}/-45_{10})_s$ laminate at the mid-thickness of the interphase (B), for realistic matrix material. (a) One-half width (b) Near the edge

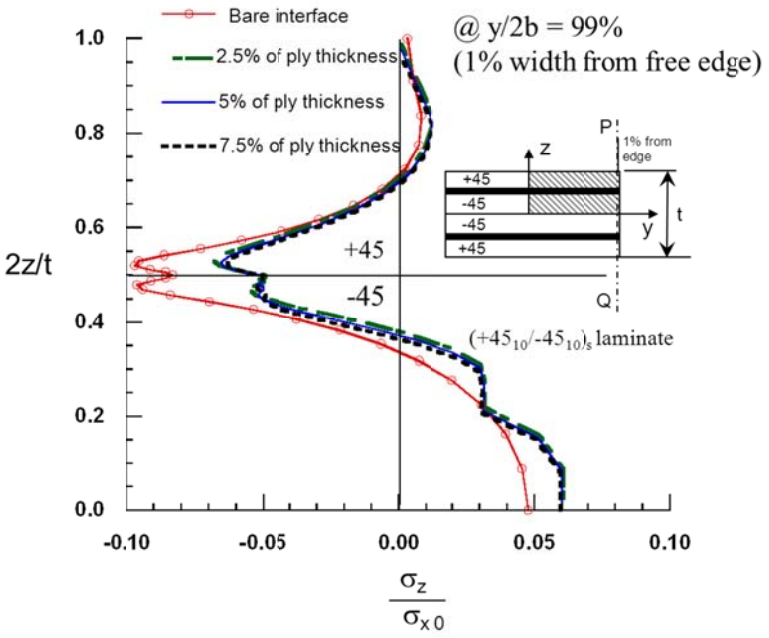

Figure C.18 Normalized σ_z Stress distribution through the thickness, for $(+45_{10}/-45_{10})_s$ laminate at 1% of width from the edge (P-Q), for realistic matrix material

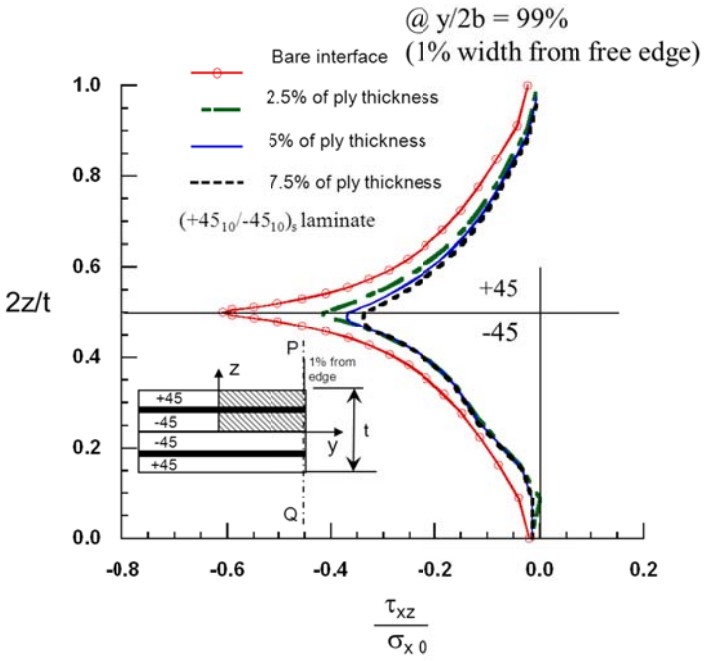

Figure C.19 Normalized τ_{yz} Stress distribution through the thickness, for $(+45_{10}/-45_{10})_s$ laminate at 1% of width from the edge (P-Q), for realistic matrix material

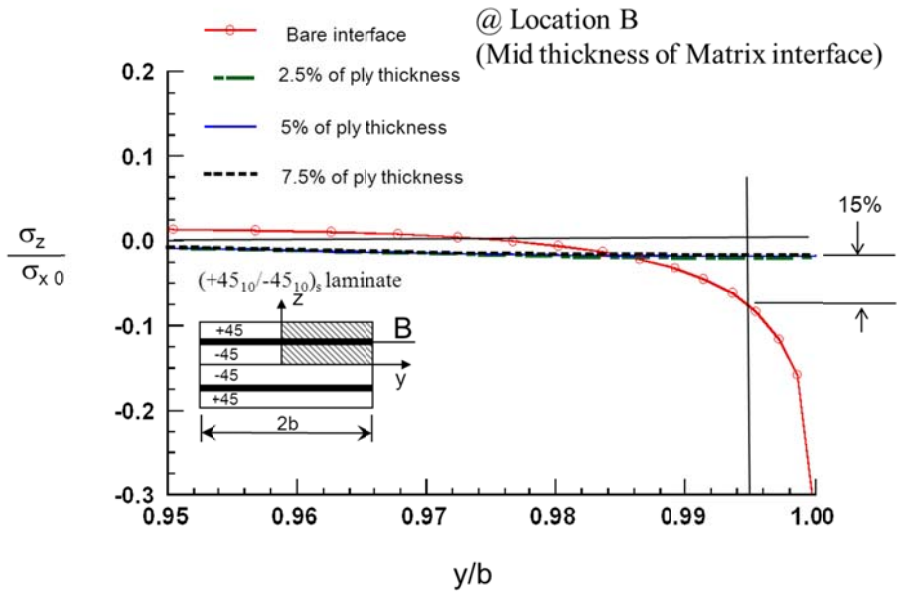

Figure C.20Normalized σ_z Stress distribution across the width for $(+45_{10}/-45_{10})_s$ laminate at the mid-thickness of the interphase (B), for Elastic-Plastic matrix material

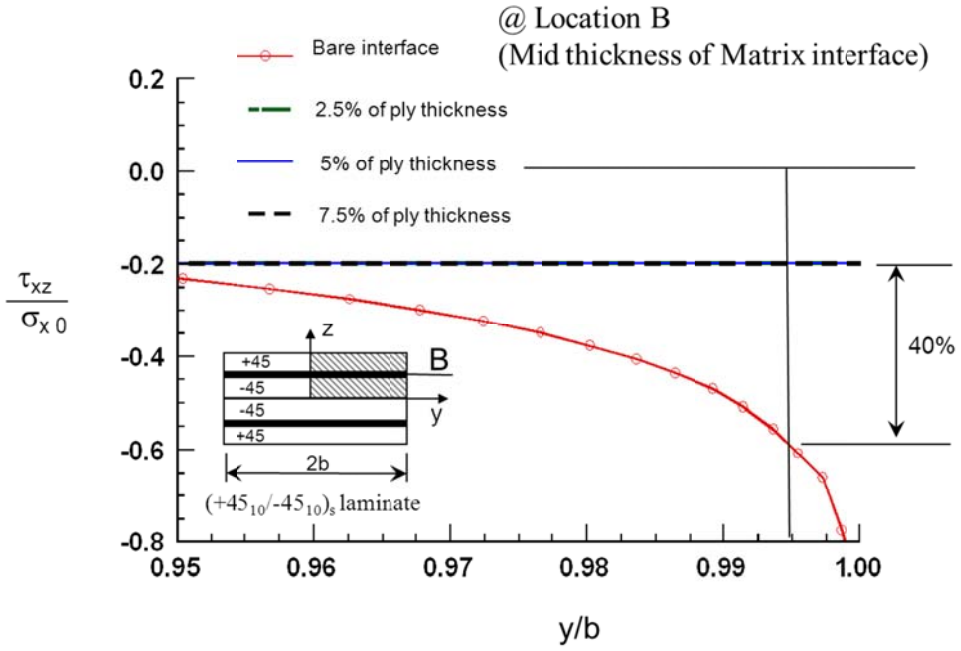

Figure C.21 Normalized τ_{xz} Stress distribution across the width for $(+45_{10}/-45_{10})_s$ laminate at the mid-thickness of the interphase (B), for Elastic-Plastic matrix material

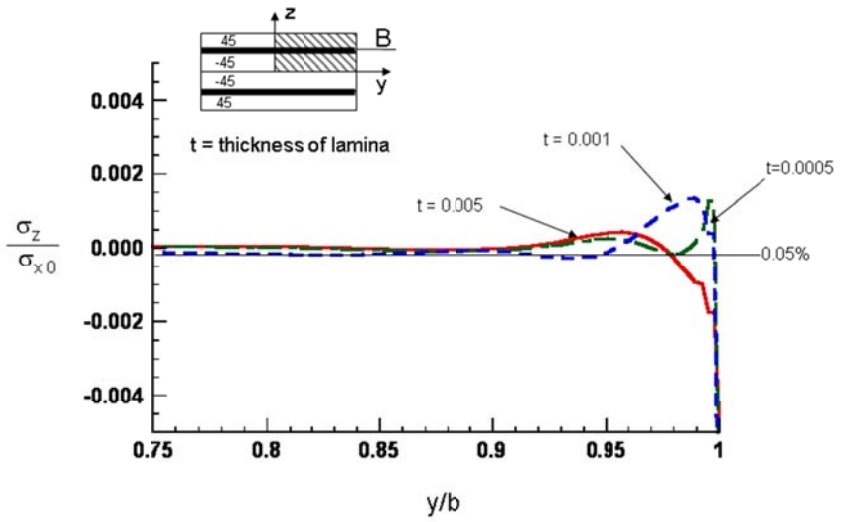

Figure C.22 Normalized σ_z Stress distribution across the width, for $(+45_{10}/-45_{10})_s$ laminate at the mid-thickness of the interphase (B) for different lamina thickness with realistic matrix material

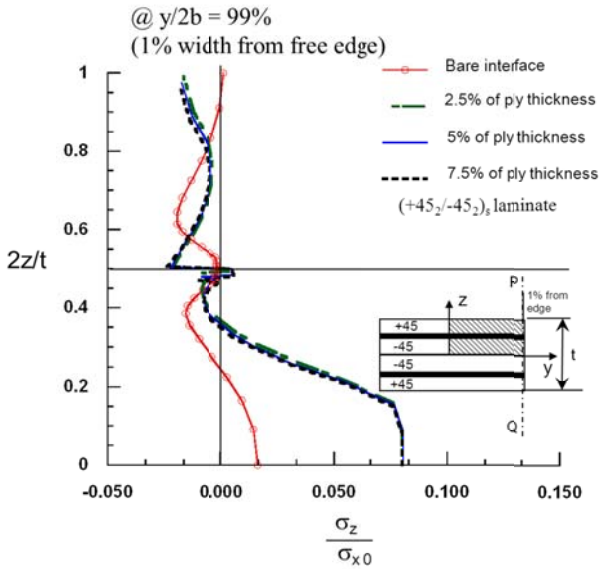

Figure C.23 Normalized σ_z Stress distribution through the thickness, for $(+45_2/-45_2)_s$ laminate at 1% from the edge (P-Q), for Elastic-Plastic matrix material

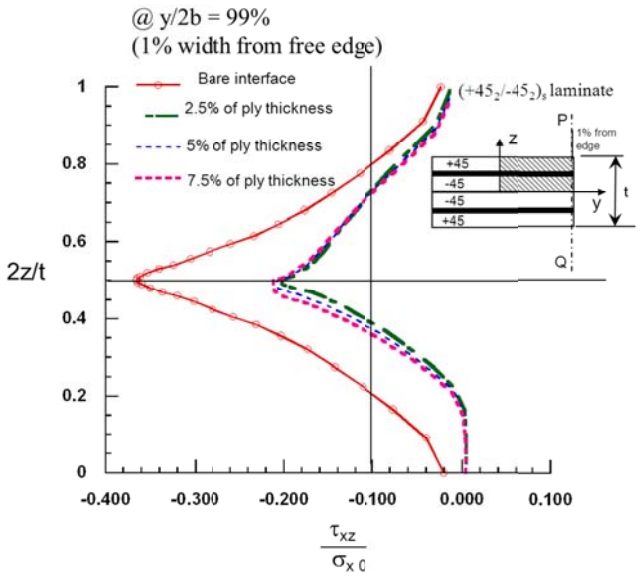

Figure C.24 Normalized σ_z Stress distribution through the thickness, for $(+45_2/-45_2)_s$ laminate at 1% from the edge (P-Q), for Elastic-Plastic matrix material

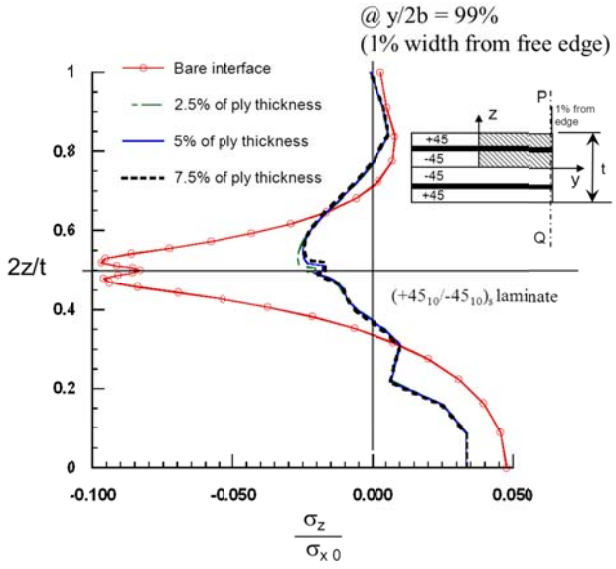

Figure C.25 Normalized σ_z Stress distribution through the thickness, for $(+45_{10}/-45_{10})_s$ laminate at 1% from the edge (P-Q), for Elastic-Plastic matrix material

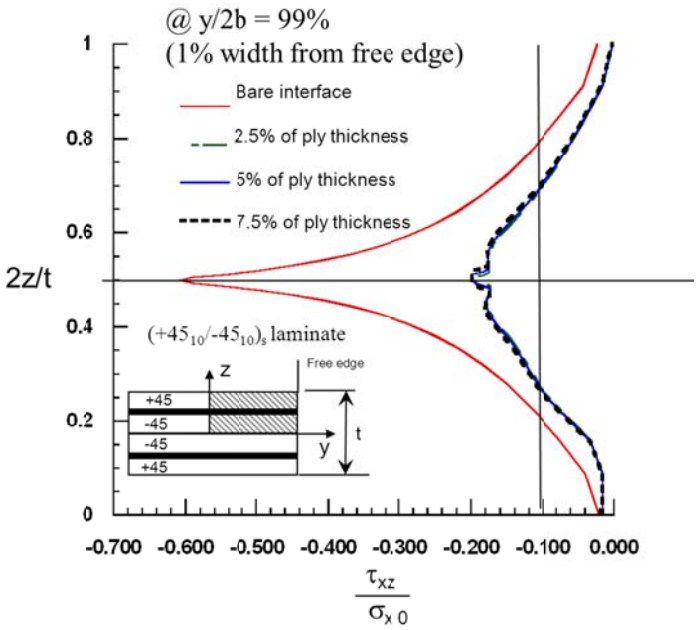

Figure C.26 Normalized σ_z Stress distribution through the thickness, for $(+45_{10}/-45_{10})_s$ laminate at 1% from the edge (P-Q) for Elastic-Plastic matrix material

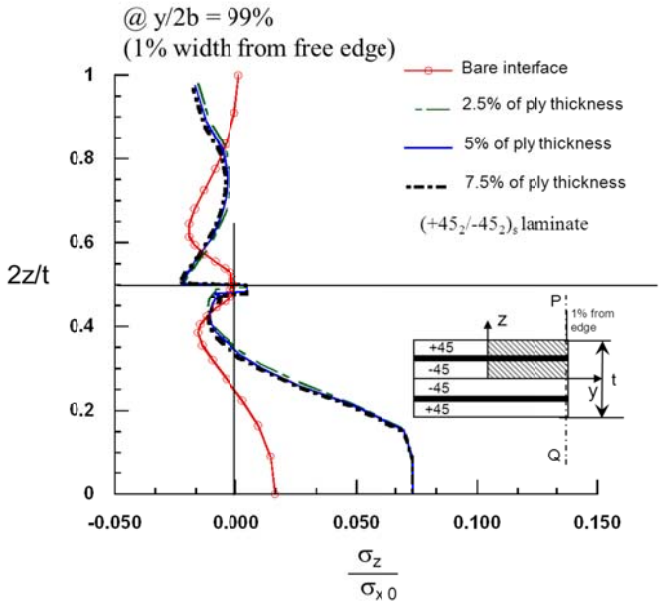

Figure C.27 Normalized σ_z Stress distribution through the thickness, for $(+45_2/-45_2)_s$ laminate at free edge, for non-linear matrix material

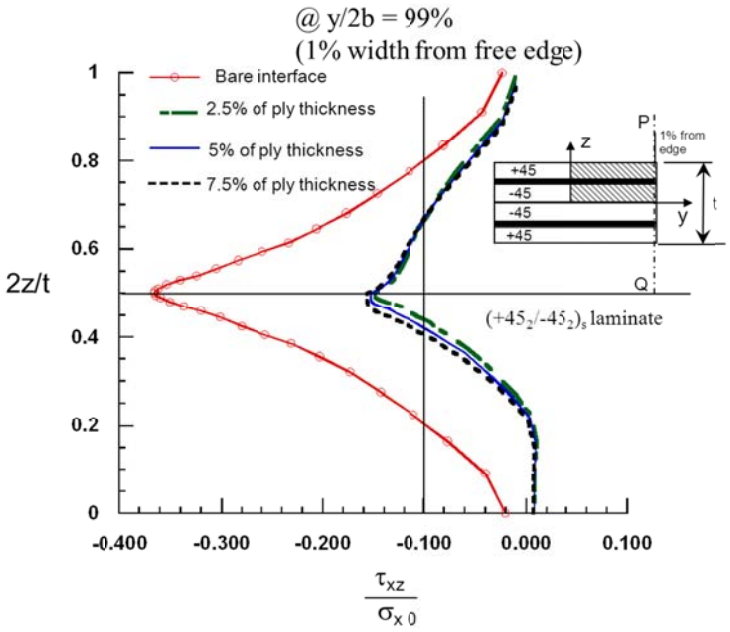

Figure C.28 Normalized σ_z Stress distribution through the thickness, for $(+45_2/-45_2)_s$ laminate at free edge, for non-linear matrix material

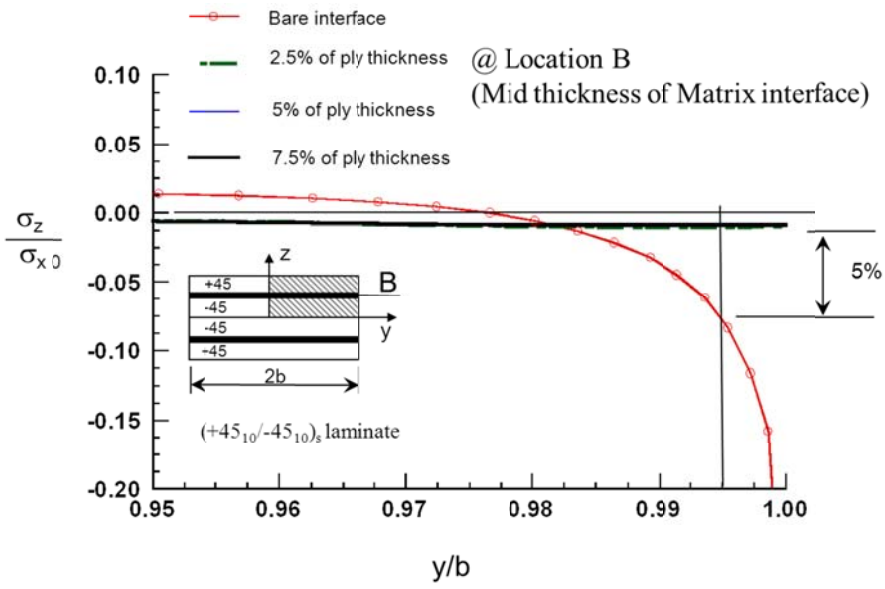

Figure C.29 Normalized σ_z Stress distribution across the width for $(+45_{10}/-45_{10})_s$ laminate at the mid-thickness of the interphase (B), for non-linear matrix material

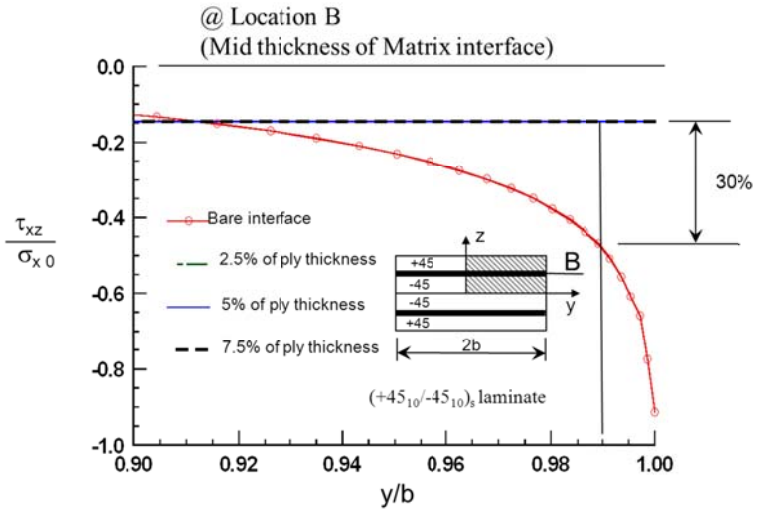

Figure C.30 Normalized τ_{xz} Stress distribution across the width for $(+45_{10}/-45_{10})_s$ laminate at the mid-thickness of the interphase (B), for non-linear matrix material

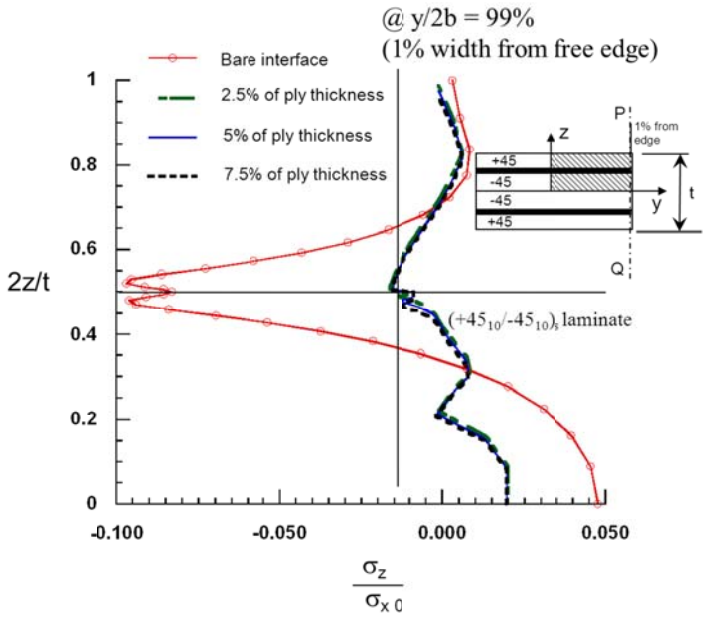

Figure C.31 Normalized σ_z Stress distribution through the thickness, for $(+45_{10}/-45_{10})_s$ laminate at 1% width from the edge (P-Q) for non-linear matrix material

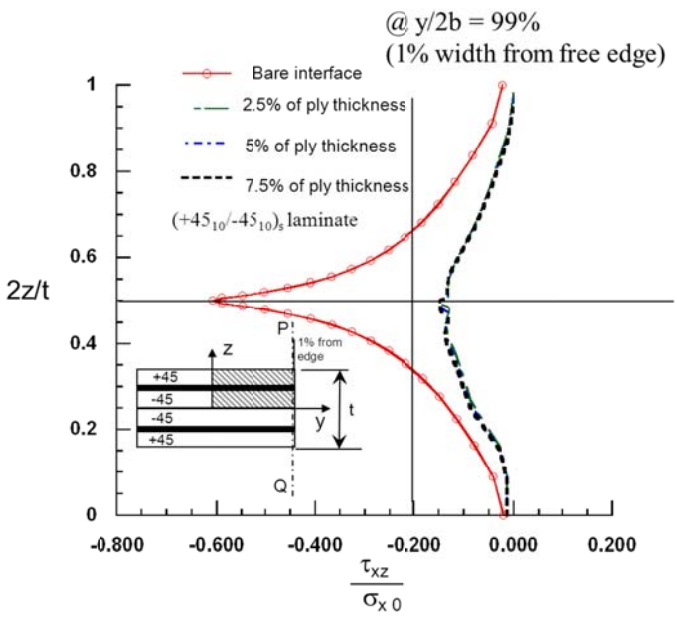

Figure C.32 Normalized σ_z Stress distribution through the thickness, for $(+45_{10}/-45_{10})_s$ laminate at 1% from the edge (P-Q) for non-linear matrix material

APPENDIX D

ADDITIONAL FIGURES FROM CHAPTER 4

In this section some of the figures that have been referred in chapter 2 and not critical for the overall conclusions have been shown here. Studies to show the effect of the width of the laminate and the ply thickness, also, the through the thickness plot comparing the existing literature for the thermal specimen and the interphase analysis have been shown here. , Figure D1 to D3 $(0_2/90_2)_s$ laminate Stress distribution of different interphase material, Figure D4 to D $(0_{10}/90_{10})_s$ laminate Stress distribution of different interphase material, Figure D7 to D8$(45_{10}/45_{10})_s$ laminate Stress distribution of Elastic Material, Figure D9 to D11 $(0_{10}/90_{10})_s$ laminate Stress distribution for different interphase material, Figure D12 to D14 $(45_{10}/45_{10})_s$ laminate Stress distribution of different interphase Material,

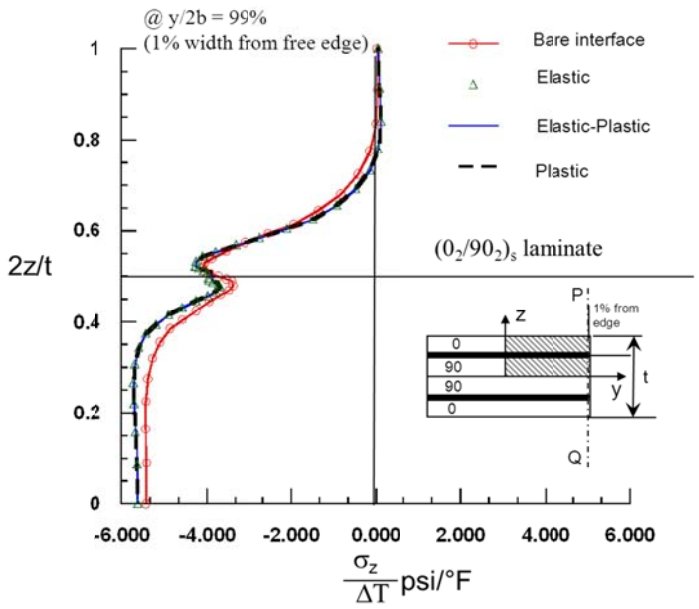

Figure D.1 Normalized σ_z Stress distribution through the thickness for $(0_2/90_2)_s$ laminate at 1% width from edge (P-Q), for comparing different matrix material

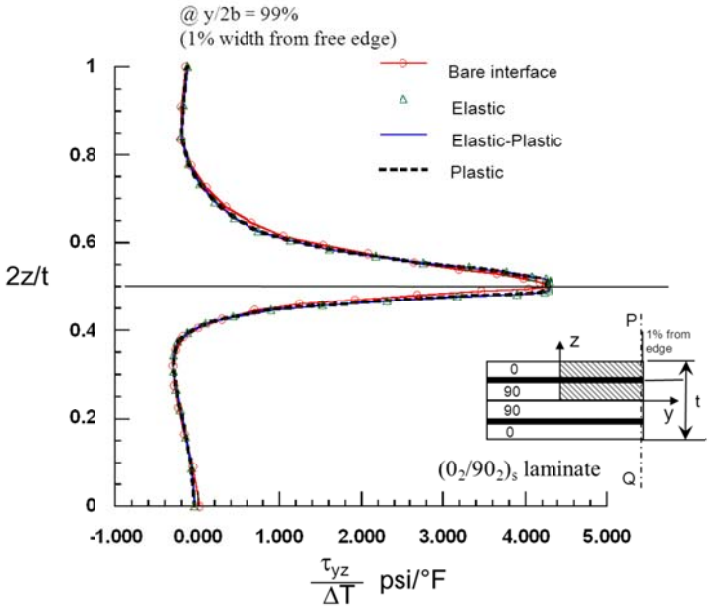

Figure D.2 Normalized τ_{yz} Stress distribution through the thickness for $(0_2/90_2)_s$ 1% of width from the edge (P-Q), for comparing different matrix material

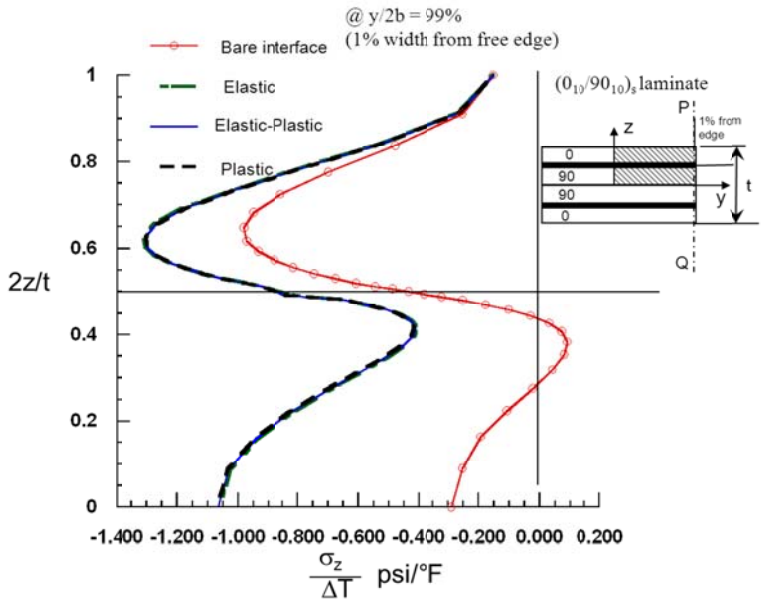

Figure D.3 Normalized σ_z Stress distribution through the thickness, for $(0_{10}/90_{10})_s$ laminate at 1% width from the edge (P-Q), for comparing different matrix material

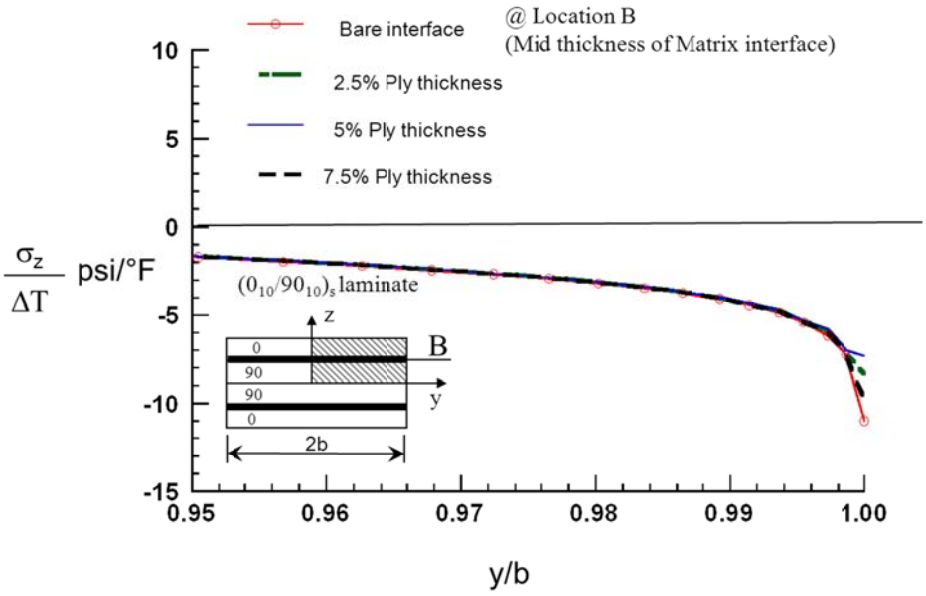

Figure D.4 Normalized z Stress distribution across the width for (010/9010)s laminate at the mid-thickness of the interphase (B), for comparing different matrix material thickness

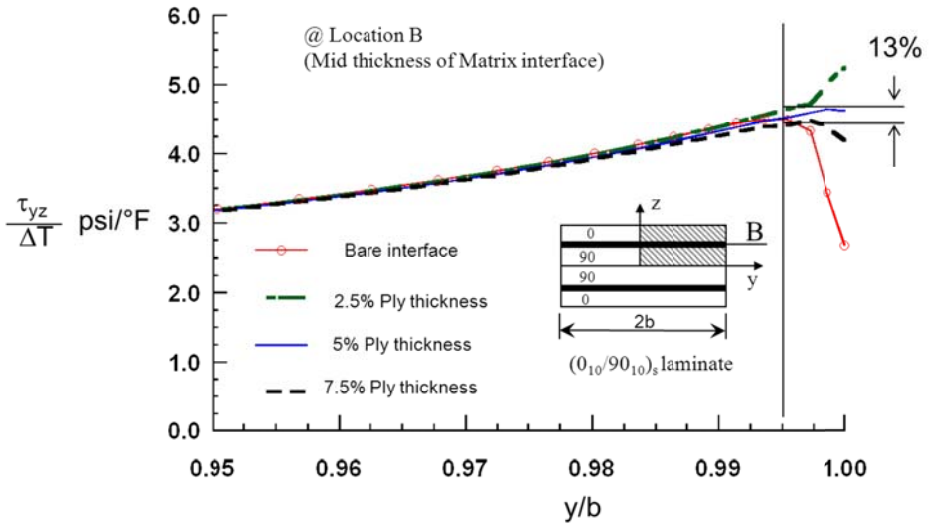

Figure D.5 Normalized τ_{yz} Stress distribution across the width for $(0_{10}/90_{10})_s$ laminate at the mid-thickness of the interphase (B), for comparing different matrix material thickness

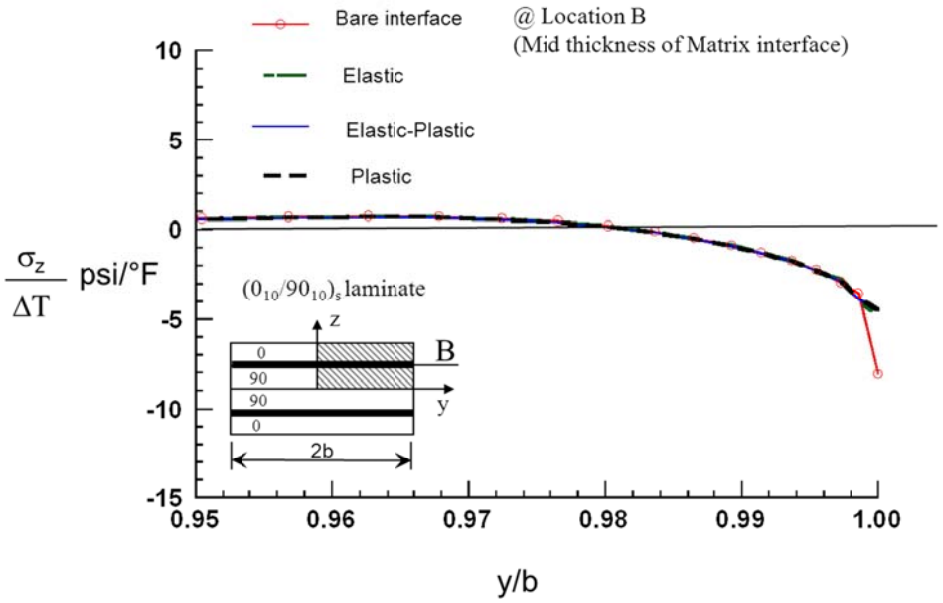

Figure D.6 Normalized σ_z Stress distribution across the width for $(0_{10}/90_{10})_s$ laminate at the mid-thickness of the interphase (B), for comparing different matrix material near the edge

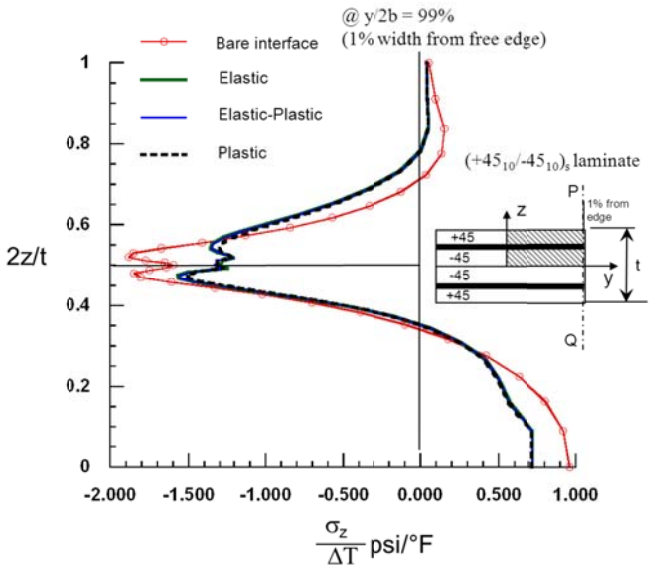

Figure D.7 Normalized σ_z Stress distribution through the thickness, for $(+45_{10}/-45_{10})_s$ laminate at 1% of width from the edge (P-Q), for comparing different matrix material

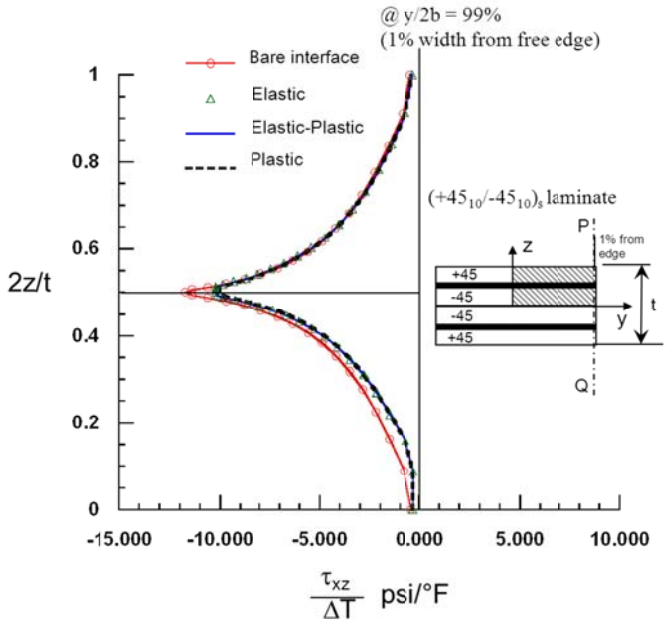

Figure D.8 Normalized τ_{yz} Stress distribution through the thickness, for $(+45_{10}/-45_{10})_s$ laminate at 1% of width from the edge (P-Q), for comparing different matrix material

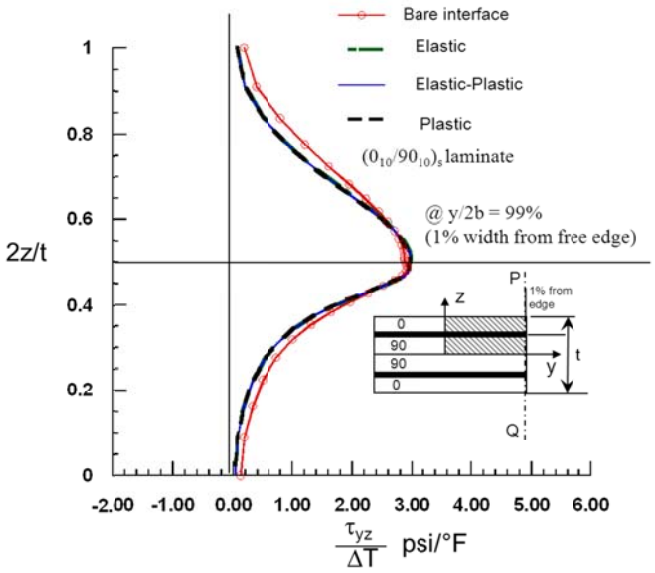

Figure D.9 Normalized τ_{yz} Stress distribution through the thickness, for $(0_{10}/90_{10})_s$ laminate at 1% from the edge (P-Q), for comparing different matrix material

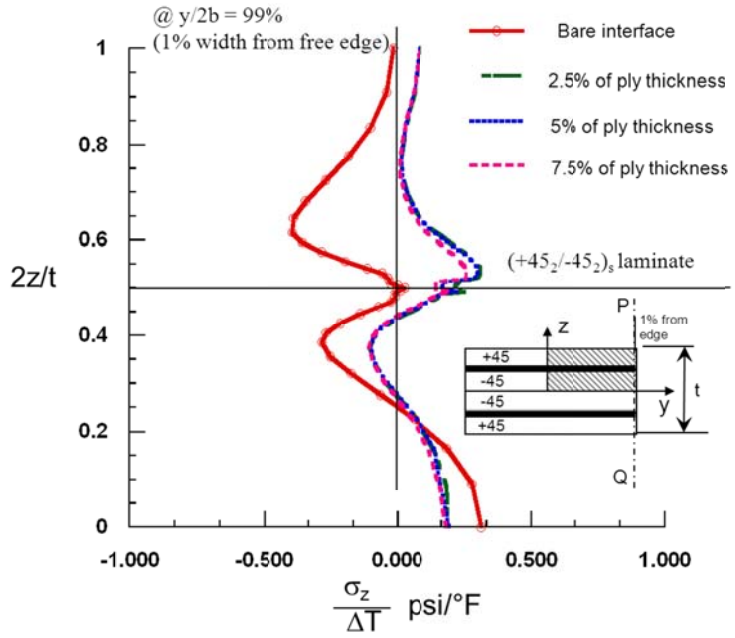

Figure D.10 Normalized σ_z Stress distribution through the thickness, for $(+45_2/-45_2)_s$ laminate at 1% width from the edge (P-Q), for comparing different matrix material

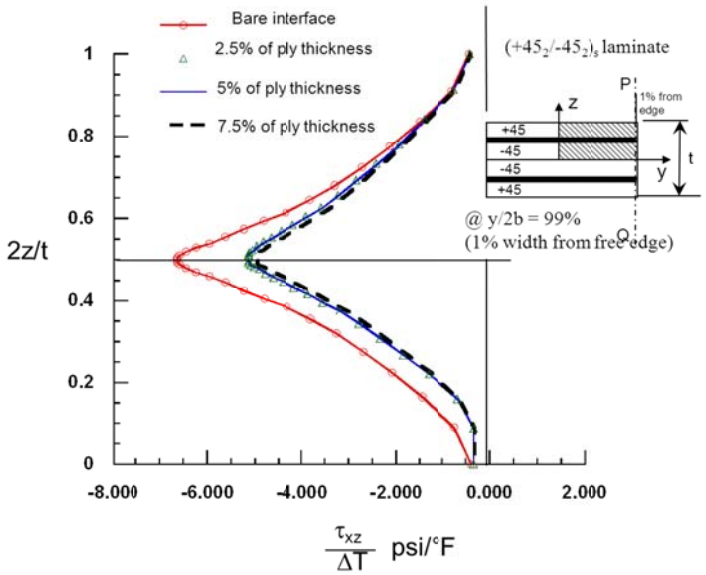

Figure D.11 Normalized τ_{xz} Stress distribution through the thickness, for $(+45_2/-45_2)_s$ laminate at 1% width from the edge (P-Q), for comparing different matrix material

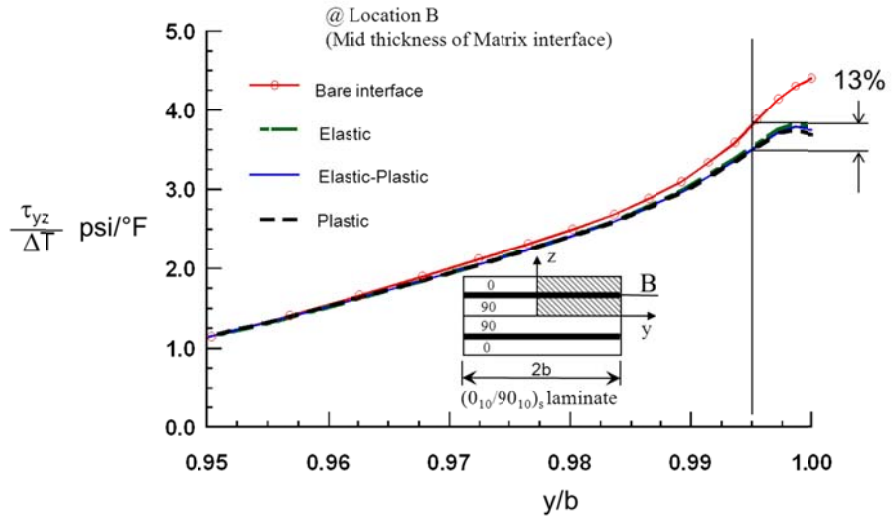

Figure D.12 Normalized τ_{yz} Stress distribution across the width for $(0_{10}/90_{10})_s$ laminate at the mid-thickness of the interphase (B), for comparing different matrix material near the edge

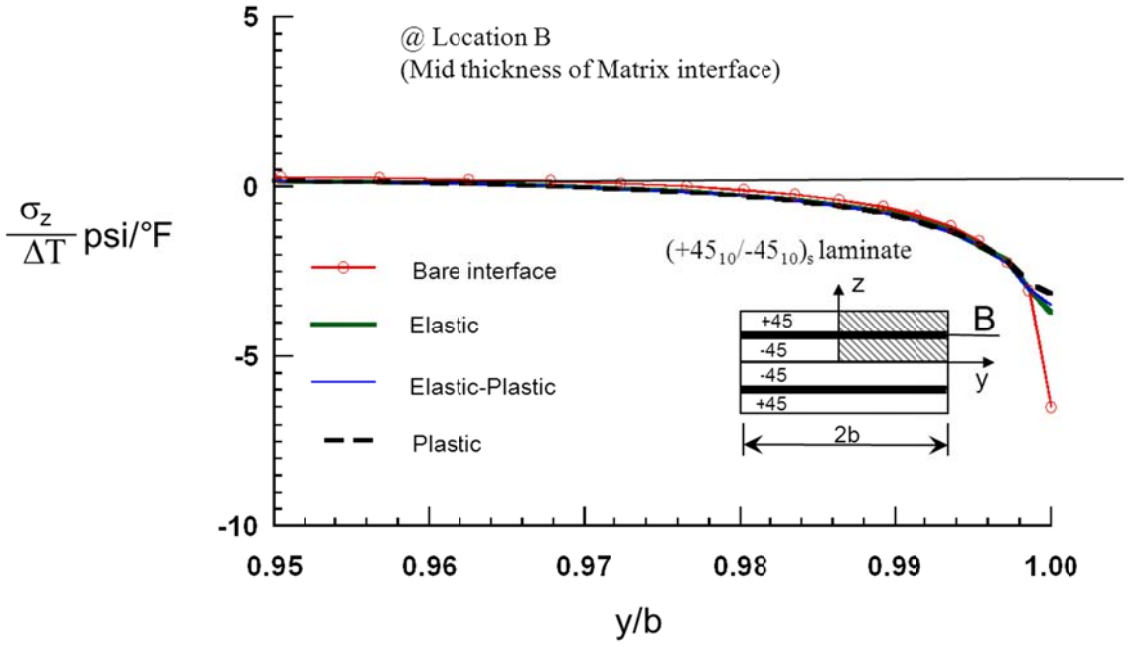

Figure D.13 Normalized σ_z Stress distribution across the width for $(+45_{10}/-45_{10})_s$ laminate at the mid-thickness of the interphase (B), for comparing different matrix material near the edge

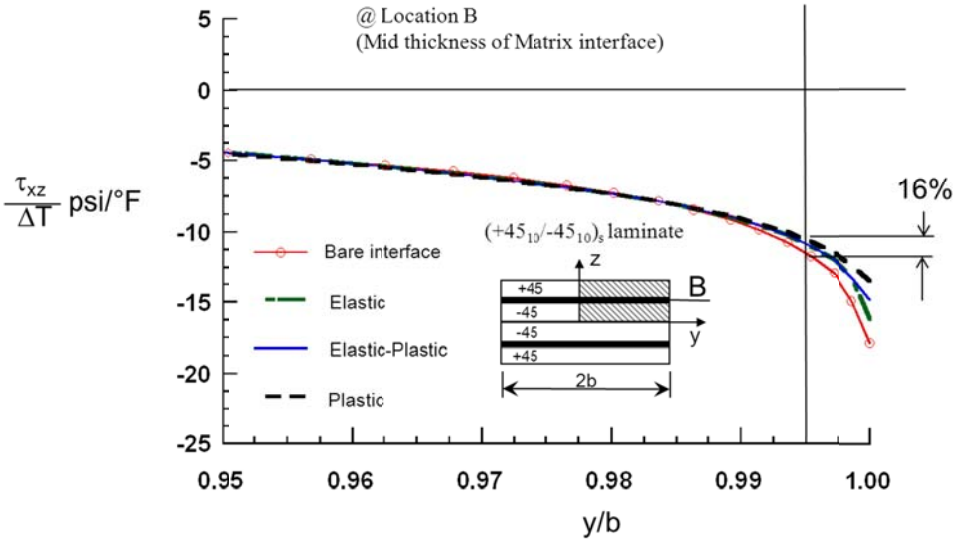

Figure D.14 Normalized τ_{xz} Stress distribution across the width for $(+45_{10}/-45_{10})_s$ laminate at the mid-thickness of the interphase (B), for comparing different matrix material near the edge